COMMISSION OF THE EUROPEAN COMMUNITIES

AGRESTE PROJECT

Agricultural resources investigations in Northern Italy and Southern France

Nasa landsat satellites investigations Nr. 28790

(E78-10199) AGRESTE PROJECT: AGRICULTURAL RESOURCES INVESTIGATIONS IN NORTHERN ITALY AND SOUTHERN FRANCE Final Report (Commission of the European Communities) 176 p HC A09/MF A01 CSCL 02C G3/43

N78-31497

Unclas 00199

Final Report

June 1978

COMMISSION OF THE EUROPEAN COMMUNITIES

AGRESTE PROJECT

Agricultural resources investigations in Northern Italy and Southern France

Nasa landsat satellites investigations Nr 28790

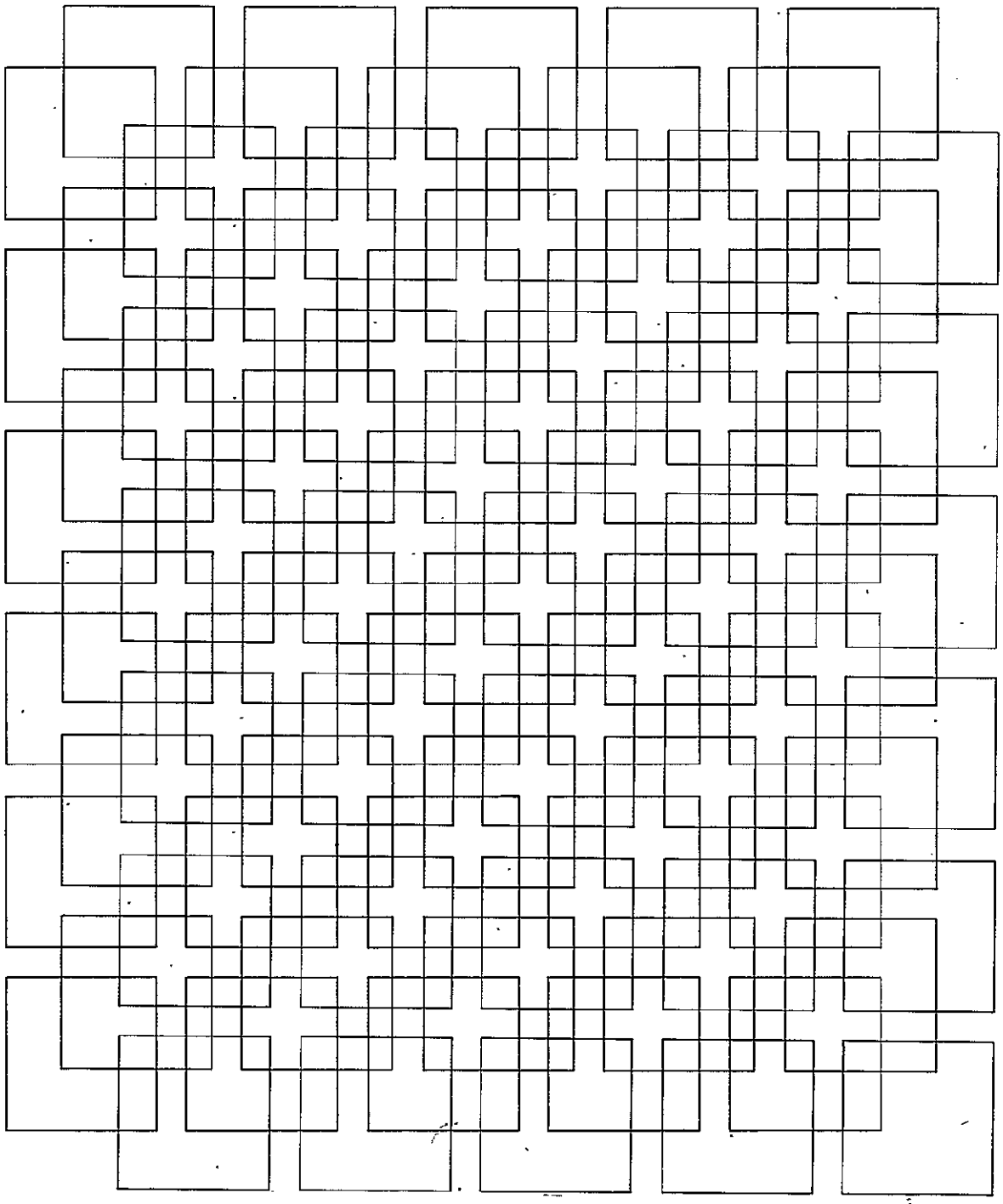

Final Report

June 1978

AGRICULTURAL RESOURCES INVESTIGATIONS IN NORTHERN ITALY AND SOUTHERN FRANCE

A joint publication from several French and Italian interdisciplinary laboratories reporting the results of a Remote Sensing Programme

General coordination:

Commission of the European Communities
Joint Research Centre - Ispra Establishment
21020 Ispra (Varese) - Italy

Coordination for the French test sites:

Centre d'Etude Spatiale des Rayonnements
9, Avenue Colonel Roche
31029 Toulouse Cedex - France

Edited by:

A. Berg, JRC - Ispra Establishment
G. Flouzat, C.E.S.R , Toulouse
S. Galli De Paratesi, JRC - Ispra Establishment

TABLE OF CONTENTS

INTRODUCTION

1. GENERAL GUIDE-LINES

The AGRESTE Project has been conceived as a pilot experiment applied to some sectors of agriculture selected in order to cover a typical range of European conditions, including man-made ecosystems (rice irrigated fields, poplar groves) and more natural ecosystems (conifer and beech forests). The choice of these specific sectors was determined by the value of examples provided by the important resources gained from the concerned ecosystems, not only in Europe but also in developing countries (rice), and by the urgent need for a global inventory of these natural resources.

The aim of the experiment was to evaluate the potentiality of remote sensing facilities under such European conditions as a support to agronomic research and land-use management, identification and inventory of rice fields, of poplar groves, of conifer and beech forests, definition of parameters allowing a prediction of rice production by remote observation of the vegetative vigour.

It was evident from the beginning that the realization of such a project with a global approach necessitated the collaboration of complementary competences and facilities existing at national levels with those existing at the Joint Research Centre of Ispra and in other services of the Commission of the European Communities (General Directorates for Agriculture, for Research, Science and Education and for Aid to Development). The idea of a consortium of national laboratories working together with the Commission of the European Communities was retained for efficiency reasons and for being a good way to promote remote sensing methods applied to agriculture in Europe. Furthermore, the contribution of different laboratories to single research items allowed a comparative evaluation of results obtained under different conditions, on the French and Italian test sites, respectively.

Test sites of limited area have been chosen, thus counterbalancing the wideness of the investigation sectors. They were selected for providing well controlled training fields, in order to obtain accurate ground truth measurements and to concentrate efforts on a minimized amount of data, to reduce computer and interpretation time. The geographic location of the European test sites in Southern France and Northern Italy is given in Fig. 1. An African test site located in Madagascar (surroundings of

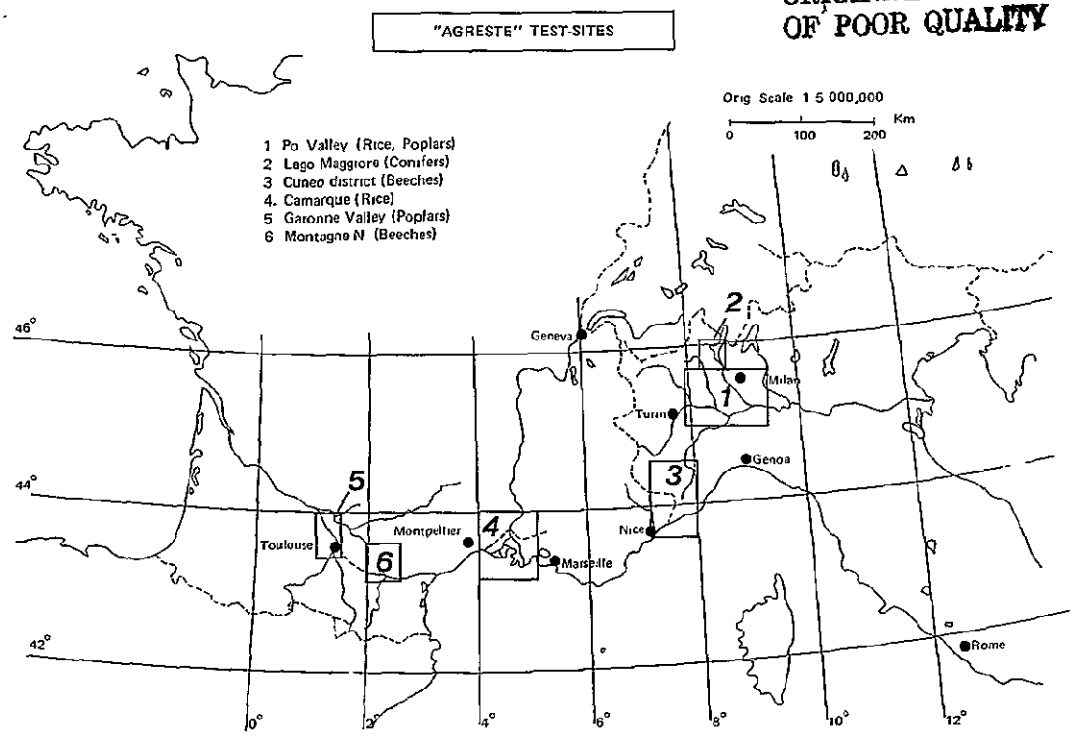

Fig. 1 - Geographic location of the European test sites in Southern France and Northern Italy

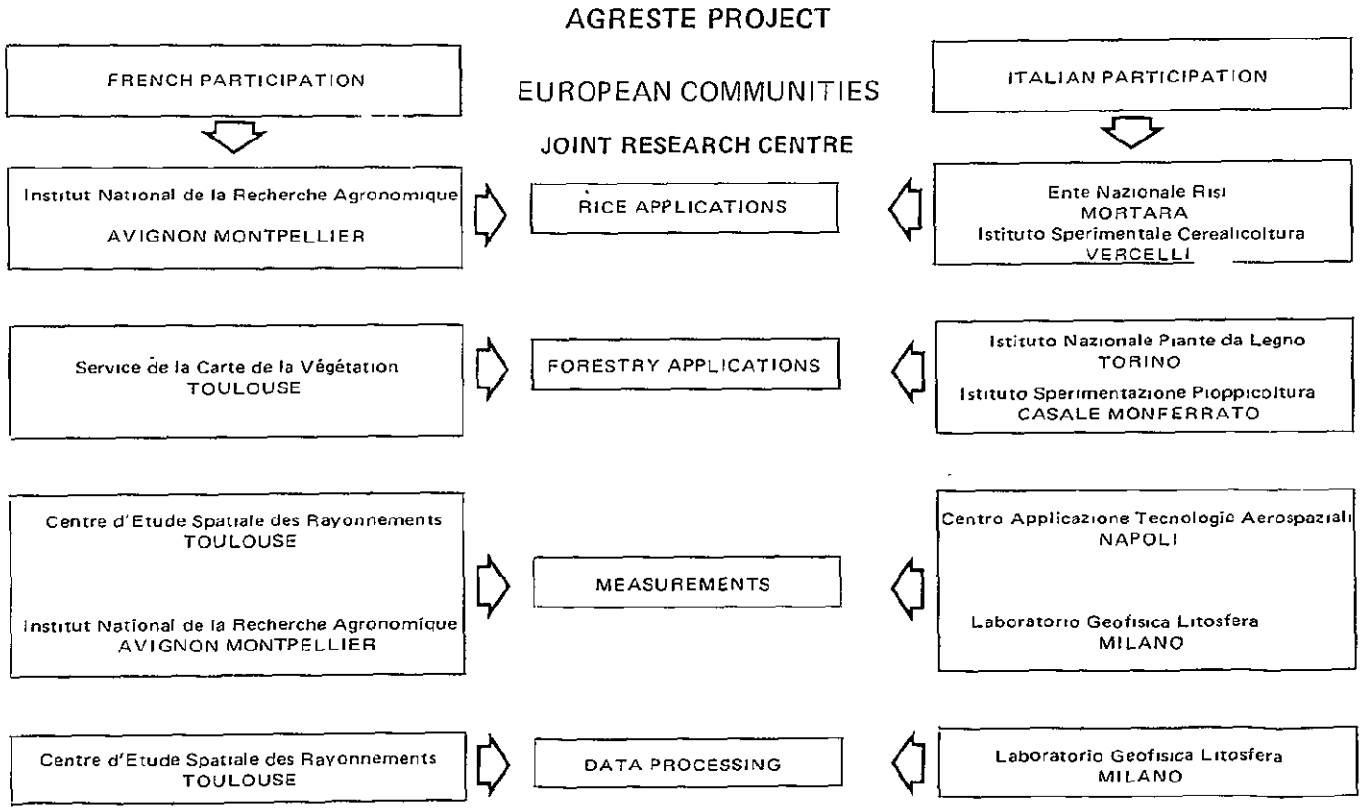

Fig. 2 - Participation in the AGRESTE Project

Lake Alaotra) was tentatively included in the rice sector of investigation, in order to add another category of totally different ecologic and agrarian conditions to those prevailing in Europe, taking at the same time profit of the exhaustive ground truth available.

The remote sensing imagery used for the realization of the AGRESTE Project consisted of that provided by LANDSAT 1 and LANDSAT 2, as well as that provided by national existing airborne facilities (aerial photography and aircraft MSS). These two types of imagery allowed the studies performed in France and Italy to reach a good level of complementarity.

In the rice investigations, a single LANDSAT imagery taken in spring over the Po Valley assumed a particular interest, whereas most French work on the Camargue was based on a multi-temporal study. On the other hand, the data acquired from aircraft were used in France as digitalized aerial photographs with the aim of textural analysis, whereas MSS records did lead in Italy to an identification of varieties.

In the poplar investigations, the LANDSAT imagery allowed in Italy a good estimate of the productive classes, whereas discrimination of poplar groves from other wood formations was not possible in the Garonne Valley in France. On the other hand, the aircraft data (mostly colour infrared) have been used in Italy for constructing ground truth maps in order to estimate the classification capabilities of satellite imagery in the Po Valley. In France the aircraft data have been used with the specific aims of establishing a timber yield prediction and of recognizing various clones.

In the forest investigation (beech and conifers), interesting results of classification have been achieved applying two complementary tests for checking the goodness of classification (performance matrix and digitalization of the reference map).

Finally, conceived as a complement to an existing ERTS-A French investigation (ARNICA Project), the AGRESTE Project did constitute a useful link between cartographic vegetation investigations, agronomic research and land-use management.

The present report represents the synthesis of all the work performed in the framework of the AGRESTE investigation. This synthesis concerns the specific research themes as well as the observed test areas and the methods used in the research.

2. PARTICIPATION IN THE AGRESTE PROJECT

Table 1 provides a list of all the organizations and institutes which were involved in the setting up and the realization of the AGRESTE Project. The specific contributions of the single institutes are indicated along the report in the description of the various research chapters (see also Fig. 2).

Table 1 - Participation in the AGRESTE Project

	Organizations and Institutes		Abbrev.
European Communities	Directorate General for Agriculture	Brussels	DG-VI
	Directorate General for Aid to Development	"	DG-VIII
	Directorate General for Research, Science and Education	"	DG-XII
	Statistical Office	Luxemburg	SOL
	Joint Research Centre	Ispra	JRC
	Biology Group DG-XII	Ispra	BGI
Italian Institutes	Ente Nazionale Risi	Mortara	ENR
	Istituto Sperimentale Cerealicoltura	Vercelli	ISC
	Istituto Sperimentazione Pioppicoltura	Casale Monferrato	ISP
	Istituto Nazionale Piante da Legno	Torino	INPL
	Istituto Patologia Vegetale	Milano	IPV
	Laboratorio Geofisica Litosfera	Milano	LGL
	Centro Applicazione Tecnologie Aerospaziali	Napoli	CATA
French institutes	Centre d'Etude Spatiale des Rayonnements	Toulouse	CESR
	Service de la Carte de la Végétation, CNRS	Toulouse	SCV
	Station d'Amélioration des Plantes	Montpellier	INRA-M
	Station de Bioclimatologie	Avignon	INRA-A

3. BIBLIOGRAPHY

The activities performed in the framework of the AGRESTE Project have been the object of regular Progress Reports, of internal JRC reports (AGRESTE Project Reports) and of numerous papers published mostly in the Proceedings of Specialized Symposia on Remote Sensing. General bibliography is presented below whereas specific bibliography will be presented at the end of each specific research theme.

GENERAL BIBLIOGRAPHY

(Anonymous) (Staffs of the European Communities and of the French and Italian Institutes of the AGRESTE Project):

- "Agricultural Resources Investigations in Northern Italy, Southern France and Madagascar", CEC, JRC-Ispra Establishment, AGRESTE Project Report No. 4 (1975); Proc. Symp. on European Earth Resources Satellite Experiments, Frascati (Italy), Jan. 28 - Feb. 1, 1974
- "Agricultural Resources Investigations in Southern France and Northern Italy", CEC, JRC-Ispra Establishment, AGRESTE Project Report No. 6 (1975); Proc. 9th Int. Symp. on Remote Sensing of Environment, Ann Arbor, April 15-19, 1974
- "AGRESTE's Activity on the Italian Test Sites - Annual Report 1974", CEC, JRC-Ispra Establishment, AGRESTE Project Report No. 10 (1975)
- "AGRESTE's Activity on the Italian Test Sites - First Semi-Annual Report 1975", CEC, JRC-Ispra Establishment, AGRESTE Project Report No. 21 (1975)

(Anonymous) (Institutes of the AGRESTE Project and JRC Remote Sensing Staff):

- "LANDSAT-2 Satellite Follow-on Investigation No. 28790. Agricultural Resources Investigations in Northern Italy and Southern France, (AGRESTE Project)",
  - 1st Progress Report (Aug. 15 - Nov. 15, 1975),
  - 2nd " " (Nov. 15, 1975 - Feb. 15, 1976),
  - 3rd " " (Feb. 15 - May 15, 1976),
  - 4th " " (May 15 - Dec. 31, 1976),
  - 5th " " (Jan. 1 - March 31, 1977).

(Anonymous) (Remote Sensing Staff, Ispra)

- "Objective 2.53.0 - Remote Sensing of Earth Resources, JRC Progress Report 1974"

(Anonymous) (French Remote Sensing Staff)

- "AGRESTE Programme - Part 2 French Test Sites":

  . 1-st Progress Report (Dec. 1975 - Jan. 1976),
  . 2nd " " (March - June 1976),
  . 3rd " " (July - Dec. 1976).

- MEGIER, J., BALDI, G., CELLERINO, G., DE CAROLIS, C., LAPIETRA, G., "Classification automatique des données du satellite LANDSAT appliquée à agriculture et sylviculture", Rivista Il Riso, 25, 4 (1976)

- DEJACE, J., MEGIER, J., MEHL, W., "Computer-aided Classification for Remote Sensing in Agriculture and Forestry in Northern Italy", 11th Int. Symp. on Remote Sensing of Environment, Ann Arbor, Mich., April 1977

- DEJACE, J., GALLI DE PARATESI, S., MEGIER, J., MEHL, W., "Contribution of the AGRESTE Investigation to the Identification and Inventory of Agricultural Resources in Europe", COSPAR/IAMAP (IUGG) Symp. on the Contribution of Space Observations to Global Food Estimation System, Tel Aviv, June 1977.

CHAPTER I - IDENTIFICATION AND INVENTORY OF RICE FIELDS

Contributors to the Text

LE TOAN, T. (CESR, Toulouse)
MEGIER, J. (JRC-Ispra Establishment)

Scientific Collaborators

France: CASSIRAME, P. (CESR, Toulouse)
MARIE, R. (INRA, Montpellier)
QUACH, J. (CESR, Toulouse)

Italy: BALDI, G. (ENR, Mortara)
DEJACE, J. (JRC-Ispra Establishment)
DORPEMA, B. (JRC-Ispra Establishment)
GREGOIRE, J-M. (JRC-Ispra Establishment, post-graduate student)
MALAGONI, R. (ENR, Mortara)
MEHL, W. (JRC-Ispra Establishment)
RUSSO, S. (ISC, Vercelli)
STEIN, A. (JRC-Ispra Establishment)

The investigations described in this chapter were performed in the regions of intensive rice cultivation of Southern France and Northern Italy (test sites No. 1 and 4). They were essentially aimed at identifying, by the setting up of reliable automatic classification methodologies, the surfaces occupied by rice cultivation in view of their synoptic and repetitive inventory. Because of quite different environmental conditions prevailing on the two test sites, the French and Italian investigations provide complementary results. Furthermore, a certain amount of effort has been dedicated, on the Italian test site, to the problem of recognition of various important rice varieties.

1. GENERAL DESCRIPTION OF RICE FIELDS

1.1 France

Water and sun requirements of rice plants make that rice culture in France remains confined to the Rhône delta in the form of irrigated fields. This region of the Provence, called Camargue, lies at a very low altitude (scarcely above sea level) and is essentially marshy.

The typically mediterranean climate is characterized by a dominant N-S cold wind (mistral) which reduces the frequency of rice diseases relative to the Italian test site.

The arrangement of rice fields in the test site depends on the ecological and agricultural conditions of the region. Areas of rice cultivation consist of adjacent parcels, the size of which mainly depends on local topography. The plots are leveled so that water depth can be controlled to within one centimeter. This implies that the plots be narrow and that they follow contour lines. Most of the rice fields are therefore divided into small parcels (40 - 50 cm wide and 100 - 400 m long). After flooding, the fields look like a mosaic of rectangular plots.

Several varieties are cultivated: Delta, Balilla 28, Euribé, Cigalon, Cristal, Arlésienne, RB, etc. and this affects the irrigation conditions which are based on the water requirements of the plants. The cover rate during the vegetative stage can vary from parcel to parcel in relation to the cultivated variety.

In the Northern part of the test site, rice fields are surrounded mainly by vineyards and cereal fields (wheat, barley, corn, etc.) and in the South, mainly by natural water bodies and marshes. Some difficulty may therefore arise in the identification of rice fields because of possible confusion with natural water bodies at the sowing stage and with marshes at the vegetative stage.

1.2 Italy

Most of the Italian rice fields (91.4% in 1975) are concentrated in the Northern part of the country, along the Po Valley, in the provinces of Milan, Pavia, Novara and Vercelli. Rice cultivation is very extended in this region contained in the AGRESTE test site No. 1 (with a global surface of rice fields of 1620 km^2 in 1975). Its concentration increases from East to West, with rice fields of progressively larger size.

As in France, the rice fields are organized in continuous parcels separated by little dams from 10 to 80 cm thick for the main dams. The parcels are flooded at sowing time with a layer of water of an average depth of 10 cm ($\pm$ 3 cm). The average dimension of the parcel is about 1 ha (10,000 m^2) with wide variations from 0.1 to 5 ha and a general rectangular shape. Inside a large rice area which is "seen" by LANDSAT as a continuous water body during the sowing period, dams and ditches which bring water to the parcels, constitute 5 to 6% of the total surface.

The main rice varieties cultivated in Northern Italy are Balilla and Balilla GG (28.2% of the total cultivation area in 1975), Padano (12.7%),

Ribe (10.6%), Arborio (8.7%), Roma (8.3%) and Ringo (7.5%). Other less important varieties are present, including Europa (3.3%) and Romeo (2.6%). Four of the mentioned varieties, together with two others, have been investigated in section 4. The other main cultivations present in the test area (situated immediately to the South of the town Mortara, 40 km to the South-West of Milan) are, in order of decreasing importance: corn, wheat, oat and similar, poplars, beets, potatoes, melons and water melons.

Water bodies are not present in the test area apart from the Po River and some of its tributaries.

2. GROUND DATA COLLECTION

2.1 France

2.1.1 The following indicative phases in the phenological cycle of the rice plant were considered as significant for application of remote sensing techniques (beside bare soil):

- sowing phase: soil is covered by a thin layer of water (10 cm), brought through a complex irrigation system. The sowing period extends from April 20 to May 15 approximately, in relation to irrigation water availability and water temperature conditions;
- vegetative phase: the young plant emerges about 3 weeks after sowing and one month later the leaves cover up the field (tillering/heading);
- maturation phase: characterized by a strong colour change of the plant and by the reappearance of the water layer;
- harvest phase: the fields are dried out about one month before harvesting.

A series of 5 to 6 LANDSAT scenes taken during the course of rice development should therefore be available for the best identification of rice fields.

2.1.2 During 1975. a vast amount of ground data was collected simultaneously with the passages of LANDSAT-2.

2.1.2.1 Rice phenology was followed for the 3 most commonly cultivated rice varieties in the Camargue region, i.e. Delta, Euribé and Balilla 28. Table 2 summarizes development stages and soil conditions observed at LANDSAT-2 passages (for development stage definition, see ref. 1).

Table 2 - Development stages of rice plants and soil conditions at passages of LANDSAT-2, 1975, French test site

Date of passage	Development Stage			Soil Conditions
	Delta	Euribé	Balilla 28	
April, 7	-	-	-	wet
April, 25	-	-	-	dry
May, 13	emergence	emergence	emergence	
May, 31	"	"	"	under water
June, 18	beg. of tillering	"	"	" "
July, 6	beg. of stem elongation	beg. of tillering	beg. of tillering	" "
July, 24	boots just visible	beg. of stem elongation	beg. of stem elongation	" "
Aug., 11	mid flowering	beg. of heading	boots just visible	" "
Aug., 29	early milk stage	mid flowering	mid flowering	" "
Sept., 16	early dough stage	early milk stage	early milk stage	" "
Oct., 4	caryopsis loosening at daytime	caryopsis hard	early dough stage	beginning of drying
Oct., 22	-	caryopsis loosening at daytime	caryopsis hard	-
Nov., 9		harvested	harvested	-

Contemporaneously, the following meteorological parameters were recorded in an experimental rice field: maximum, minimum and mean temperatures, soil temperature and minimum actino-thermal index (at 10 and 50 cm soil depth), direction and average velocity of wind, duration of insolation, number of hours with an air relative moisture below 40% and above 80%, rain fall (Table 3).

2.1.2.2 On the other hand, an experiment was performed with the aim to follow the phenology of 5 rice varieties in relation to time of sowing intentionally spread out in time (from April 21 to May 15) (Table 4). One can note that important differences in development stage are induced by time of sowing during the first phases, but these differences progressively decrease during the course of development. It follows that the spectral response of rice fields in the test site exhibits a wide variation range during the first stages (before tillering). On the other hand, spectral dis-

Table 3 - Measurements recorded in the "Mas de Gouine" area

DATE OF PASSAGE	AIR TEMPERATURES			MIN ACTIONO-THERMAL INDEX		WIND		SOIL TEMPERATURES a-10 cm		a-50	SUN	RELATIVE HUMIDITY		RAINFALL
	Mini	Maxi	moy	At 10 cm	At 50 cm	DIR	MOY (m/s)	Mini	Maxi	cm	(h)	<40 %	>80 %	mm
75.03.02	11,5	13,5	12,5	3,2	5,0	-	-	9,5	10,0	9,6	-	0	11	0,0
75.03.20	0,4	8,5	4,5	6,1	3,0			7,3	8,9	8,8	-	0	16	49,8
75.04.07	5,0	15,5	10,3	0,0	1,0	8	2,6	8,0	9,5	9,0	5,6	0	11	0,2
75.04.25.	9,2	29,0	19,1	5,2	7,1	8	6,8	14,5	15,1	15,1	12,3	20	0	0,02
75.05.13	10,7	21,7	16,2	8,1	9,8	8	3,6	11,4	15,5	14,1	12,0	0	6	0,0
75.05.31	13,1	17,0	15,1	8,9	11,4	1	2,8	15,8	19,4	18,4	1,8	0	18	11,1
75.06.18	9,9	21,9	15,9	4,2	7,7	8	5,7	15,4	20,0	20,4	13,0	0	0	0,0
75.07.06	16,8	25,0	20,9	14,2	15,8	8	1,6	16,9	20,2	20,9	11,5	0	13	0,0
75.07.24	17,2	30,7	24,0	15,8	16,9	9	1,8	20,7	26,4	24,2	9,2	0	2	0,0
75.08.11	18,0	28,5	23,3	15,6	16,4	8	0,8	21,4	26,5	26,0	12,8	0	11	0,0
75.08.29	16,4	25,2	20,8	14,0	16,0	9	1,4	16,4	22,7	21,4	2,2	0	15	0,1
75.09.16	13,5	24,8	19,2	12,0	13,0	5	1,4	14,0	19,5	20,5	0,8	0	14	0,0
75.10.04	13,5	27,7	20,6	11,9	12,9	8	3,1	13,0	20,7	19,7	9,5	0	9	0,0
75.10.22	6,5	18,0	12,3	3,0	5,0	9	0,8	8,0	13,6	13,5	0,7	0	18	0,2
75.11.09	5,6	9,4	7,5	2,8	3,7	9	2,6	6,0	10,2	12,5	0,0	0	24	18,3

Table 4 - Developmental stages of 5 rice plant varieties in relation to time of sowing

VARIETY	SOWING	First leaf	Beginning of Tillering	Beg. of Stem Elongation	Boots just visible	Heading to flowering	End of flowering	Early milk stage	Early dough stage	Caryopsis hard	Good for harvest	OBSERVATIONS
BALILLA 28		07.05	08.06	25.07	06.08	12.08	20.08	27.08	04.09	18.09	08.10	
CIGALON		07.05	08.06	12.07	23.07	31.07	08.08	13.08	21.08	08.09	22.09	Abnormaly long
CRISTAL	21.04	07.05	08.06	25.07	06.08	10.08	20.08	25.08	06.09	21.09	03.10	cycle
DELTA		07.05	08.06	20.07	26.07	03.08	09.08	20.08	02.09	15.09	27.09	Heterogeneous
EURIBE		07.05	08.06	22.07	06.08	11.08	23.08	04.09	15.09	28.09	05.10	emergence
BALILLA 28		12.05	04.06	20.07	31.07	09.08	14.08	27.08	03.09	22.09	05.10	
CIGALON		12.05	04.06	12.07	20.07	30.07	08.08	13.08	21.08	07.09	22.09	
CRISTAL	29.04	12.05	04.06	20.07	29.07	06.08	12.08	18.08	27.08	15.09	30.09	
DELTA		12.05	04.06	12.07	20.07	02.08	09.08	18.08	25.08	09.09	22.09	
EURIBE		12.05	04.06	26.07	02.08	11.08	19.08	29.08	09.09	25.09	05.10	
BALILLA 28		15.05	06.06	28.07	03.08	09.08	18.08	25.08	09.09	25.09	14.10	
CIGALON		15.05	06.06	12.07	19.07	31.07	08.08	13.08	21.08	09.09	22.09	
CRISTAL	07.05	15.05	06.06	26.07	02.08	09.08	16.08	23.08	30.08	20.09	03.10	
DELTA		15.05	06.06	15.07	22.07	03.08	11.08	21.08	27.08	11.09	25.09	
EURIBE		15.05	06.06	30.07	06.08	12.08	21.08	28.08	09.09	22.09	07.10	
BALILLA 28		25.05	10.06	28.07	04.08	09.08	21.08	27.08	11.09	25.09	14.10	
CIGALON		25.05	10.06	12.07	19.07	31.07	09.08	18.08	25.08	12.09	25.09	
CRISTAL	15.05	25.05	10.06	30.07	04.08	08.08	16.08	24.08	03.09	16.09	06.10	
DELTA		25.05	10.06	17.07	25.07	05.08	12.08	21.08	28.08	10.09	25.09	
EURIBE		25.05	10.06	25.07	03.08	12.08	23.08	04.09	18.09	30.09	15.10	Disease

crimination of rice varieties would be possible only after tillering (for example at mid July for the most usual sowing dates).

2.1.2.3 Finally, a ground truth campaign was systematically performed during 1975 in conjunction with each satellite passage. It included rice field inventory, mapping of rice varieties and disease detection.

2.2 Italy

2.2.1 The phenological stages considered are the same as on the French test site, but they are somewhat anticipated in time. Table 5 presents the phenological stages and soil conditions in the test area of Mortara, collected by ENR in correspondence to LANDSAT-2 passages in 1975, for the most important varieties Balilla and Balilla GG.

Table 5 - Development stages of rice plants and soil conditions at LANDSAT-2 passages, 1975, for varieties Balilla and Balilla GG, Italian test site

Date of passage	Development Stage	Soil Conditions
April, 22	sowing (April, 17-18)	under water
May, 10	no information collected	" "
May, 28	emergence	" "
June, 15	beginning of tillering	" "
July, 3	tillering - field coverage not compl.	" "
July, 21	tillering - complete field coverage - beginning of booting	" "
Aug., 8	late flowering (beg. Aug., 5-6)	" "
Aug., 26	late milk stage	drained
Sept., 13	late dough stage	"
Oct., 1	harvest (Sept. 29-Oct. 6)	"
Oct., 19	harvested	"

2.2.2 Ground truth maps providing the location of the rice fields were established for two test areas in collaboration with ENR. A test area of 120 km^2 was chosen for the year 1973 around the village of Ferrera, between the town Mortara and the Po River (test area "Ferrera"); for the year 1975, an area of about 250 km^2 was considered, including the town Mortara and the test rice fields of ENR (test area "Mortara"). For a limited part (44 km^2) of the test area "Mortara", a ground truth map of some rice varieties was established.

Furthermore, numerous other ground data were collected on some test fields of ENR concerning water temperature, water depth, vegetation mass temperature, vegetation biomass, etc.

3. DATA PROCESSING FOR RICE INVENTORY

3.1 France

3.1.1 Preliminary study of the aerial images

A B 17-flight was organized on June 20, 1975 over the test site, at 7000 and 1500 m) by the GDTA*. The following products were used:

- Daedalus Scanner recordings (7000 m),
- IRC images (7000 m) acquired with the Camera Wild RC8,
- Black and white images (1500 m).

Photo-interpretation of 7000 m IRC images provided the location of several samples of rice fields and other object categories in the area: vineyards, wheat fields, marshes and urban areas. On June 20, rice fields were under a 10 cm layer of water, and the various varieties exhibited different development stages: from emergence (Delta) to beginning of tillering (Euribé, Balilla 28). On IRC images, rice fields appear as blocks of mixed blue and pink tones (Fig. 3).

Displays of Daedalus scanner recordings were studied, especially those from the 2 channels closest to the LANDSAT MSS 5 and 7 (channels 7, 650-700 nm; channel 10, 900-1100 nm). Ambiguity exists on channel 7 between rice and some other cereals while, in channel 10, rice fields are confused with temporarily flooded plots (vineyards, market gardens).

The photo-interpretation also reveals the diversity of land use classes in the Northern and the Southern part of the zone with the Upper Camargue, of fluvial origin, mainly occupied by agriculture and urban areas, and the lower Camargue where natural water bodies and marshes are abounding.

In order to facilitate the computer-aided classification, the test site was subdivided into 4 rectangular areas (Fig. 4), presenting a certain homogeneity in ground occupation: 1. Arles (about 20 x 20 km); 2. Aigues Mortes (about 20 x 11 km); 3. Saintes Maries de la Mer (about 11 x 11 km); 4. Port St. Louis (about 15 x 20 km).

---

*Groupement pour le Développement de la Télédétection Aérospatiale.

Fig. 3 - IRC image of part of the test site (7000 m - Camera Wild RC 8; f = 152 mm). 1. rice; 2. wheat; 3. vineyard; 4. marsh

3.1.2 Study of rice field responses

Photo-interpretation of aerial images provided directives for the study of homogeneity of rice field responses. An area is considered as homogeneous when the gradient at all points is zero or less than a threshold determined by the measurement noise. In addition to this concept of instrumental homogeneity, a concept of ground object homogeneity, related to the resolution problem, is applied. With LANDSAT resolution, such agricultural grounds as vineyards or orchards (structure of alternating vine and soil, trees and soil) appear as stable composites and the extracted samples exhibit homogeneous responses.

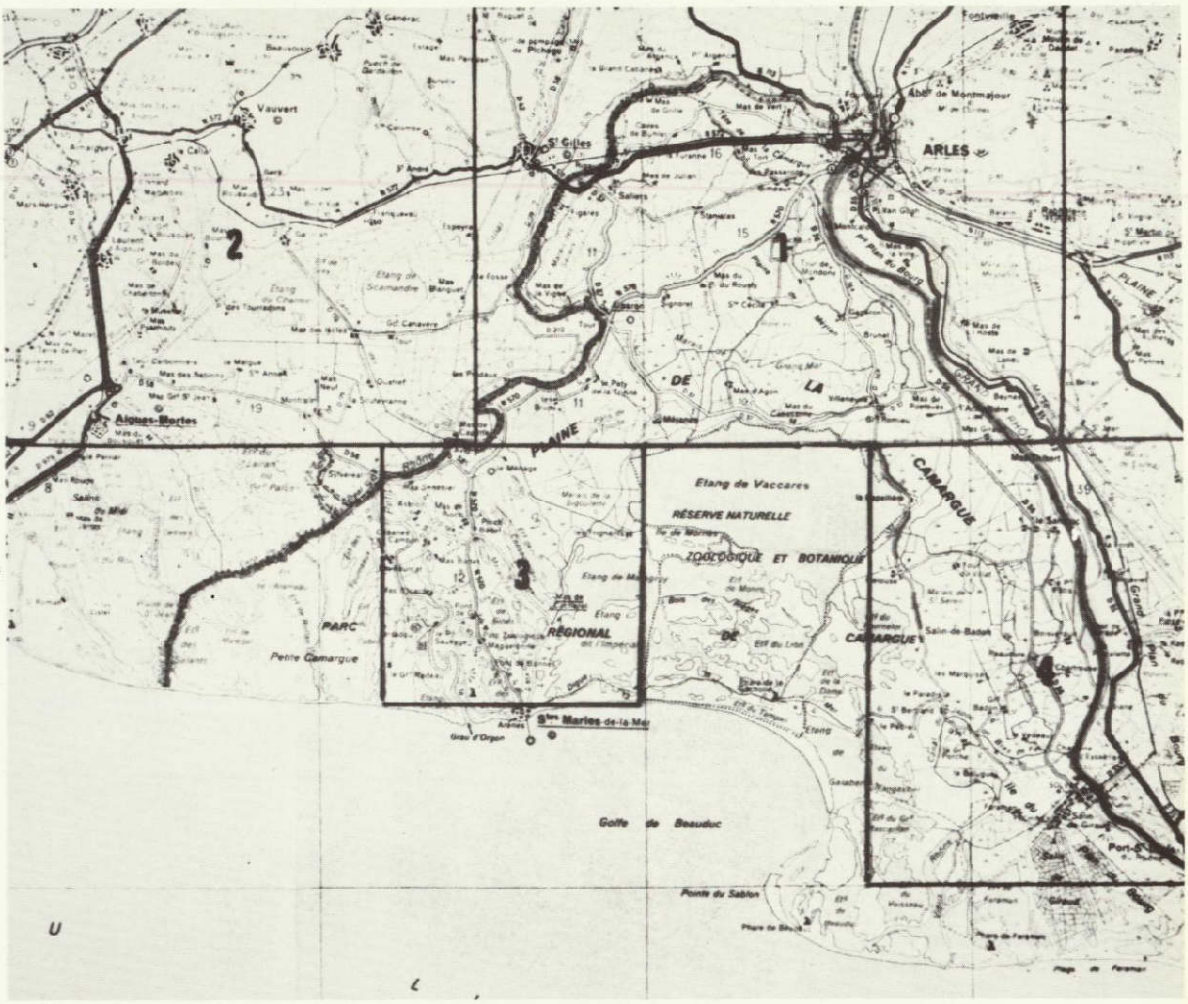

Fig. 4 - French test site No. 4 (about 55 x 20 km)

The study of rice field homogeneity was performed on both aerial and LANDSAT images.

3.1.2.1 Study on aerial images

1500 m IR black and white images (sensitivity in the band 0.25 - 0.92 um) were digitized by means of a Joyce-Loebl microdensitometer, delivering an 8 bits coded optical density for every pixel of about 2 x 2 m.

Several grey level manipulations leading to an algorithm of edge detection were performed on the digitized image with several simulated resolutions obtained by averaging pixel matrices. On 10 x 10 m and 20 x 20 m resolution images, smoothing and sharpening techniques and an edge detection algorithm were successively applied, using the Eberlein-

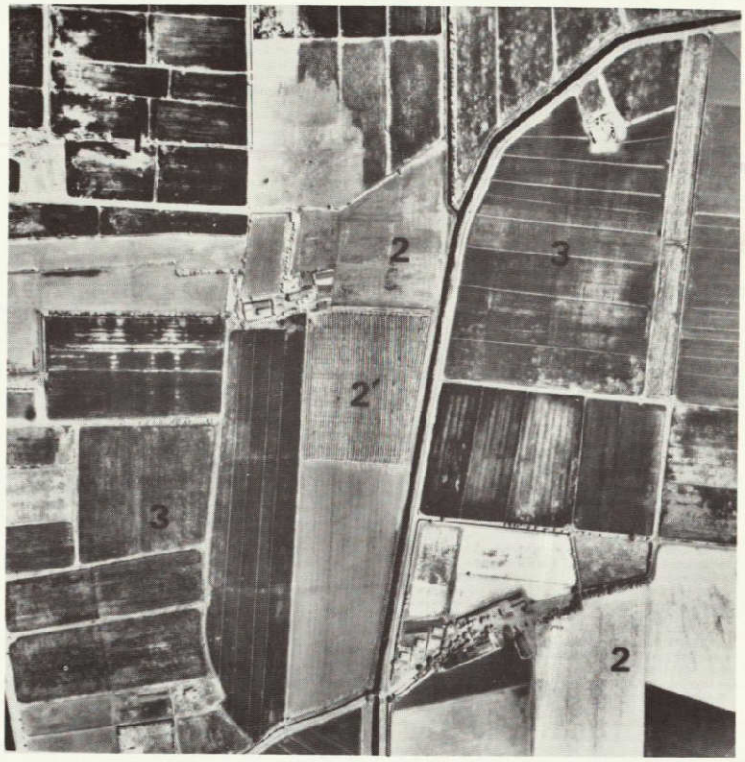

Fig. 5 - IR Black and White, 1500 m, scale 1 : 10,000. 1 = rice; 2 = wheat; 2'= harvested wheat; 3 = corn

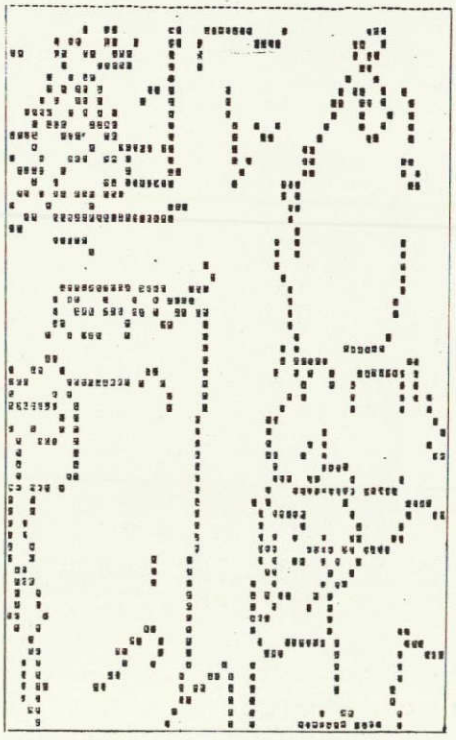

Fig. 6 - Results of edge-detection performed on aerial image of Fig. 5

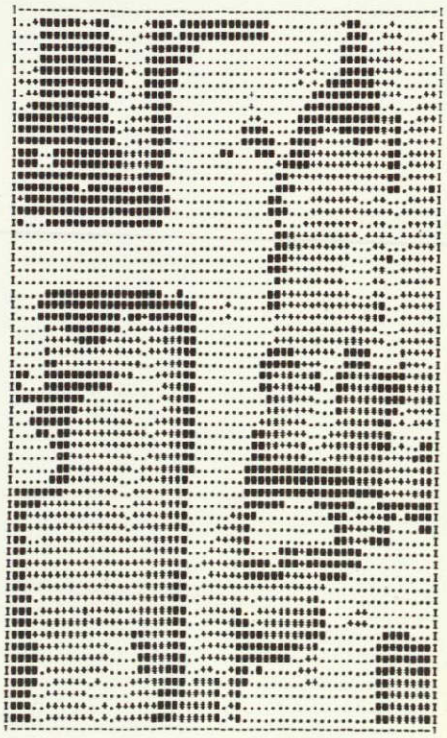

Fig. 8 - Results of classification on same image (see text)

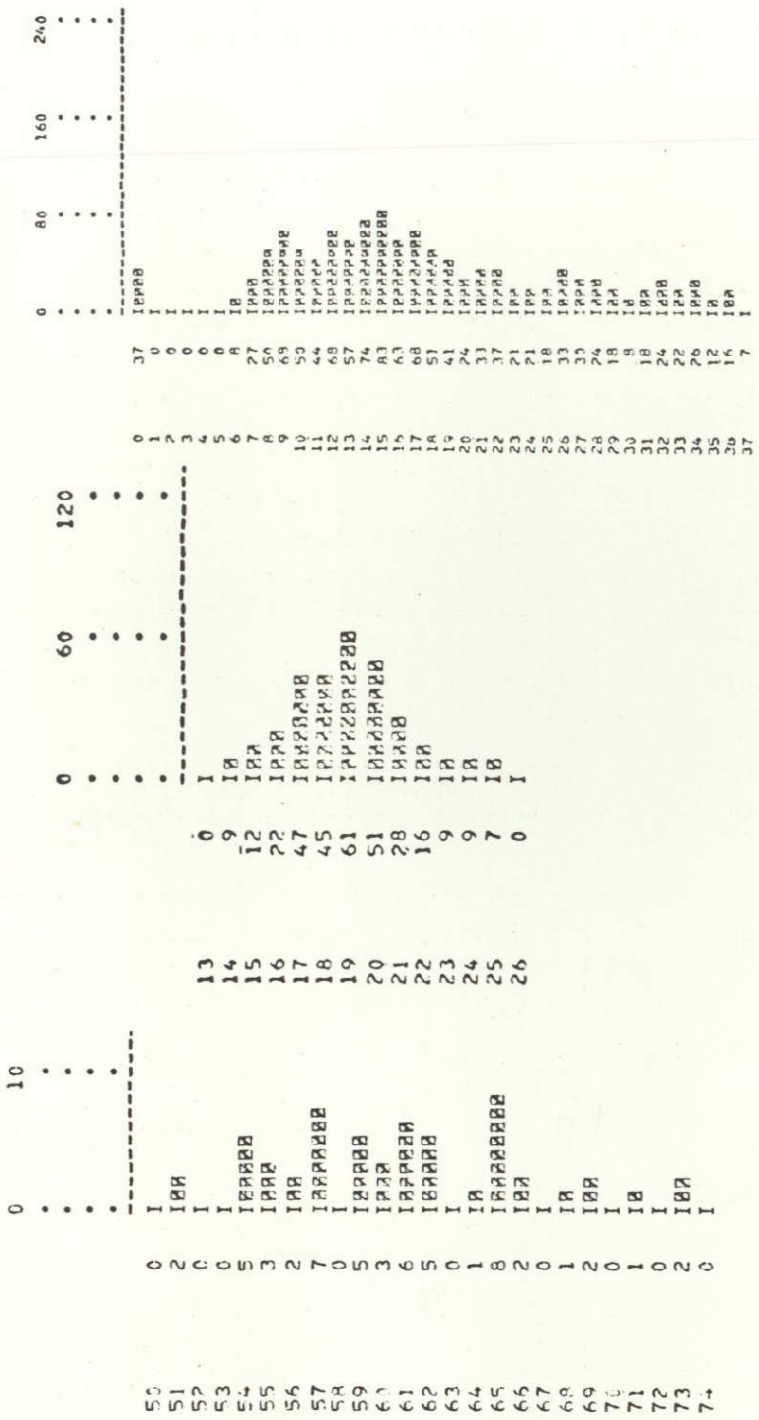

Rice N = 1180
σ = 7.85
χ^2 = 322.6

Wheat N = 320
σ = 2.64
χ^2 = 19.2

Rice N = 55
σ = 5.25
χ^2 = 39.5

Fig. 7 - Comparison of rice and wheat histograms extracted from aerial images (above) and histogram of a rice sample extracted from LANDSAT MSS 7 (below), July 6, 1975

quired during the period from emerging to tillering.

3.1.2.2 Study on LANDSAT images

Statistics of rice field responses were determined for each spectral LANDSAT band for the scenes of July 6, July 23 and August 11. On the July scenes, statistics of samples indicated a wide range of rice responses with respect to cereals, vineyards and meadows, whereas the inverse is found on the August image. Table 7 presents an example of statistics computed on 3 rice samples compared with 3 wheat samples of the same size (about 60 pixels), for the July 23 and August 11 scenes.

The dispersion of rice responses in July can be explained by the great differences in development stages in the parcels: beginning of tillering, stem elongation, boots just visible. On August 11, after the vegetative phase, the fields appear phenologically more homogeneous (mid flowering for the Delta variety, beginning of heading for the Euribé variety).

Table 7 - Statistical parameters of LANDSAT responses of some fields

Date	Samples	MSS 5		MSS 7	
		mean value	standard deviation	mean value	standard deviation
July 23, 1975	Rice	28.86	5.46	31.79	3.95
		23.58	6.31	29.08	5.09
		33.50	4.68	31.08	4.12
	Wheat	43.04	2.10	23.03	1.16
		46.71	2.16	27.75	1.03
		41.71	1.95	24.20	1.38
August 11, 1975	Rice	22.31	1.27	36.18	3.26
		19.95	1.30	35.75	2.45
		18.29	1.73	37.48	2.54
	Wheat	38.92	4.01	46.86	3.92
		40.50	3.13	51.21	3.43
		31.21	2.92	37.85	5.80

The above study on homogeneity of rice fields can guide the choice of the classification technique to apply to images acquired during the vegetative phase of rice.

The first conclusion is that the normal distribution hypothesis for rice response cannot be assumed. The χ^2-values, computed from the formula

$$\chi^2 = \sum_{i=1}^{n} \frac{(f_i - Np_i)^2}{Np_i} ,$$

where N = number of pixels,
f_i = frequency associated to level i,
p_i = probability associated to level i, calculated by the Gauss-Laplace formula,

actually exceed the acceptable limit for normality assumption. In this case, techniques based on the normal assumption should be substituted by techniques using for instance Mahalanobis or Sebestyen distance (see Appendix, section 4.1.2).

The second conclusion of the study is the correlation existing for rice between MSS 5 and MSS 7 in July (correlation between water and rice responses) while the responses are rather independent for vineyard and for the other cereals (see example of Fig. 9 and of Table 8).

Table 8 - Example of correlation between MSS-5 and MSS-7 responses, July 6, 1975

Class	5	7	
Rice	4.37	6.44	-0.117
Vineyard	4.48	3.57	-0.012
Cereals	7.57	5.15	-0.005

The slope of the axis along which the response values x_i, y_i are located, can be calculated from the following formula, if we assume that the cloud formed by plotted sample points of every class is an ellipse[3]:

$$\operatorname{tg} 2\theta = \frac{-2r\sigma_x\sigma_y}{\sigma_x^2 - \sigma_y^2}$$

This correlation can be exploited by choosing a linear classifier in MSS-5 - MSS-7 plane. The linear function can easily be determined on the following diagram (Fig. 9). The plane is then divided into 2 regions (rice and others). One must, however, ascertain that region 1 does not include other water bodies and marshes.

Another example of the possibility of application of the linear classifier method is illustrated by a bitemporal diagram computed in a preliminary study (Fig. 10) from March and May 1973 scenes. In this case, where rice

Fig. 9 - Bispectral diagram of the responses of samples on MSS 5 and MSS 7 channels (1: rice fields; 2: vineyards; 3: cereals)

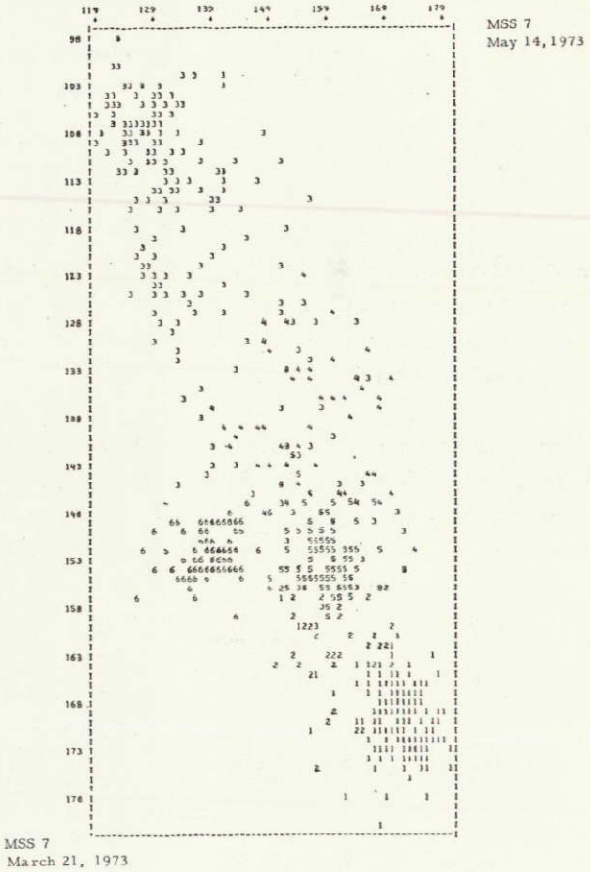

Fig. 10 - Bitemporal diagram of the responses of samples on MSS 7 channel (1: meadows; 2: vineyards; 3: Rhône; 4: Petit Rhône; 5: town (Arles); 6: rice fields)

fields are ploughed in March and flooded in May, the density technique applied on MSS 7 image gives mixed rice fields and water bodies.

3.1.3 Comparison between the different classification techniques

The classification methods applied in this section are briefly described in the Appendix (section 4.1).
The performances of the various algorithms have been tested on LANDSAT data of August 11, 1975. This date actually appears as the most suitable one for rice field inventory, according to the results of the data reduction study (see following section 3.1.4).

Fig. 11 shows the reference map of a 6.7 x 9.5 km area of the test site (120 x 120 pixels) with the location of rice fields, wheat fields and vineyards. The following results are obtained:

Fig. 11 - Reference map of a 6.7 x 9.5 km area. Pink: rice; yellow: wheat; green: vineyard

- Barycentric and quadratic methods: the reference rice fields are mapped with 3% difference between computed surface and owner estimation (Figs. 12 and 13). Vineyards are subdivided into 2 classes, relating to their soil conditions.
- Fix-Hodges method: rice fields are mapped with 5% difference. Vineyard is classified as one class, including meadows, market gardens and bare soil (Fig. 14). For rice fields, the method can fit to their non-normal spectral responses. However, it requires a very good sample selection which is difficult to perform on such parceled agricultural sites.
- Unsupervised methods: results are obtained with clustering techniques using euclidean, Mahalanobis and χ^2-distance. Rice fields and vineyards are partly merged as expected, whereas wheat fields are divided into 2 classes which do not correspond to differences in cultural conditions.

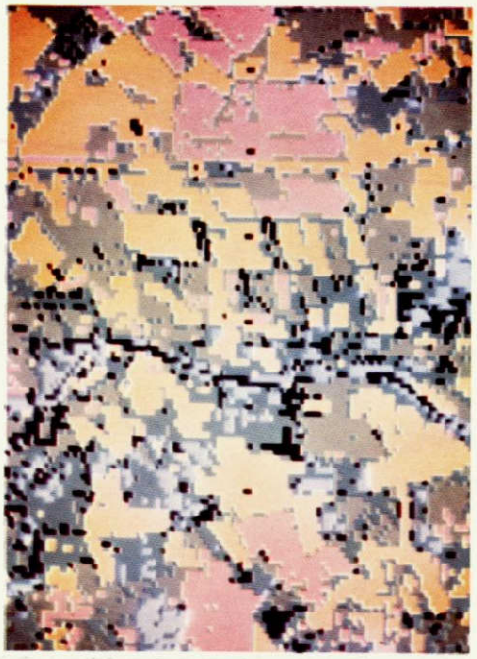

Fig. 12 - Supervised method, euclidean distance

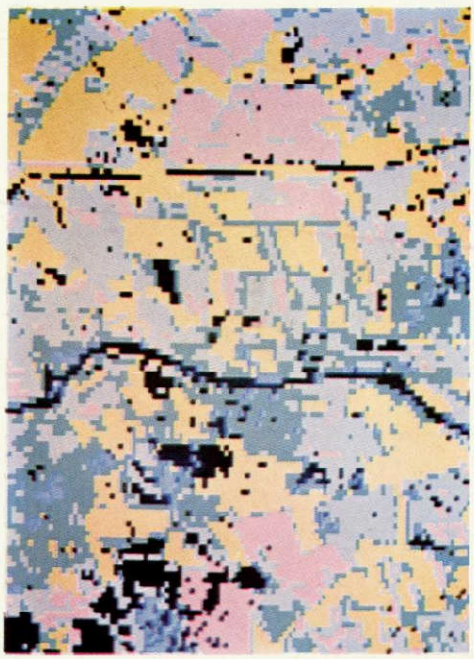

Fig. 13 - Supervised method, quadratic distance

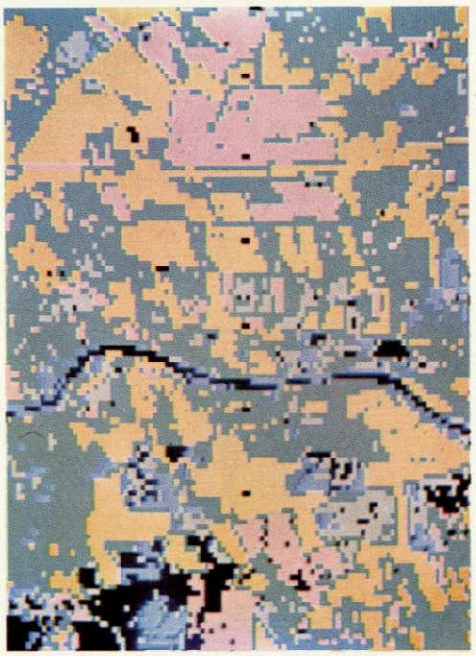

Fig. 14 - Supervised Fix-Hodge method

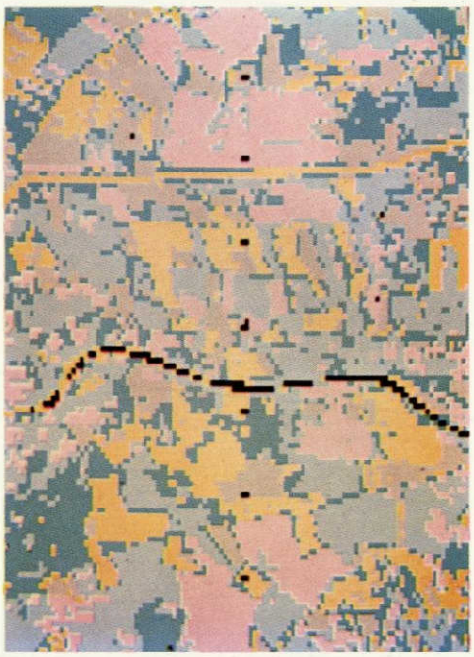

Fig. 15 - Unsupervised method, Mahalanobis distance

Comparison of classification methods
Pink : rice Yellow : wheat Green : vineyard

rice fields were flooded. The study of the sample responses reveals the clustering of the main classes: water bodies, vineyards, cereals. The recognition of rice fields is possible by means of a density slicing method, although the result also includes all natural water bodies and the edges of the river (Fig. 16).

A multitemporal analysis on the scenes of March 21 and May 14, 1973 provided a second mapping. On March 21, rice fields were just wet ploughed plots. A study of the sample responses indicates possible discrimination of rice fields from water bodies (Fig. 10). Euclidean distance method applied on MSS-7, MSS-5 data of May 14 and March 21, provided a better discrimination of rice fields (Fig. 17).

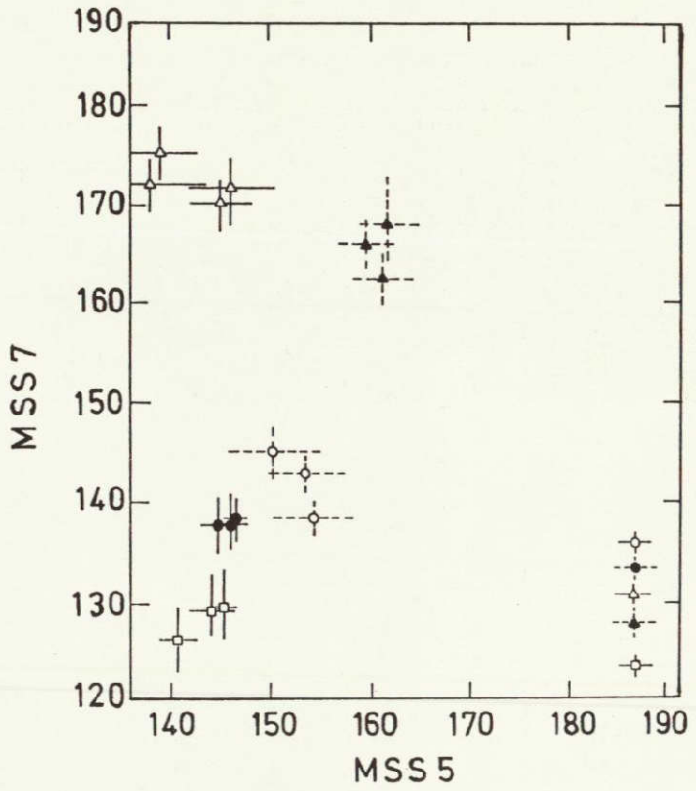

Fig. 16 - Diagram of MSS 5 - MSS 7 data, May 14, 1973. Rice fields (sowing), rice fields (just flooded), cereal, vineyard, Rhône river

3.1.4.2 Study on 1975 scenes

A previous data reduction was performed (12 channels for 3 dates), providing at the same time adequate information in order to define the best conditions for data acquisition in the future (spectral bands and dates).

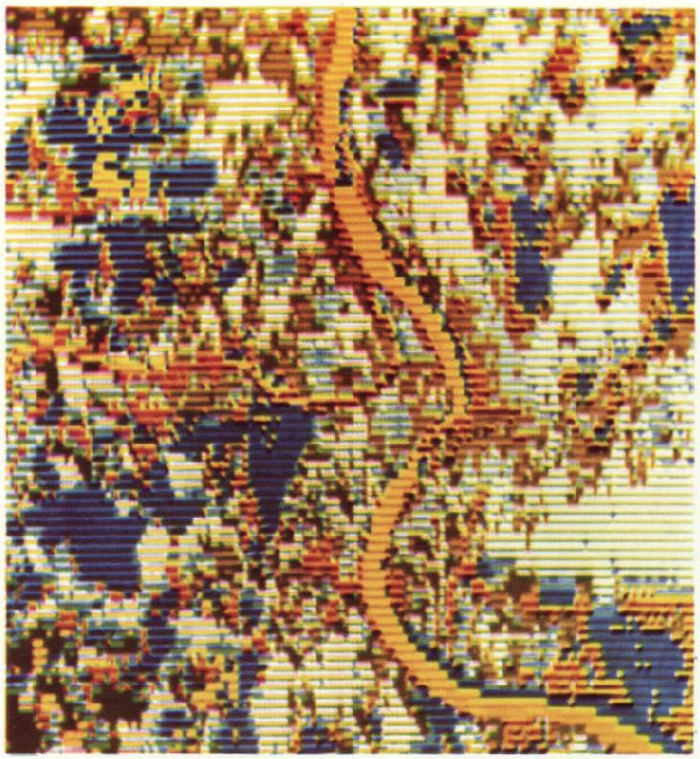

Fig. 17 - Mapping of rice fields in 1973 by multitemporal data classification (March, 21 and May, 14). Dark blue: rice fields; dark green (bottom left): marshes

To determine the best combination of spectral bands and dates among the 3 x 4 channels (July 6, July 23 and August 11 LANDSAT scenes) suitable for the discrimination of rice fields from their surroundings, samples were extracted and divided into two groups.

The discrimination function (in this case Sebestyen-distance is used) is computed from the first group and applied to the second one for calculation of the well-classed percentage.

The best combinations of 2, 4, 5 channels for the discrimination of wheat, vineyard, rice are shown in Table 10. The August scene appears as the best for rice recognition: rice (flowering, heading) is then well separated from wheat (harvested) and vineyard (maximum foliage on bare soil). The July 23 scene provides the least performing set of data. Unfortunately, for inventory purposes on the global test site, the August image had to be combined with another image, the test site being partly

covered by clouds on August 11.

Table 10 - The best combinations of spectral bands and dates for discrimination of rice, wheat, vineyard

	MSS 7, MSS 5, Aug. 11			MSS 7, MSS 5, Aug. 11 MSS 7, July 6 MSS 4, Aug. 11			MSS 7, MSS 5, Aug. 11 MSS 7, July 6 MSS 4, Aug. 11 MSS 5, July 23		
computed / original	rice	wheat	vine-yard	rice	wheat	vine-yard	rice	wheat	vine-yard
Rice	209	11	12	214	5	13	214	5	13
Wheat	3	172	33	12	176	20	7	183	18
Vineyard	12	7	79	3	9	86	3	6	89
	well classed perc: 85.50% well classed perc. for rice: 90%			well classed perc.: 88.48% well classed perc. for rice: 92%			well classed perc.: 90.33% well classed perc. for rice: 92%		

3.1.5 Conclusions for data processing

For rice field identification and inventory purposes, the following conclusions can be drawn from the 1973 and 1975 LANDSAT and aerial data.

1973 - May 14 (flooded rice fields, before emerging): density slicing applied on MSS 7, but the result includes marshes and natural water bodies. The solution consists in combining the May scene with another one when rice fields are drained (in this case March scene).

1975 - June 20 (emerging, beginning of tillering): recognition of rice fields by edge detection and texture analysis, evaluation of unproductive surfaces within a block of rice fields.

The method might be applied to aerial images and extended to future satellite images.

1975 - July 6 and 23 (vegetative stage: tillering, stem elongation): classification by linear discrimination (LANDSAT images), possible confusion with marshes on July 6 and other irrigated plots on July 23.

- August 11 (reproductive stage: flowering, heading): classification using euclidean or quadratic distance.

The following combinations proved to be useful in multitemporal analysis:

- August 11 and July 6: classification using euclidean distance on MSS MSS 5 bands.
- August 11, July 6 and July 23: classification using euclidean distance MSS 7 - MSS 5 bands of August 11, MSS 7 July 6 and MSS 5 July 23.

Fig. 18 - Mapping of the sub-test area No. 1 (black signs: rice fields)

Fig. 19 - Reference map of rice fields (in black) within the test area "Ferrera", 1973. Approx. area: 45 km^2

Fig. 20 - Map of classified rice fields (in black) obtained by level slicing of LANDSAT channel 7 on May 10, 1973, test area "Ferrera"

Table 11 - LANDSAT-2 available scenes over rice test area, 1975

ID NBr.	Date	Growth Stage
2144 - 09331	June, 15	Beginn. of tillering
2162 - 09331	July, 3	Tillering
2234 - 09320	Sept., 13	Late dough stage

No early LANDSAT data were available at the end of May before emergence of the plants above water level. The tillering stage prevailing in the June and early July scenes introduces a great heterogeneity in the data due to variation of vegetation coverage from field to field and to variation of aspect of the rice plants from variety to variety. The scene of September 13 has not yet been processed.

The concept of supervised classification was used.* The heterogeneity of the data convinced us, on the basis of previous studies, to use a quadratic rather than a linear classifier, but with a special care to define and choose the training sets. As a matter of fact, the maximum likelihood method (ML) was chosen, with supervised classes described by normal parameters. If the class distributions taken into account are not normal, as is generally the case, the ML scheme does not provide any more the best theoretical classifier. It results, however, in a very reasonable and efficient quadratic classifier, provided the class distributions are unimodal or nearly so. A further question arises from the evaluation of the a priori probability $P(C_k)$ for class C_k, but the supervised context allows here to use equal existence probabilities for the classes of interest and thus to ignore them in the classification process.

3.2.2.1 Processing of data from June 15, 1975

The study was made on the reduced test area "Mortara" (see section 2.2.2). In a first stage the training sets for rice were chosen by combining a clustering method with a uniformity mapping procedure, both using euclidean distance as similarity measure between two points in order to put in evidence clusters of points suitable in the sense of uniformity and of geographic location. The same was done for non-rice classes, mainly poplar groves and corn fields. A first classification and mapping provided a basis to identify - in connection with the ground truth map - reliable sampling areas to define training sets for unimodal rice classes. No care was purposely devoted to the fact that the new classes were largely overlapping (owing to the large variance values) in order to keep the entire variance of the rice data. The mean and standard deviations of the rice training classes are given in Table 12. The training sets for rice represented less than 4% of the total area processed.

* see Appendix, section 4.2.2

Table 12 - Mean and standard deviation values for rice classes, June 15, 1975

	LANDSAT-2 Channels			
	4	5	6	7
R_1 μ	24.3	21.7	46.9	19.1
R_1 σ	1.1	1.0	3.0	1.8
R_2 μ	28.8	20.8	43.2	17.2
R_2 σ	1.1	0.9	6.0	3.7
R_3 μ	25.3	22.8	45.2	18.3
R_3 σ	1.2	1.5	3.4	2.2
R_4 μ	27.8	26.1	48.0	19.1
R_4 σ	1.4	1.8	3.5	1.8
R_5 μ	25.1	23.4	45.3	17.9
R_5 σ	1.4	1.7	4.6	3.0

The classification and mapping results using this second set of five classes together with three non-rice classes, showed that a trade-off was needed between non-recognition of rice zones and misclassification as rice of non-rice zones by setting a proper "membership threshold" on rice classes. The classification results are mapped in Fig. 22 and can be compared to the ground truth displayed in Fig. 21. They were obtained by setting on each rice class a rejection threshold of 3% of the maximum probability of the corresponding class distribution.

The overall rice percentage area was found to be 43%, whereas the ground truth value is 35.5%, thus with an overestimation by 21% of the rice covered areas.

3.2.2.2 Processing of data from July 3, 1975

At the time this work was done, a procedure had been set up to construct a digitized version of ground truth maps by discrete elements following the scanning grid of LANDSAT (see Chapter 4 - § 2.2.3.1 for more details). A discrete version of the ground truth map with rice varieties for the limited test area "Mortara" was thus realized. It was then possible to localize training samples within the different varieties with a fair accuracy. Due to the reduced dimensions of the fields, each training sample was rather small (from 4 to 20 pixels) and several samples were merged for each variety. The training sets represented about 5% of the total processed area. The statistical parameters of some retained varieties are presented in Table 13.

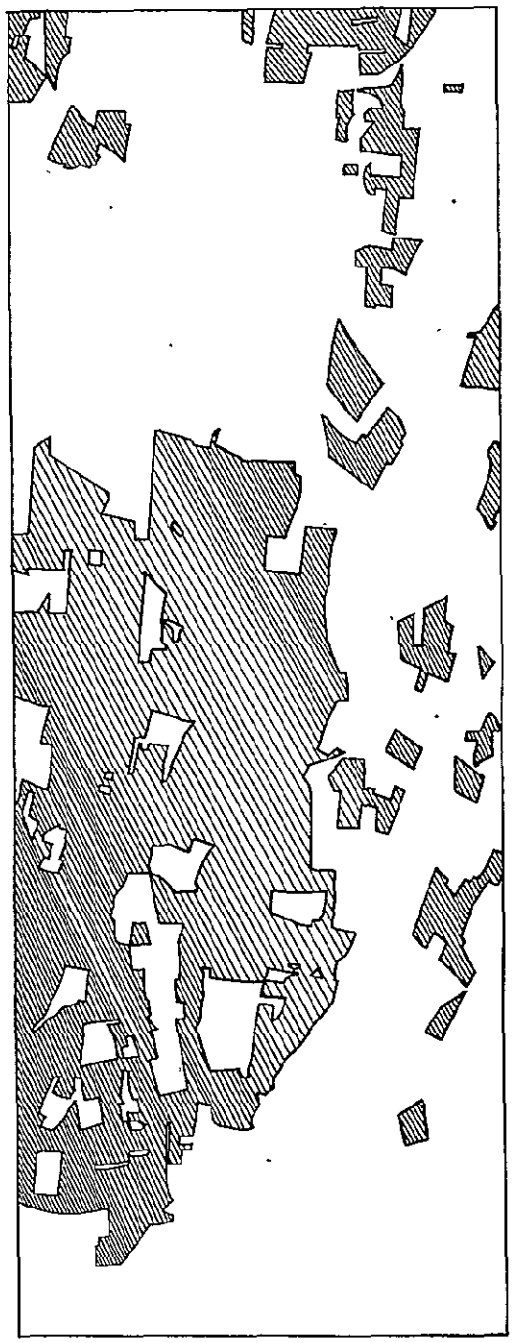

Fig. 21 - Ground truth map for the limited test area "Mortara", 1975. Hatched areas represent rice fields. Approx. scale 1 : 60,000

Fig. 22 - Classification display of test area "Mortara" with data of June 15, 1975, ML method. Rice fields in black

Table 13 - Mean and standard deviation for various rice varieties, July 3, 1975

		LANDSAT-2 Channels			
		4	5	6	7
Arborio	μ	23.7	21.2	65.6	31.8
	σ	1.3	0.63	5.5	3.9
Balilla GG	μ	21.7	19.2	48.9	21.7
	σ	1.3	1.5	5.1	3.3
Gritna	μ	22.1	20.4	58.7	28.3
	σ	1.2	1.0	4.5	2.7
Carnaroli	μ	22.6	20.1	48.7	21.0
	σ	1.5	1.5	4.6	2.5

The classification work was then performed with the ML method, starting from 4 rice classes corresponding to the 4 varieties and from some other non-rice classes. This time no rejection threshold was set for the classes.

A pixel-by-pixel comparison between discrete ground truth and classification results was performed under the form of a performance matrix shown in Table 14. It is organized in rows corresponding to the various ground truth categories (R = rice, NR = non rice) and in columns corresponding to the various classes resulting from classification. The first number of each square is considered in the sense category-class, thus indicating the percentage of pixels correctly classified into the corresponding class and misclassified into the other class. The second number of each square is considered in the sense class-category.

For example, on the righthand side of the R column, one has indicated in each row the percentage of pixels classified as "rice" which actually belong to the ground truth category R (row R), but also to category NR (row NR). The same is done on the righthand side of column NR. The overall result RC1/RGT (total number of pixels classified as "rice"/ total number of pixels belonging to the category rice on the ground truth) is also given. This presentation allows an objective and complete evaluation of the classification performances.

From the detailed results of Table 14 it is seen that 90% of rice present on the ground truth was correctly recognized, but with 18% misclassifications within the pixels classified as rice.

As an overall result (RC1/RGT), it is seen that rice covered areas are overestimated, this time, by 9%. Two circumstances may explain the

Table 14 - Performance matrix (expressed in %) for data of July 3, 1975, ML method. RC1/RGT = 109%

Class / Ground truth	R	NR
R	90/82	10/20
NR	33/18	67/80

improvement of the results, as compared to those obtained by processing the data of June, 15. On the one hand, the development stage (more advanced tillering) may be more favourable to the discrimination of rice from non-rice; on the other hand, sampling over the actual varieties may improve the representation of the intrinsic reflectance features of rice. The last assumption seems to be reinforced by the fact that sampling rice independently of the varieties location brings a degradation of the results.

It must be added, however, that, although the consideration of rice varieties as training classes improved the accuracy of rice classification as a whole, the problem of discriminating varieties with LANDSAT data is not yet solved. Preliminary results in this sense show that two groups of varieties can be rather well discriminated from each other, Carnaroli and Balilla GG from Arborio and Gritna.

3.2.3 Conclusions for rice inventory in Italy with LANDSAT data

The generality of any conclusion is naturally restricted by the fact that, up to now, the test areas studied are limited as compared to the extension of the rice cultivated areas in Italy, although the test areas were chosen as typical of rice cultivation. In this respect, a comparison should be made over a wide region between recognized rice areas at the flooded stage (corrected from other water bodies) and coverage data given by ENR from cadastral maps updated every year.

Extrapolation from results obtained for a 15 km^2 test zone allows to expect good performances in the inventory of rice areas over wide regions, such as Northern Italy, with a global accuracy not inferior to 95%. Such an accuracy is obtained by using LANDSAT data during the period between sowing and emergence of rice. The suitable time interval extends over 3 to 4 weeks; a cloudfree LANDSAT scene should there-

fore be obtained within this short period. This might prove to be difficult to realize; actually we did not succeed for the year 1975, even by considering LANDSAT-1 as well as LANDSAT-2 passages, thus with a coverage period of 9 days.

Using data acquired at later development stages, does not bring the same precision in inventory. A global accuracy of 90% has nevertheless been reached. This conclusion is also limited by the reduced extension of the studied area (44 km^2). The last result was obtained by using the scenes acquired on June 15 and July 3; however, an exhaustive multi-temporal analysis combining these scenes with the last scene available, acquired on September 13, is still to be done.

In a preliminary estimation, one could evaluate to a minimum of 5 or 6 the number of successive LANDSAT scenes necessary for an exhaustive rice inventory. The actual availability of LANDSAT data over the test area chosen did not allow to fulfill this requirement. One of the reasons for this was that the test area for the year 1975 is situated toward the edge of one of the two overlapping LANDSAT frames (in the sense East-West). This unfavourable circumstance was not given sufficient importance when choosing the testarea.

4. PROCESSING OF AIRBORNE SCANNER DATA FOR IDENTIFICATION OF RICE VARIETIES

4.1 Characteristics of the data

The data were acquired on August 7, 1975, between 9.11 and 10.32 a.m. by a Bendix M^2S scanner at a date on which the various rice varieties should be in the flowering stage (Table 5) considered to be favourable for the scope of the operation.

The technical data of the scanner are reported in Table 15. The data from channels 1, 2 and 10 were not used, however, due to an unacceptable level of noise. The resolution of the data at the altitude of 1500 m is 3.8 m. The flight was made over a part of the test area "Mortara"; the strip of data processed here covers a zone approximately 3 km^2 in area, where six rice varieties are present, labeled in the following way on the ground truth document (Fig. 23): Gritna (G), Balilla GG (B), Arborio (A), Carnaroli (C), Rocca (RC), Romeo (RO). The other symbols correspond to Corn (M) and wet meadows (MR).

4.2 Ground truth preparation

The work was done in collaboration with ENR (see section 2.2.2). The final document (Fig. 23) was prepared following the procedure described

Table 15 - BENDIX M^2S scanner technical data

	Chan. no.	Center (μm)	Width (μm)	Chan. no.	Center (μm)	Width (μm)
Scan angle 100^o	1	0.410	0.06	7	0.680	0.04
	2	0.465	0.05	8	0.720	0.04
Roll compensation	3	0.515	0.05	9	0.815	0.09
$\pm 10^o$	4	0.560	0.04	10	1.015	0.09
Geometric resolution	5	0.600	0.04	11	11.0	6.0
$2.5 \cdot 10^{-3}$ rad	6	0.640	0.04			

in chapter 4, section 2.2.3.1, but in a much easier context owing to the resolution of the data. Not all the rice fields present in the strip were characterized from the point of view of rice variety. Fields containing unidentified varieties or mixtures of varieties - what often occurs in the studied zone - are black on the ground truth, together with roads, field ways and some inhabited areas.

4.3 Classification methodology (see also Appendix, section 4.2.2)

The classification was exhaustive, including also the zones uncharacterized on the ground truth. The ML and MED methods were used. No rejection threshold was applied to any of the classes and no point was therefore left unclassified. The training of the algorithms was done on little portions of the ground truth classes as seen in Fig. 23. Care was taken that the statistical distributions in the training sets be nearly unimodal although training sets of the same ground truth class could present noticeable differences between the respective distributions. Better global results were obtained, however, with the ML method by merging together all the sub-distributions of the same class, than by processing such "subclasses" separately. The opposite was true, on the average, with the MED method, particularly class A and class M were divided respectively into three sub-classes.

4.4 Atmospheric corrections

As the total scan angle of the Bendix M^2S scanner is 100^o, it is well known that the variation of the thickness of the atmosphere between the scanner and the ground along a scan line has a systematic effect on the acquired data and may then cause a degradation of the classification results. The "long track averaging" procedure used here to correct this effect, assumes that, in absence of the above mentioned atmospheric effect, the mean and variance for each channel along a column of data (i.e. following the flight axis) would have the same value for all the columns (i.e.

from edge to edge in the strip of acquired data). The routine set up calculates then in a first step the mean and the variance of the columns from edge to edge of the strip and transforms in a second step the data of each column in order that all the columns have the same mean and variance. This procedure is repeated separately for each channel. The correction on the variance has proved to be useful to correct what appears as a lack of contrast towards the edges of the strip in a somewhat accurate visualization of the raw data. This correction method has been applied to all data.

4.5 Outline of the results

The results are presented in the confusion matrices displayed in Tables 16 to 18, where UC means uncharacterized areas on the ground truth from the point of view of rice varieties, and O stands for roads, inhabited zones and other non-vegetal items. In the classification process, UC and O are grouped under the label 0. In the last row, labeled "total classified/total ground truth", the overall classification results for each category are indicated.

Table 16 - Rice varieties performance matrix for ML 8 channels

	G	B	A	MR	M	C	RC	RO	O
G	71.4	7.9	9.8	0.0	2.4	0.2	2.5	0.2	5.4
B	2.9	76.4	1.2	0.1	3.1	1.7	0.4	0.3	13.9
A	11.3	1.3	86.8	0.0	3.9	0.2	3.2	0.9	12.3
MR	0.1	0.9	0.4	83.5	2.2	0.0	0.1	0.0	13.8
M	0.8	0.0	0.2	0.1	80.1	0.0	0.1	0.0	19.2
C	0.8	10.3	0.3	0.0	1.0	64.7	14.7	2.5	5.6
RC	0.9	1.3	4.5	0.0	1.3	0.5	78.3	10.2	3.0
RO	0.2	1.7	8.8	0.0	1.2	0.1	26.0	51.2	10.8
O	0.5	1.2	0.1	1.6	2.8	0.1	0.1	0.1	93.5
UC	2.0	12.0	3.4	0.4	13.8	3.6	1.9	0.6	62.3
Tot cl./ tot. GT	105	97	83	89	108	68	210	84	

The best result was obtained, as expected, with the ML method using all the 8 channels available (Table 16). It is seen that the discrimination is on the average very good between rice varieties on the one hand, between rice and other vegetal species on the other hand. The percentage of ground truth classified as such varies from 65 to 83%, apart from variety RO. The data compression by principal components analysis (P.C.) from 8 to 5 dimensions affects very little the results (Table 17) but the calculation time is decreased from 29 to 18 min (CPU time with IBM 370/165, 134320 pixels processed); the fraction of the

Table 17 - Rice varieties performance matrix for ML after data compression from 8 to 5 dimensions by P.C. analysis

	G	B	A	MR	M	C	RC	RO	O
G	69.1	7.4	11.5	0.0	3.0	0.6	3.1	0.2	5.0
B	2.9	74.4	1.2	0.0	4.4	2.7	0.4	0.3	13.6
A	15.2	1.0	63.7	0.0	6.4	0.2	2.8	0.9	9.7
MR	0.0	0.0	0.5	85.4	3.9	0.0	0.0	0.0	10.1
M	0.3	0.0	0.3	0.2	78.0	0.0	0.1	0.0	21.1
C	1.1	11.7	0.4	0.0	1.2	62.4	14.6	2.8	5.7
RC	2.1	1.3	5.4	0.0	1.3	0.6	76.3	10.3	2.5
RO	0.2	1.5	11.9	0.0	1.2	0.2	27.0	47.9	9.7
O	1.1	1.4	0.4	1.4	5.4	0.2	0.2	0.1	89.7
UC	2.5	11.9	3.6	0.4	17.6	4.0	2.0	0.5	57.4
Tot.cl./ tot. GT	111	96	82	90	117	67	204	83	

Table 18 - Rice varieties performance matrix for MED 8 dimensions after P.C. transformation

	G	B	A	MR	M	C	RC	RO	O
G	61.1	6.6	10.0	0.0	3.5	0.1	0.8	0.1	14.9
B	1.9	65.8	0.5	0.0	4.5	1.1	0.3	0.1	25.8
A	13.4	1.8	60.4	0.0	3.9	0.0	2.0	0.4	16.1
MR	0.3	0.0	0.2	68.2	0.7	0.0	0.0	0.0	30.6
M	0.2	3.2	1.9	0.0	69.3	0.0	0.0	0.0	25.4
C	1.4	23.5	0.5	0.0	2.2	43.4	10.9	0.8	17.2
RC	1.5	2.7	20.8	0.0	0.7	0.1	56.7	9.9	7.5
RO	1.1	5.4	26.8	0.0	0.7	0.0	20.1	29.8	16.0
O	0.2	1.8	0.3	0.4	1.6	0.0	0.0	0.0	95.5
UC	2.3	15.1	3.4	0.2	10.5	2.3	0.7	0.3	65.3
Tot. cl./ tot. GT	98	104	89	70	100	45	150	48	

total variance conserved in the transformation is 99.2%. The classification results are displayed in Fig. 24 for this last case. It is seen that the uncharacterized rice fields (in black) on the ground truth are mainly classified as mixtures of varieties with the exception of zones where rice was not recognized; it must be said in this respect, that other varieties, not identified on the ground truth, are present in the same region and were not sampled here.

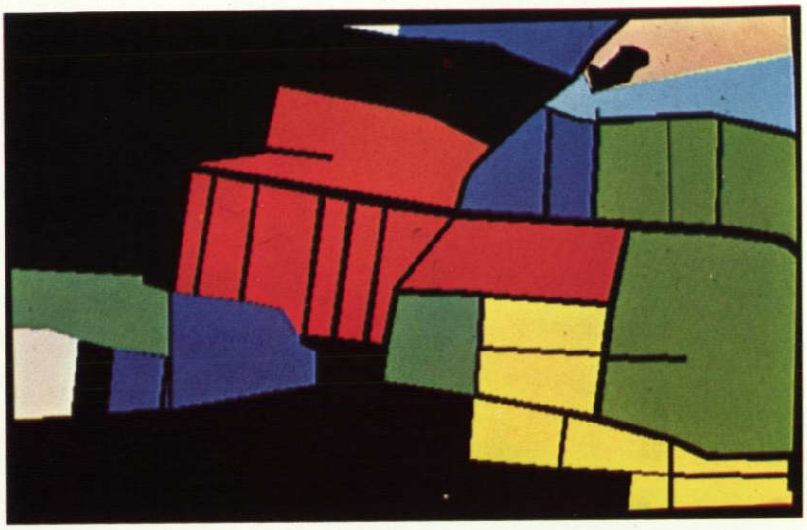

Fig. 23 - Ground truth document for rice varieties (discrete version). White = wet meadows; yellow = corn; the six other colours correspond to six rice varieties (see text). Black areas are uncharacterized rice fields, roads and inhabited zones.

Fig. 24 - Classification results of rice varieties with ML method after data compression from 8 to 5 dimensions, by principal components analysis.

- LE TOAN, T., "Etude spécifique d'une culture (riz) par télédétection: cartographie et évaluation de production", Quatrième Symp. Canadien sur la Télédétection, Québec, Canada, May, 1977

- DEJACE, J., GALLI DE PARATESI, S., MEGIER, J., MEHL, W., "Contribution of the AGRESTE Investigation to the Identification and Inventory of Agricultural Resources in Europe", COSPAR/IAMAP (IUGG) Symp. on the Contribution of Space Observations to Global Food Estimation System, Tel Aviv, June 1977

- LE TOAN, T., CASSIRAME, P., "Utilisation des données LANDSAT-2 pour l'étude d'une culture spécifique", Journées de Télédétection GDTA, Paris, Septembre 1977

- QUACH, J., LE TOAN, T., "An Attempt of Image Objects Discrimination by Spectral and Textural Parameters", International Symp. on Image Processing-Interactions with Photogrammetry and Remote Sensing, Graz, Austria, October 1977

- CASSIRAME, P., "Méthodes de classification des données multi-dimensionnelles en Télédétection", Application à la cartographie d'une région agricole (Camargue), Thèse du 3e cycle, Université Paul Sabatier, Toulouse (1977).

CHAPTER 2 - SPECTRAL FEATURES OF RICE CULTURES AT THE VARIOUS PHENOLOGICAL STAGES AND THE ESTABLISHMENT OF RELATIONSHIPS FOR YIELD PREDICTION PURPOSES

Contributor to the text:

BERG, A. (JRC-Ispra Establishment)

Scientific Collaborators:

AGAZZI, A. (JRC-Ispra Establishment)
BALDI, G. (ENR, Mortara)
CAVELIER, M. (BGI, Ispra, Post-graduate student)
MALAGONI, R. (ENR, Mortara)
MALET, Ph. (INRA, Avignon)
MARACCI, G-C. (JRC-Ispra Establishment)
RUSSO, S. (ISC, Vercelli)

Investigations aimed at establishing the spectral signature of rice in relation to the phenological stages of the plant have been performed over a wide spectrum of culture conditions (greenhouses, lysimeters, open fields) in order to point out the most significant conclusions. At the same time special attention has been devoted to establishing valid relationships between spectral features of rice and final grain production with a view to the possible use of reflectance data for yield prediction purposes.

All the experimental work reported in this section was performed on the Italian test sites, both at the JRC (lysimeters of the Biology Group, Ispra) and in the institutes involved in this project (ISC, Vercelli; ENR, Mortara). The Bioclimatological Station of Avignon, France (INRA-A) did contribute to the theoretical aspects involved in section 5 of this chapter. These investigations have already been the object of various earlier reports or scientific publications (see bibliography). Their integrated results are presented here in a more concise form and with an attempt to draw some general conclusions.

Radiometric measurements were made from a short distance above the plants in the four LANDSAT channels using an EXOTECH model 100 radiometer or over the 300-1050 nm wavelength region with a bandwidth of 5 nm using the OPTRONICS model 740 spectroradiometer. The reflec-

tance of rice was calculated from radiance measurements in reference to a grey panel of known reflectance (according to the formula of equality of radiance and reflectance ratios).

1. PRELIMINARY RESULTS UNDER GREENHOUSE CONDITIONS

1.1 General

Measurements were made via OPTRONICS automatic wavelength scanning at Vercelli, during the whole vegetation cycle of rice. Integration of the measured radiances over the four MSS LANDSAT channels was performed and the corresponding reflectance values were calculated.

The ten pots concerned two rice varieties (Arborio - Roma) and two N-fertilization levels (40-140 kg N/ha). Production of caryopsis (grain), leaf and stem biomass and total biomass were measured.

1.2 Results

In spite of the variability introduced purposely by rice variety and fertilization, two different sun irradiation levels in the greenhouse exerted a first order effect on rice development and on final production.

The grain productivity data can actually be regrouped in two different classes, with mean values around 150 and 100 g rice/pot at harvest, respectively for pots no. 1 to 5 and no. 6 to 10. From a radiometric point of view, this two-class regroupment is shown up by extracting reflectance for the LANDSAT bands 4 and 6. The evolution in time of the mean values of these parameters, starting from germination time, is shown in Figs. 25 and 26. It can be seen that the curves diverge significantly for the two production classes from day 76 (ρ_6 and ρ_4 on Fig. 25) and from day 96 (ρ_6/ρ_4 on Fig. 26) after germination. This latter date corresponds to the time of earing/flowering and is characterized for the higher productive rice class (pots 1-5) by a maximum value of the ratio ρ_6/ρ_4 which subsequently decreases during the maturation phase. This maximum is significantly postponed for the lower productive rice class (pots 6-10), thus indicating a delay in the plant growing cycle related to the lower amount of incoming solar energy.

1.3 Conclusion

This experiment seems to indicate that radiometric features of rice might become useful indicators of anomalies in the growing cycle of the plant and thus may be indirectly related to the final yield.

2. SPECTRAL FEATURES OF RICE CULTURES AT VARIOUS NITROGEN FERTILIZATION LEVELS

2.1 Introduction

In order to follow, throughout the development cycle, the reflectance of a rice culture as a parameter to be correlated to the final yield, two experiments have been set up, under controlled conditions (lysimeters) and under field conditions respectively. For these experiments, nitrogen was chosen as the experimental variable, since it is known to be strongly correlated to the yield and to be able to create morphological and physiological differences between treatments, which can be correlated to the canopy reflectance.

2.2 Experiment under controlled conditions (Lysimeters, Biology Group, Ispra)

2.2.1 Methods

Two varieties of rice (Arborio - Roma) were studied from planting (beginning of June) to harvesting (end of September) in 20 lysimeters 2.5 x 2.5 m (2 varieties; 5 N-levels at 0, 60, 120, 180 and 240 kg N/ha; 2 repetitions). The mode of plantation was by groups of 4 plants, at 25 cm intervals.

Eight series of measurements along the growing season; reflectance was measured as vertically as possible in the 4 LANDSAT channels with an EXOTECH mod 100 radiometer.

The following agronomical data were collected on small samples: dry (green) biomass, leaf area index (leaf surface per unit of culture surface), chlorophyll content.

2.2.2 Results (concerning mostly the Arborio variety)

2.2.2.1 Agronomical data

- Phenological stages

These are presented in Table 19, in correspondence with the measurement series, relative to an arbitrary day 0, taken early in July at a mid-tillering stage.

- Chlorophyll index (in mg/m^2 culture; see Fig. 27)

This parameter is characterized by a maximum reached around day 48 (earing). On the other hand, a strong increase of the parameter with the increase of N-level is observed.

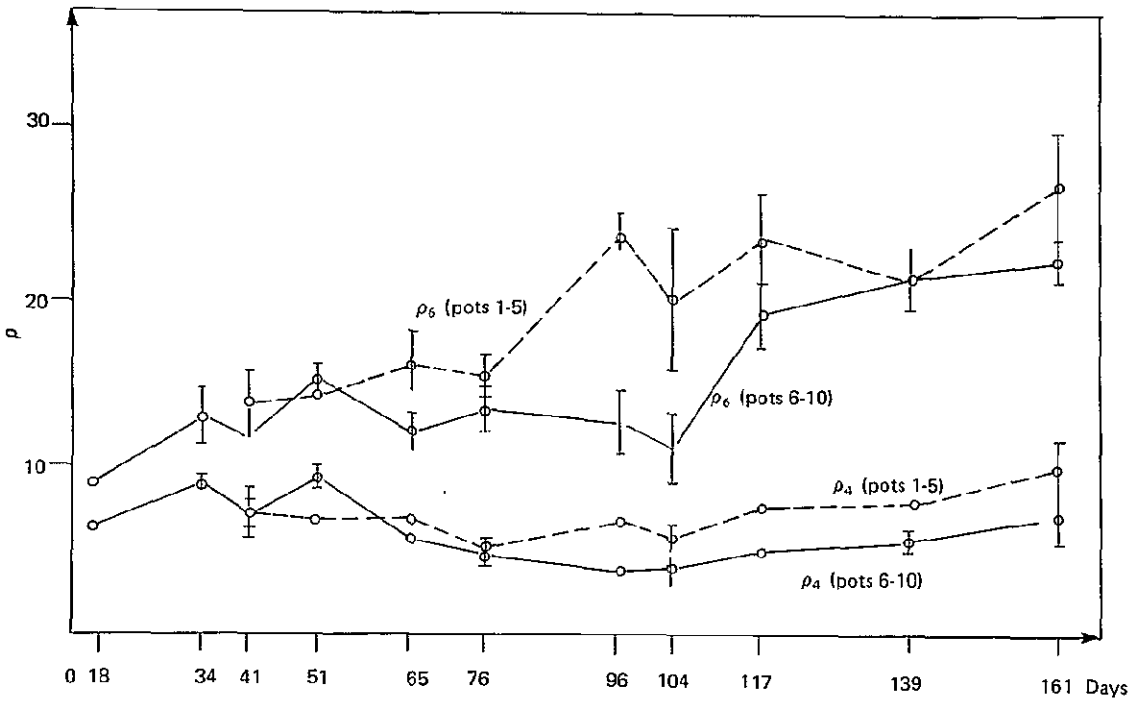

Fig. 25 - Evolution of reflectance ρ_4 and ρ_6 with time

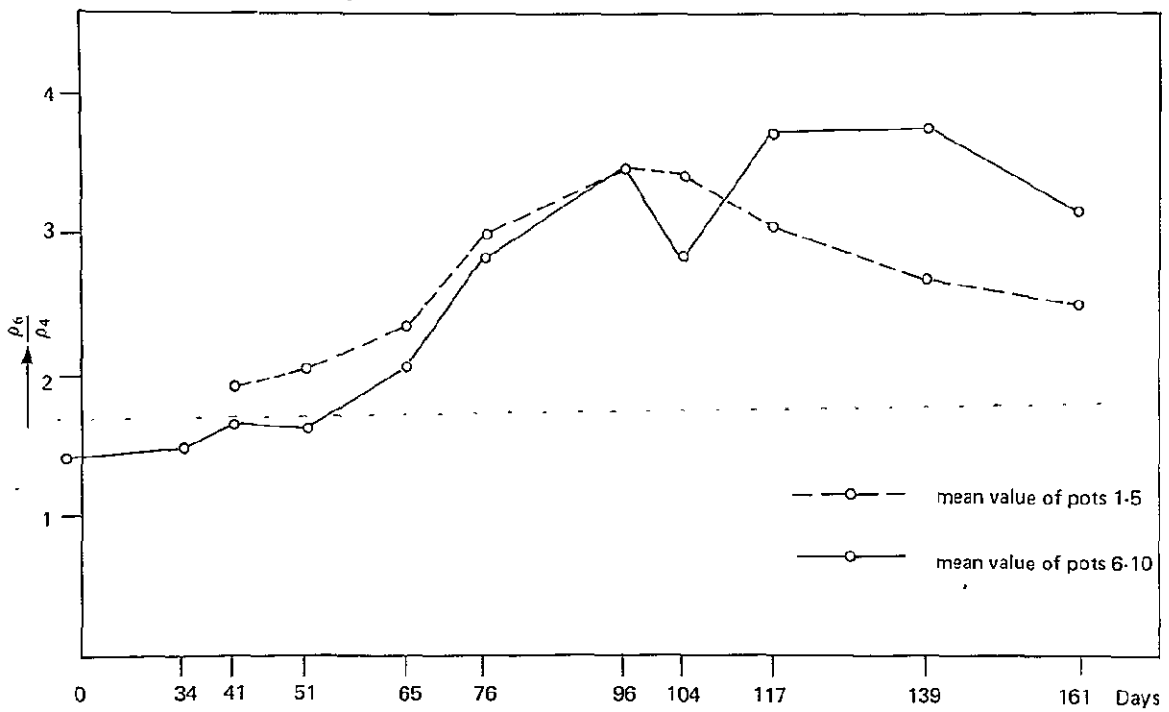

Fig. 26 - Evolution of ratio ρ_6/ρ_4 with time

Table 19 - Rice Phenology

Phase	Day	Date	Stage
	0	7/ 2	mid-tillering
Vegetative			end-tillering
	23	7/25	appearance of flower primordia
			expansion
Generative	38	8/ 9	booting
	48	8/19	earing
	55	8/26	flowering
	64	9/ 4	milk ripening
Maturation	72	9/12	wax ripening
	83	9/23	full ripening

- (Green) leaf and stem biomass (in g/m^2 culture; see Fig. 28)

  This parameter reaches a maximum value at the beginning of the maturation phase (day 55-72 between flowering and wax ripening). On the other hand, a general increase of the biomass with the increase of N-level is observed, until a saturation is reached at high levels (180 and 240 kg N/ha) at least before flowering.

- Leaf area index (see Fig. 29)

  This parameter already exhibits an early maximum at the beginning of the generative phase (day 38 at booting). The subsequent decrease is due to the senescence of the leaves. On the other hand, positive correlation with N-level is evident.

  The general increase with N-level of the three foregoing parameters must be attributed to an increased number of tillers (Fig. 30) and not to an increased dry weight of a single tiller (which seems to be independent of the N-level). At low N-levels, rice seems to regulate the number of halms according to nutrient availability.

  At the planting density used (64 plants/m^2), the density at the end of the season remains limited (130-300 halms/m^2), even at high N-levels (max. 308 halms/m^2), whereas the normal field density might be higher (300-400 halms/m^2).

- Biomass

  Fig. 31 illustrates the typical evolution in time of the biomass (leaf and stem, panicle, total biomass). It is evident that after flowering, growth of the panicle biomass substitutes the growth of the leaf and stem biomass. The relationships of dry weights at harvest to N-levels

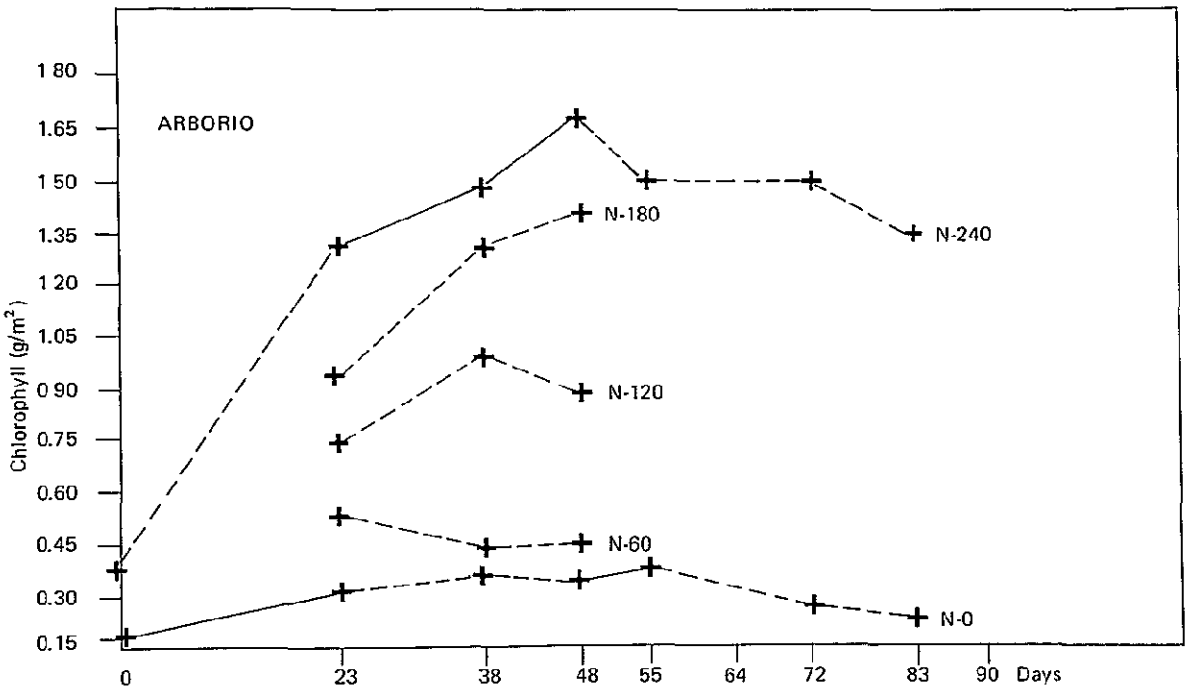

Fig. 27 - Evolution of chlorophyll index with time

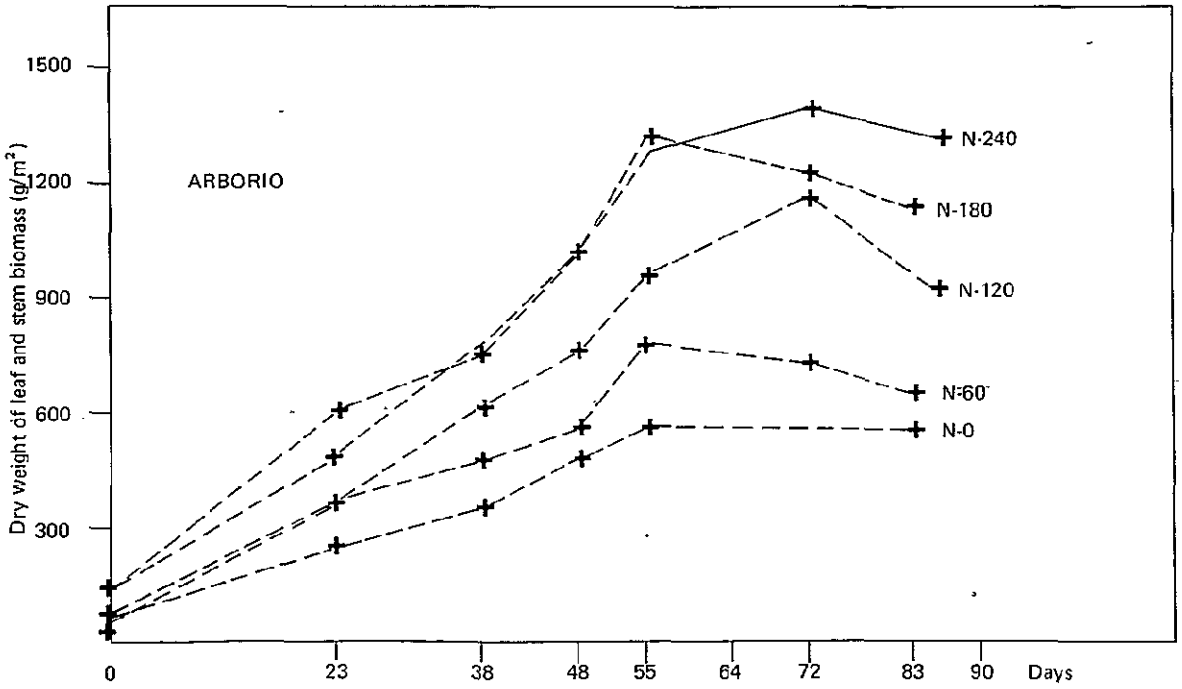

Fig. 28 - Evolution of leaf and stem biomass with time

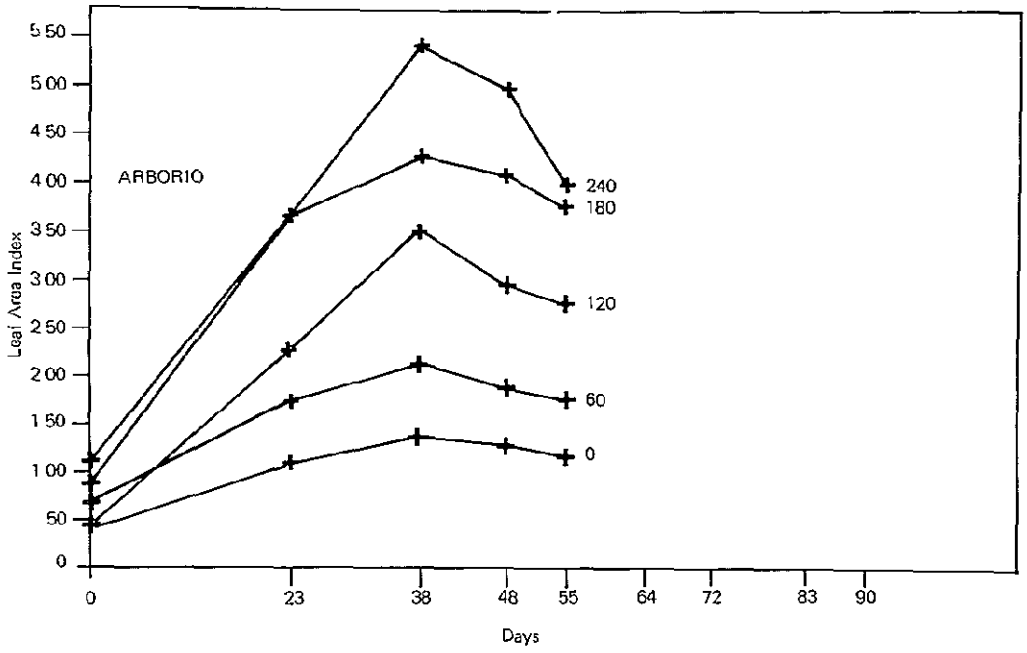

Fig. 29 - Evolution of leaf area index with time

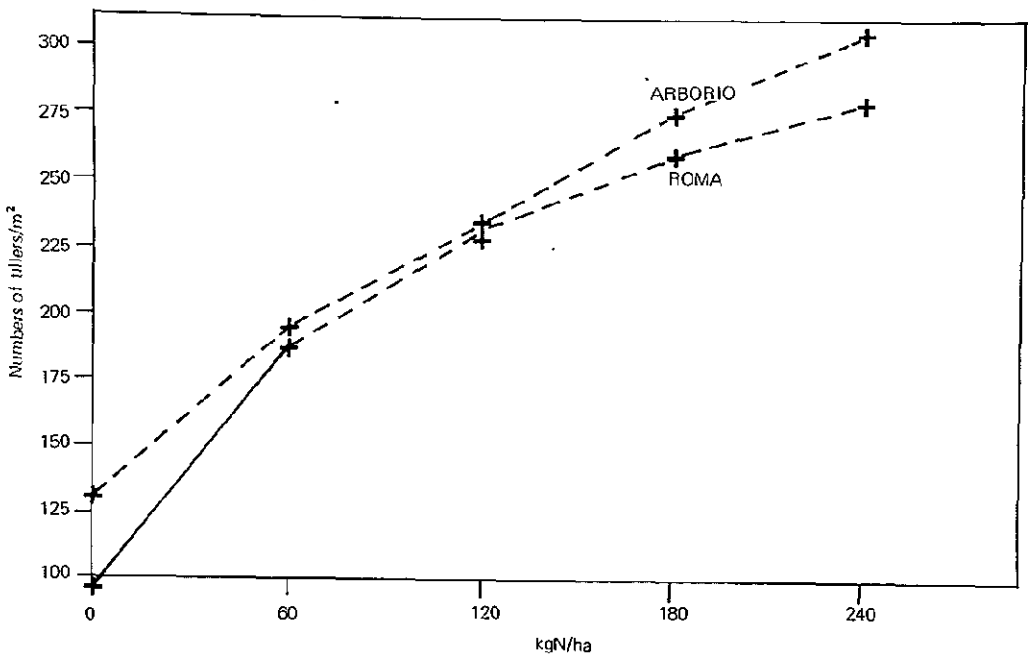

Fig. 30 - Number of tillers in relation to N-fertilization level

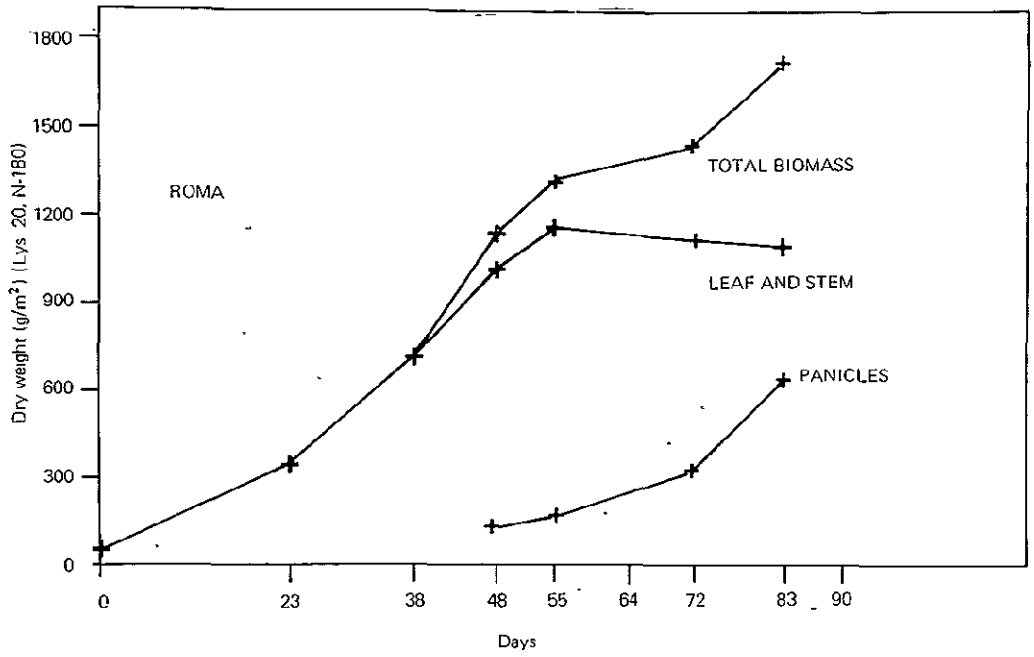

Fig. 31 - Evolution of biomass with time

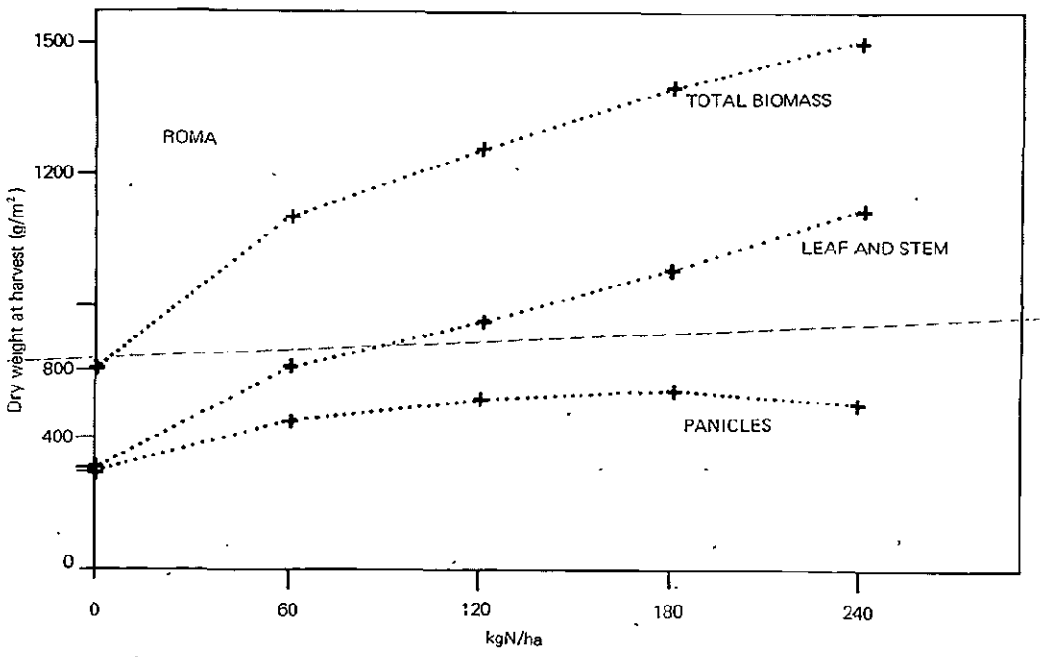

Fig. 32 - Biomass in relation to N-fertilization level

are presented in Fig. 32. A clear plateau is reached for panicle production at the highest N-levels whereas the other biomasses increase continuously with N. For this reason, the "yield coefficient" (panicle dry weight/total dry weight) shows a negative correlation with N (Fig. 33, Table 20).

2.2.2.2 Spectral data

Figs. 34 and 35 show the reflectance data in channels 5 and 7 respectively (ρ_5 - ρ_7, which are similar to data in channels 4 and 6 respectively).

It is evident that reflectance in visible red shows a typical tendency to decrease when N increases, whereas the opposite is true in close infrared. The strong correlation between the chlorophyll index and N-level, as described above, is responsible for this behaviour of reflected red by the vegetation canopy. The near infrared is only slightly absorbed by the leaves and highly reflected at the various leaf layers after transmission through the canopy. The near infrared reflectance is thus sensitive to variations of the leaf area index, at least up to complete covering of soil, and is a very good indicator of total biomass.

Table 20 - Yield coefficient at various N-levels

Lys. No.	N-level (kg N/ha)	Yield coefficient
11	0	0.489
19	0	0.491
14	60	0.447
17	60	0.405
12	120	0.412
16	120	0.402
13	180	0.369
20	180	0.382
15	240	0.338
18	240	0.300

The divergence of the behaviour of ρ_5 and ρ_7 is also evident as far as evolution in time is concerned. Therefore the ratio ρ_7/ρ_5 is a useful indicator of the reflectance behaviour both in time and in relation to the N-level (Fig. 36). Since this ratio is very sensitive to foliage senescence[1], it should be a very good indicator of the proportion of green biomass in total biomass, as evident also from the correlation with the

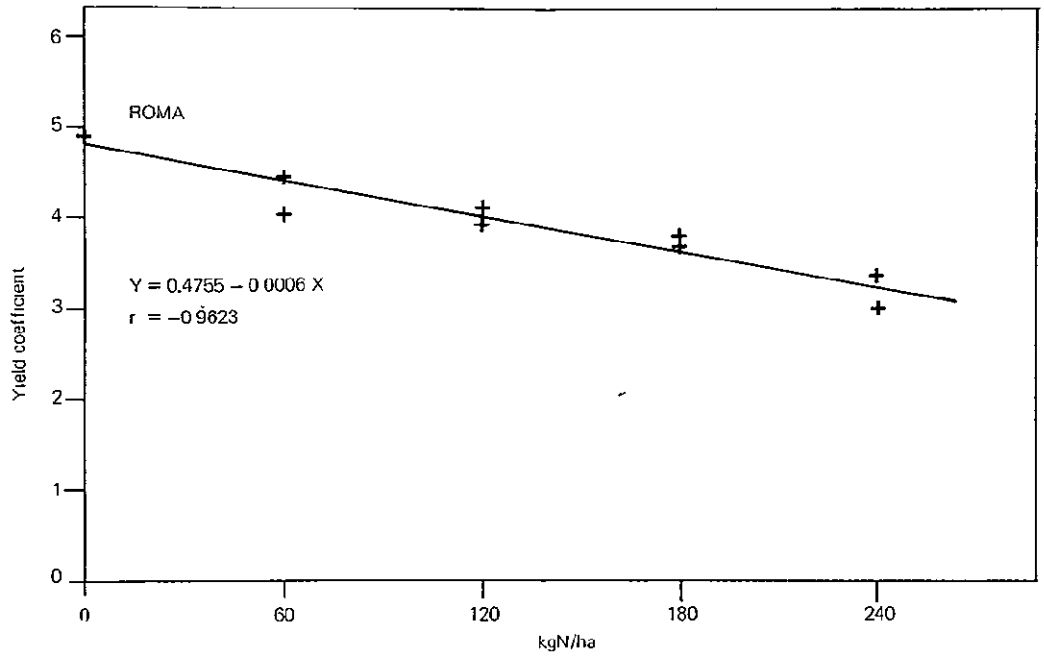

Fig. 33 - Correlation between yield coefficient and N-level

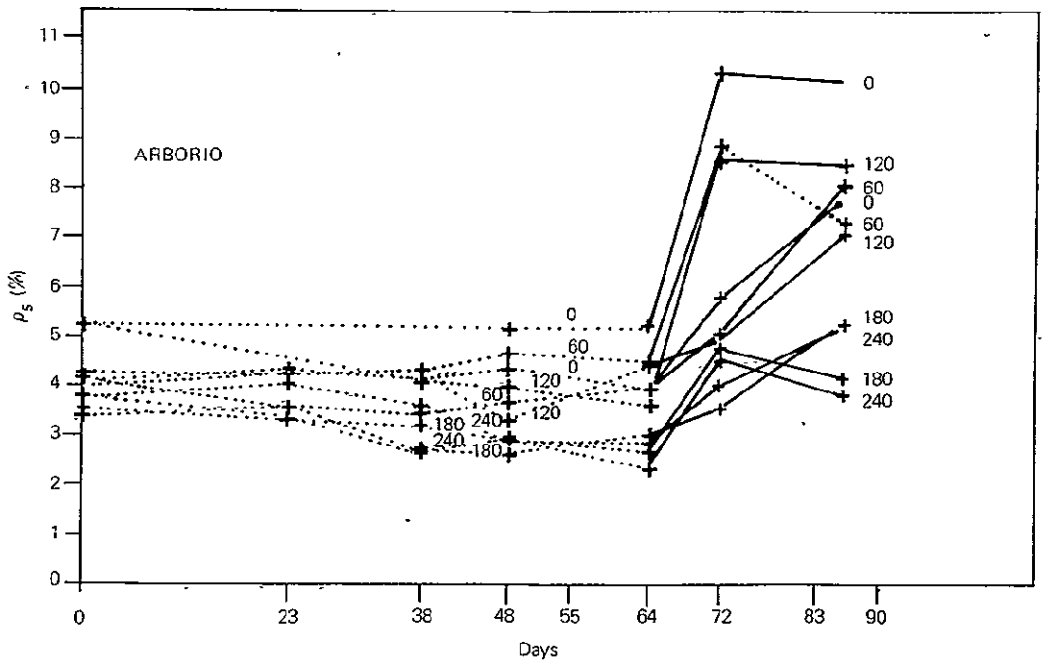

Fig. 34 - Evolution in time of the reflectance data in channel 5

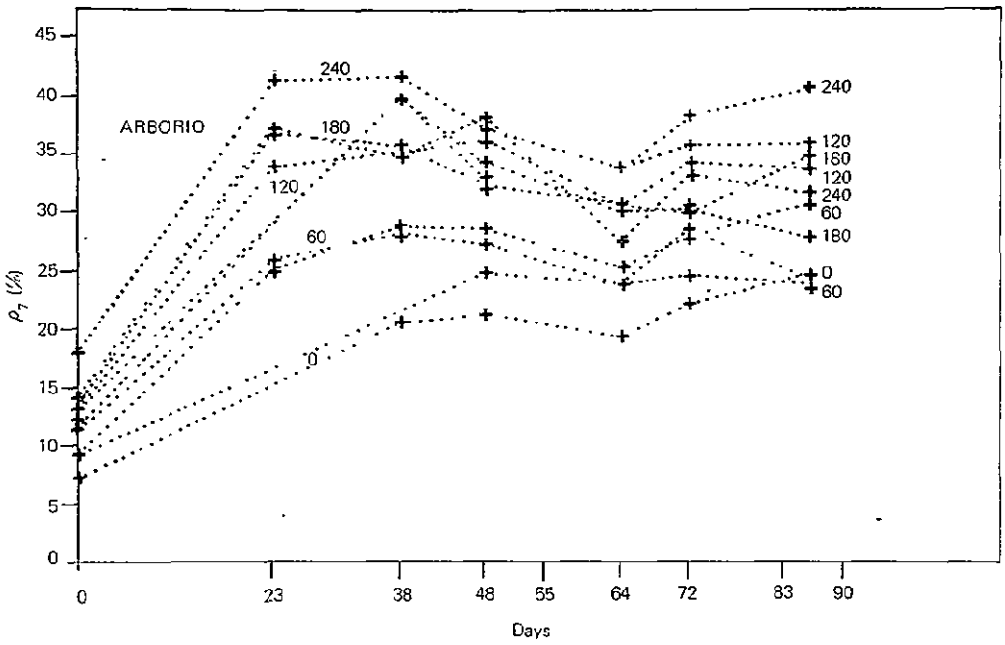

Fig. 35 - Evolution in time of the reflectance data in channel 7

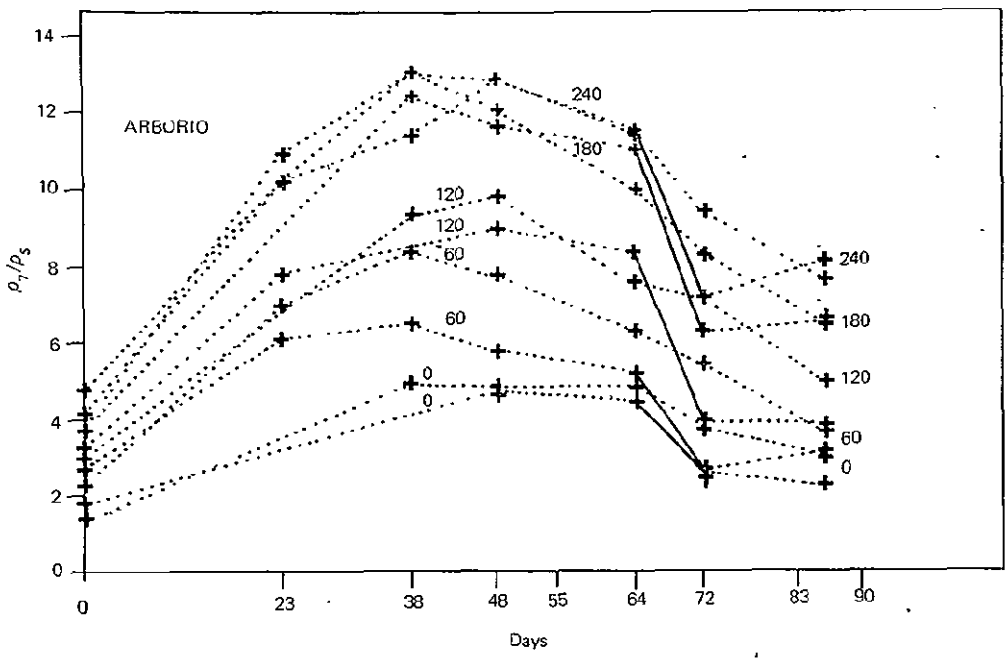

Fig. 36 - Evolution of reflectance ratio ρ_7/ρ_5 with time

leaf area index (Fig. 37). Another advantage of this ratio lies in the fact that it is insensitive to solar height and might therefore be used over a long period of the growing season[2]. The coefficient of variability of the ratio ρ_7/ρ_5 in this experiment is in fact much lower (2.37%) than that of the single reflectances (around 7-8%).

One can see from Fig. 36 that the reflectance ratio ρ_7/ρ_5 exhibits a characteristic evolution in time with a maximum value around earing (day 48). On the other hand, there is an obvious tendency for the reflectance ratio to reach a plateau at very high N-levels (above 180 kg N/ha), at the end of tillering (day 23, 7/25) and at booting (day 38, 8/9). This trend indicates a temporary saturation of reflectance which disappears with the subsequent development of the vegetation structure.

2.2.2.3 Yield prediction

The correlation parameters have been calculated between reflectance ratios measured in 10 lysimeters during the development cycle and total biomass at harvesting. All of them appear highly significant, especially for reflectances measured at earing (Fig. 38; r = 0.964). The same is true for the negative correlation between reflectance ratios and yield coefficient (Fig. 39; r = -0.955). Through the regression coefficients of these correlations, it is possible to calculate grain yield from reflectance ratio values. These calculated values of grain yield compare well with the actual values (Fig. 40). Under the conditions of the experiment, where nitrogen is the only source of systematic variability, it may thus be inferred that yield prediction might be achieved with satisfactory precision on the basis of reflectance data (or of total biomass data) collected at the stages of earing-flowering (mid-August).

However, the preceding discussion has shown that any parameter like the reflectance ratio, which would be a good indicator of total biomass and could be correlated to the same biomass at harvesting, could be used for the prediction of grain yield only on the basis of the yield coefficient. In the experiment described here, a correlation could be found between nitrogen level and yield coefficient. But under normal field conditions, this last parameter may vary considerably in relation to various factors. This would make the achievement of yield prediction much more difficult.

2.3 Experiment under field conditions (Experimental fields ISC, Vercelli)

2.3.1 Methods

One rice variety (Roma) was investigated from the end of July (end of booting) to the end of September (harvesting), in seven cells of about 80 m^2 each, corresponding to seven N-fertilization levels (0, 50, 75, 100, 125, 150, 200 kg N/ha).

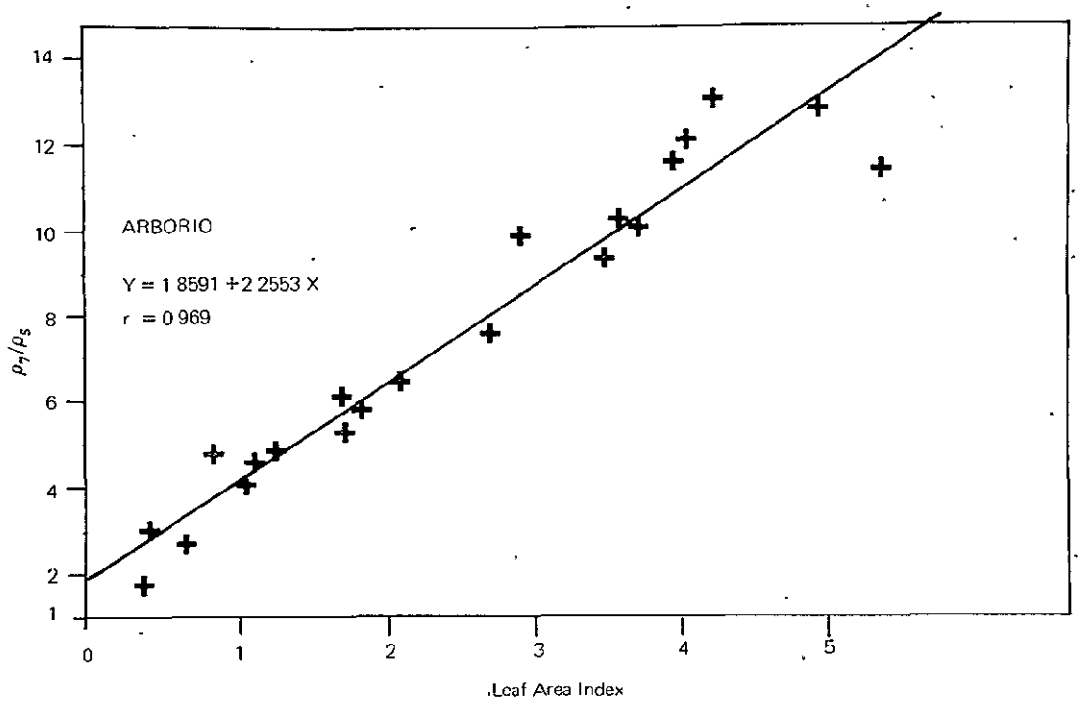

Fig. 37 - Correlation between reflectance ratio ρ_7/ρ_5 and leaf area index

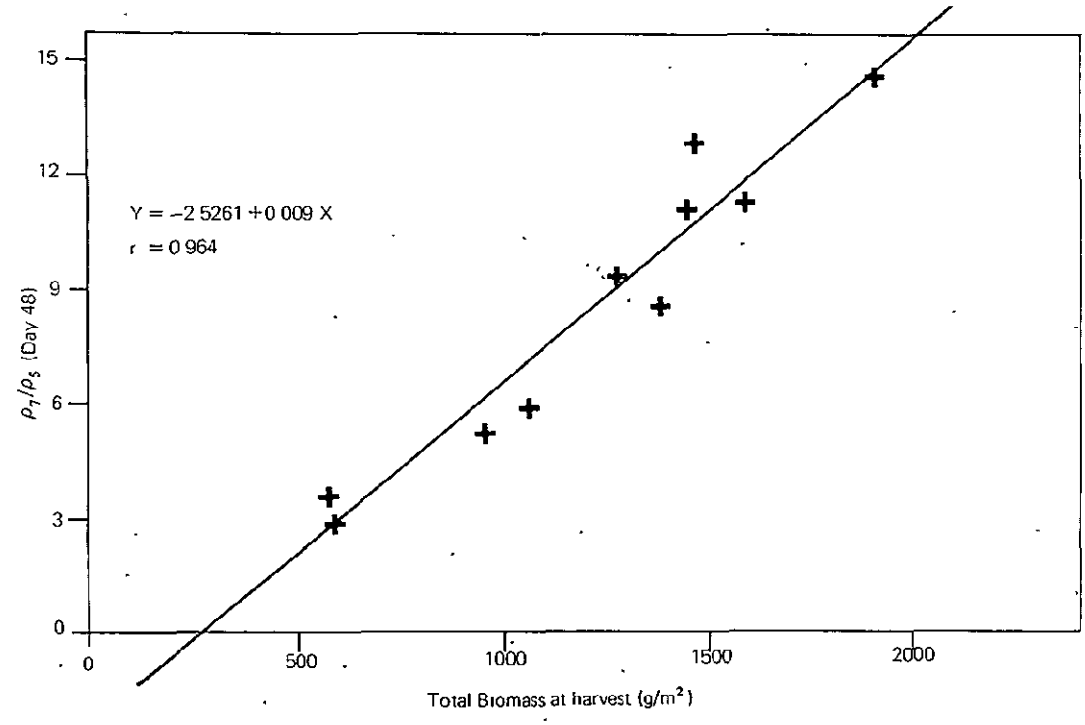

Fig. 38 - Correlation between reflectance ratio ρ_7/ρ_5 and total biomass at harvesting

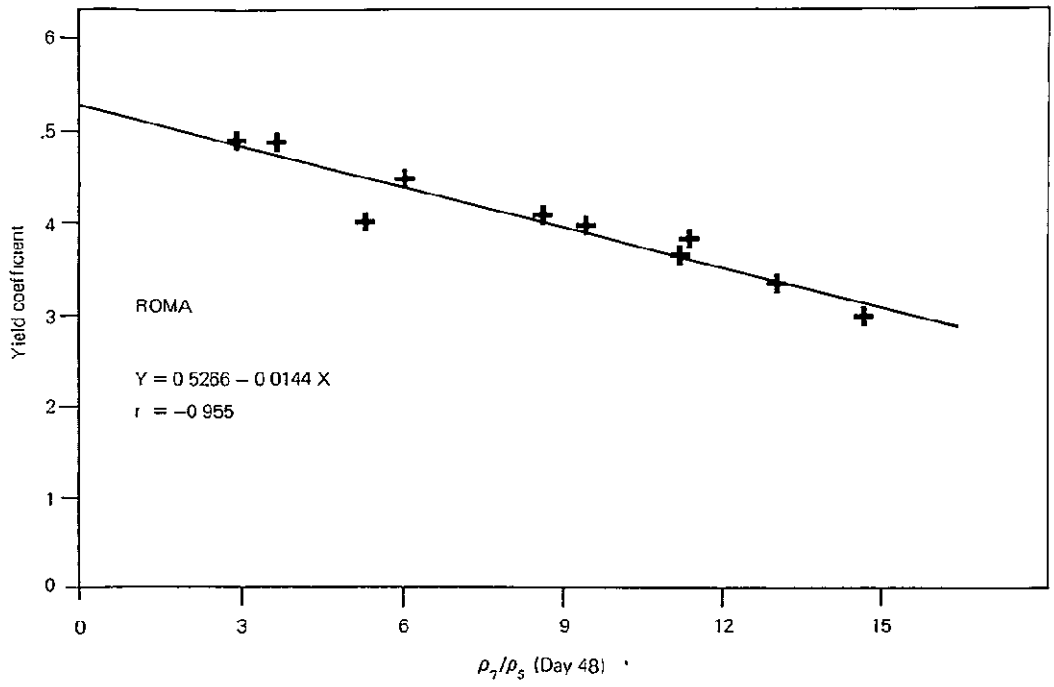

Fig. 39 - Correlation between yield coefficient and reflectance ratio ρ_7/ρ_5

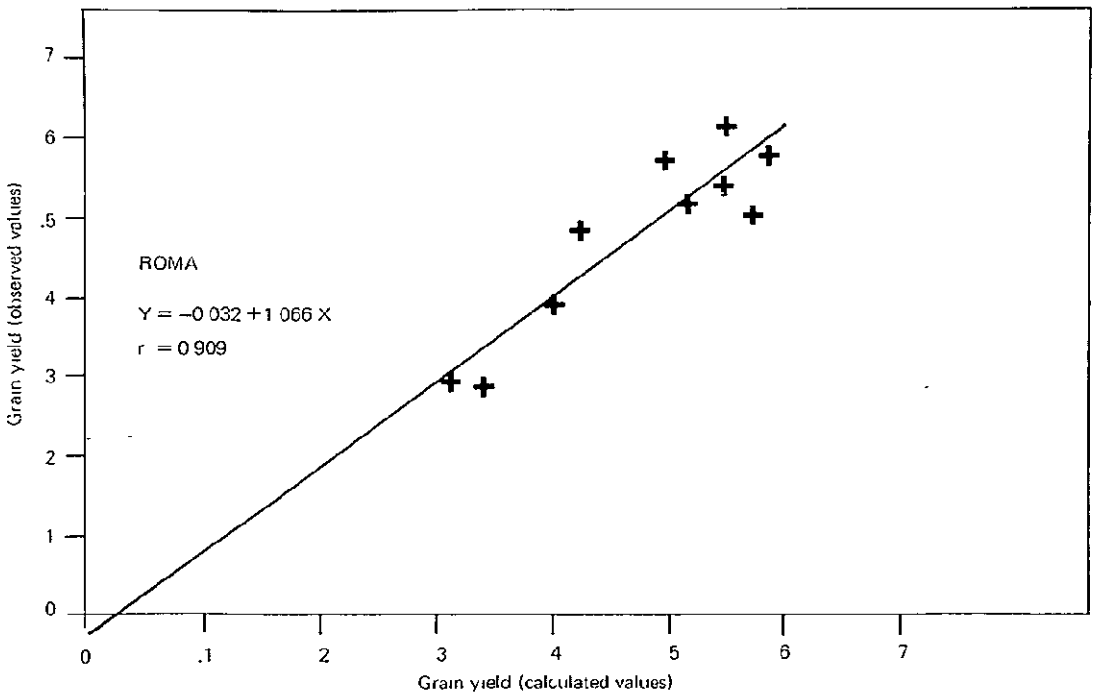

Fig. 40 - Comparison between effective and calculated grain yields

Six series of measurements were performed during the growing season; reflectance was measured by means of an EXOTECH model 100 radiometer placed about 5 m above the vegetation, with a field of view of 15 degrees.

At harvest the dried overground biomass and the weight of rice grain were measured.

2.3.2 Results

2.3.2.1 Agronomical data

- Phenological stages

  These are presented in Table 21 (for the cell at 125 kg N/ha) in correspondence with the measurement series, relative to an arbitrary day 0, taken at the end of July (end of booting).

- Harvest data

  These are presented in Table 22 and in Fig. 41. There is a fairly linear correlation between total biomass and N-level. In spite of an anomaly in the curves a and b, the trend of the continuous increase of the dried biomass with N-fertilization level is evident, whilst a characteristic plateau is reached for grain production over 125 kg N/ha.

Table 21 - Rice phenology (at 125 kg N/ha)

Day	Phenological Stage
0	end of booting
7	earing
29	wax ripening
37	full ripening
49	" "
59	harvesting

Table 22 - Harvest data

N-level (kg N/ha)	Dried Biomass (qntls./ha)	Rice Production (qntls./ha)	Total Biomass (qntls./ha)	Yield Coefficient
0	45.50	38.04	83.54	0.455
50	55.18	59.17	114.35	0.517
75	55.61	67.33	122.94	0.548
100	69.90	55.68	125.58	0.442
125	62.97	74.43	137.40	0.542
150	70.57	73.42	143.99	0.510
200	99.66	68.47	168.13	0.407

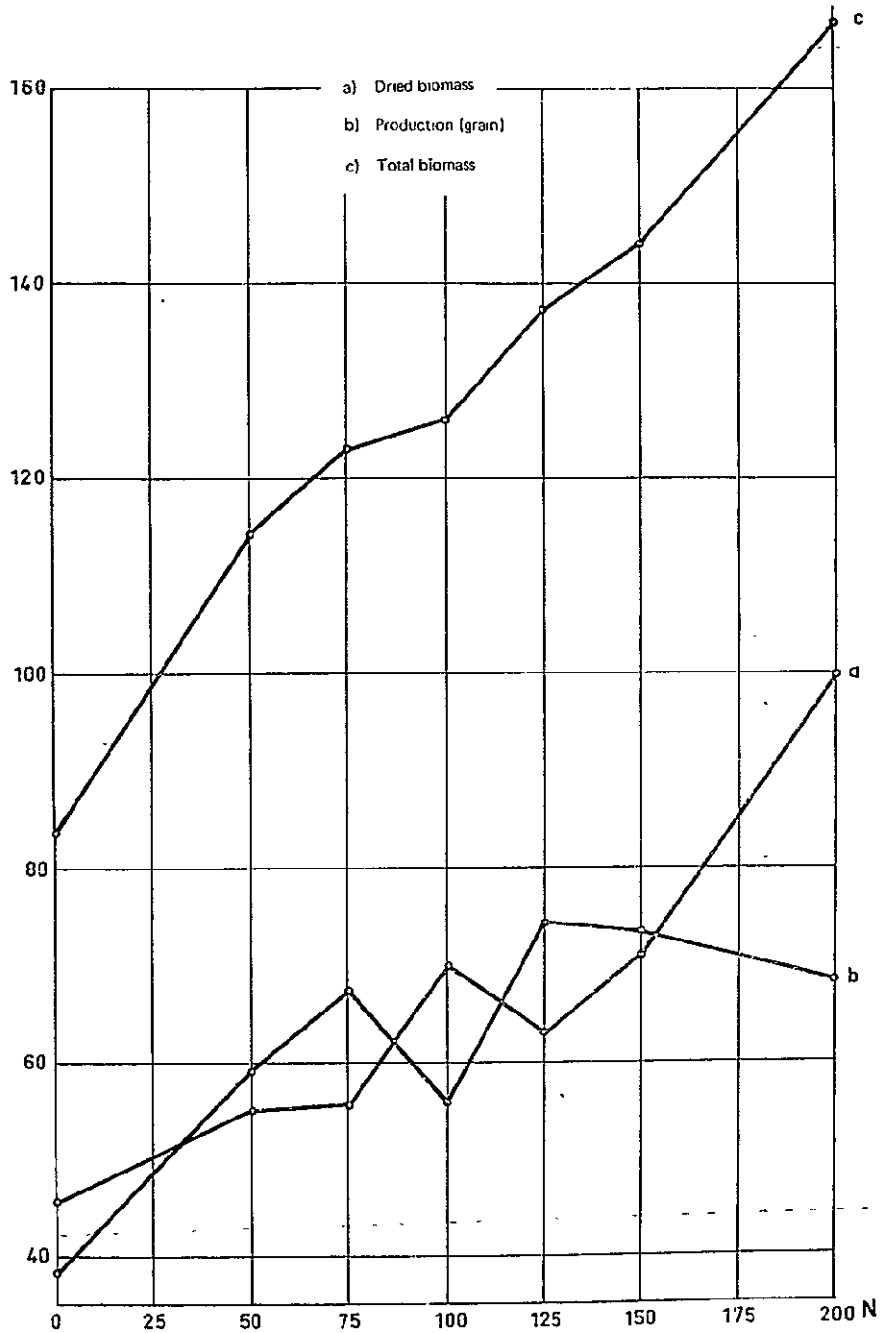

Fig. 41 - Biomass in relation to N-fertilization level

2.3.2.2 Spectral data

- Relation of reflectance data to N-level

Fig. 42 presents the reflectance in the four channels versus N-level

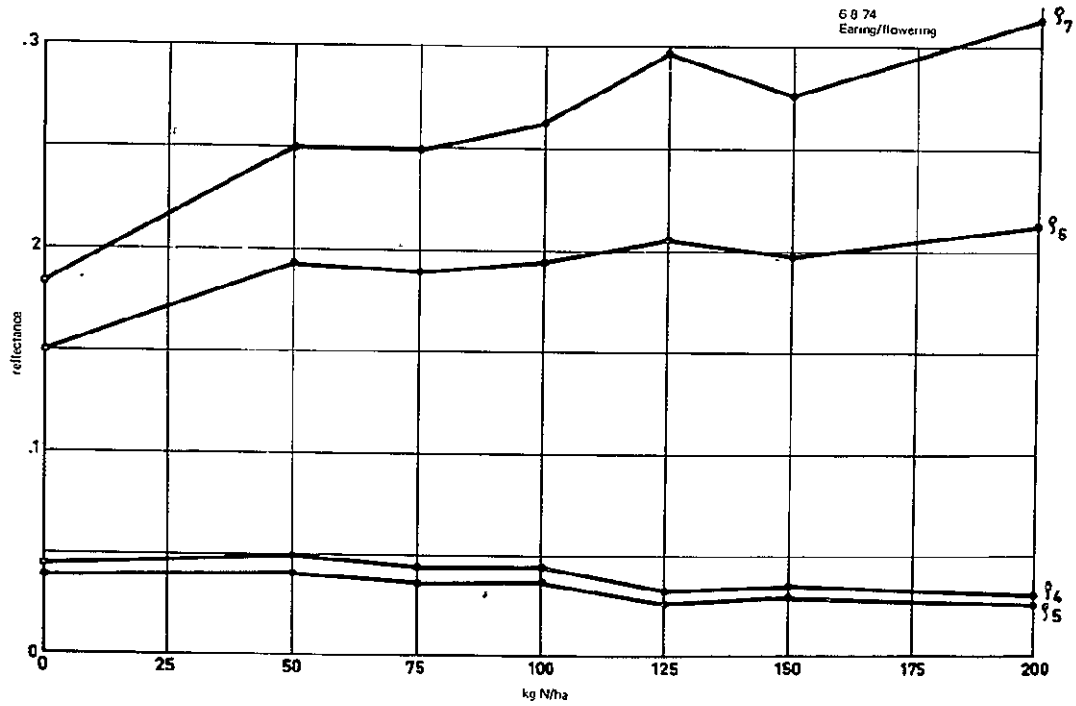

Fig. 42 - Reflectances in relation to N-fertilization level

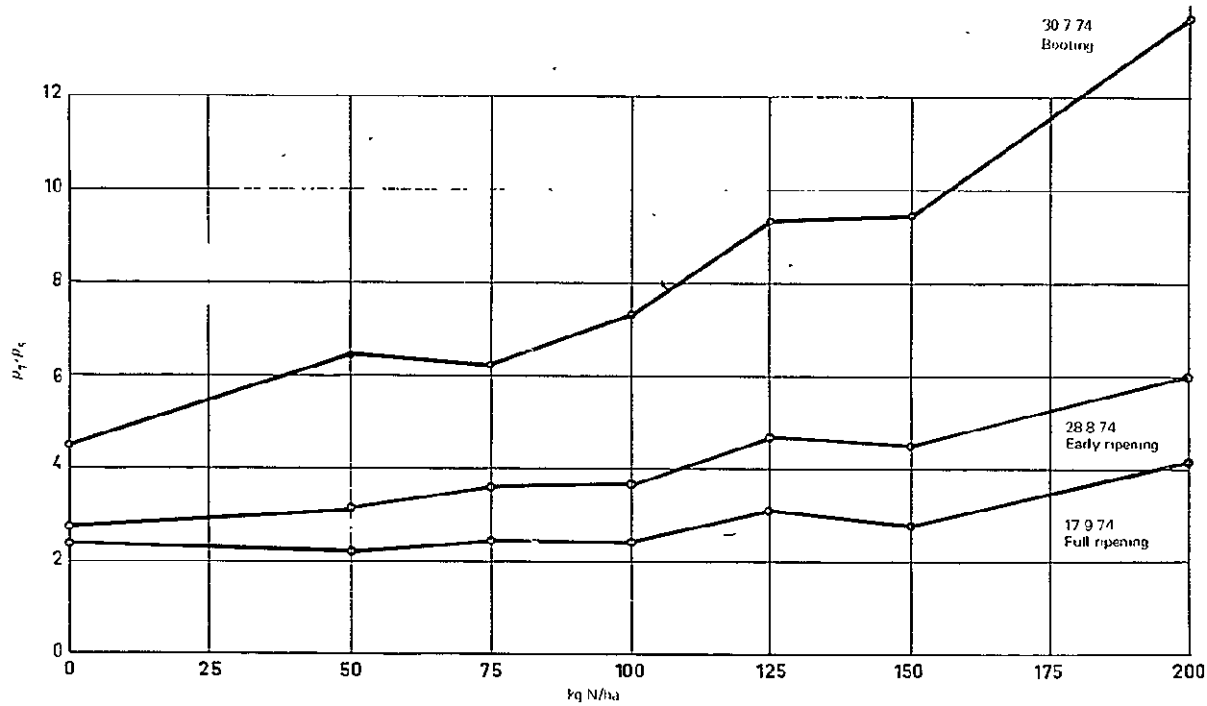

Fig. 43 - Reflectance ratio in relation to N-fertilization level

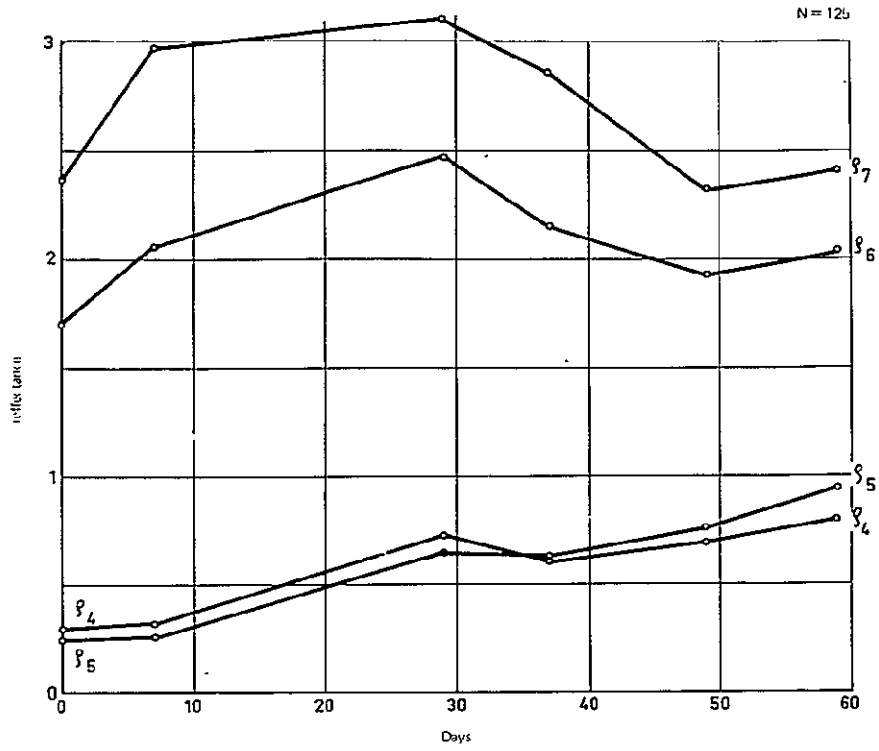

Fig. 44 - Evolution of reflectance with time, at 125 kg N/ha

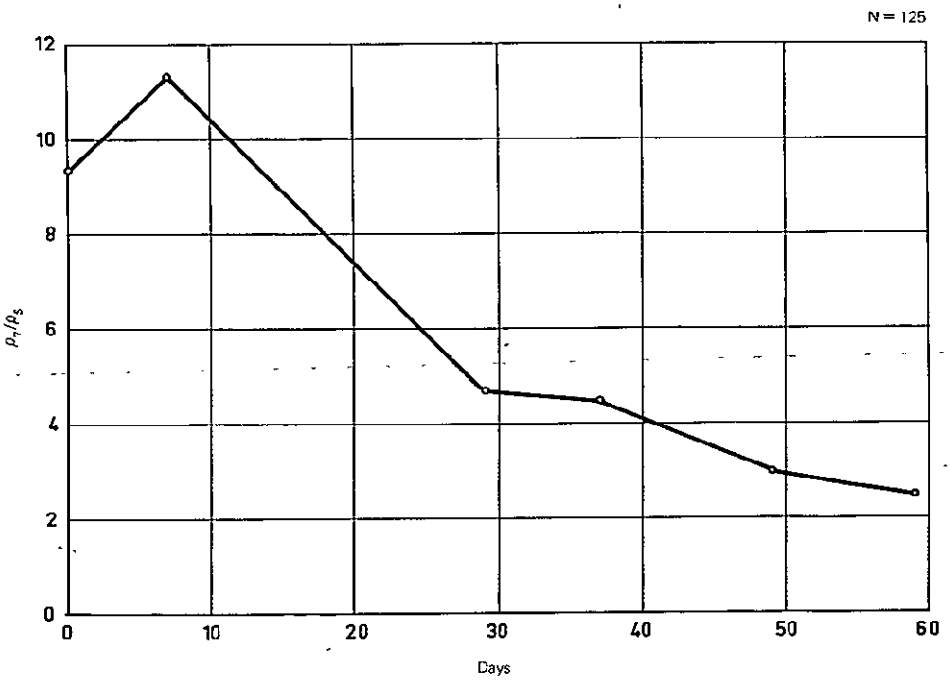

Fig. 45 - Evolution of reflectance ratio ρ_7/ρ_5, at 125 kg N/ha

at the second measurement (early August at earing/flowering). As already noted in the lysimeter experiment, there is a generally positive correlation between the reflectance in the near infrared channels and N-level (more accentuated for channel 7) and a generally negative correlation between the reflectance in the visible channels and N-level. The reflectance measurements taken during the whole growing season indicate the same characteristic trends, from booting to harvesting.

Because of the divergent behaviour of reflectance in visible and infrared regions, the ratio ρ_7/ρ_5 appears to be an adequate parameter to enhance the radiometric response to the biomass variations. Fig. 43 illustrates the behaviour of ρ_7/ρ_5 in relation to N-level at three successive development stages. One notes beside the clear positive correlation the decrease of the regression slope during the course of the development. By comparing the 6 sets of reflectance measurements, it appears that the decrease in regression slope is not progressive but discontinuous in time.

- Evolution in time of reflectance data

Fig. 44 illustrates this relation for the single reflectances at 125 kg N/ha. The diagrams drawn at the other N-levels are fundamentally similar. The reflectances ρ_7 and ρ_6 are characterized by a maximum value which appears on the diagram at the first stage of ripening, whilst the reflectances ρ_5 and ρ_4 present a gradual increase during the period of observation. It should be emphasized that an observation gap between days 7 and 29 (from earing to ripening) unfortunately prevents any definite conclusion about the exact location, during this period, of the maximum infrared reflectance.

As a direct consequence of the evolution in time of the single reflectances, the ratio ρ_7/ρ_5 exhibits in time a typical behaviour which is illustrated in Fig. 45 at 125 kg N/ha. A maximum of the reflectance ratio is observed at the beginning of the observation period, around earing, but the uncertainty about the time of maximum infrared reflectance also makes any definite conclusion impossible in this case.

2.3.2.3 Yield prediction

It was of the utmost importance to check whether the correlation described in the lysimeter experiment between reflectance ratios and total biomass at harvesting would also be found under field conditions. Using the values of reflectance ratio measured during the whole observation period, the regression formulae presented in Table 23 were found ($y = \rho_7/\rho_5$; x = total biomass in quintals/ha).

The functions of reflectance ratios at various phenological stages versus total final biomass can thus all be assumed to be linear, with the best

Table 23 - Regressions of reflectance ratio versus total biomass at harvesting

Development Stage	Date	y = a + bx	r
End of booting	7 - 30	y = -10.83 + 0.14 x	0.983
Earing	8 - 6	y = - 6.96 + 0.11 x	0.997
Ripening	8 - 28	y = - 2.8 + 0.052x	0.992
Full ripening	9 - 5	y = - 3.57 + 0.055x	0.981
Full ripening	9 - 17	y = - 2.06 + 0.035x	0.944
Harvesting	9 - 27	y = - 1.04 + 0.026x	0.933

correlation occurring in a period around earing-flowering. The significance of these stages for the investigation on rice growth by means of radiometric techniques is thus fully confirmed. On the basis of such correlations, the prediction of final biomass can be achieved with a satisfactory precision about 2 months before harvesting.

On the other hand, prediction of grain production from final biomass data requires the estimation of the yield coefficient. From the last column of Table 22, one notes that it is impossible to indicate a relationship between the values of the yield coefficient and the reflectance ratio ρ_7/ρ_5, probably because of the great variability in production which should be tested at several points in a large open field.

The conclusions of this experiment are thus in accordance with expectations based on the lysimeter experiment. If the reflectance ratio ρ_7/ρ_5 can be used also in the field as an indicator of the rice development for prediction of the total biomass at harvesting, variations of the yield coefficient prevent an extension of this prediction to the grain production, even in the present simplified situation where nitrogen constitutes the only factor of experimental variability.

3. SPECTRAL FEATURES OF A RICE CULTURE AT VARIOUS DENSITIES (Experimental fields, Ente Nazionale Risi, Mortara)

3.1 Methods

The purpose of this experiment was to ascertain whether differences in total biomass induced by differences of plant densities (and no longer by different N-fertilization levels) could be sensed by reflectance measurements.

A strip of normal rice field was subdivided into 10 cells of about 80 m^2 each. The same variety (Padano) was seeded at different densities in

order to obtain a theoretical halms density of 150 to 600, with an increment of 50. Twelve measurement series were performed from beginning of June (early tillering) to the beginning of October (harvesting); reflectance was measured as in the previous experiment (see section 2.3.1). Harvesting data (dried overground biomass and rice grain) were collected in the experimental cells at the end of the experiment. In order to follow the evolution in time of biomass and to evaluate the open field variability, samples in close contact with the experimental cells were taken randomly in a field with a normal density. The actual densities and rice production at harvest of such reference samples are shown in Table 24.

3.2 Results

3.2.1 Agronomical data

- Phenological stages (see Table 25)
- Actual density (see Table 26)

It will be observed that the actual density after tillering follows in an irregular manner the theoretical density at seeding and exhibits a narrower range.

Table 24 - Data on reference samples

Cell	Density (halms/m^2)	Rice Production (qntls./ha)
A	275	79.2
B	360	80.2
C	349	66.7
D	300	48.1
E	379	62.3
F	385	89.7
G	356	60.7
H	396	64.6
I	306	66.3

- Evolution in time of biomass

Fig. 46 presents the data collected during the entire experiment on the cells distributed in a normal density field. The overground (leaf and stem) biomass reaches a plateau around flowering. This interruption of growth is substituted, from then on, by the growth of the panicle biomass.

Table 25 - Rice phenology

Day	Date of measurement	Phenological Stage
0	6- 4-74	early tillering
16	6-20-74	tillering
38	7-12-74	"
48	7-22-74	"
58	8- 1-74	booting
70	8-13-74	flowering
78	8-21-74	milk ripening
87	8-30-74	end of milk ripening
94	9- 6-74	wax ripening
101	9-13-74	advanced wax ripening
119	10- 1-74	full ripening
128	10-10-74	harvesting

Table 26 - Agronomical data on experimental cells

Cell	Theoretical Density (halms/m^2)	Actual Density (halms/m^2)	Rice Production (qntls/ha)
1	150	212	69.2
2	200	287	78.9
3	250	280	75.2
4	300	254	71.3
5	350	338	84.5
6	400	366	78.7
7	450	445	76.8
8	500	498	88.1
9	550	429	78.4
10	600	473	80.2

- Rice Production towards density (Fig. 47)

It is apparently difficult to make any simple interpretation of the results. It would seem, however, than an increase of production occurs at the lower densities (from 200 to 300 halms/m^2) and perhaps at the higher ones (above 450 halms/m^2). The central part of the figure corresponds to densities found in normal fields (300 to 400 halms/m^2). At these densities, rice production appears to be independent of density and to be characterized by great variability (see Fig. 48) in the observed cells under normal field conditions.

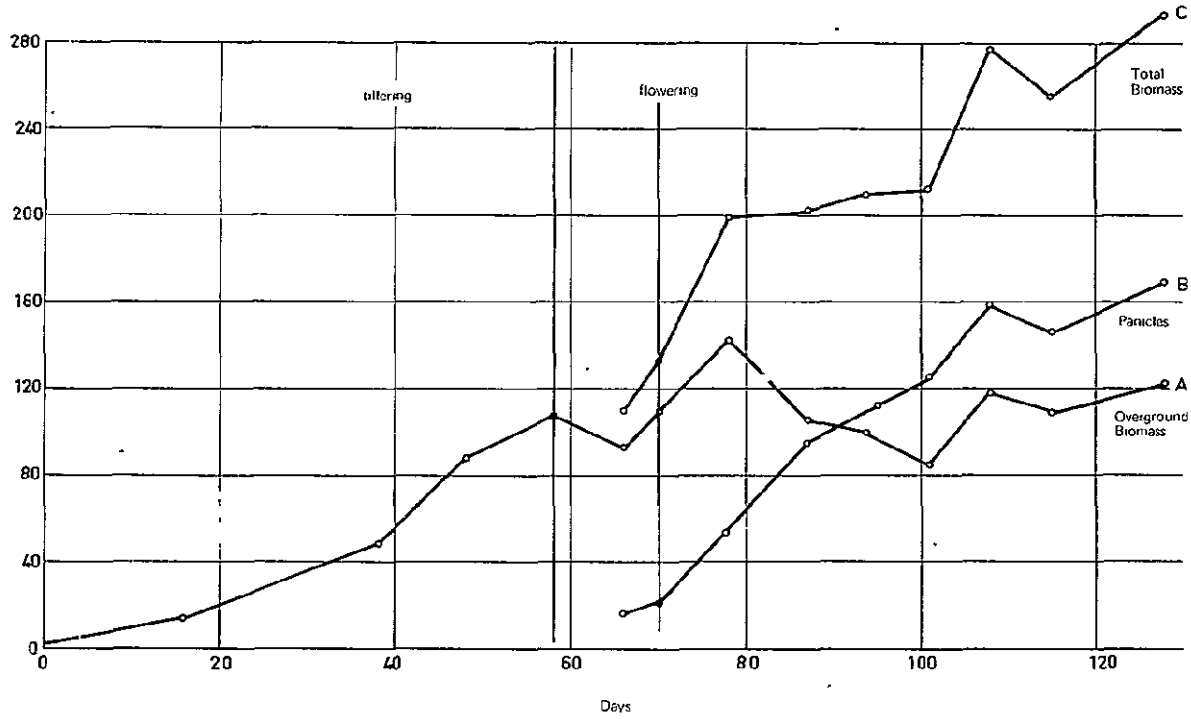

Fig. 46 - Evolution of biomass in the reference samples with time

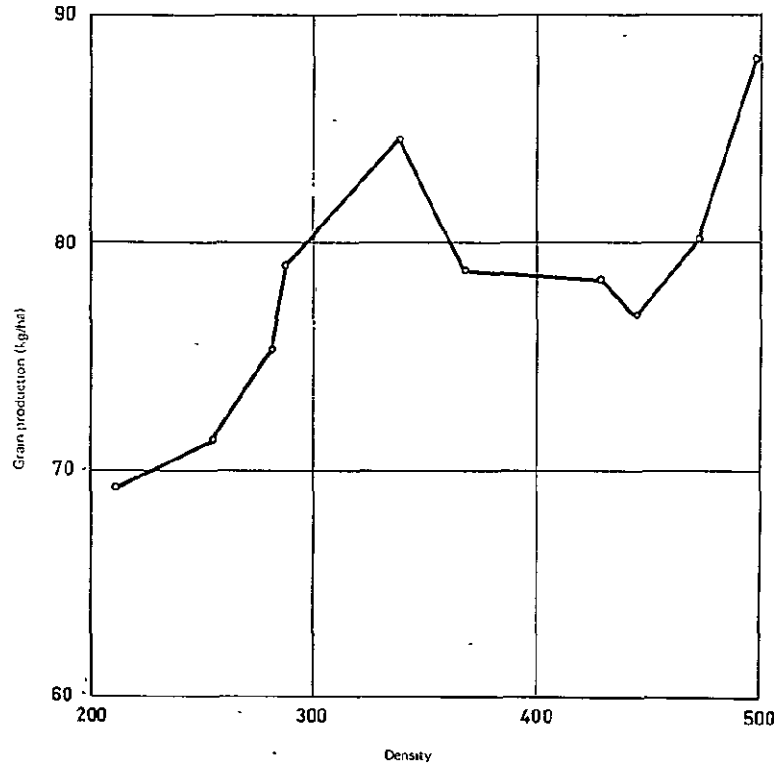

Fig. 47 - Grain production in relation to density, in the experimental cells

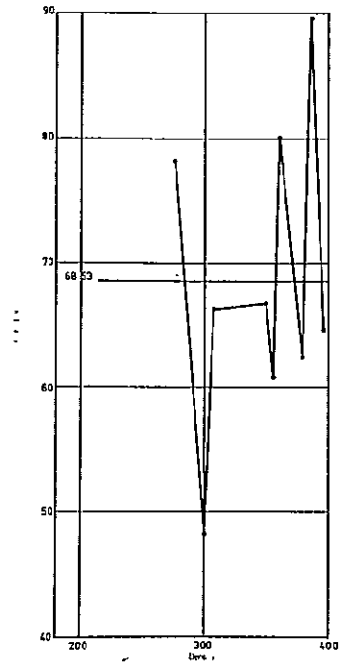

Fig. 48 - Grain production in relation to density, in normal density field conditions

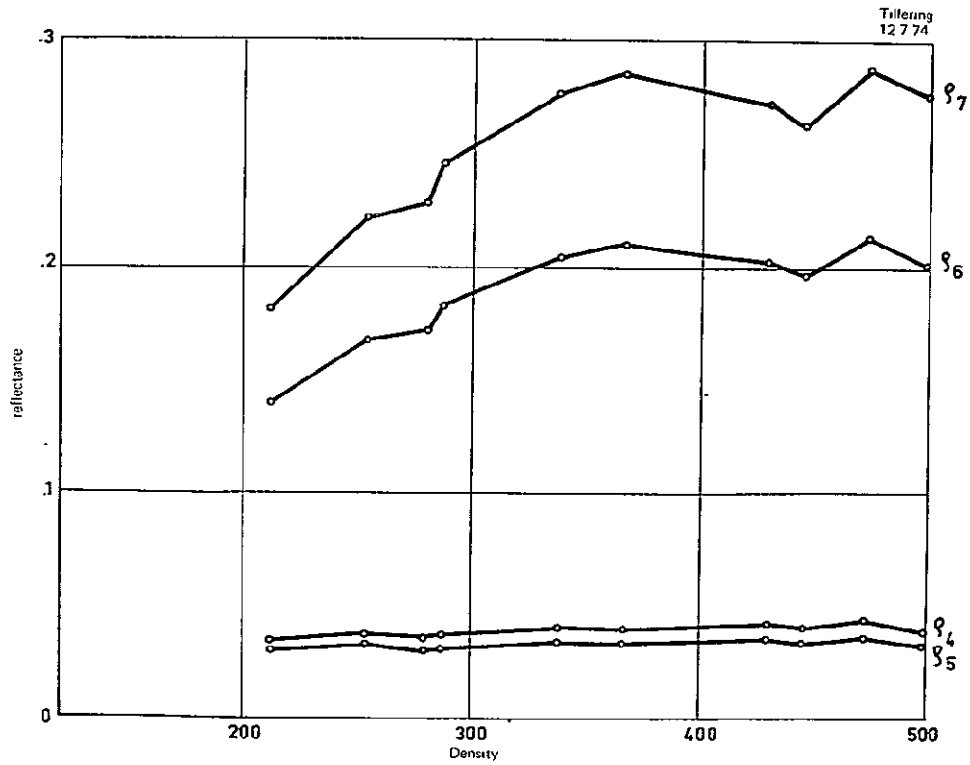

Fig. 49 - Reflectances in relation to density during tillering

3.2.2 Spectral data

3.2.2.1 Relation of reflectance to density

The relationships between reflectance in the four channels and the actual density can be referred to three main groups: early tillering, tillering and from booting to maturity.

- Early tillering (6-4-74)

  The reflectances exhibit a very irregular behaviour in relation to density. This is due to the fact that rice vegetation is still sparse and mixed with algae and other plants. These reflectance data are irrelevant to our investigation.

- Tillering (from 6-20-74 to 7-22-74)

  Fig. 49 characterizes reflectance behaviour during this period. While ρ_5 and ρ_4 appear to be constant with density, ρ_7 and ρ_6 increase until about 350 halms/m^2; at higher densities, infrared reflectance appears to be constant with density

- Booting to harvesting (from 8-1-74 to 10-10-74)

  Figs. 50 (at booting) and 51 (at milk ripening) are characteristic of this period; the trends are similar to the ones described for tillering except that infrared reflectance, after a sharp increase at the lowest density, appears uniform above a density of about 250 halms/m^2.

One would be tempted to interpret the behaviour of infrared reflectance at higher densities on the basis of a hypothesis of saturation of such reflectance. The contribution to the total radiant emittance detected by channels 7 and 6 would be mainly given by the overall horizontal green surface seen by the radiometer, whilst the inner biomass would be somewhat shielded by the upper layers of leaves.

In fact, such a hypothesis of reflectance saturation is not at all supported by the results obtained on lysimeters in 1975, to be described later. These results indicate a clear positive correlation between infrared reflectance and leaf area index up to densities as high as 450 halms/m^2. This correlation is a consequence of the development of the vegetation structure occurring at booting, which favours the penetration of infrared through the canopy layers (see section 4.2.2.1). On the other hand, the hypothesis of reflectance saturation is not supported by the evolution of reflectance with time in the present experiment (see section 3.2.2.2). This evolution indicates a further increase of infrared reflectance between tillering and flowering in relation to the increase of overground biomass.

The constancy of infrared reflectance with density could probably find a plausible interpretation on the basis of the development of the vegeta-

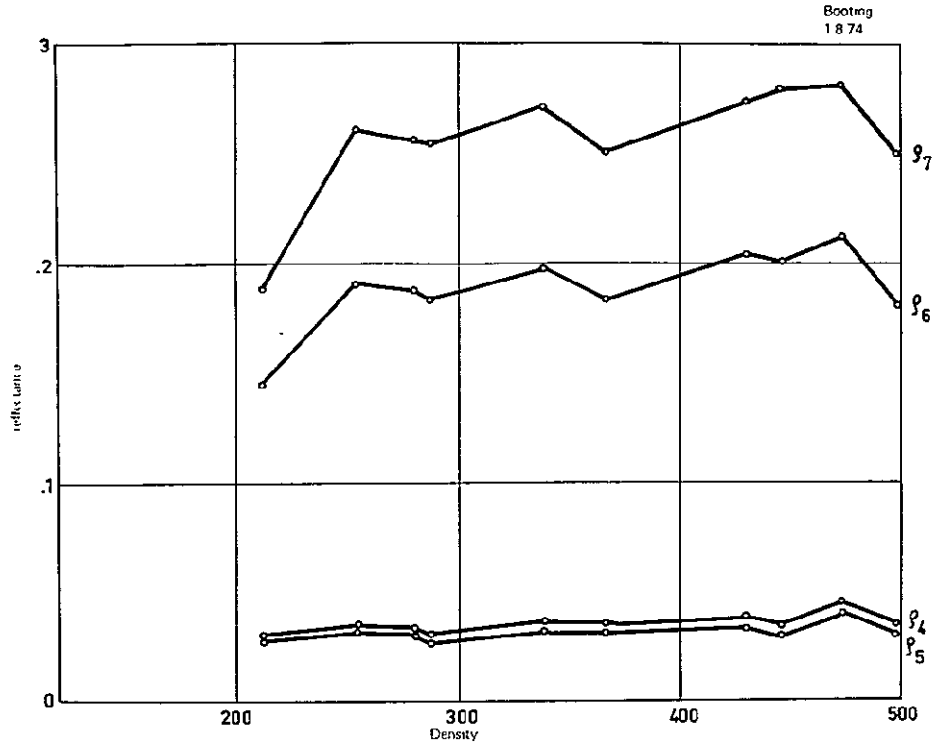

Fig. 50 - Reflectances in relation to density during booting

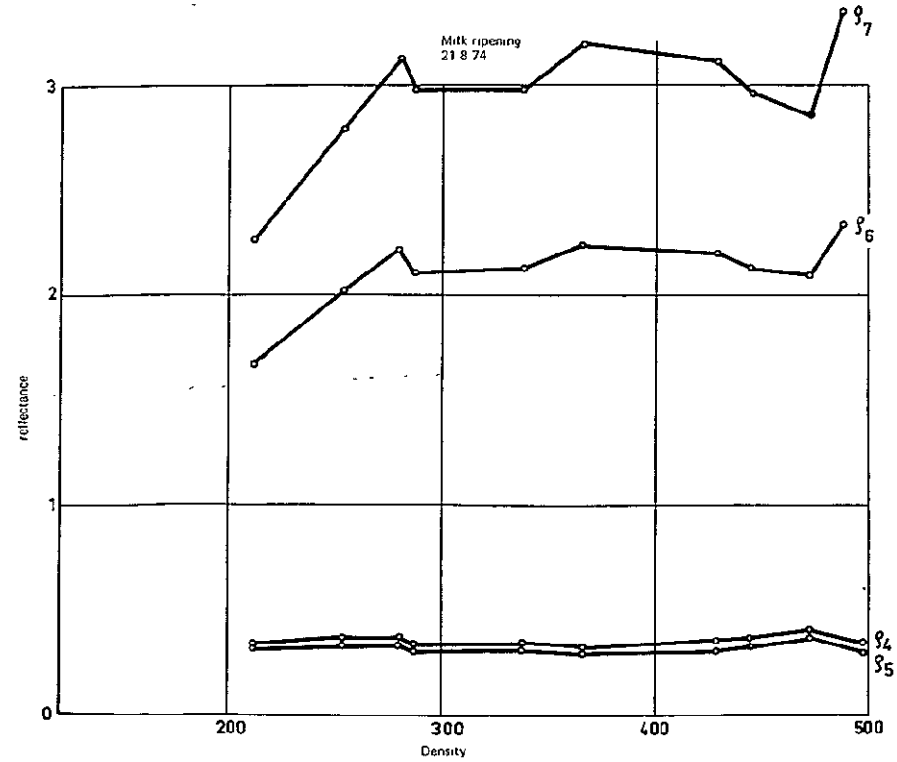

Fig. 51 - Reflectances in relation to density at milk ripening

tion structure in the investigated rice variety (Padano). Unfortunately, it was not possible, under the field conditions considered here, to achieve an exhaustive collection of data on vegetation structure.

As far as the reflectance ratio ρ_7/ρ_5 is concerned, there is no advantage in using this ratio in relation to density since ρ_5 does not significantly vary with density.

3.2.2.2 Relation with reflectance to time

The evolution of reflectance with time is shown in Figs. 52, 53 and 54 at three different densities. The following features are observed:

- increase of ρ_7 and ρ_6 during tillering with a saturation which is reached at the end of tillering,
- flowering (around day 70) is characterized by a clear peak of infrared reflectances,
- general decrease of visible reflectances (ρ_5 and ρ_4) from day 0 to day 70, followed by a clear increase during the maturation phase.

These reflectance trends cause the reflectance ratio ρ_7/ρ_5 to be a very good indicator of the plant development (Figs. 55, 56 and 57), with a very sharp peak occurring around flowering (day 70). This evolution of reflectance with time is in general agreement with the results of the preceding experiments. The postponement of the maximum reflectance and reflectance ratio from earing to flowering in the present experiment might well be due to the observation gap during the two first weeks of August when earing actually took place.

The importance of the generative phase in the evolution of reflectance with time is thus emphasized. It is significant that reflectance measurements are able to identify this essential phenological stage which indicates the maturity of the plant turning toward the accomplishment of the final goal of seed production.

3.2.3 Yield prediction

Results of previous experiments have shown that yield prediction can be attempted on the basis of the relationships between reflectance measurements and total biomass, and of the estimation of the yield coefficient.

Results of the present experiment under field conditions do not allow any relationship to be drawn between reflectance data and halms density. Under such conditions, total biomass cannot be related to reflectance. On the other hand, the yield coefficient itself will probably vary widely with density.

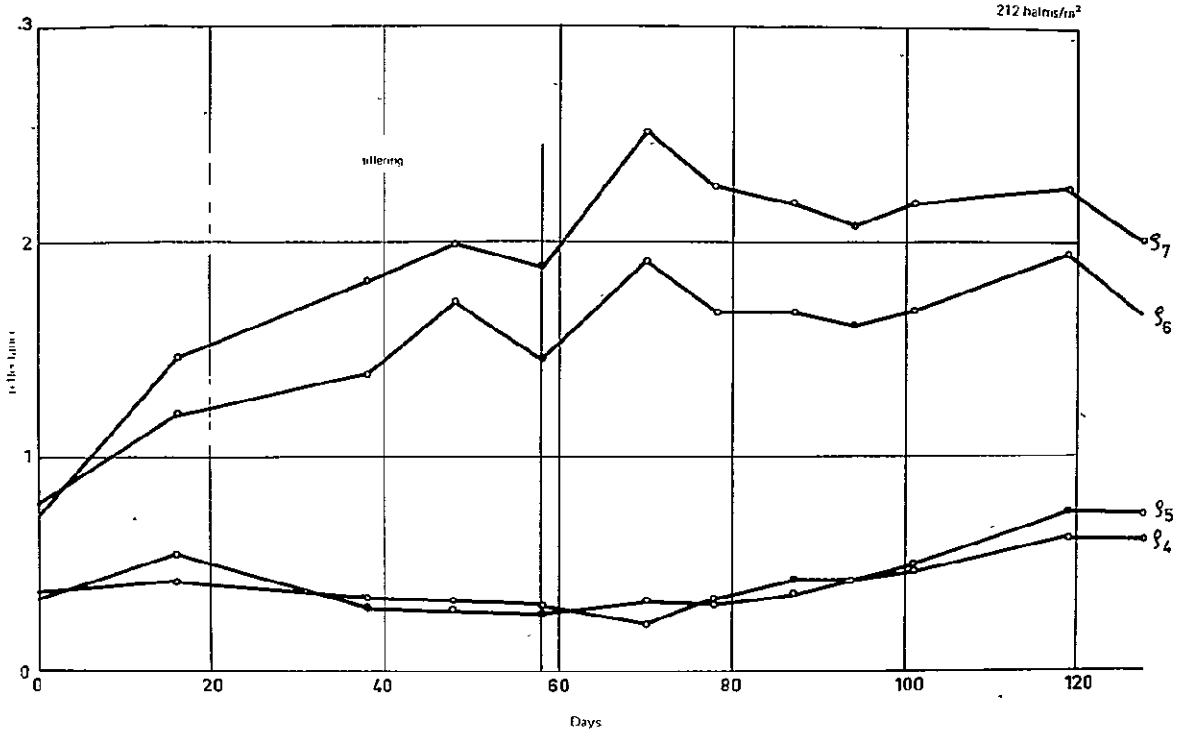

Fig. 52 - Evolution of reflectances with time, at density 212 halms/m^2

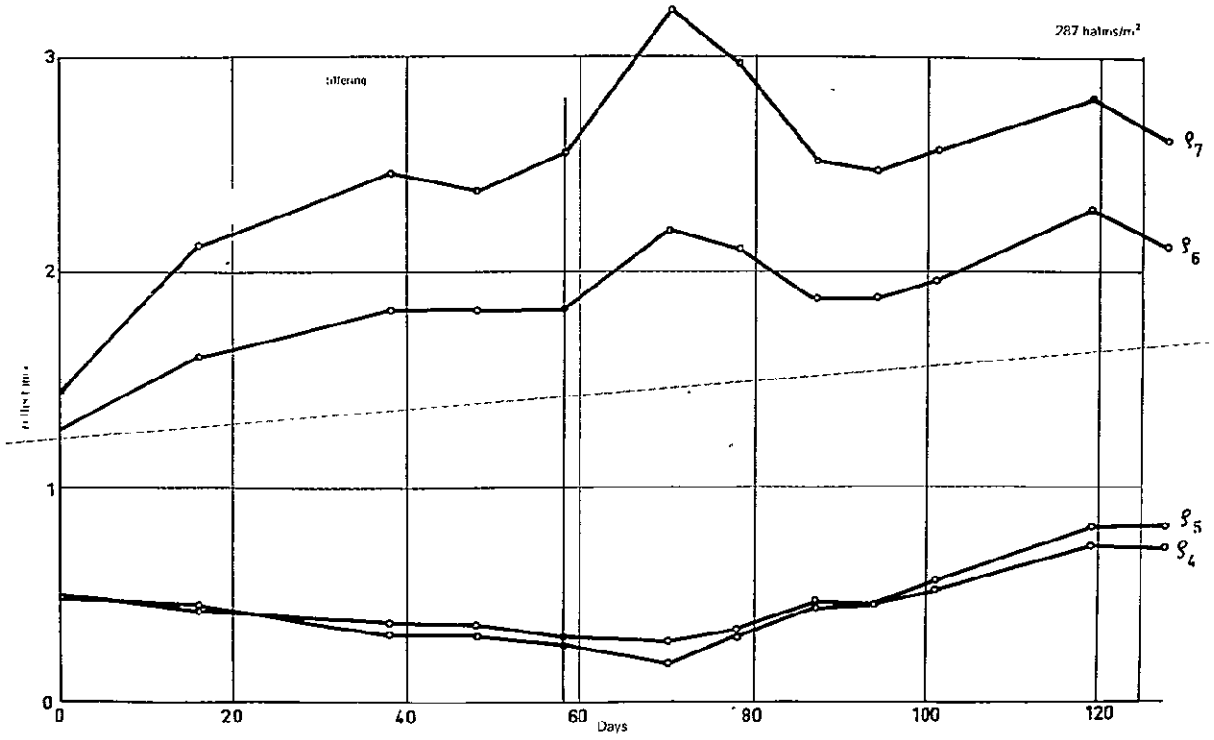

Fig. 53 - Evolution of reflectances with time, at density 287 halms/m^2

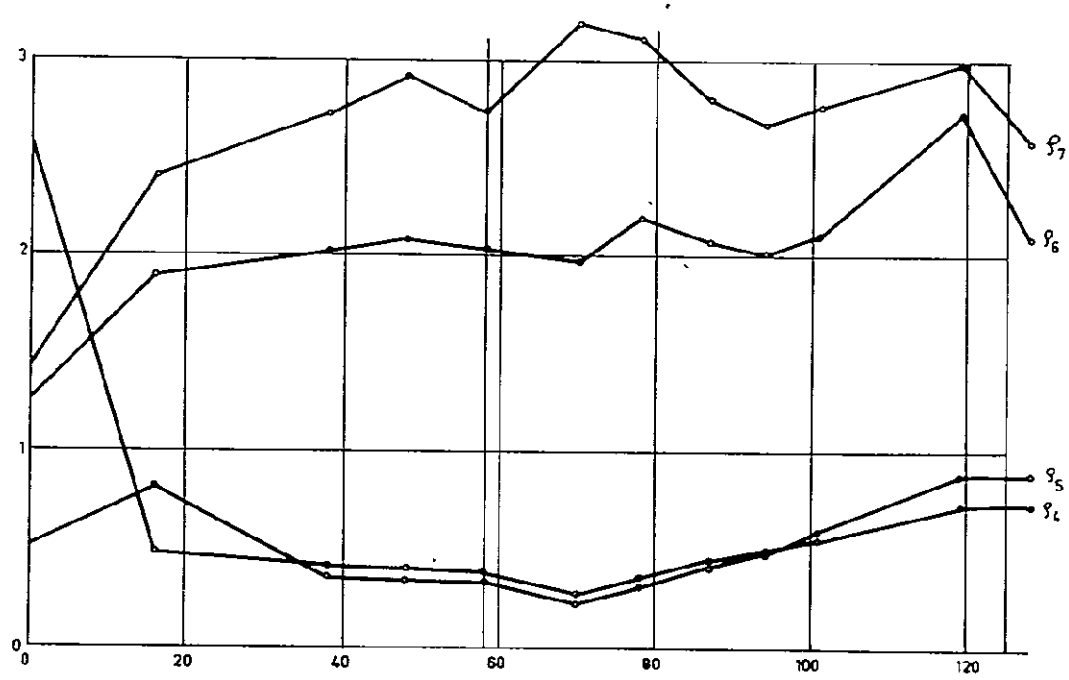

Fig. 54 - Evolution of reflectances with time, at density 429 halms/m^2

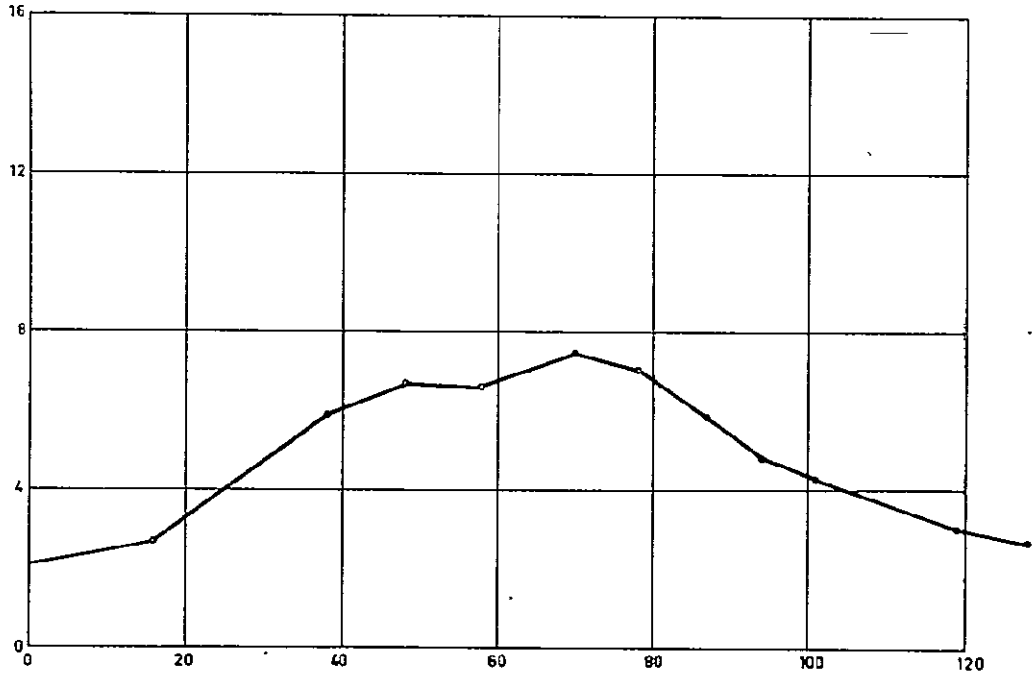

Fig. 55 - Evolution of reflectance ratio ρ_7 / ρ_5 with time, density 212 halms/m^2

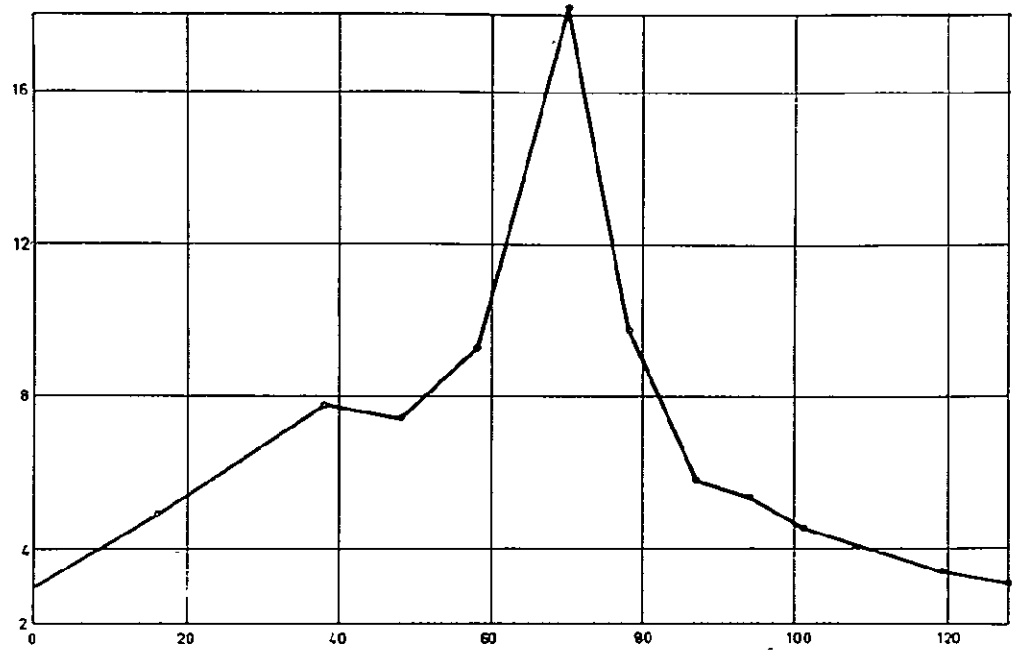

Fig. 56 - Evolution of reflectance ratio ρ_7/ρ_5 with time, at density 287 halms/m^2

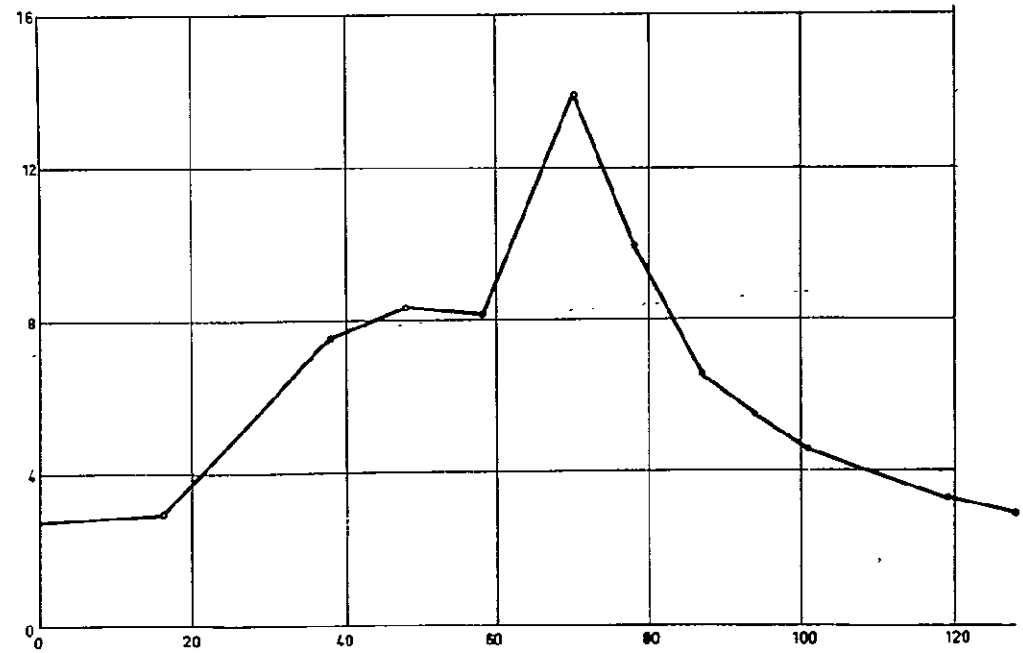

Fig. 57 - Evolution of reflectance ratio ρ_7/ρ_5 with time, at density 429 halms/m^2

It must be emphasized, however, that the conclusions of the present experiment must be considered as provisional. Actually this experiment under field conditions suffered in its interpretation from an evident lack of more detailed basic information on the behaviour of rice reflectance. Collection of such information needs research under more controlled conditions such as the one performed in lysimeters during 1975 (see following section 4). In this sense the experiment performed here under field conditions was somewhat premature and its conclusions will therefore have to be revised later.

4. SPECTRAL FEATURES OF A RICE CULTURE IN RELATION TO SEVERAL CULTURAL FACTORS (Lysimeters Biology Group, Ispra, 1975)

4.1 Methods

Three different treatments were applied, with 5 repetitions each, in the same lysimeters as in 1974, on the rice variety Arborio. The treatments differed in the mode of planting (in groups or by single plants; planting density 64/m^2) and in mode of N-fertilization (in one or two applications).

Treatment 1 - one N-application at planting (12 g N/m^2);
- planting in groups of 4 plants.

Treatment 2 - one N-application at planting (12 g N/m^2);
- planting by single plants.

Treatment 3 - two N-applications (8 g N/m^2 at planting plus 4 g N/m^2 at the second node stage;
- planting by single plants.

Reflectance measurements began one month after planting (early July) at a variable frequency (generally 4 to 10 days) according to the phenological stage (see Table 27). Regular samplings took place in order to follow continuously the development of the vegetation structure (see Table 27), growth in weight of the culture and of the individual halms, total leaf area index, partial leaf area index (in 10 cm vertical layers).

4.2 Results

4.2.1 Agronomical data

- Phenological stages

They have been observed in an accurate manner and are described in Table 27, together with the dates of sampling and of spectral measurements. A delay in the phenological development is evident for treatment 1.

Dates 1975	Day (from planting)	Development stages			Samplings	Reflectance meas	
		Tr. 1	Tr. 2	Tr. 3		Exotech	Optronics
6/10	0						
	–						
	–						
7/7	27						
	28						123
	29	3	3		12		
	30			3	3		
	35						123
	36	3	3		12		
	37			3	3		
	46						123
	47						
	48	4			1		
	49		4	5	23		
	50					123	
	51						
8/1	52					123	123
	55			7			
	56						
	57	6	7		12		
	58			8	3	123	
	59						123
	64					123	
	69	10	10 2		12		
	70			10 3	3	123	123
	73		10 3				
	77		10 5 1		2	3	
	78	10 3			1		
	79						3
	80			10 5 2	3		
	81					12	
9/1	83						
	84						
	85					3	
	91					123	
	92	10.5.3			1		
	93		11 1		2		
	94				3		
	95					123	
	99					123	
	102					123	123
	105	11 1 11 2			1		
	106		11 2		2	12	
	107			11 2	3		
10/1	113					123	
	114					123	
	115						
	116						123
	119					123	
	123		harvest		2		
	126					12	
	127			harvest	3	1	
	128						
	129	harvest			1		
	130						

Vegetative Phase		3	Tillering
GENERATIVE PHASE	BOOTING	4	Leaf sheath begins to elongate
		5	Pseudo-extension of stem
		6	First node
		7	Second node
		8	Last leaf visible
		9	The ear swells; last leaf sheath which is now visible
		10	The leaf sheath is pulled by ear pressure
	EARING	10.1	Beginning of earing
		10.2	A quarter of the ears has emerged
		10.3	Half of the ears has emerged
		10.4	Three quarters of the ears have emerged
		10.5	All the fertile halms have eared
	FLOWERING	10.5.1	Beginning of flowering
		10.5.2	Complete flowering at the ear top
		10.5.3	Complete flowering at the ear bottom
		10.5.4	End of flowering and grain formation
MATURATION PHASE		11.1	Milk ripening
		11.2	Wax ripening
		11.3	Hard grain ripening

Legend to Table 27

Table 27 - Survey of the phenological stages according to Feekes[3] (see legend) and chronology of samplings and of reflectance measurements (Radiometer Exotech and spectroradiometer Optronics). In the columns Samplings and Reflectance measurements, the numbers 1, 2 and 3 refer to treatments 1, 2 and 3 respectively.

- Halm growth and vegetation density

The mean growth curve of a single halm is clearly synchronous in the 3 treatments (Fig. 58) whereas the vegetation density strongly depends on the mode of culture (Fig. 59). It is thus evident, as noted in previous experiments, that regulation of the biomass is achieved via the number of halms and not via the biomass of a single halm.

- Development of leaf cover

Fig. 60 represents the evolution in time of the leaf area index which exhibits in the 3 treatments a sharp maximum at the second node stage (day 57). The vertical distribution of the leaf surface (expressed in partial leaf area index) is illustrated for treatment 2 on Fig. 61: it is evident how the planiform distribution characteristic of tillering becomes erectiform in the following phases of development.

- Development of tillers

The histograms of Fig. 62 show for the 3 treatments, during the entire development cycle, the frequencies of various weight classes of tillers. From a thorough discussion of these data, the following conclusions can be drawn:

a) a cereal culture is characterized by its very great heterogeneity;

b) processes of competition occur among tillers, mostly at the end of tillering and beginning of booting (day 36-57). They are responsible for a two-mode distribution in "major" and "minor" tillers. After flowering (day 80), these two modes are separated by vacant weight classes and their segregation becomes complete because of the sterility of the minor tillers. These competition processes differ widely among the 3 treatments in relation to a different N-availability (treatments 2-3) and to a different vital space (treatments 2-1).

- Final grain yield and its relationships with competition

Data of Table 28 show that the total biomass and the number of panicles per m^2 are very similar for the 3 treatments whereas final grain yield as well as yield coefficient differ widely, assuming the highest values in treatment 3 (in relation to a better balanced N-availability) and the lowest values in treatment 1 (as a consequence of excessive competition processes). Fig. 63 shows how grain yield is conditioned very soon after flowering by the different growth rates of the panicle.

It appears thus evident that competition between plants (due to some limiting factor, such as nitrogen or light deficiency) exerts a negative effect on grain yield. One might interpret this effect as a consequence of the disturbance, by excessive competition, of the compensatory mechanisms by which a plant tends to occupy a maximum of space (by in-

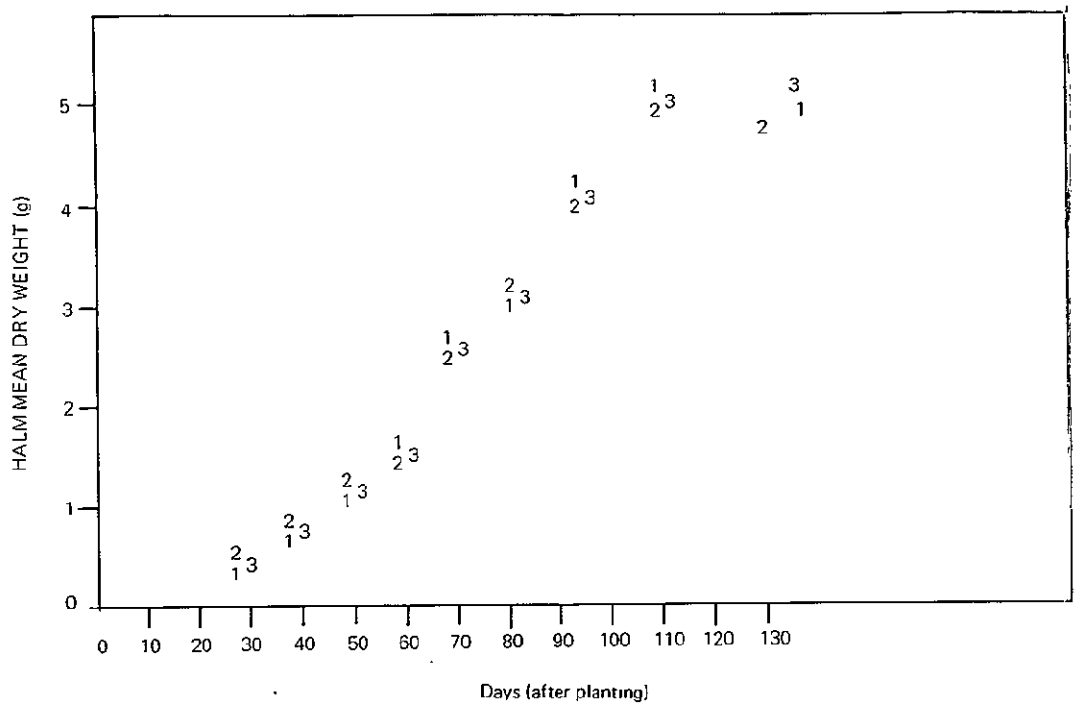

Fig. 58 - Halm growth in the three treatments

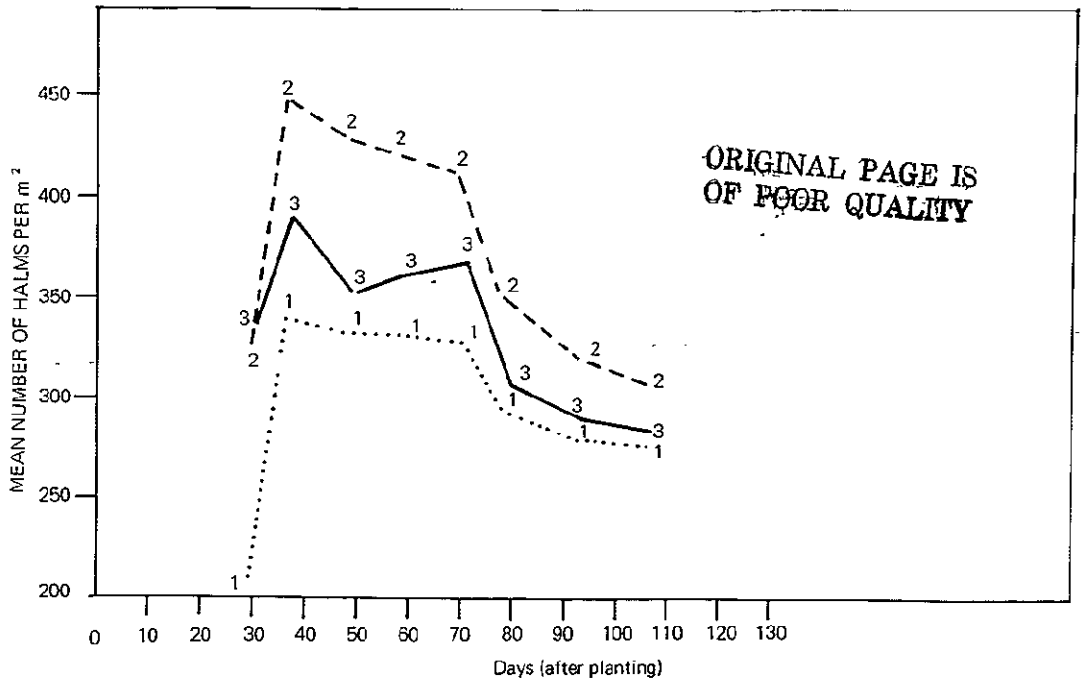

Fig. 59 - Evolution of vegetation density with time in the three treatments

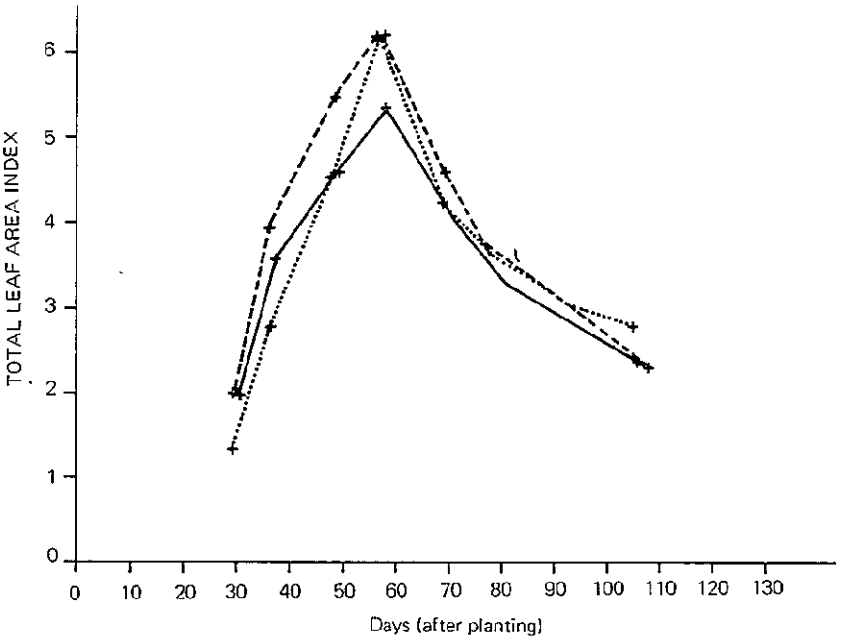

(.....) treatment 1 (-----) treatment 2 (———) treatment 3

Fig. 60 - Evolution of leaf area index with time in the three treatments

creasing the number of tillers or by developing the foliar surface of each tiller).

4.2.2 Spectral data

4.2.2.1 Near Infrared (NIR) (Fig. 64)

During early tillering, when the canopy is still far from covering the water surface, the lowest reflectance is observed for treatment 1, as a consequence of its lowest leaf area index and the low NIR reflectance of water. On the other hand, the difference between reflectance in treatments 2 and 3 (same leaf area index) should be due to a different vegetation structure, with a more planiform distribution of the leaves (and hence more "covering") in treatment 2.

A general correlation is evident between leaf area index and NIR reflectance (ρ_6) (Fig. 65). This correlation explains that ρ_6 reaches a maximum during booting (just before day 60) in correspondence with the maximum leaf area index (Fig. 60). But this correlation cannot explain all the differences of reflectance observed among treatments after tillering. During booting (day 50 to 60), treatment 1 exhibits a higher NIR reflectance than the other treatments, whereas their leaf area indexes are similar.

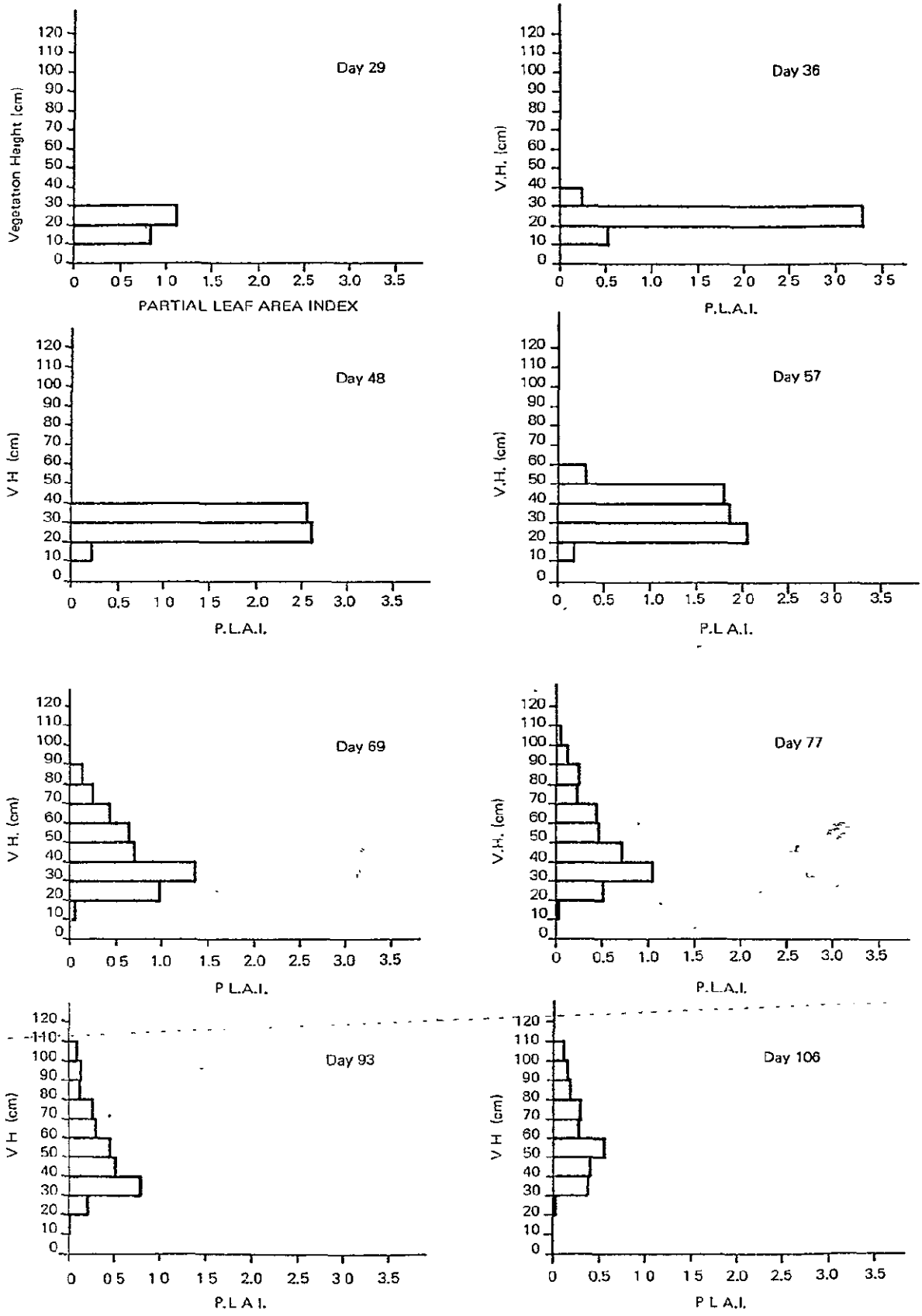

Fig. 61 - Vertical distribution of leaf surface in treatment 2 (expressed as partial leaf area index)

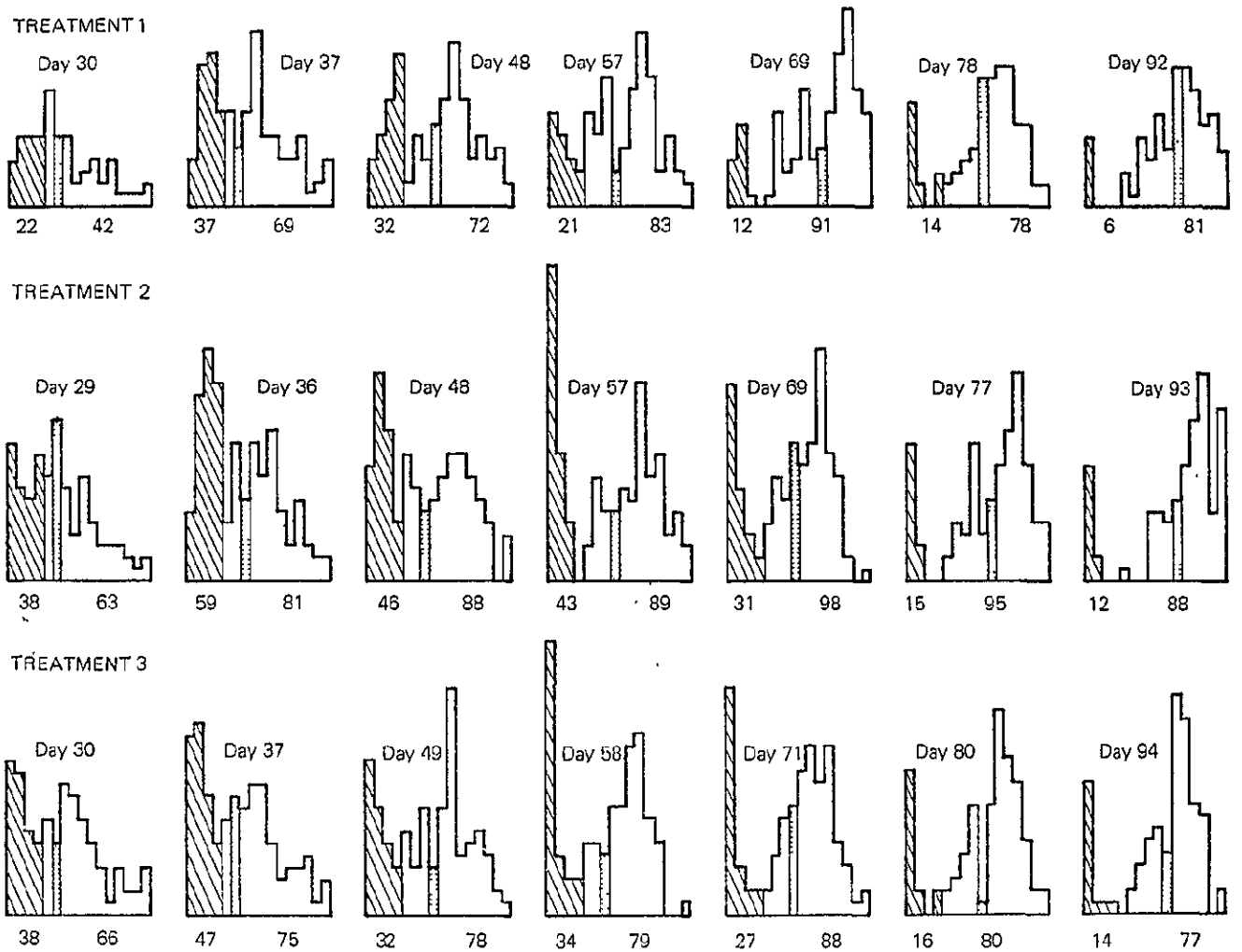

Fig. 62 - Frequency distribution of halm weights in 7 successive samplings on 5 x 4 plants
- at the left side: dashed surfaces representing "minor" tillers
- at the right side: "major" tillers
- the dotted frequency class represents the general mean weight
- the indicated numbers refer to the numbers of minor and major tillers respectively

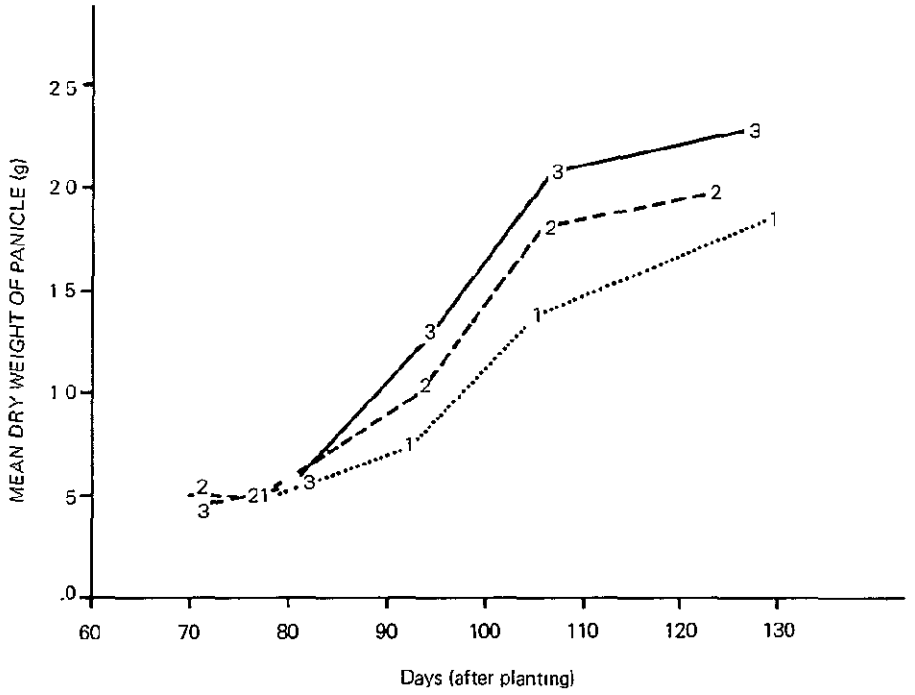

Fig. 63 - Growth rate of panicle in the three treatments

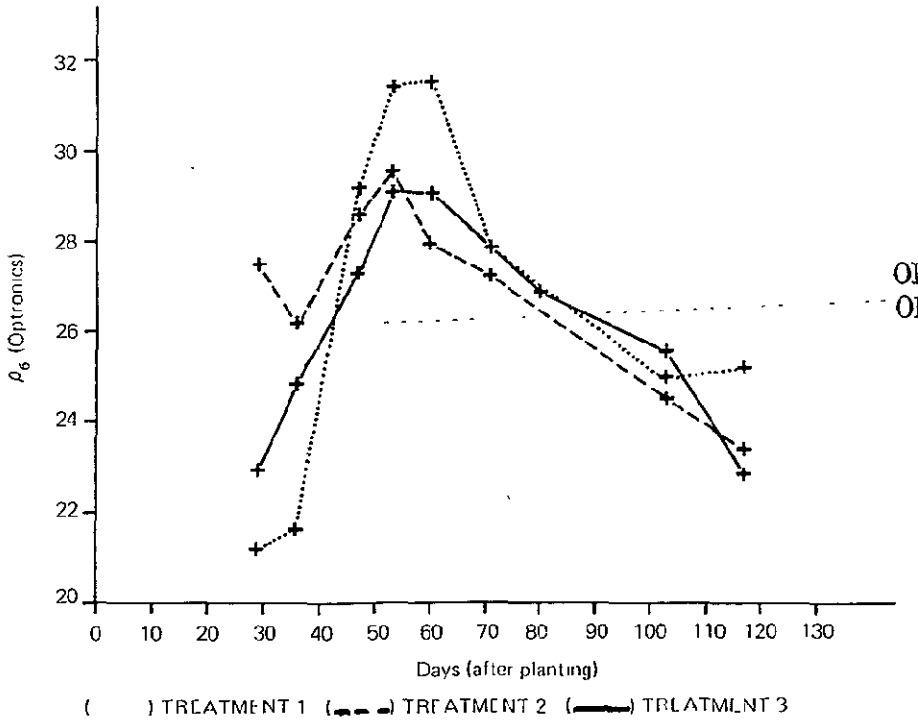

ORIGINAL PAGE IS
OF POOR QUALITY

Fig. 64 - Evolution of near infrared reflectance (Optronics) with time

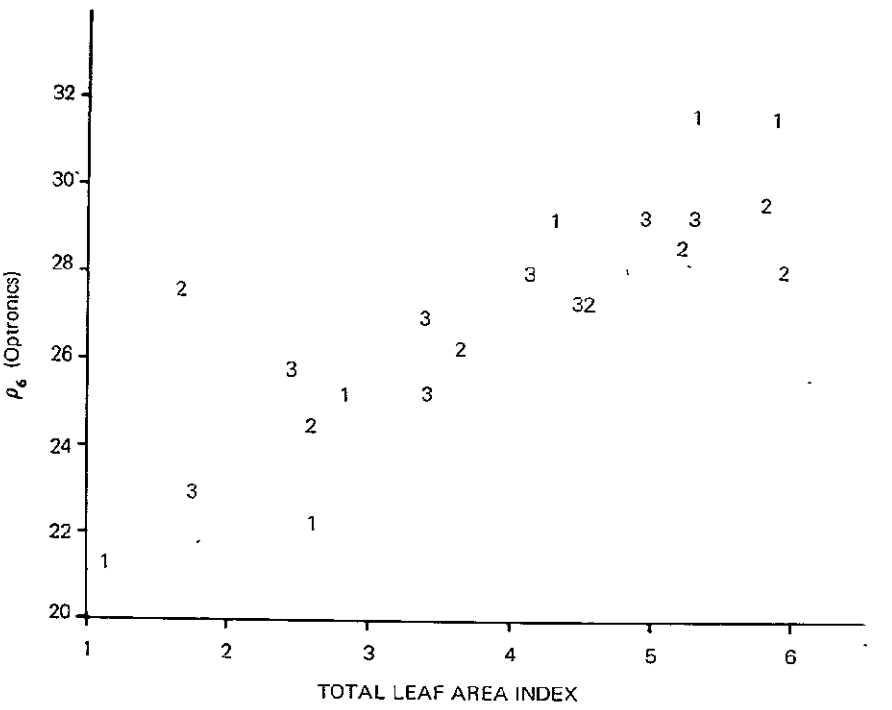

Fig. 65 - Near infrared reflectance in relation to total leaf area index

This difference is to be related to the distribution of plants (in groups of 4) which would allow a better diffusion of the NIR through the vegetation.

The vertical distribution of the leaf surface (Fig. 61) represents another component of the vegetation structure which exerts an effect on NIR reflectance. Fig. 66 shows the differences among treatments as far as that component is concerned. This figure indicates, after day 40, a predominant development of the highest leaf layers in treatments 1 and 3, and of the intermediate ones in treatment 2. This difference in vegetation structure can be correlated to the higher NIR reflectance of treatment 1 and 3 relative to treatment 2, after day 60 (Fig. 64).

Since the differences in vegetation structure can be easily interpreted as a consequence of the different mode of culture, it appears thus evident that the spectral signature of a rice culture is strongly governed by agricultural practices, within a general framework of temporal evolution of reflectance data which is conditioned by plant growth and development.

During the maturation phase, the development of panicles and their inclination due to their own weight, are responsible for the further decrease of the NIR reflectance in the three treatments.

Table 28 - Production components at harvesting

	Dry Weight (g/m^2)				Number of panicles per m^2	Yield coeffic. (3)/(1)+(2)+(3)
	senescent stems (1)	dead leaves (2)	panicles (grain) (3)	total (1)+(2)+(3)		
Treatment I	653	168	434	1255	228	0.35
	656	197	411	1264	229	0.33
	640	206	451	1297	234	0.35
	650	187	457	1294	233	0.35
	720	204	426	1350	246	0.32
Mean	664	192	436	1292	234	0.34
Stand. Dev.	32	16	19	37	7	0.01
Treatment II	535	230	477	1242	228	0.38
	560	215	483	1258	250	0.38
	585	215	486	1286	243	0.38
	690	225	504	1419	248	0.36
	645	220	464	1329	241	0.35
Mean	603	221	483	1307	242	0.37
Stand. Dev.	64	7	15	71	9	0.01
Treatment III	580	221	577	1378	254	0.42
	640	219	592	1451	261	0.41
	471	169	496	1136	208	0.44
	650	195	481	1326	222	0.36
	630	210	566	1406	235	0.40
Mean	594	203	542	1339	236	0.41
Stand. Dev.	74	22	50	122	22	0.03

4.2.2.2 Visible light (Channel 4) (Fig. 67 Optronics; Fig. 68 Exotech, from day 52)

The following phases can be distinguished:

- Tillering (day 27-46). In spite of the interference of water reflectance, one notes a general decrease of reflectance in relation to the development of the vegetation cover. According to a different foliar index, treatment 2 exhibits a lower reflectance than treatment 3.
- Beginning of booting (day 46-52). A transition plateau is reached while the leaf surface is still increasing. This type of saturation should be

caused by an excessively closed vegetation but the development of a new type of plant structure causes a rapid evolution of the situation towards the following phase.

- Booting, earing (day 52-75). The new plant structure causes a further decrease in reflectance, especially in treatment 3 (second N-distribution at day 55) where the leaf surface is distributed more vertically.
- Flowering, maturation (day 75-120). The reflectance increases progressively in relation to leaf senescence (which is more accentuated in treatment 2), in spite of the interference of the panicles.

4.2.2.3 Reflectance ratio ρ_6/ρ_4 (Fig. 69 Optronics; Fig. 70 Exotech)

This ratio is characterized by two increasing phases followed by a decreasing one. The first increasing phase extends over the whole vegetative phase (tillering, day 0-46). After a short interruption at the beginning of booting (day 46-52), the reflectance ratio increases again during booting until earing (day 52-70-78 for treatment 1).
The decreasing phase extends from flowering to maturation.

The evolution in time of the reflectance ratio is thus characterized by a maximum value attained during the earing phase. As illustrated by the figures, it is during this phase that the best differentiation can be achieved between the 3 treatments.

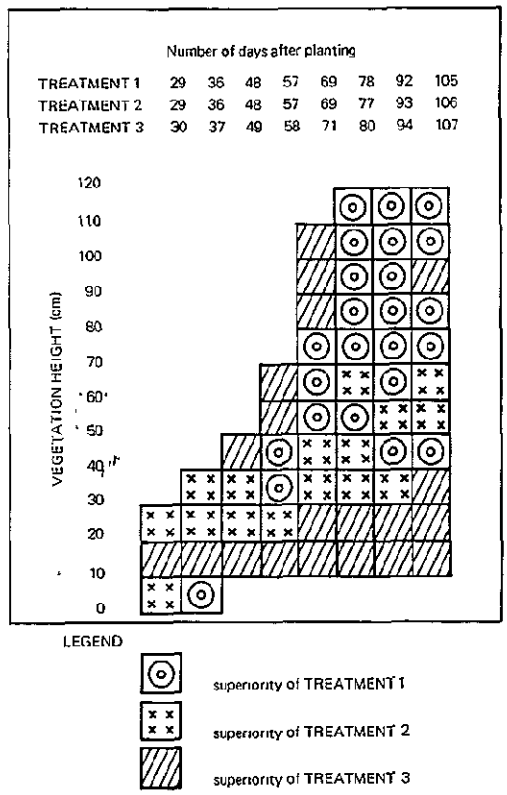

Fig. 66 - Comparison between treatments, relative to the importance of their leaf layers at various levels, during time

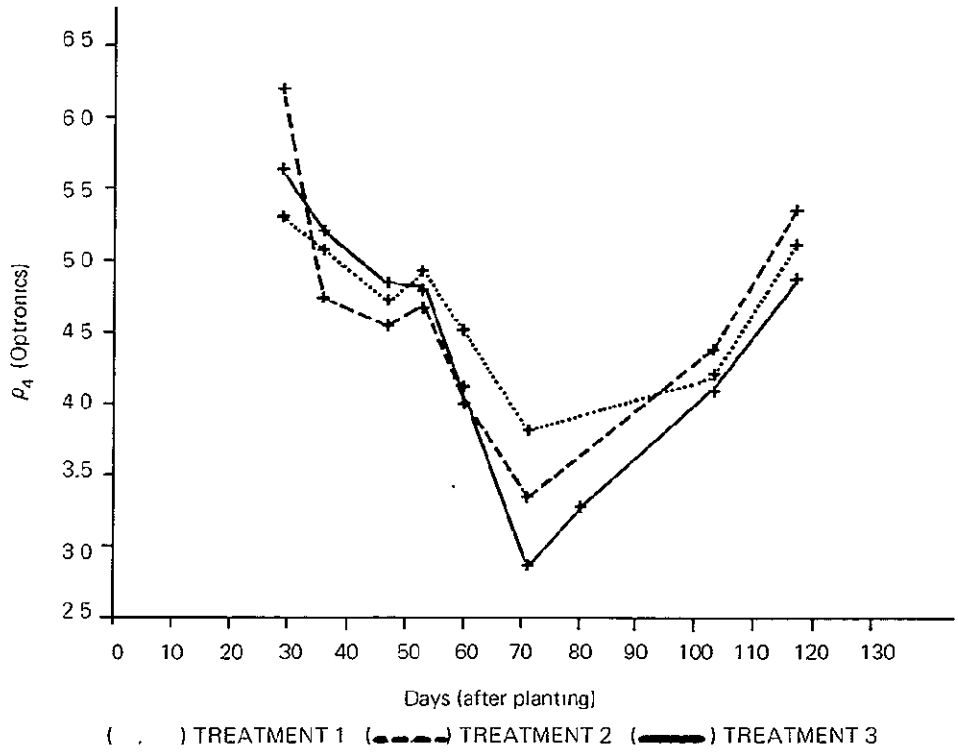

Fig. 67 - Evolution of visible light reflectance (ρ_4, Optronics) with time

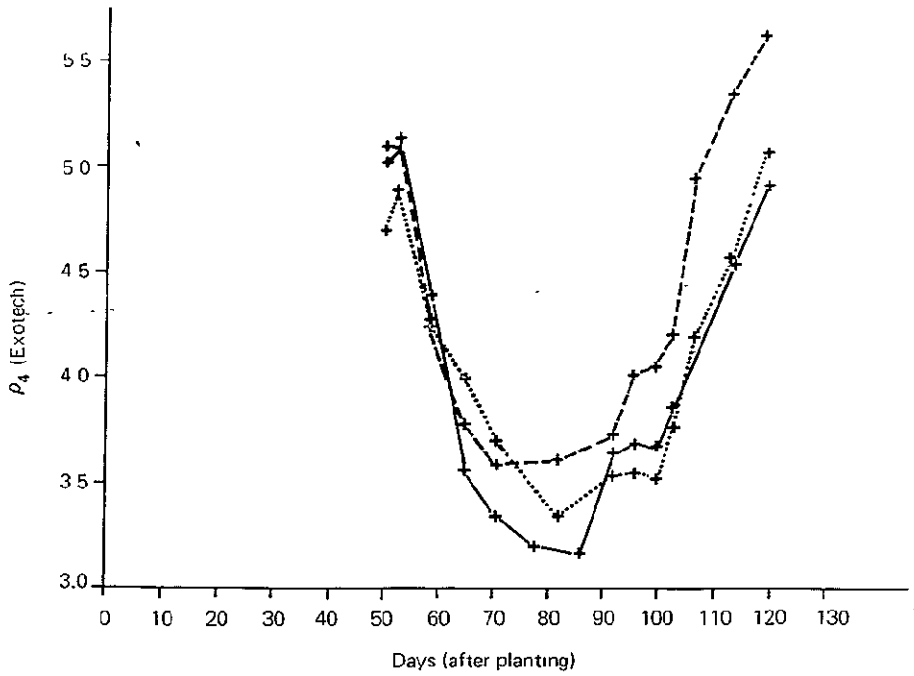

Fig. 68 - Evolution of visible light reflectance (ρ_4, Exotech) with time

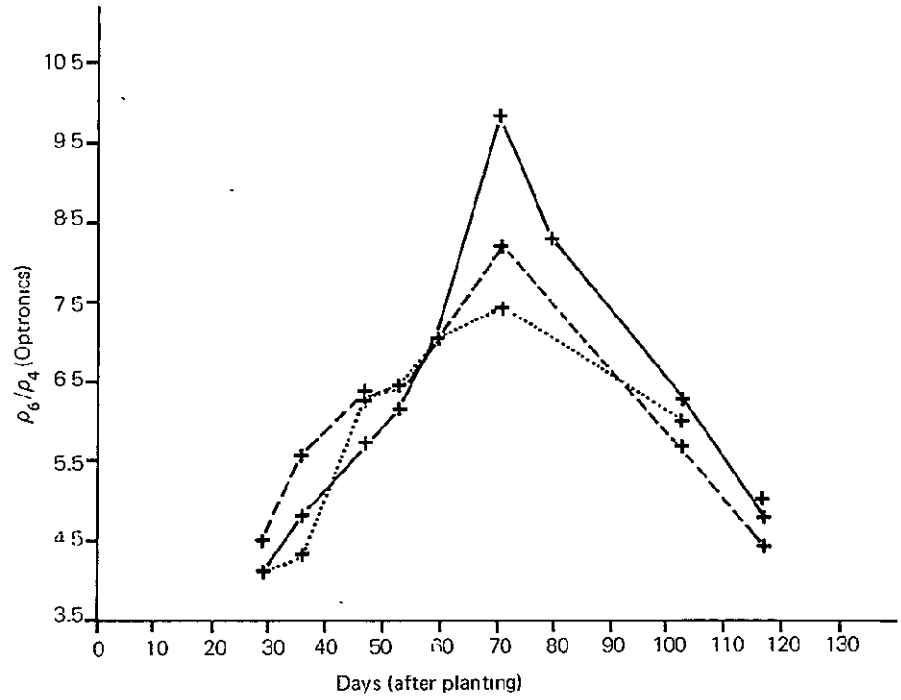

Fig. 69 - Evolution of reflectance ratio ρ_6/ρ_4 (Optronics) with time

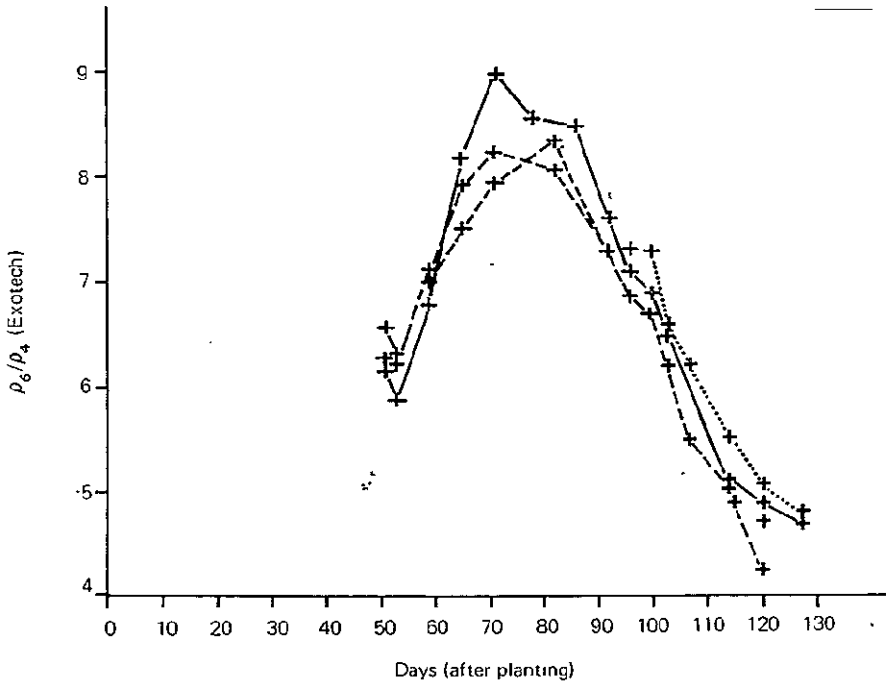

Fig. 70 - Evolution of reflectance ratio ρ_6/ρ_4 (Exotech) with time

4.2.2.4 Seasonal model of reflectance

From the above considerations a seasonal model of reflectance can be established. Table 29 presents such a model, where - or + represent respectively a decrease or increase of the parameter, and MIN or MAX respectively minimum or maximum values. This model is valid for the 3 treatments except that the minimum of reflectance in channel 4 is postponed from earing to flowering (stage 10.5) for treatment 3.

Table 29 - Seasonal model of reflectance

Stage of Development	Channel 4	Channel 6	Ratio ρ_6/ρ_4	FEEKES scale(3)
Tillering	-	+	++	3
Early booting	0	+	+	4-5
Maximum Leaf Area Index	-	MAX	++	7
Earing	MIN	-	MAX	10.3
Flowering and Maturation	+	-	-	10.5-11

4.2.3 Approach of a yield prediction based on radiometric data

It has been shown in the present experiment how cultivation practices influence the vertical distribution of the leaf surface. This important parameter of vegetation structure itself governs the light distribution between the vegetation layers and its utilization towards the translocation of the plant assimilates to the panicles. It is therefore allowed to apply the term "productive structure"(4) to a cereal structure best adapted to grain production. In this sense, a structure which favours the best penetration of light inside the culture is much more productive than a structure which exposes only the top of the vegetation to light.

Examination of Table 28 indicates a mean grain production which decreases in the following order of treatments: 3 (542 g/m^2) > 2 (483) > > 1 (436). The same decreasing order is observed on day 70 for the reflectance ratio ρ_6/ρ_4 (Figs. 69 and 70), although the maximum value of the latter parameter is reached on day 81 for treatment 1. In spite of such a relationship found for the mean values of the 3 treatments, no correlation at all can be drawn on the basis of the values available for the 15 lysimeters.

On the other hand, it was shown in the lysimeter experiment of 1974 that grain production is the result of the combined action of two production parameters: total biomass and yield coefficient. The present experiment shows how vegetation structure integrates these two production parameters by conditioning the potential efficiency of total biomass to produce definite levels of final grain production. The problem is therefore to define a reflectance parameter which could be correlated to the vegetation structure and thereby to the intensity of the productive potential of vegetation in order to be used for yield prediction purposes.

From that point of view the reflectance ratio at earing might not be the most adequate because it is not only conditioned by the leaf structure but also by the panicles. Since the new type of vegetation structure is elaborated during booting, an adequate reflectance parameter should include this period and take into account the increase of reflectance data rather than their instantaneous values.

The EXOTECH measurements taken every six days in the present experiment allow us to search for such a parameter. The best correlation was found to be the following (including the single data of 15 lysimeters):

$$y = \text{Grain production} = a + bx$$

$$x = 10^3 \frac{r_2 - r_1}{r_2} \cdot \frac{r_3 - r_2}{r_3}$$

where r_1, r_2 and r_3 represent the values of the reflectance ratio ρ_6/ρ_4 at day 52, 58 and 64 respectively (during booting).

Experimental values of the regression coefficients are a = 386.8 and b = 7.857, with a correlation coefficient r = 0.959.
This relationship appears to have a more general significance than those described in the 1974 lysimeter experiment, since it integrates quantitative, as well as qualitative aspects of rice culture. Such a relationship makes possible, in the present experiment, under various culture conditions, the estimation of the productive potential of a rice culture, two months before harvesting. The yield prediction should be improved subsequently on the basis of the effect, on the potential plant productivity, of meteorological conditions occurring after the earing stage. From that point of view, the estimation by radiometric methods, of a parameter such as the "stress degree day"[5] could allow prediction of final yield from the previous estimation of the potential culture productivity.

5. SPATIAL VARIABILITY OF RICE REFLECTANCE IN RELATION TO THE PHENOLOGICAL STAGES

5.1 A structural model for growth and development in annual plants

When annual plants, e.g. wheat[6] or corn[7], initiate a new organ, leaf, flower, fruit, etc., their growth rate decreases more or less perceptibly (Fig. 71). This leads to noteworthy statistical consequences on populations of field-grown plants.

Genetics, climate and soil microvariations slightly shift the dates of initiation among plants, and, hence, shift their growth curves. If those shifts do not modify the growth rate law from one plant to another, which may be the case of a short phase between two development stages, growth curves remain parallel and included between two extreme curves (Fig. 72).

It can be shown[8] that the growth level variance S^2y depends on the time of measurement:

$$S^2y = a^2\left(\frac{dy}{dt}\right)^2 + b^2\left(\frac{d^2y}{dt^2}\right)^2 + c^2$$

where a, b and c are constant.

Therefore, as soon as the growth rate law is not modified, the growth variance is minimum when growth rate dy/dt and acceleration d^2y/dt^2 are zero, that is when plants are just going over into a new development stage.

Under the same conditions, the law of skewness may be established too: growth distributions are symmetrical only when the instantaneous growth rate is zero (i.e. when reaching a stage) or when it is maximum (Fig. 73).

Unfortunately, shifts in development usually modify the growth rate from one plant to another during slow development phase, or phases including intermediate stages. Moreover, the growth rate decreases more or less, according to the stages: the decrease is usually clear during the heading of wheat or silking of corn, but rather less during the other stages. At last, the growth rate can be reduced by other causes, such as climatic limiting factors (temperature, water, etc.).

Then, it may only be asserted that growth variance and/or skewness are likely to show a noticeable change in their evolution when reaching the stages of development at which growth rate is considerably reduced. The same phenomenon may then be expected relating to any

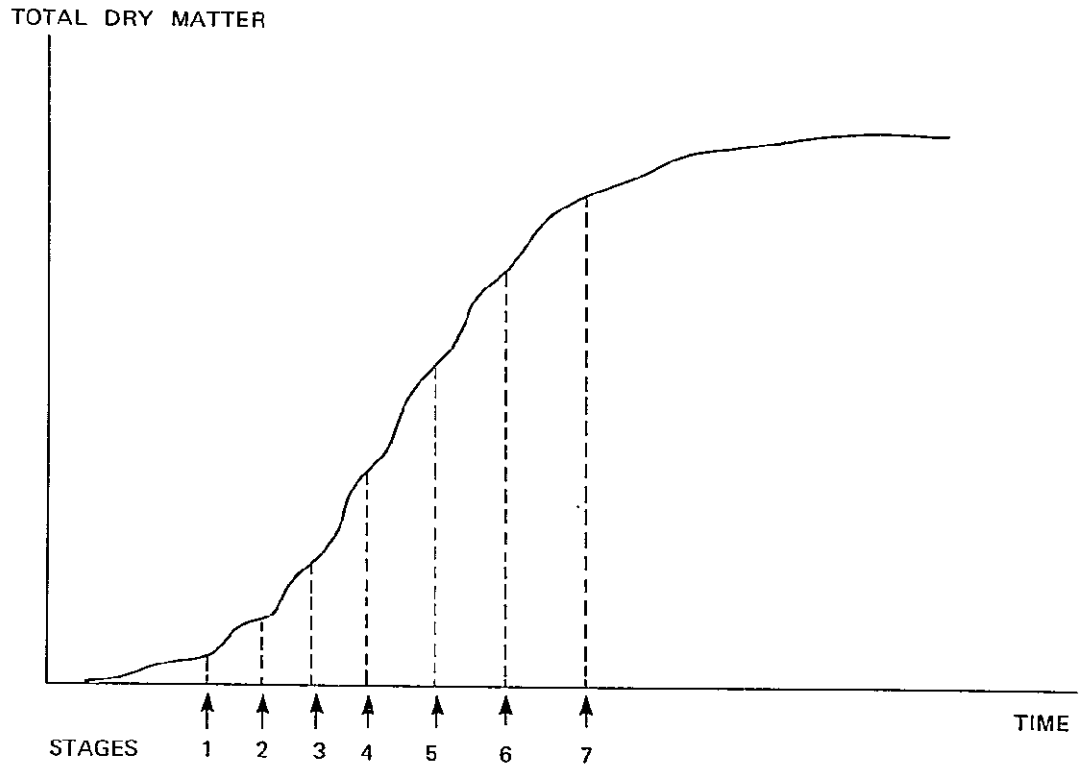

Fig. 71 - Theoretical growth curve of a plant with 7 development stages

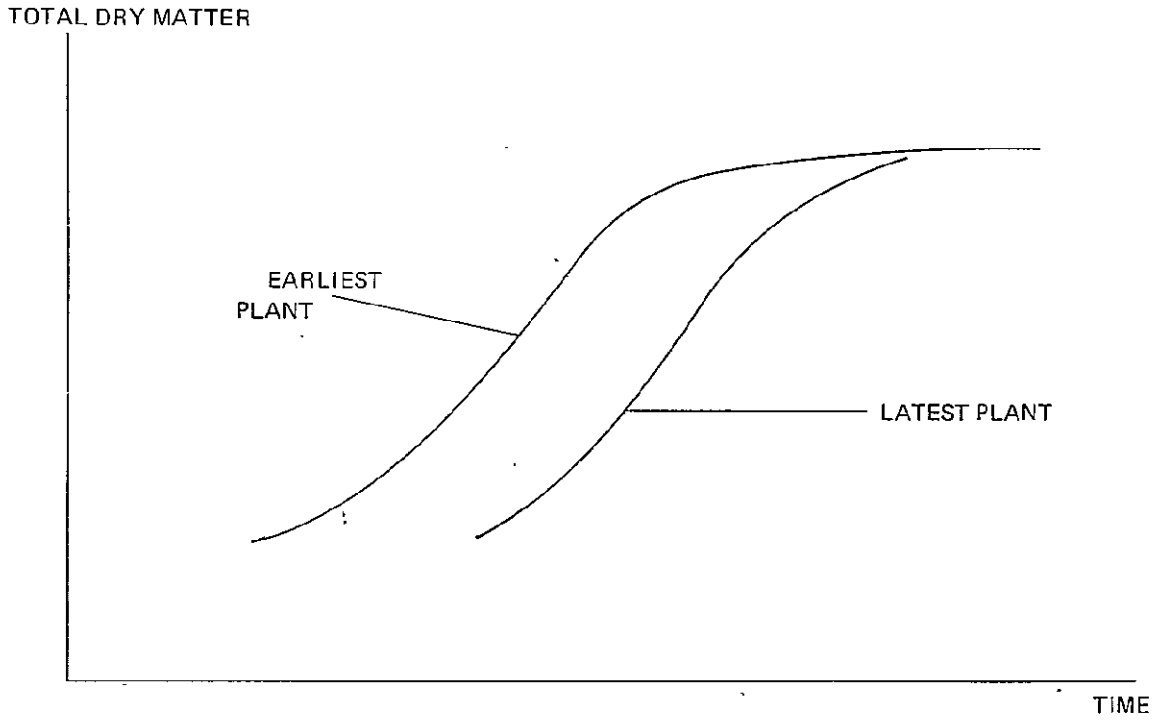

Fig. 72 - Growth curves of a plant population during a fast development phase

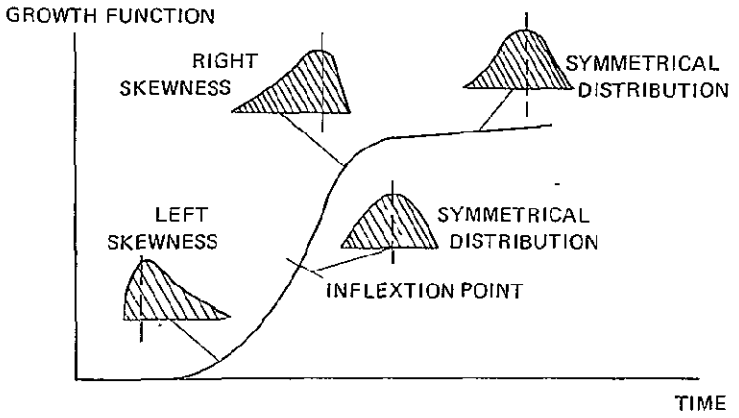

Fig. 73 - Theoretical evolution of distribution in a vegetal population during growth

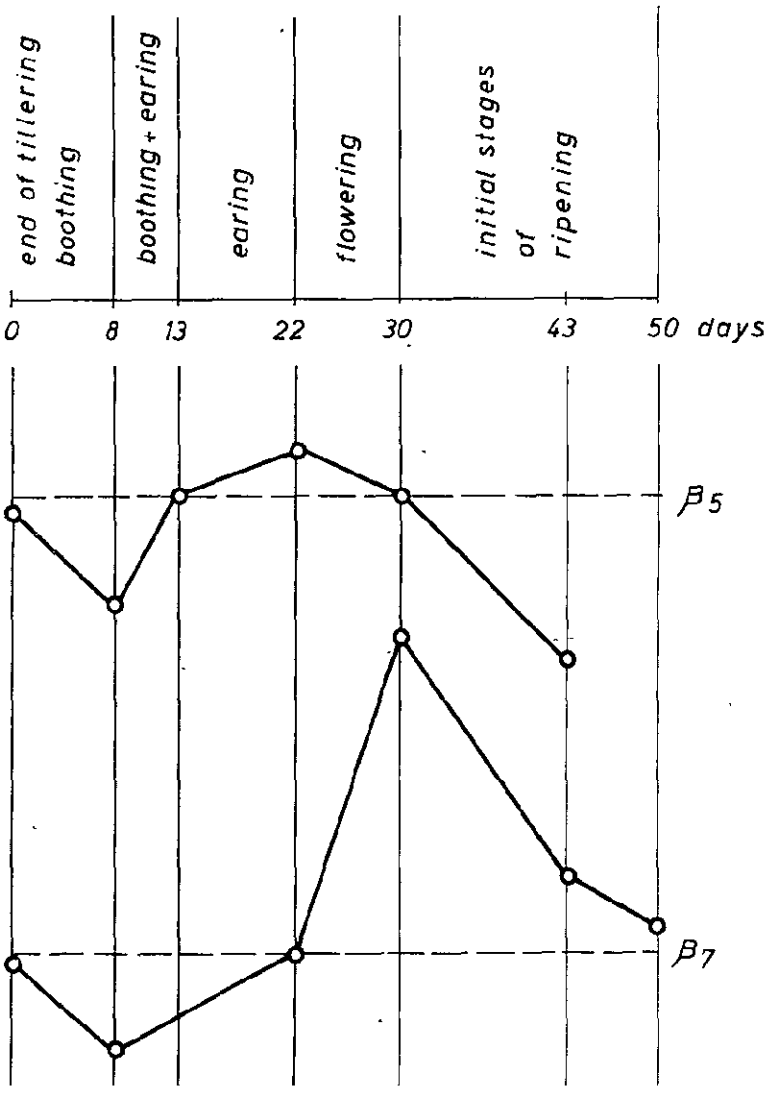

Fig. 74 - Evolution of Pearson coefficient for channels 5 and 7 versus different phenological stages of rice

physical measurement, such as reflectance, for which evolution rate would be the same as growth rate.
An attempt has thus been made to detect the stages of development in rice through the evolution of variance and skewness (Pearson's β_1) of reflectance.

5.2 Experimental results on an open field rice cultivation

During 1975, a measurement campaign was carried out in order to try a first validation of the model outlined in section 5.1.

For this purpose a rice field of the "Istituto Sperimentale per la Cerealicoltura" in Vercelli was subdivided into thirty ideal cells on which every week (from July to October) measurements of reflectance in the four LANDSAT channels have been performed on two points randomly selected on each cell, by means of an EXOTECH mod. 100 radiometer.

On the data collected (60 measurements each time), the following parameters have been calculated:

- mean value (μ),
- standard deviation (σ),
- Pearson coefficient ($\beta_1 = \left\{\frac{1}{N}\sum(x_i-\mu)^3\right\} / \sigma^3$) where x_i are measured reflectance values.

In Fig. 74 the values of the Pearson coefficient for channels 5 and 7 (β_5 and β_7) have been plotted against time in correspondence with different phenological stages. One can observe some peculiar coincidence in correspondence of well defined days, which are summarized in the following table.

Table 30 - Evolution in time of the Pearson coefficient

time	β_5	β_7
0	0	0
8	min	min
13	0	-
22/23	max	0
29/31	0	max
43/45	min	min

We note on Fig. 74 that the sequence of all the characteristic phenological stages connected with rice plant development produces either a change in sign or an inversion, or at least a slope change in the Pear-

son coefficient curves.

At this stage of the research it is not considered wise to try and enter into more detailed analysis on the basis of the few measurements performed at Vercelli in only a few large spectral bands. Nevertheless, it would appear that variability analysis is probably a very useful tool for the identification of rice phenological stages and hence a good start towards the determination of a time-dependent model of plant growth and development.

6. SUMMARY AND CONCLUSIONS

6.1 Visible and near-infrared reflectance of a rice culture exhibit a characteristic evolution in time in the course of plant development. This evolution of rice reflectance with time can be interpreted in relation to the modifications of cultural parameters (leaf area index, vegetation structure) induced by plant growth, and in relation to the phenological stages.

6.2 A seasonal model of rice reflectance can thus be drawn, which allows the identification, on a radiometric basis, of several important phenological stages. In particular, the reflectance ratio ρ_7/ρ_5 (or ρ_6/ρ_4) exhibits a sharp maximum in correspondence with earing.

6.3 Variations of a single cultural factor such as nitrogen fertilization, induce variations of the total rice biomass at harvest, which can be correlated closely to the values of the reflectance ratio at earing. When grain production itself is correlated to total biomass (in controlled conditions), prediction of yield can thus be achieved on the basis of reflectance data measured two months before harvest.

6.4 Variations of several cultural factors (such as the modes of planting and of nitrogen fertilization) induce variations of the vegetation structure which can be sensed by reflectance measurements. Since the type of vegetation structure developing at the beginning of the generative phase (booting) exerts a strong influence on grain production, a correlation between reflectance and rice production is thus likely to be found, making possible the prediction of yield on radiometric basis. A reflectance parameter adequate for such predictions is proposed here. It is based on the increase of the reflectance ratio occurring during booting, rather than on its maximum value reached at earing.

6.5 Several important phenological stages of a rice culture can be identified under normal field conditions on the basis of variability parameters (Pearson coefficient) of rice reflectance in visible and near-infrared light.

BIBLIOGRAPHY

External:

(1) COLWELL, J.E., "Grass Canopy Bidirectional Spectral Reflectance", Environmental Research Inst. of Michigan, Ann Arbor, Mich. (1973)

(2) KANEMASU, E.T., "Seasonal Canopy Reflectance Pattern of Wheat, Sorghum and Soybean", Remote Sensing of Environment, 3, p. 43-47 (1974)

(3) FEEKES, W., "De tarwe en haar milieu", Verslag XVII Techn. Tarwe Commissie, Groningen, 12, p. 523-588 (1941)

(4) SAEKI, T., KUROIWA, S., "On the Establishment of the Vertical Distribution of Photosynthetic System in a Plant Community", Bot. Mag. Tokyo, 72, p. 27-35 (1959)

(5) IDSO, S.B., JACKSON, R.D., REGINATO, R.J., "Remote Sensing of Crop Yields", Science, 196, p. 19-25 (1977)

(6) VINCENT, A., KOLLER, J., FARCY, E., SUTY, L., "Fonctionnement intégré du blé", Note de travail Stat. Amélior. Pl., Dijon, 30 p. (1976)

(7) BARLOY, J., "Rapport d'activité pour les années 1973-1975 (extraits du Rapport Général)", Laboratoire de Phytotechnie, Ecole Nationale Supérieure Agronomique de Rennes, 62 p. (1976)

(8) MALET, Ph., "Relations entre la vitesse de croissance et les paramètres statistiques dans des populations de mesures de croissance", Note interne INRA Bioclimatologie, Montfavet, 16 p. (1975)

Internal:

- CAVELIER, M., "Réponse spectrale d'une culture de riz irrigué à diverses fumures azotées", AGRESTE Project Report No. 17, JRC-Ispra Establishment (1975)

- AGAZZI, A., FRANZETTI, G., "Effects of Rice Biomass and Yield on Reflectance in the LANDSAT Channels", AGRESTE Project Report No. 15, JRC-Ispra Establishment (1975)

- CAVELIER, M., "Réflectance d'une culture de riz irrigué en fonction de quelques facteurs culturaux", Thèse de doctorat Agronomie, Univ. Cath. Louvain (1977)

- AGAZZI, A., MALET, Ph., RUSSO, S., "Utilization of the Spatial Variability of Reflectance for Rice Phenologic Stages Determination", COSPAR - W. Nordberg Memorial Symposium, Tel-Aviv, 8-10 June, (1977).

CHAPTER 3 - IDENTIFICATION OF RICE DISEASES

Contributor to the text:

DE CAROLIS, C. (IPV, Milan)

Scientific Collaborators:

BALDI, G. (ENR, Mortara)
KNOLL, G. (JRC-Ispra Establishment, post-graduate student)
LECHI, G. (LGL, Milan)

1. GROUND AND AERIAL INVESTIGATIONS OF RICE FIELDS

The aim of this research was the study of the spectral behaviour in the whole range, from Visible to Infrared, of rice fields under different health conditions. Particular attention was paid to a rice virus disease, called "giallume". The disease causes the yellowing of leaves, stunting, and therefore a serious underproduction of rice.

Before carrying out the multispectral investigation, 8 extended rice cultivation areas (about 100 ha altogether) were chosen. During the days before and after flying, each field was checked carefully, in order to know exactly the distribution and the variation of the parameters which might affect the measurements. The following field parameters were considered as being the most appropriate for the purpose of investigation: rice variety; shift of average vegetative status from the rice surrounding area; anomalies in nutritional status; eventual crisis due to transplanting or herbicides; transplanting areas or thinnings; algae infestation (distinguishing between green and blue algae, with or without algicides); weeds (distinguishing between large and narrow leaf infestant, with or without herbicides); aphids attack; "giallume" spots. The type of cultivation at the field boundaries, presence of any rice nurseries, uncultivated areas, rivers, trees, etc. were also noted down.

The scene of each field of the test site was periodically filmed with Nikon cameras equipped with Wratten filters Nr. 12, 21, 25, 87. Either Kodak-Aero 2443 Infrared Film or Kodak B/W 2424 Infrared Film were used. The results of these photographic surveys, carried out in a complete and systematic manner, revealed to be of little interest. A good chromatic contrast can help (better than that of normal panchromatic films) to distinguish between diseased and healthy rice spots.

Another series of measurements was performed, viewing the diseased rice spots from a 23 m high cherry-picker by means of an AGA-Mod. 680 thermocamera. The objective of this experiment was a) a knowledge of the thermal behaviour of rice spots infested by the disease, in particular with respect to the surrounding rice in the field, b) from these measurements - taken from pre-dawn to sunset - the determination of the day period when the maximum thermal contrast occurs between healthy and diseased rice; this allows one to choose the optimal time for flying with an airborne thermal scanner. These surveys revealed that the radiating power emitted by the diseased areas is greater than that from the healthy ones. The maximum thermal contrast is equivalent to some degrees of black-body temperature and was observed within the test-zones at around 1 o'clock in the afternoon. Up to now it is difficult to get quantitative results in terms of normal absolute leaf temperature, because we do not yet know the precise emissivity value, either for healthy or diseased rice.

Moreover, as far as the 3-5.6 μm band is concerned, an appreciable amount of reflected energy exists, and has been accurately detected. However, in this phase of research, we are more interested in the differential thermal behaviour than in the exact measurement of absolute temperature.

In a third phase of investigation, two near-infrared and two thermal aerial surveys were performed. A set of Nikon photocameras was employed using Wratten filters Nr. 12, 21, 25 with Kodak panchromatic colour films and Kodak-Aero 2443 Infrared films. This particular arrangement of cameras, filters and films, was the same as that used in the previously described ground surveys, thus allowing an accurate comparison of the results of the two different kinds of observations. Referring to the diseased areas (yellowish in the infrared film), we can easily distinguish them from thinnings and from healthy rice. This is quite important because it permits discrimination between the thermal contribution of water and that of the diseased rice, thus making correct interpretation of the AGA thermo-imagery possible.

A Daedalus Mod. DS/1220 scanner (dual channel) was employed for the thermal infrared aerial surveys. The flights were performed at 1500 m. a. s. l. The local atmospheric conditions caused an absorption of about 15%. In order to give a quantitative meaning to the thermographic strips interpretation, an analog electronics slicing device was designed and built. This slicer allows simultaneous discrimination between six contiguous voltage levels of the electrical signal driving the printer by means of which they are converted into six corresponding grey-levels on the film. The total amplitude of the six voltage levels is a constant and the resolution of the final description of the scene on the thermographic strip only depends on the amplitude of the input signal up to the limit of the scanner sensitivity. An improvement of the interpretation of the in-

formation was obtained by performing the same process in a colour composition. Some other analog elaborations were also performed, such as a) making the difference between the two channels, b) ratioing the channels, in order to investigate the emissivity variations, c) making the difference between the derivative and integral functions of one channel at a time, thus trying to detect small variations from the mean value of the phenomenon.

In conclusion, the set of photographic imagery allowed us to interpret correctly the AGA thermographs, mainly as far as the discrimination of the thermal contribution of water from that of the diseased rice was concerned. It has been verified, both on-ground and from aircraft, that the diseased rice areas behave like thermally anomalous areas. The order of magnitude of the increase in black-body temperature for the diseased rice areas in comparison to the healthy ones is the same as that observed by on-ground thermovision. This thermal contrast corresponds to some ^{o}C of black-body temperature. Results and conclusions such as those referred to the aforementioned example have been gathered for all the investigated rice zones infested by disease.

2. EVOLUTION IN TIME OF THE THERMAL BEHAVIOUR OF RICE AFFECTED BY THE "GIALLUME" DISEASE

This evolution was investigated under controlled conditions. A lysimeter with 5 cells, each of 2 x 2 m with a central separated area of 1 x 1 m was used. Ten days after the transplanting of rice plants, an affected plant carrying infected aphids was planted in the centre of three cells and the central square metre of each cell was covered with a fine-mesh gauze (Fig. 75). After 3 days the gauze was removed and all the cells were treated with insecticide.

The measurements started on the fifth day after the infection, one series at 13.00 h and one at 24.00 h (solar time) and were continued without interruption until the 19th day after the infection. For the measurements a cherry-picker was used on which an AGA-Thermovision Mod. 750 heat-camera and a photographic camera with normal colour films and infrared false colour films were installed.

The first symptoms of the disease were only noticed on the 13th day after the infection; there were no symptoms in the cells which were not infected. On the contrary, slight difference in the thermal behaviour of the central zone of cell No. 3 and the peripheral zone of cell No. 1 (both artificially infected) was already noted by the 7th day after infection. On the 9th day this difference was such as to show at least $2^{o}C$ thermal difference between the central "suspect" zone of cell No. 3 and the surrounding plants. The possible influence of the presence of water can be excluded, in that the significant measurements were made

at the time of maximum thermal contrast (13.00 h solar time).

On the other hand, the measurements at night time did not seem to exhibit such a significant thermal difference as the ones at day time. Thus the results of the previous experiments seem to be confirmed, with the addition of the possibility of "fore-warning" the progress of the disease.

3. EVALUATION OF THE DETECTABILITY OF DISEASED RICE BY MEANS OF SPECTRORADIOMETRIC TECHNIQUES

3.1 Spectroradiometric measurements on rice lysimeters

A series of spectroradiometric measurements was performed on some controlled rice lysimeters where the "giallume" disease had been deliberately inoculated. The measurements were made with an EG&G spectroradiometer, using a continuous wavelength variation in the range 0.4 - 1.0 μm. The disease was introduced into the lysimeters by means of a flying vector at the end of June. Radiometric observations were performed from July 7 to 15, when it was expected that the disease would diffuse in the lysimeter. Continuous spectral reflectances of different lysimeters on different days were obtained as well as reflectances in the four LANDSAT channels. Unfortunately, the disease did not attack all the infected lysimeters. Only one lysimeter (No. 18), presenting 7% of clerotic leaves, could be considered as really affected by "giallume".

From Fig. 76 one may compare the spectral reflectance of an infested (No. 18) and a non-infested (No. 19) lysimeter, both at the beginning of the measurement campaign (thin line) and at its end (thick line). It can be seen that the infested lysimeter presents a higher reflectance in the visible range (0.55 - 0.70 μm) and a lower one in the NIR range, than a non-infested lysimeter. These results are also reported in Table 31, where the integral reflectances in the four LANDSAT bands are shown for four lysimeters, of which only No. 18 was attacked by "giallume".

In order to extend the results obtained here under conditions of low infestation (7% of clerotic leaves) to normal conditions of higher impact of the disease, a theoretical investigation was performed on the basis of the Suits canopy model.

3.2 Theoretical investigation using the Suits canopy model

The Suits model[1] gives the directional spectral reflectance of a vegetative canopy. It is based on both geometric and spectral characteristics of individual components of the considered canopy. Input data for the mathematical model are:

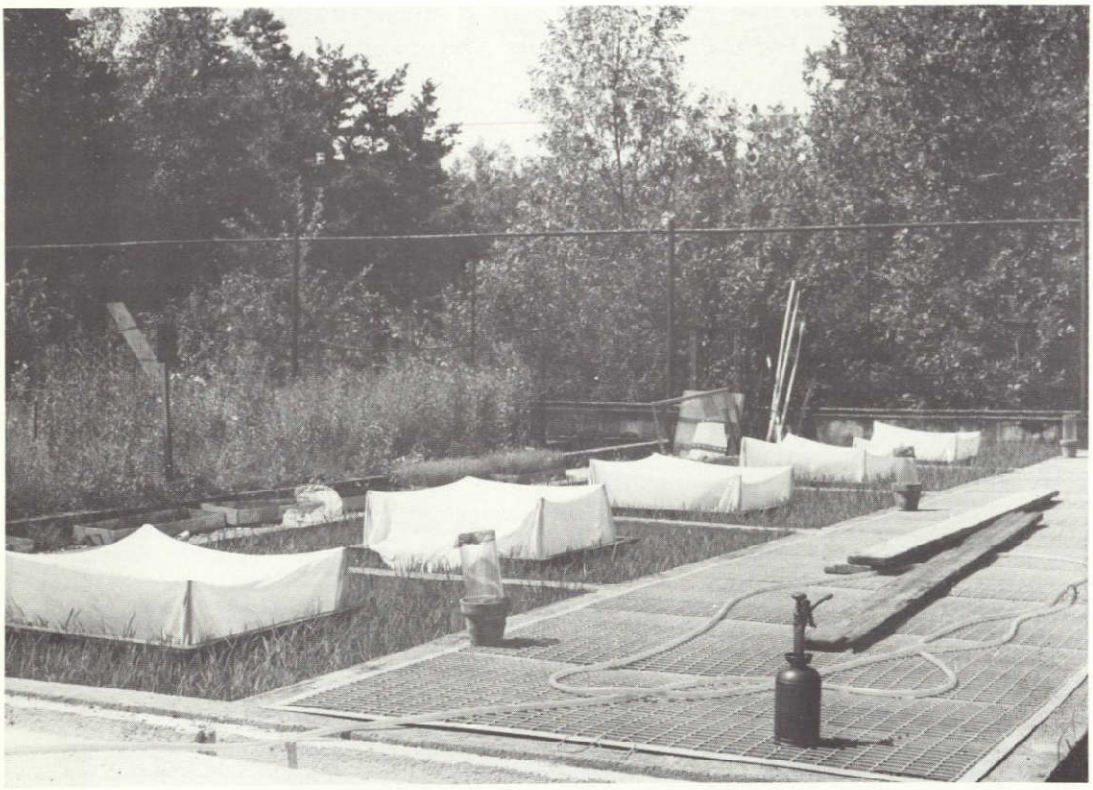

Fig. 75 - General view of the rice lysimeters used for inoculation of the "giallume" disease

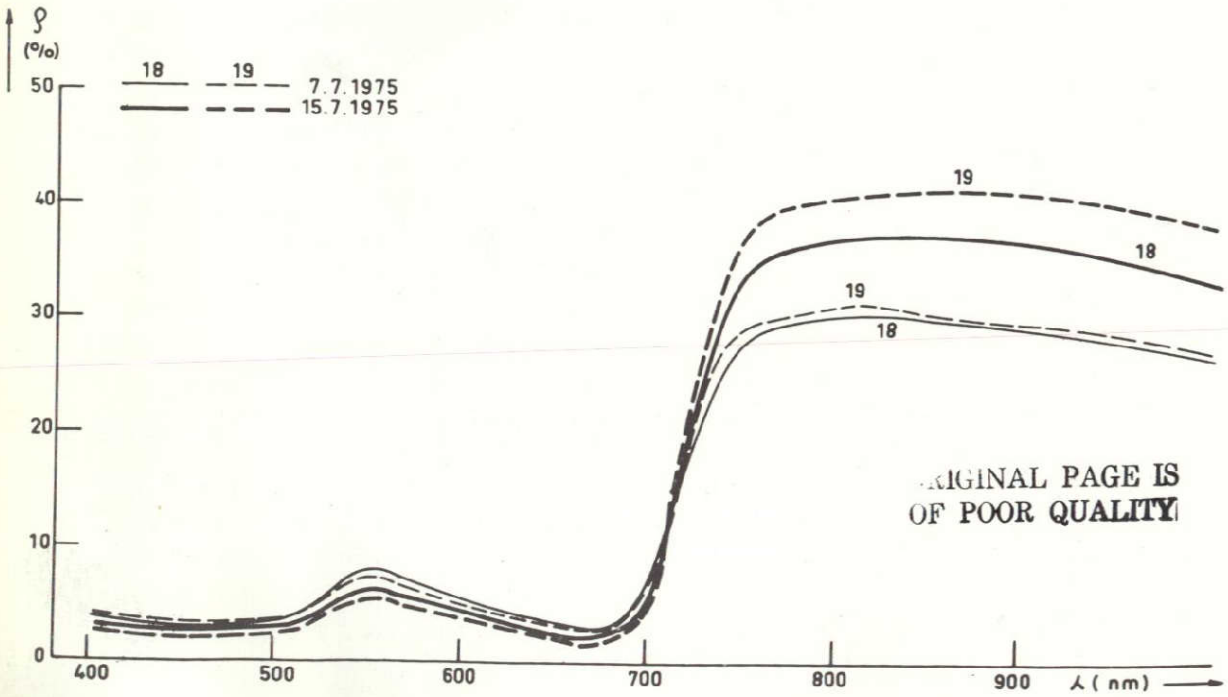

Fig. 76 - Measured spectral reflectance of rice lysimeters No. 18 and 19

Table 31 - Reflectance in LANDSAT bands 4, 5, 6, 7 for lysimeters 17, 18, 19, 20

7/7, 11, 15/75		Band 4	Band 5	Band 6	Band 7	Band 7/ Band 5
Lys. 17	7. 7.75	0.0570	0.0535	0.2631	0.3083	5.7626
	7.11.75	0.0574	0.0528	0.2839	0.3398	6.4317
	7.15.75	0.0478	0.0455	0.3324	0.4329	9.5212
Lys. 18	7. 7.75	0.0628	0.0570	0.2500	-0.2935	5.1507
	7.11.75	0.0657	0.0590	0.2708	0.3282	5.5577
	7.15.75	0.0534	0.0518	0.3036	0.3756	7.2562
Lys. 19	7. 7.75	0.0686	0.0542	0.2590	0.3006	5.5431
	7.11.75	0.0590	0.0510	0.2867	0.3404	6.6713
	7.15.75	0.0458	0.0432	0.3177	0.4086	9.4574
Lys. 20	7. 7.75	0.0595	0.0524	0.2453	0.2905	5.5464
	7.11.75	0.0560	0.0471	0.2616	0.3185	6.7559
	7.15.75	0.0441	0.0431	0.3365	0.4264	9.8996

Table 32 - Geometric characterization of lysimeters No. 18 and No. 19 (7.8.1975)

Lysimeter No. 18				
X	-14		-23	
CLASS I	0.05565	0.05928	0.05286	0.04725
CLASS II	0.00419	0.00446	0.00398	0.00356
CLASS III	0.0	0.0	0.00426	0.01970
Lysimeter No. 19				
X	-17		-25	
CLASS I	0.07173	0.09147	0.06813	0.07804
CLASS II	0.0	0.0	0.0	0.0
CLASS III	0.0	0.0	0.00487	0.02205

Note:

X level of layers (cm); 0 = top of canopy
CLASS I horizontal (left) and vertical (right) leaf area index of healthy leaves
CLASS II idem, of diseased leaves
CLASS III idem, of stalk

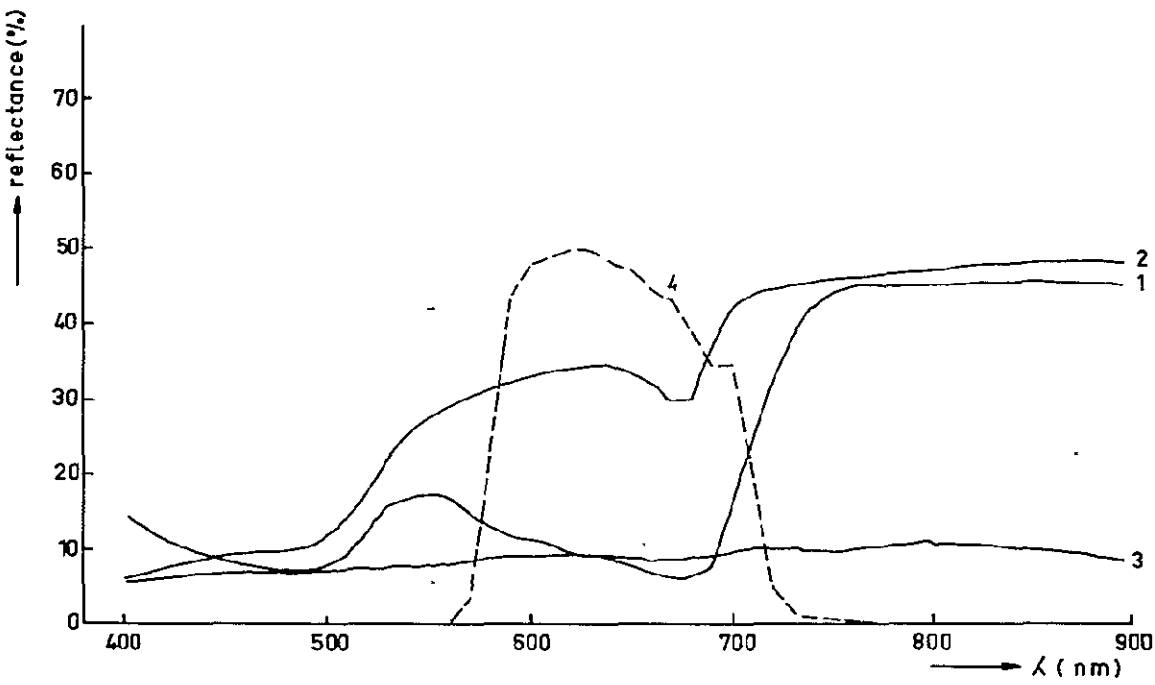

Fig. 77 - Diffuse reflectance of 1) green leaves, 2) yellow leaves, 3) water, 4) band-pass of LANDSAT band 5

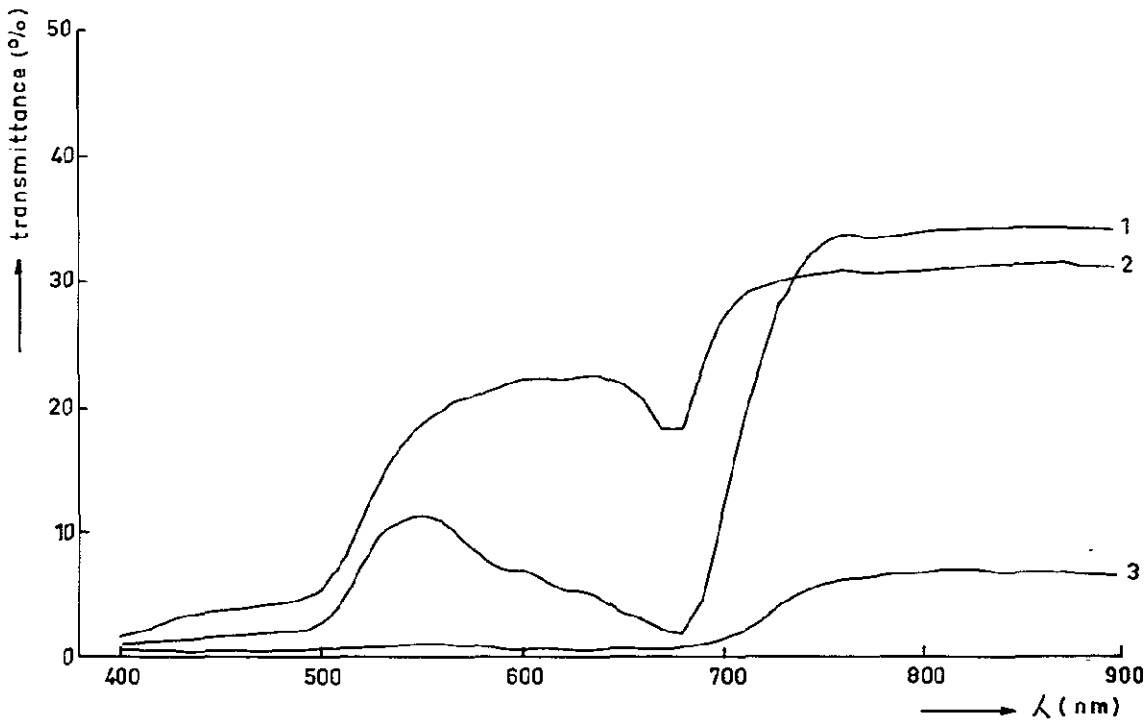

Fig. 78 - Transmittance of 1) green leaves, 2) yellow leaves, 3) stalk

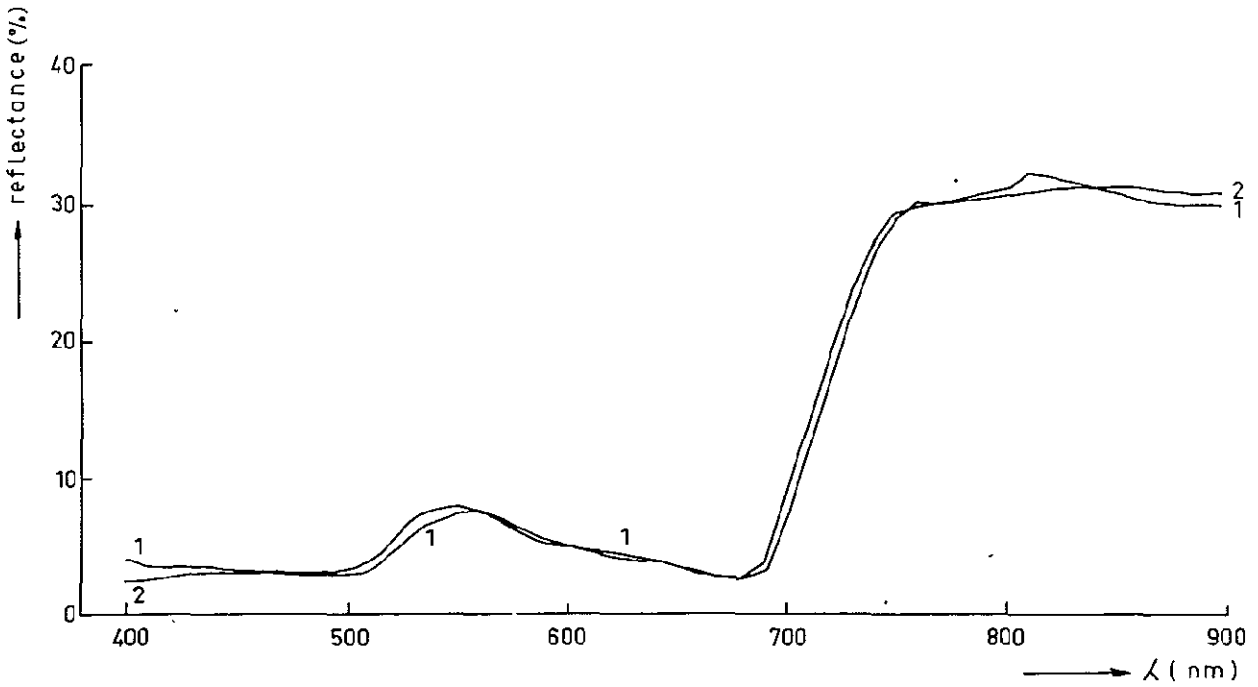

Fig. 79 - Comparison between calculated reflectance (2) and radiometric measurement of reflectance (1), disease 0%

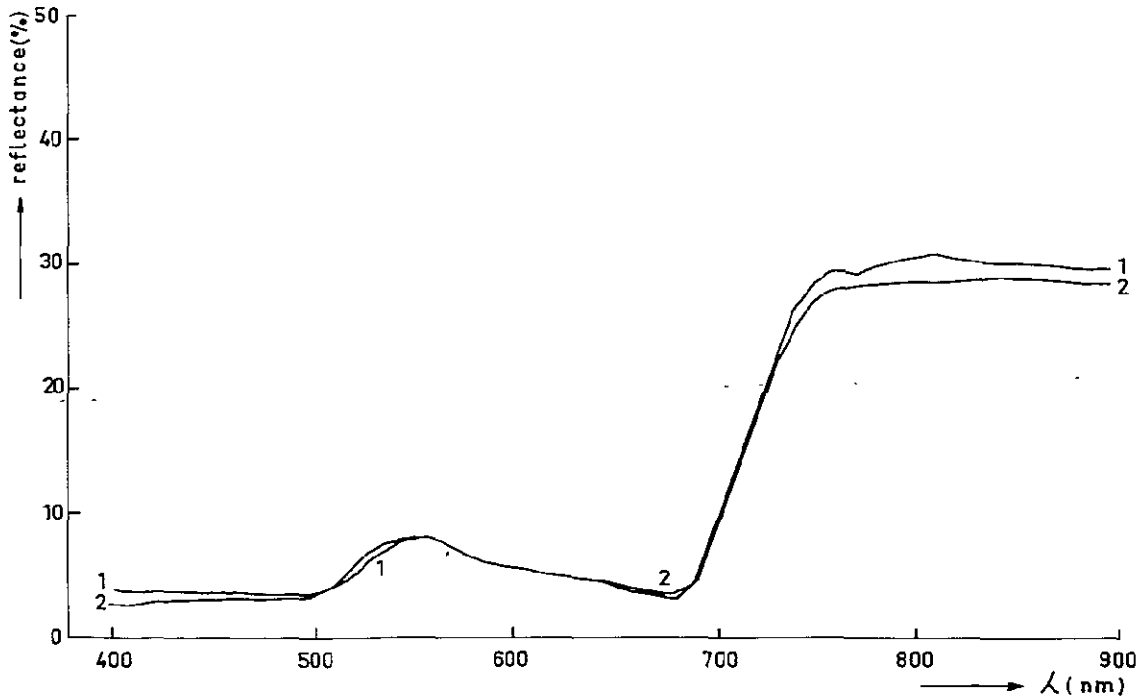

Fig. 80 - Comparison between calculated reflectance (2) and radiometric measurement of reflectance (1), disease 7%

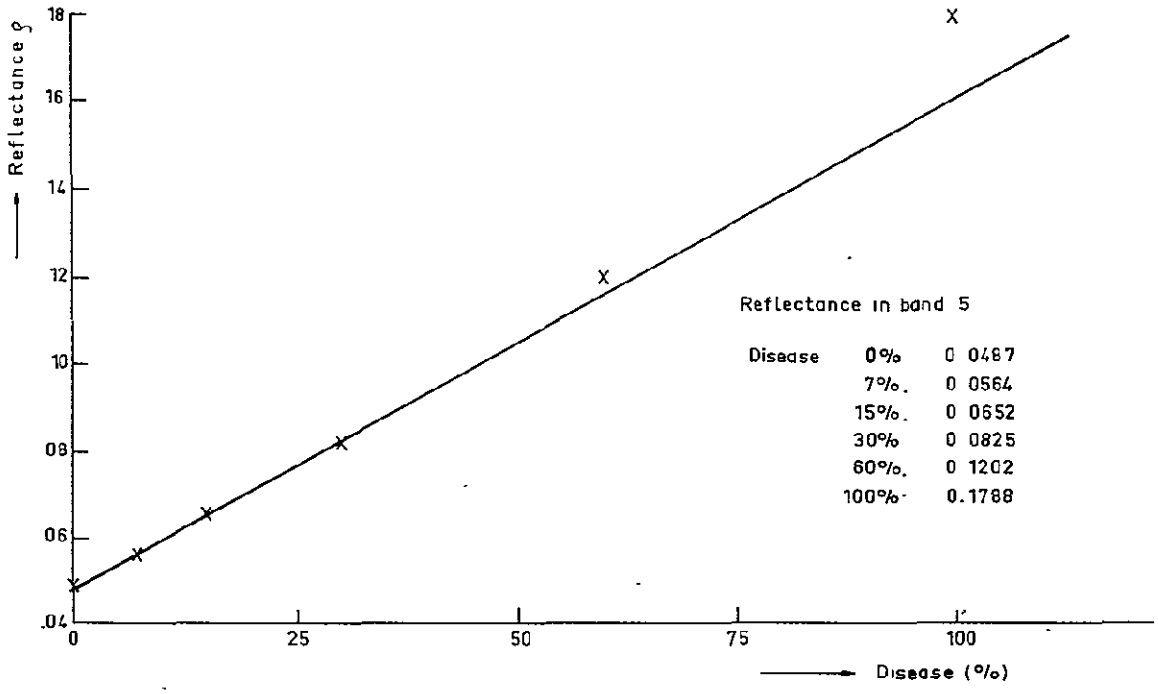

Fig. 81 - Reflectance in LANDSAT band 5 as a function of disease level

BIBLIOGRAPHY

External:

(1) SUITS, G. M., "The Calculation of the Directional Reflectance of a Vegetative Canopy", Mich. Symp., 1972, p. 117-125 (1972)

Internal:

- LECHI, G. M., DE CAROLIS, C., "Rilievi da terra e dall'aereo nell'infrarosso fotografico e termico su campi di riso affetti da "giallume"", Il Riso, 13, 1, p. 19-41 e 12, 3, p. 159-172 (1974)
- KNOLL, R., "Tatigkeitsbericht zu einem Studienaufenthalt", Agreste Project Report No. 29, Comm. Eur. Comm. JRC-Ispra Establishment, 26 p (1976)
- DE CAROLIS, C., BALDI, C., GALLI DE PARATESI, S., LECHI, G., "Thermal Behaviour of Some Rice Fields Affected by a Yellowing Type Disease", 9th Int. Symp. on Remote Sensing of Environment, Ann Arbor, Mich., April 1974.

CHAPTER 4 - IDENTIFICATION AND INVENTORY OF POPLAR GROVES

Contributors to the text:

FLOUZAT, G. (CESR, Toulouse)
MEGIER, J. (JRC-Ispra Establishment)

Scientific Collaborators:

CELLERINO, G-P. (ISP, Casale Monferrato)
DEJACE, J. (JRC-Ispra Establishment)
DORPEMA, B. (JRC-Ispra Establishment)
KOHL, M. (JRC-Ispra Establishment)
LAPIETRA, G. (ISP, Casale Monferrato)
MEHL, W. (JRC-Ispra Establishment)
STEIN, A. (JRC-Ispra Establishment)

Collaborators on the French Test Site:

The following collaboration from official and private organizations has been highly appreciated:

Mr BONITON (Coopérative Forestière de la Garonne, Toulouse)
Mr BOUISSOU (Service Régional d'Aménagement Forestier, Toulouse)
Mr de PIBRAC (Centre d'Etudes Techniques et Economiques Forestières)
Mr CABROL (Centre Régional de la Propriété Forestière de Midi-Pyrénées)
Mr CHARDENON (Secrétaire Général de la Commission Internationale du Peuplier)
Mr JARNY (Centre Régional de la Propriété Forestière)
Mr LAINEZ (Service Régional d'Aménagement Forestier, Toulouse)
Mr MONCHANT (Centre d'Etude Spatiale des Rayonnements)
Mr VIART (Centre Technique Forestier, Nogent/Vernisson).

The investigations reported in this chapter have been performed in a complementary way by the French and Italian Coinvestigators in the AGRESTE Project.

The processing of satellite data with a mean resolution applied to the study of ground objects of small dimensions, required as complementary operations, an accurate ground data collection together with the collection and processing of airborne flights data, in order to properly evaluate the obtained performances.

1. GROUND DATA COLLECTION

1.1 Test sites and ground truth preparation

Four Italian and French test areas have been investigated. The three Italian test areas, situated in the Po region in AGRESTE test site No. 1 (TA_1, TA_2 and TA_3) occupy surfaces of 40, 30 and 45 km^2 respectively. The French test area, situated in AGRESTE test site No. 5, has a length of 20 km along the Garonne Valley and a mean width of 1 km. These areas represent typical zones for poplar cultivation in Italy and Southern France, which assume a great importance for packing and wood pulp industries.

The relevant ground truth data were collected by two remote sensing aircraft flights which delivered infrared colour photographs at a 1 : 10,000 scale. These flights were performed in May 1975 over the Garonne Valley and in August 1975 over the Po region.

1.2 Interpretation and cartography

An exhaustive conventional photo-interpretation of all the poplar groves was made by research workers of the specialized institutes involved in the AGRESTE Project.

Following the criterion established by ISP, the poplar plantations of the Garonne Valley were subdivided into 4 classes corresponding to various ranges of ground coverage percentage, i.e.:

- Class 1 : 0 - 5% ground coverage
- Class 2 : 5 - 25% " "
- Class 3 : 25 - 75% " "
- Class 4 : more than 75% ground coverage.

The reference map obtained from such cartographic criteria is presented in Fig. 82.

In the case of the Italian test site, poplar groves were grouped in two comprehensive classes:

- Class A : young groves with ground coverage less than 25%
- Class B : intermediate and adult groves with ground coverage over 25%

and were reported on the available UTM map, scale 1 : 25,000.

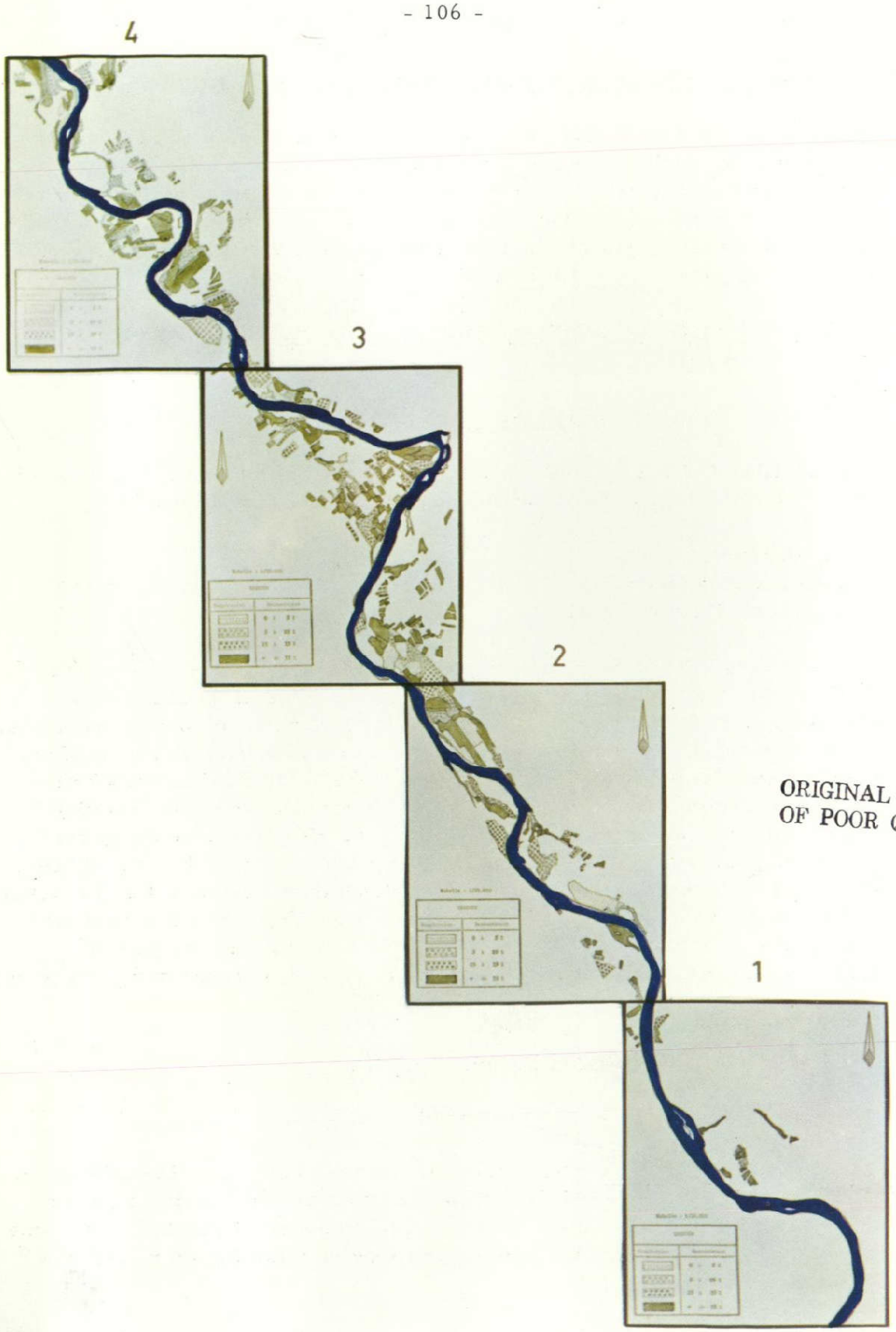

Fig. 82 - Reference map of poplar groves in the Southern part of test site No. 5 (Garonne Valley), scale 1:100,000

1.3 Relationship between coverage classes and age classes

Representative ground truth surveys were performed in order to establish the relationship between the poplar classes identified by aircraft remote sensing and the plantation age. Figs. 83 and 84 illustrate such relationship for the Po region and the Garonne Valley respectively. Comparison clearly points out the higher productivity of poplar groves under the ecological conditions of the Italian test areas.

2. IDENTIFICATION OF POPLAR GROVES BY LANDSAT IMAGERY

2.1 Monotemporal LANDSAT data analysis on the Garonne Valley

The LANDSAT-2 scene used for this investigation is that of July 7, 1975. The following classification methods were applied (see Appendix,4):

- rectangular method,
- barycentric method (BM),
- maximum likelihood (ML).

The most significant results obtained by the BM-method are presented in Fig. 85. The great difference between these classification results and the map reference (Fig. 82) is due to the fact that it was not possible, in the course of the sampling operations, to localize samples of poplars, spontaneous woodland and productive fruit-trees with sufficiently different spectral signatures. Therefore, all the areas covered by woodland vegetation are classified in one single group. Moreover, young poplar groves appear under very different aspects according to the soil upkeep. If ground is covered by high herbaceous vegetation, classes 1 and 2 seem to be older classes. No discrimination is thus achieved in the woodland vegetation (green in Fig. 85) for an adequate recognition of poplars. The discrimination of agricultural land (grey) and of water surfaces (blue) remains, however, satisfactory.

2.2 LANDSAT data analysis in the Po region

2.2.1 Particular conditions of the study

The dimensions of the poplar groves in the test areas considered, range from some hectares to 100-200 hectares, so that the training sets for classification had to be defined on reduced numbers of pixels (from some pixels to some tens of pixels) in order to avoid sampling on mixed pixels at the edges of the groves.

Another characteristic of the problem was that the retained training sets belong only to the forementioned class B; in fact, it was not possible to

Dimension classes	Plant age (years)											Ground Coverage
	1		2									< 25%
	2		2	3								
	3				4	5	6					25 - 75%
	4						6	7	8	9	10	> 75 %

Fig. 83 - Relationship between coverage classes and age, Po Valley

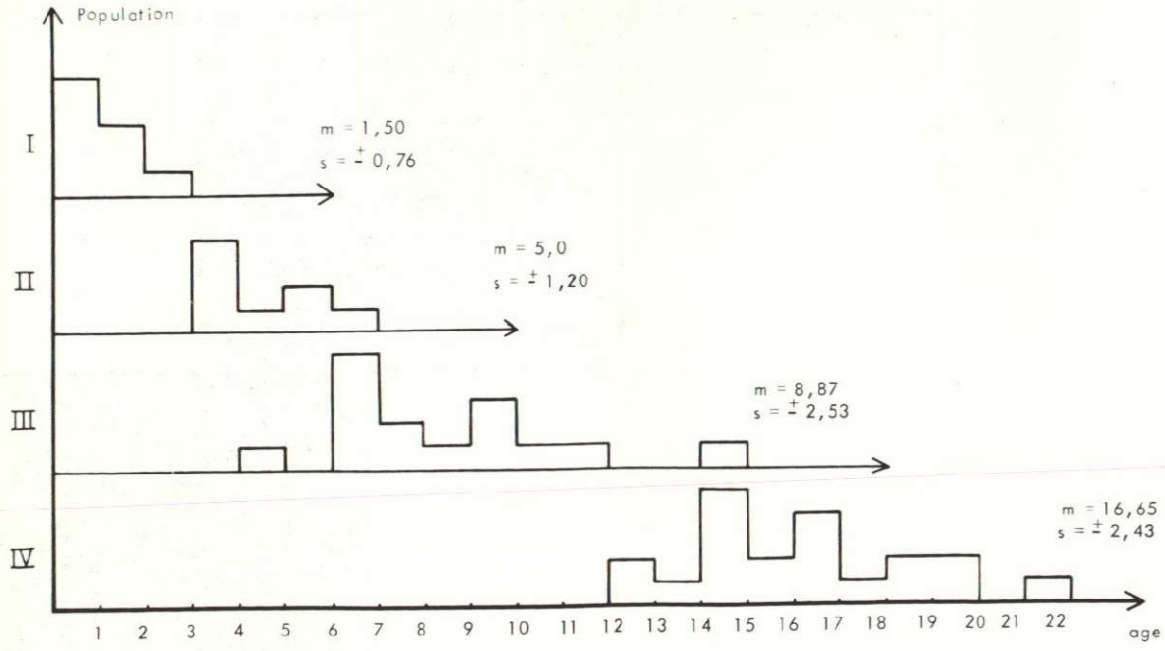

Fig. 84 - Relationship between coverage classes and age, Garonne Valley

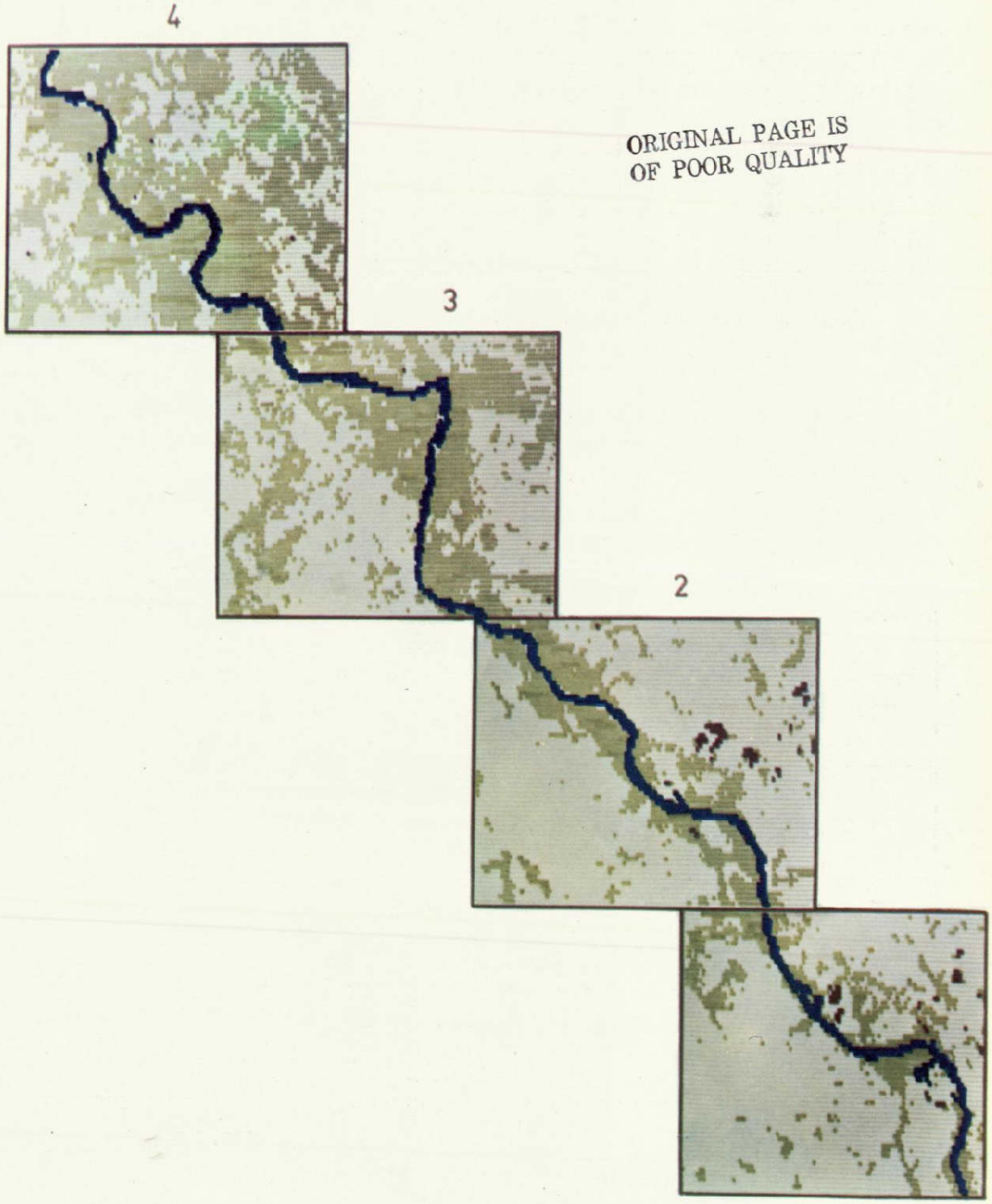

Fig. 85 - Classification results obtained from a monotemporal LANDSAT data analysis on the Garonne Valley (green: woodland vegetation without discrimination of poplars; grey: agricultural land; blue: water)

retain training sets for class A because the insufficient ground coverage causes too much dispersion in the data and hence in the classification results, owing to the great variability of the ground conditions. It must be noted, however, that, although recognition of class A would provide a valuable production forecasting, recognition of class B is sufficient for an evaluation of the amount of wood available for industrial needs. Actually class B contains about 90% of the total amount of wood present in the two classes and the whole amount of timber available each year for industry.

The last point to be stressed is that the ground truth document did not provide reliable information on ground coverage, other than poplar groves and water bodies. Three ways are open to overcome this difficulty:

- setting membership thresholds for the classes of interest in order to leave as unclassified the pixels which actually do not belong to these classes(1);
- using auxiliary classes defined by an unsupervised clustering process on the uncharacterized parts of the ground truth(2);
- using some "pseudo-classes" with wide variance, defined also on the uncharacterized parts of the ground truth, when the clustering process is not successful. In this last case, the pixels which actually do not belong to the classes of interest, are likely to be attributed to the "pseudo-classes" in the course of the classification process(3).

For the task of identifying poplar groves in flat areas, the last two approaches were found feasible (unlike what happened for inventory of natural forests in mountainous regions, see Chapter 6). They were therefore applied preferentially to the first approach in order to avoid the problem of defining thresholds for the various classes. Moreover, the second approach, which defines unidentified but homogeneous clusters of pixels outside the characterized zones of the ground truth, was found suitable for most of the cases.

2.2.2 Analysis of 1972-1973 data (preliminary results)

Some preliminary results have been obtained by using two LANDSAT-1 scenes of October 7, 1972 and May 10, 1973. The 1972 ground truth document was made for TA_1 where poplar groves are located along the Sesia river, close to the confluence with the Po river. For the year 1973, the area TA_2 was considered where poplar groves are situated in the vicinity of the Po river, about 60 km downstream from the first area.

A comparison was made between various classification methods and it was concluded that the maximum likelihood scheme (ML) used in a "supervised" context with normal parameters to describe the training classes, gave on the whole better and more reliable results (see Appendix, 4.2.2, DMAP).
The training sets were situated in both cases outside the part of the ground truth document utilized in the study.

The comparison between classification results and ground truth was done in a rough way in the case of data from October 7, 1972. It allowed, however, to ascertain that the bulk of intermediate and adult groves (class B) was actually recognized.

The various surfaces in the ground truth for the data of May 10, 1973 were evaluated and the surface percentage of ground truth document covered by poplars was compared to the classification results. Since the problem of superposition of small areas between ground truth and classification results was not yet solved, it was difficult to evaluate the amount of pixels wrongly classified as "poplar". The global result indicated, however, that about 70% of intermediate and adult groves (class B) were correctly recognized.

2.2.3 Analysis of 1975 data

2.2.3.1 Discrete ground truth construction

The ground truth document was established (according to the procedures described in section 1.2) on the TA_3 area situated also along the Po river, immediately to the North of the town Valenza. Such a reference map was then gridded into discrete elements corresponding to the LANDSAT pixels and stored on magnetic tape to be compared afterwards with the classification results. The gridding was done by following an iterative process between reference map and classification results for a given LANDSAT scene in order to ascertain the direction of the satellite scanning on the map and the location of some "one pixel" marks both on map and LANDSAT data. The interpreted areas were then obtained from the corresponding discrete contours (given as input) by running a contour-follower routine (see Appendix, DMAP). Obviously, as three different LANDSAT scenes over the same zone were utilized, the same pixel-to-pixel correspondence had to be established between the three individual scenes.

The overall accuracy of the superposition procedure is crucial for the reliability of the classification results, on account of the reduced dimensions of the individual areas studied, which can even be one pixel in size in extreme cases. In this situation it was decided to discretize the continuous document (ground truth on U.T.M. map) and deform it in order

The best overall results could be those given for the September 13 scene since 78.4% of poplars P_B and 52.2% of poplars P_A were correctly recognized. But on the other hand, it should be noted that although 57.7% (40.7 + 17.0) of the pixels classified as poplar actually belong to this category, 42.3% (4.4 + 37.9) do not. Some of these results are displayed in Fig. 87. Similar comments apply to the results of the other scenes.

The MED method provided very similar results, although lower by 1 to 4 units on the percentage figures, but with computing times reduced by a factor around 3.

2.2.3.3 Multitemporal analysis of the LANDSAT data

Three approaches were proved to combine the single processings at the three different dates (using the ML method) in order to increase the accuracy and the reliability of the results[4].

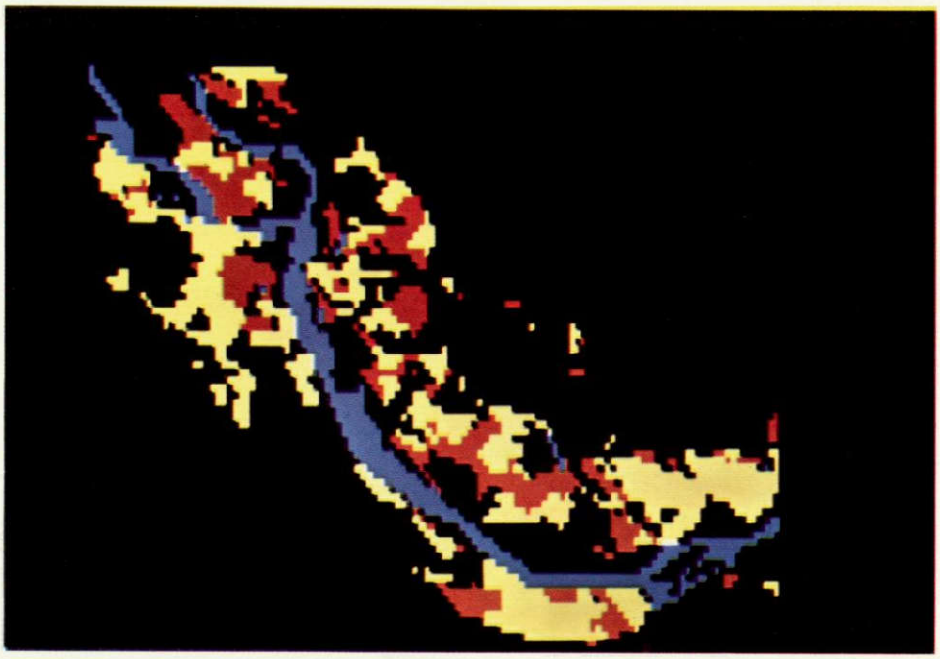

Fig. 86 - Discrete ground truth document for poplar groves, in 1975. Blue: Po River and other water bodies; red: young poplar groves (class A); yellow: intermediate and adult poplar groves (class B)

Improvements were obtained by combining the data of June 15 and September 13. No further improvement was achieved by incorporating also the data of July 3, probably because they are too much correlated to those of June 15 from the phenological point of view.

The first approach proves to minimize the misclassification in both di-

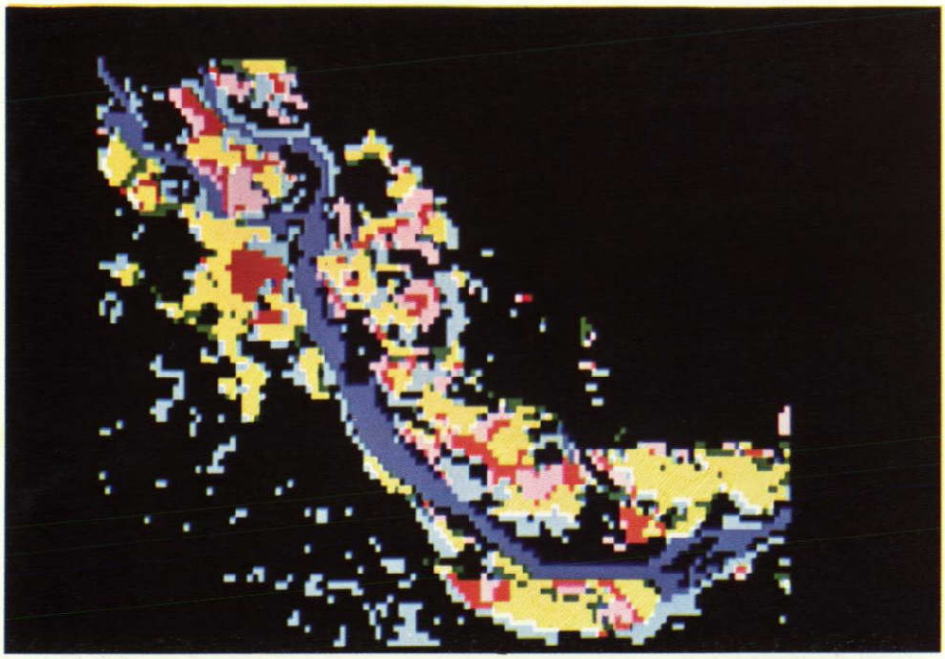

Fig. 87 - Classification results by ML method for the data of Sept. 13, 1975. Blue: water as on the ground truth; red: poplars of class A, well recognized; pink: poplars of class A, not recognized; yellow: poplars of class B, well recognized; green: poplars of class B not recognized; light blue: non-poplar items misclassified as poplars

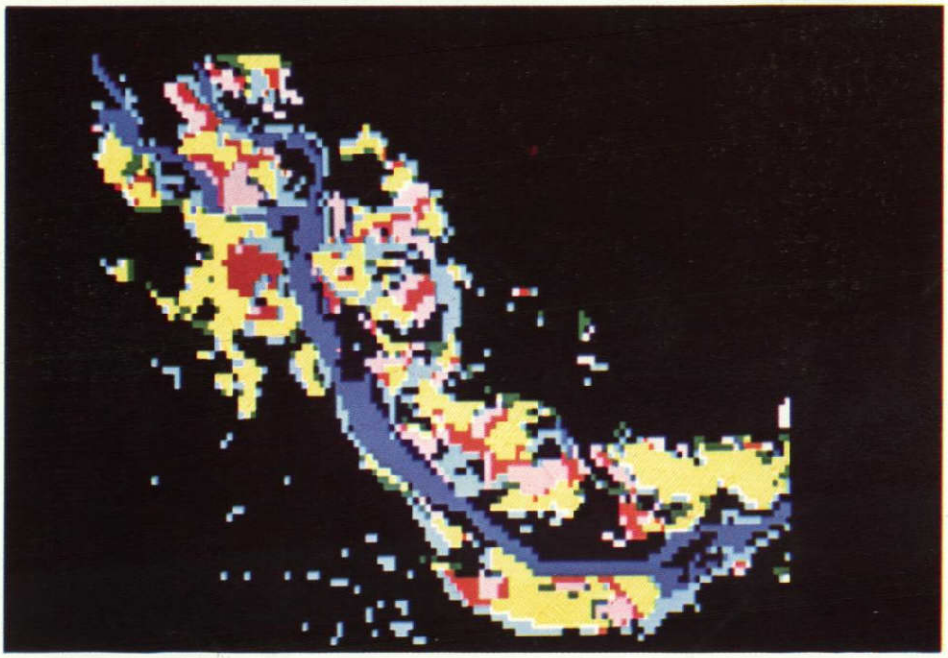

Fig. 88 - Results of multitemporal analysis using data of June, 15 and Sept., 13, 1975. The classification used the probability product scheme (Chapt. 4 - 2.2.3.3). Colours are as in Fig. 87)

rections (i.e. poplar classified as "non poplar" and "non poplar" classified as "poplar") by taking into account, in the combined processing, only the pixels classified in the same class in the separate processings. The result represents then the intersection of the successive classifications for the various classes (Table 36).

The second approach considers that the total amount of information available for the discrimination of the classes of interest, is present and integrated in the superposition, pixel-by-pixel, of the single data frames. The set of frames is then considered and processed as a single frame with 8 channel data from two LANDSAT scenes (Table 37).

The last method considered uses a probability scheme which attributes the pixel to be classified to the class for which the product of the membership probabilities for that class in each separate frame, is the highest (Table 38 and Fig. 88).

Ground-truth \ Class	W	P	R
W	54.4	9.7/ 3.6	35.9
P_A	0.9	28.9/14.9	70.2
P_B	0.3	65.8/54.0	33.9
R	1.4	8.1/27.4	90.5

Table 36 : Results (%) for intersection between scene 6/15 and scene 9/13
PCL/PGT = 75%
W: water; P: poplar of classes P_A and P_B; R: rest

Ground-truth \ Class	W	P	R
W	61.7	27.0/ 6.6	11.4
P_A	1.8	49.1/16.7	49.1
P_B	0.4	79.0/42.7	20.6
R	2.0	15.3/34.0	82.7

Table 37 : Results (%) for superposition of scenes 6/15 and 9/13
PCL/PGT = 113%
W: water; P: poplar of classes P_A and P_B; R: rest

Ground-truth \ Class	W	P	R
W	70.8	16.4/ 4.2	12.8
P_A	2.1	49.4/17.7	48.5
P_B	0.5	80.8/45.9	18.8
R	3.3	13.7/32.2	83.0

Table 38 : Results (%) for probability products for scenes 6/15 and 9/13
PCL/PGT = 108%
W: water; P: poplar of classes P_A and P_B; R: rest

Results of the three forementioned approaches can be summarized as follows:

- The "intersection" method reduces very much the number of misclassifications in the sense "non target" classified as "target", but at the same time it increases too much the misclassifications "target" classified as "non target".

- The "superposition" method reduces, on the whole, the misclassifications in both senses.

- The "probability product" method has the same effects, with slightly better results, than the superposition method; it is moreover better adapted in a "supervised" context because of the higher degree of freedom allowed in the choice of the training sets for each individual scene.

- bud stage : no discrimination possible,
- first leaves stage : efficient discrimination is achieved,
- full foliage stage : little discrimination is achieved.

Visualization of the results is given in Fig. 89, indicating that possibility of discrimination is clearly dependent on the phenological stage considered. Two performance matrices, established for 90 fields, allow to estimate the real performances obtained on the two last phenological stages. They are presented in Tables 39 and 40, by comparison between the number of fields occupied by various clones and the field aspect on IRC photographs.

Table 39 - Performance matrix of clone discrimination at full foliage stage (in number of fields)

clone aspect	I 214 Robusta	Others	Total
red	68	7	75
brown	2	13	15
total	70	20	90

Examination of Table 39 confirms that little discrimination is achieved at the full foliage stage; in particular, the two important clones I 214 and Robusta are not discriminated.

Table 40 - Performance matrix of clone discrimination at the first leaves stage (in number of fields)

clone aspect	I 214	Others	Robusta	Total
red and light-red	34	6	5	45
mixed	6	4	1	11
grey-green	2	10	22	34
total	42	20	28	90

On the contrary, at the first leaves stage (Table 40), a good correspondence is obtained between two aspects and the two important clones.

IRC photograph

date: March, 25
scale: 1 : 9,500

Phenological stage: first leaves

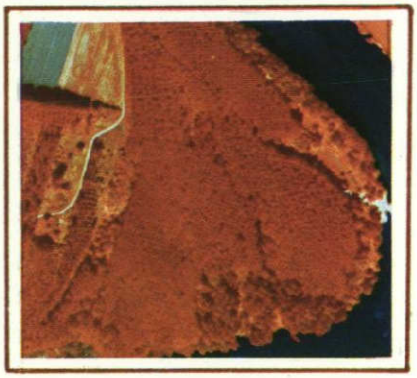

IRC photograph

date: May, 5
scale: 1 : 10,000

Phenological stage: total foliage

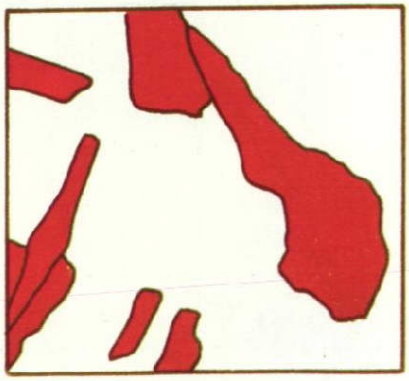

Ground Map

Localization of I 214 plantations

Scale: 1 : 10,000

Fig. 89 - Clonal identification of poplar in the Garonne Valley

Expressed in percentages, discrimination amounts to 81% for I 214 and to 79% for Robusta. According to these results, these two clones would occupy 38% and 25% of the total number of fields respectively, whereas the actual figures are somewhat higher (47 and 32% respectively).

The clonal discrimination of the two most important clones of poplar seems therefore likely to be achieved by IRC photographs taken at an adequate phenological stage.

4. INVENTORY OF POPLAR GROVES IN THE GARONNE VALLEY

4.1 Global Inventory

A "global" inventory (i.e. that does not take into account the various varieties cultivated in the area) was performed on the basis of the data provided by the map study (Fig. 82). This inventory might be compared with statistics of the Government Services. It concerned the 4 sections of the cartography and was threefold:

- quantitative inventory of the number of fields (Table 41),
- quantitative inventory of planted surfaces (Table 42),
- distribution of the various cover classes in the 4 sections (Table 43).

The significance of the total poplar surfaces is evident from their contribution (550 ha) in the 20 km^2 area of test site No. 5.

Table 41 - Quantitative inventory of the number of poplar fields (Garonne Valley)

Classes / Sections	I	II	III	IV	Total	%
1	0	1	3	14	18	4.2
2	10	14	17	27	68	15.8
3	22	24	50	97	193	44.7
4	13	15	37	87	152	35.3
Total	45	54	107	225	431	100
%	10.4	12.5	24.8	52.2	100	

Table 42 - Quantitative inventory of poplar surfaces (Garonne Valley)

Classes / Sections	I	II	III	IV	Total	%
1	0	1.68	3.12	13.44	18.24	3.3
2	34.44	27.76	36.44	50.92	149.56	27.2
3	28.64	21.64	49.48	100.56	200.32	36.4
4	10.88	34.72	36.16	100.80	182.56	33.1
Total	73.96	85.80	125.20	265.72	550.68	100
%	13.4	15.6	22.7	48.2	100	

Table 43 - Distribution of the poplar cover classes in the 4 test sections (Garonne Valley)

Classes / Sections	I	II	III	IV	Total
1	0	9.2	17.1	73.7	100
2	23.0	18.6	24.4	34.0	100
3	14.3	10.8	24.7	50.2	100
4	5.9	19.0	19.8	55.2	100

4.2 Clonal inventory

The phenological identification of the two principal clones was complemented by the estimation of the percentage of fields occupied by different cultivated varieties in the mapped zone of ground data collection (Fig. 82). This part of the study necessitated a survey performed with the help of documentation foresters of Regional Forestry Services.

Two main clone classes are considered outside the two principal clones: mixed fields (I 214 + Robusta) and the clone 45-51. Other cultivated varieties have a scarce importance (Fritzi-Pauley, Carolin, Alabama) or one localized on experimental fields (F_2, ONDA-72/51, Poitou Serotina,

Alcinde-5/2, TC-39).

Results of the survey are presented on Table 44 for the four mapped sections. They indicate an absolute predominance of the two clones I 214 and Robusta, mainly as monoclonal fields (80%) and partly as mixed fields (12%).

Table 44 - Distribution of the different cultivated varieties (in percentages of the total number of poplar fields)

Cover classes / Cultivars	I	II	III	IV	Total
I 214 (I)	5.1	5.1	12.3	25.4	47.9
Robusta (R)	2.2	1.4	11.6	17.4	32.6
Mixed (I) + (R)	2.9	0	5.1	3.6	11.6
45 - 51	1.4	1.4	0	0	2.8
Various	1.4	0	2.2	1.4	5.0

5. CONCLUSIONS

5.1 Discrimination of poplar groves from other deciduous formations is not always satisfactory with LANDSAT-2 data. When identification is possible, one may obtain a good estimation of the surfaces occupied by older age classes but an uncertainty subsists for younger classes because of their scarce rate of soil coverage.

5.2 A multitemporal analysis of LANDSAT data improves the classification results and allows a good identification of the productive classes of poplar.

5.3 The clonal identification is possible with colour infrared photography if the date of image is chosen at a significant phenological stage. The best results seem to be obtained during the first leaves stage.

BIBLIOGRAPHY

Internal:

(1) DEJACE, J., "Inventaire des hêtraies dans une région des Alpes Maritimes italiennes à partir des données du satellite LANDSAT", Coll. sur l'utilisation des Satellites en Télédétection, Paris, Sept. 1977

(2) DEJACE, J., MEGIER, M., MEHL, W., "Computer-aided Classification for Remote Sensing in Agriculture and Forestry", 11th Int. Symp. on Remote Sensing of Environment, Ann Arbor, Mich., April, 1977

(3) MEGIER, J., "Classification automatique des données du satellite LANDSAT appliquée à agriculture et sylviculture", Cinquièmes Journées d'Optique Spatiale, Marseille, Oct., 1975

(4) MEGIER, J., "Multitemporal Digital Analysis of LANDSAT data for Inventory of Poplar Planted Groves in N. Italy", Int. Symp. Image Processing, Graz, Austria, Oct., 1977

(5) FLOUZAT, G., DAGNAC, J., "Première partie de la cartographie des peupleraies de la moyenne vallée de la Garonne", National Technical Information Service. Weekly Abstracts, NASA Earth Resources Survey Program, NASA-CR-146822, July 5, 1976

(6) FLOUZAT, G., "Comparaison et première interprétation de différentes données de télédétection sur une même zone de peupleraies", National Technical Information Service. Weekly Abstracts, NASA Earth Resources Survey Program, NASA-CR-146822, July 5, 1976.

CHAPTER 5 - PREDICTION OF POPLAR TIMBER PRODUCTION FROM AIRBORNE REMOTE SENSING

Contributor to the text:

FLOUZAT, G. (CESR, Toulouse)

Collaborators on the French Test Site:

The following collaboration from official and private organizations has been highly appreciated:

Mr BONITON (Coopérative Forestière de la Garonne, Toulouse)
Mr BOUISSOU (Service Régional d'Aménagement Forestier, Toulouse)
Mr de PIBRAC (Centre d'Etudes Techniques et Economiques Forestières)
Mr CABROL (Centre Régional de la Propriété Forestière de Midi-Pyrénées)
Mr CHARDENON (Secrétaire Général de la Commission Internationale du Peuplier)
Mr JARNY (Centre Régional de la Propriété Forestière)
Mr LAINEZ (Service Régional d'Aménagement Forestier, Toulouse)
Mr MONCHANT (Centre d'Etude Spatiale des Rayonnements)
Mr VIART (Centre Technique Forestier, Nogent/Vernisson).

This part of the research has been performed in the Garonne Valley on the basis of a methodology set up by the French Co-investigators in the AGRESTE Project and of the exhaustive ground truth available.

It appears as complementary to the results exposed in the last chapter on the inventory of poplar groves.

1. GLOBAL PREDICTION OF AVAILABLE TIMBER

A "global" prediction (i.e. that does not take into account the various varieties cultivated in the area) is performed on the basis of the data of Tables 41, 42 and 43 provided by the map study.

A relationship must first be established by a representative ground truth survey, between plantation age and the poplar classes identified by airborne remote sensing. Fig. 84 did illustrate this relationship for the 4 classes. Analysis of this figure allows to consider the following theoretical bases in the prediction study:

- timber product of class 4 will be cut during the 6 years after remote sensing survey,
- age of class 3 extends over 6 years,
- age of class 2 extends over 3 years,
- age of class 1 extends over 3 years.

On the other hand, IRC photographs used for the collection of ground truth data (see Chapter 4, section 1.1) allow to measure plantation density for the 4 classes and therefore to estimate the corresponding number of trees.

From the quantitative inventory of poplar surfaces (Table 42), the forementioned data allow then a global prediction of available timber to be made (Fig. 90). This prediction, performed over a 18 year period after the remote sensing survey, concerns the poplar surfaces, the age of groves, the mean density and the total number of trees which will be available during 4 successive subperiods. If the exploitation of poplars is constant during a single subperiod, the data of Fig. 90 may be expressed per year as far as mean surfaces and number of trees are concerned (Fig. 91).

These data show that available timber will sharply decrease after 1980, as a consequence of the increase, in the last 10 years, of the extension of corn fields situated in the same ecological conditions. However, a relative recovery of planting is noted in the last few years.

In spite of a lesser accuracy, if compared to ground inventories, such a methodology study presents the advantages of rapidity of execution over an extended zone and of its possibility to be generalized to all poplar plantations. Therefore, it can be considered as a promising tool for land-planning purposes.

2. PREDICTION OF TIMBER AVAILABLE FROM VARIOUS CLONES

The data of the survey described in Chapter 4, section 4.2 (clonal inventory) allow to obtain from IRC imagery an estimation of the cover percentages for the various clones. Since such a study does not allow to change the threshold ages between the various cover classes given by Fig. 84, the same relationship is used for predicting timber production of the different cultivars.

Results are presented in Fig. 92 for I 214, in Fig. 93 for Robusta and in Fig. 94 for other clones. One notes from the first two figures the same general decrease in time noted in the global prediction (Fig. 90). This is a logical consequence of the predominant contribution (more than

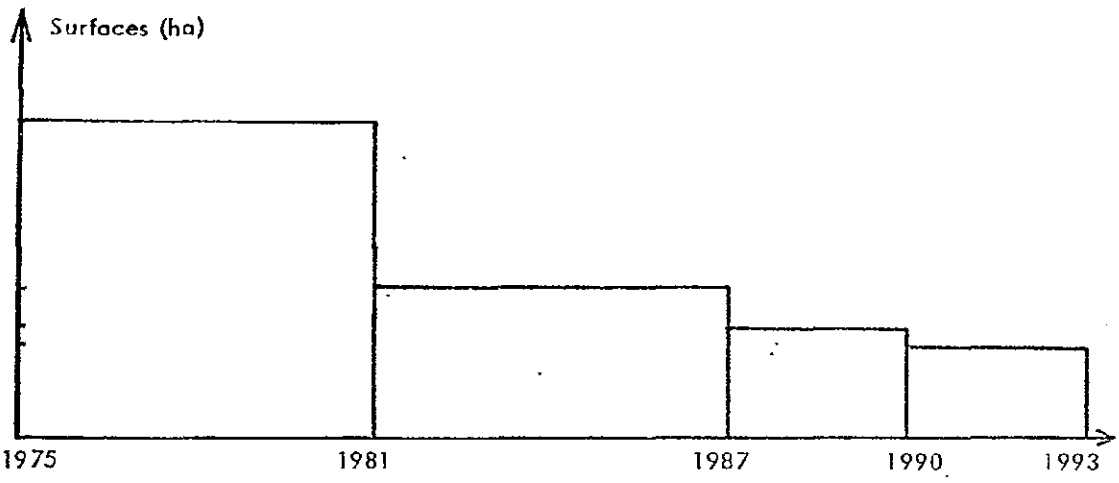

Class	IV	III	II	I
Age	more than 13 years	12 - 11 - 10 - 9 - 8 - 7 -	6 - 5 - 4 -	3 - 2 - 1
Density	312	276	282	267
Trees	82 900	34 500	24 200	20 000

Fig. 90 - Global forecast of available timber

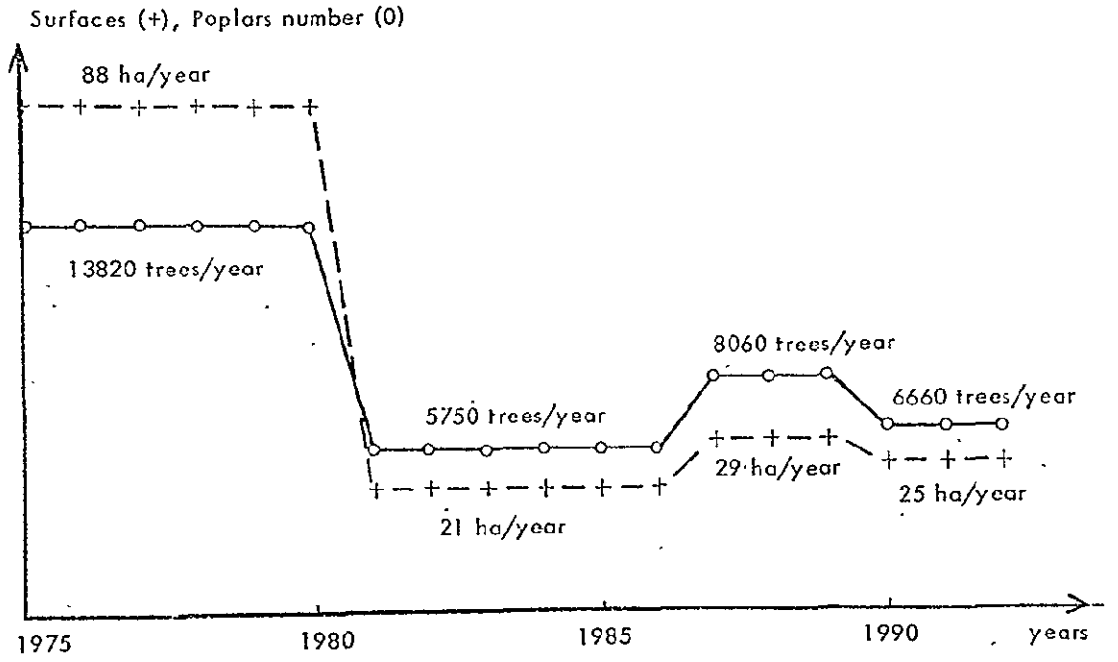

Fig. 91 - Global forecast of available timber/year

80%) of the two clones I 214 and Robusta in the total poplar area. The more stable pattern exhibited by Fig. 94 for the other cultivars (with a less than 20% contribution) cannot modify the general trend.

3. BIOMETRIC EVALUATION OF STANDING TIMBER VOLUME

3.1 Principle

The estimation of standing timber volume is done by elaboration of relationships between biometric characteristics of the studied trees and a remotely measurable parameter.

In the case of poplar groves, the remotely measurable parameter is the percentage of vegetation cover to the ground. Its measurement could be obtained by three different methods: microdensitometry, photogrammetry and model comparison. Microdensitometry has been adopted because the measurement covers a large area of the field and provides therefore more significant values.

From the cover percentage, the mean crown surface (CS) can be computed in relation with the plantation mode and the density of poplars in the field. It is this computed parameter which is used to be connected with a tree characteristic allowing the evaluation of the standing timber volume. The circumference at 1.30 m level (C) has been retained as such a biometric parameter. Therefore, it is necessary to know the C-variation in relation to CS. For realizing this objective, C-measurements were made on the ground on the same fields where CS-measurements were performed with IRC photographs.

The following ground data were collected on two sampling areas:

- cultivated variety,
- circumference (1.30 m),
- cover percentage.

This information is completed with plantation density, mode and age.

3.2 Theoretical model (maquette) and simulation

The choice of microdensitometry as the method of cover measurement induces to assess the system performances under the conditions used for the image processing (IRC photographs at a scale of 1 : 10,000). For this purpose a theoretical model was built. It reproduces at a scale 1 : 10,000 various plots where the crowns coincide in most cases with circles (see Fig. 95). Characteristics of cover percentage, plantation mode and density are known with good accuracy.

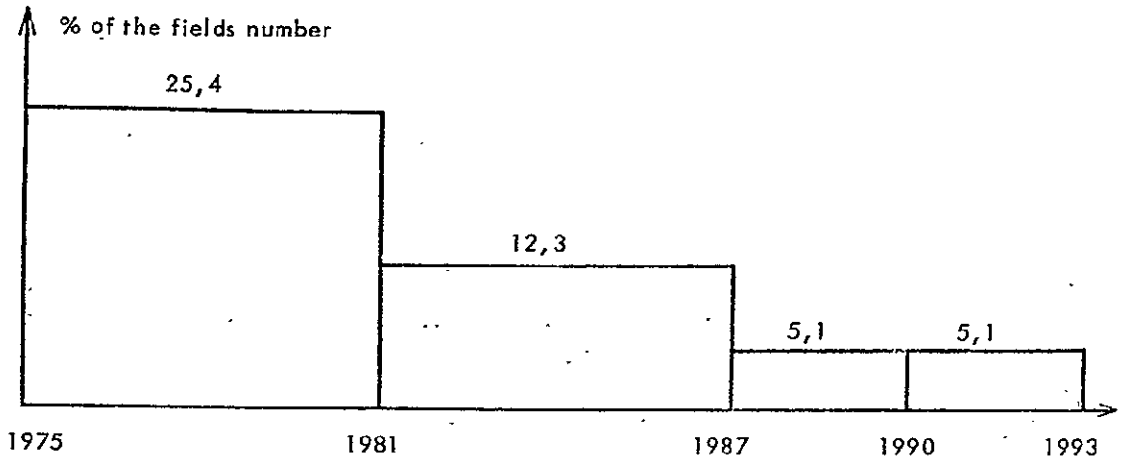

Fig. 92 - Forecast of I 214 available timber

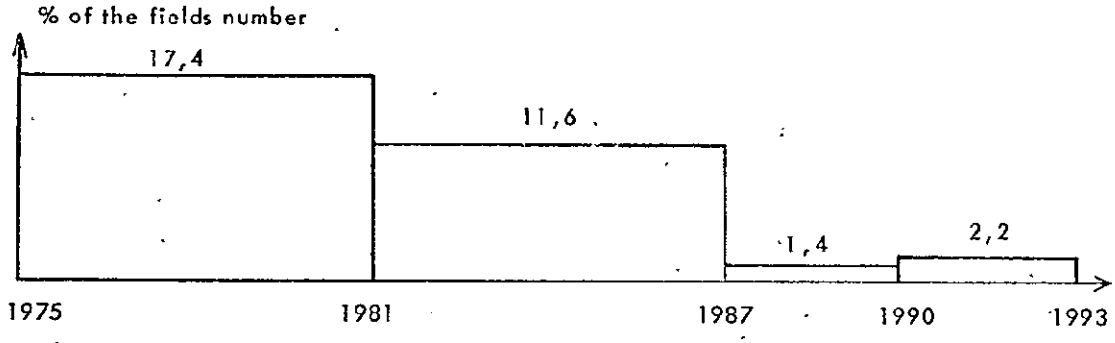

Fig. 93 - Forecast of Robusta available timber

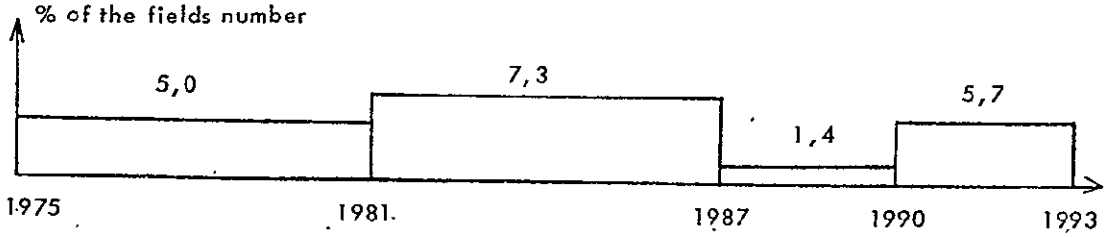

Fig. 94 - Forecast of the other cultivars available timber

The simulation of Fig. 95 was digitized with a step of 25 µm by a microdensitometer. This step corresponds to the resolution of IRC photographs. The availability of this numerical data obtained in "real dimension" allows to study the role played by the image processing. Fig. 96 gives a display of some simulated plots.

An example of assessment of the accuracy of cover measurement is shown in Fig. 97. The distribution of cover rate measurements is shown.

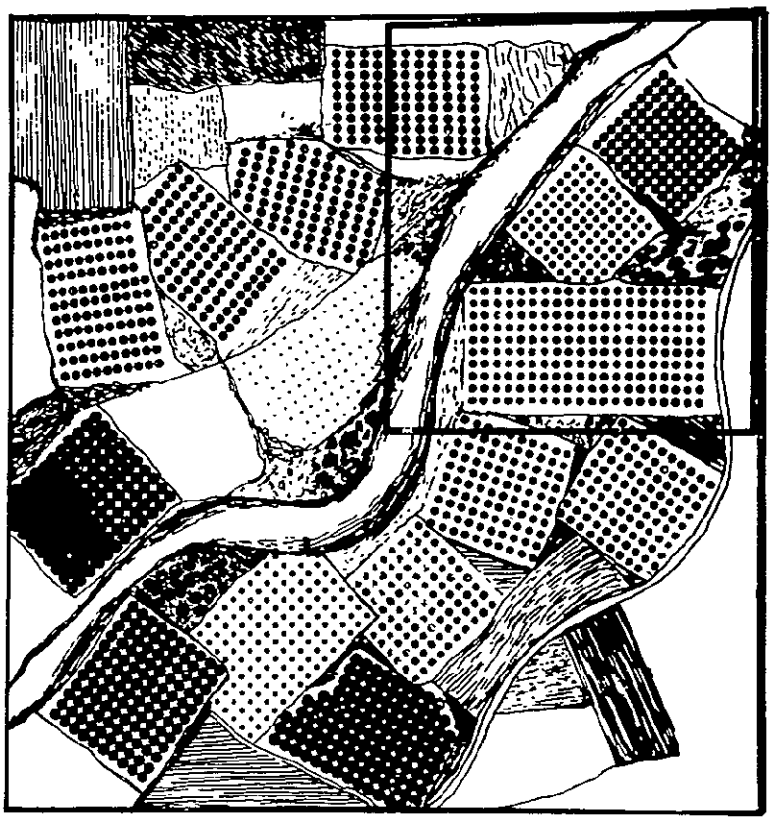

Fig. 95 - Theoretical model of poplar coverage

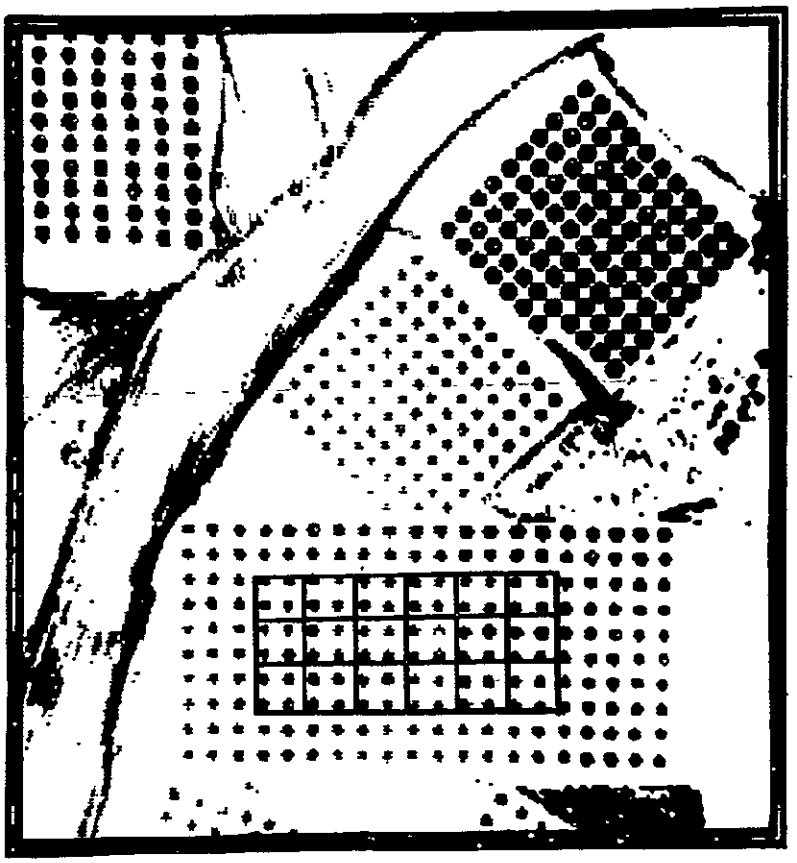

Fig. 96 - Display of some simulated plots

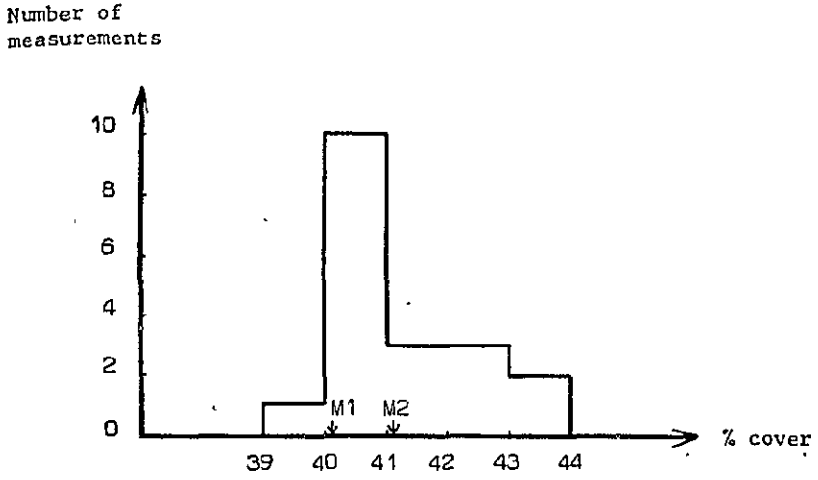

M1 = 40.1 : Cover rate of the model
M2 = 41.1 : Average of cover rate measured

Fig. 97 - Distribution of the measurements of cover rate

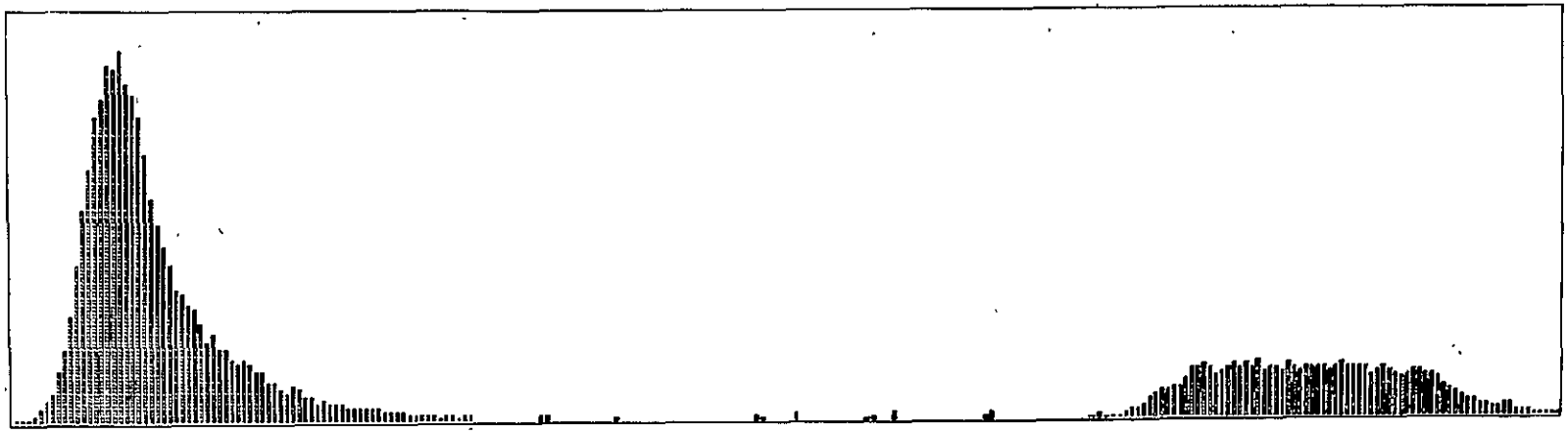

Fig. 98 - Histogram of a simulated plot

These data are obtained from computed histograms as the one exemplified in Fig. 98. The two groups of optical densities correspond respectively to the white areas on Fig. 95, and to the black circles which represent theoretical crowns of poplars. This simulation presumes that the parameter "spectral discrimination of crowns" is really known. Cover percentage of the studied model part (M1) is 40.1% while the mean of measured cover rates (M2) is 41.1%. Fig. 96 shows the squares in which the measurements are made (in green). The difference between M1 and M2 is satisfactory and allows one to think that processing of aircraft data will be accurate enough to be applied.

A systematic analysis of the theoretical model was performed in order to point out the influence of the angle value (α) between line plantation and scanning line. Fig. 99 shows the variation of the error of measurement (Em) in relation to α (Rt = cover percentage). A similar experiment gives the error in cover percentage measurements for different simulated fields where cover percentage only is varying (Fig. 100).

Such data processing on the model allows to make adequate corrections when IRC photographs are processed.

3.3 Standing timber evaluation

3.3.1 Cover percentage

The data are compiled in such a way to group the measurements obtained on a given plantation type for the same cultivated variety.

Cover rate processing is applied under the same conditions as in the theoretical model. For example, IRC transparent films of airborne data collected on the Garonne valley (see ch. 4, 1.1) are digitalized by microdensitometry. A histogram processing similar to that on Fig. 98 is done on poplar fields in given conditions. Fig. 102 shows the results obtained on poplar grove no. 4 of Fig. 101. Comparison with Fig. 98 indicates a much lower standard deviation, as a result of the small contrast between the ground objects which make up the target.

When the threshold for crown discrimination is given after display, the cover percentage is computed on the histogram. Results for field no. 4 are included in Table 45, and in this example, Fig. 103 gives the display of some poplar crowns of that plantation.

3.3.2 Crown surface

The relationships between cover percentage and crown surface (CS) must take into account the density of plantation (Fig. 104).

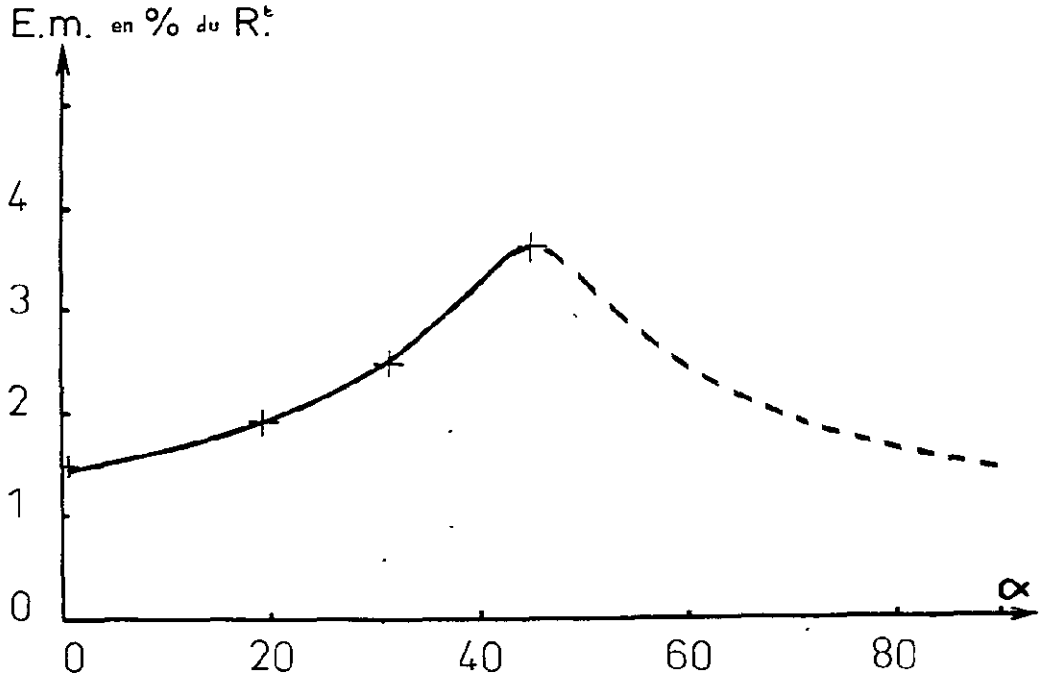

Fig. 99 - Error in cover measurement in relation to angle value between line plantation and scanning line

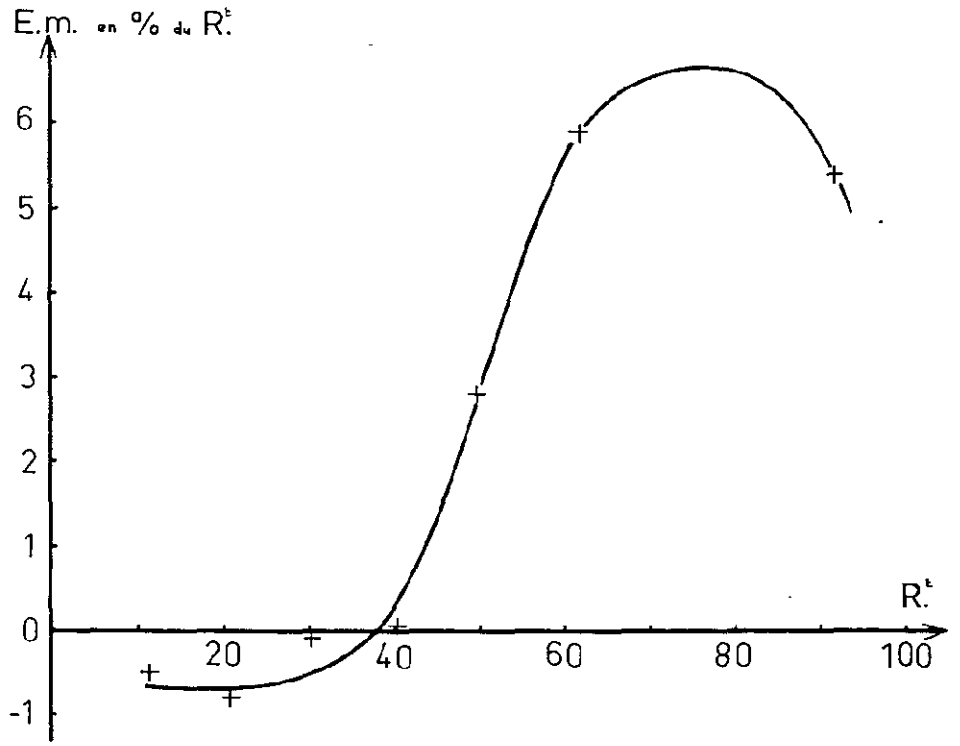

Fig. 100 - Error in cover measurement in relation to cover percentage

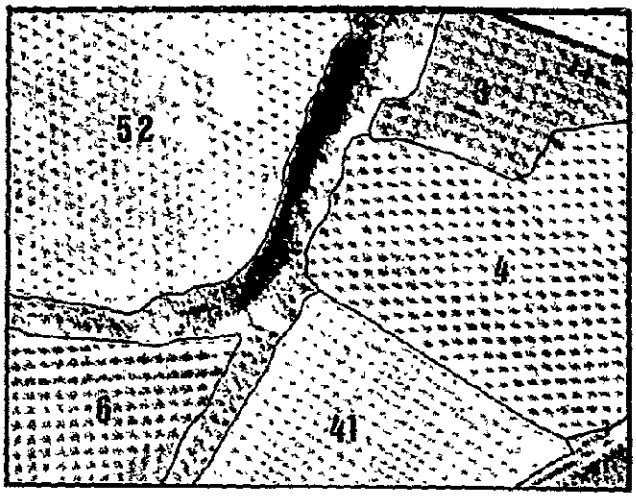

Fig. 101 - Display of poplar groves used for standing timber evaluation

3.3.3 Stem circumference

Ground measurements are performed for establishing the relationships between crown surface (CS in m^2) and stem circumference at 1.30 m level (C in m), as shown in Fig. 105 for the clone I 214 cultivated at a density of 204 plants/ha.

Remote sensing measurements on poplar groves are thus able to provide an estimate of a tree characteristic (stem circumference) which is directly related to the stem volume.

3.3.4 Example of application

An application experiment of standing timber evaluation is presented in Table 45.

The cover rate measurement which is given in the second column is already corrected according to the theoretical model analysis. The last column gives the difference between computed and ground measured circumference. Mean and standard deviation of these differences in this application experiment are -0.03 and 0.11 respectively.
Half of the estimates are thus included within one standard deviation.

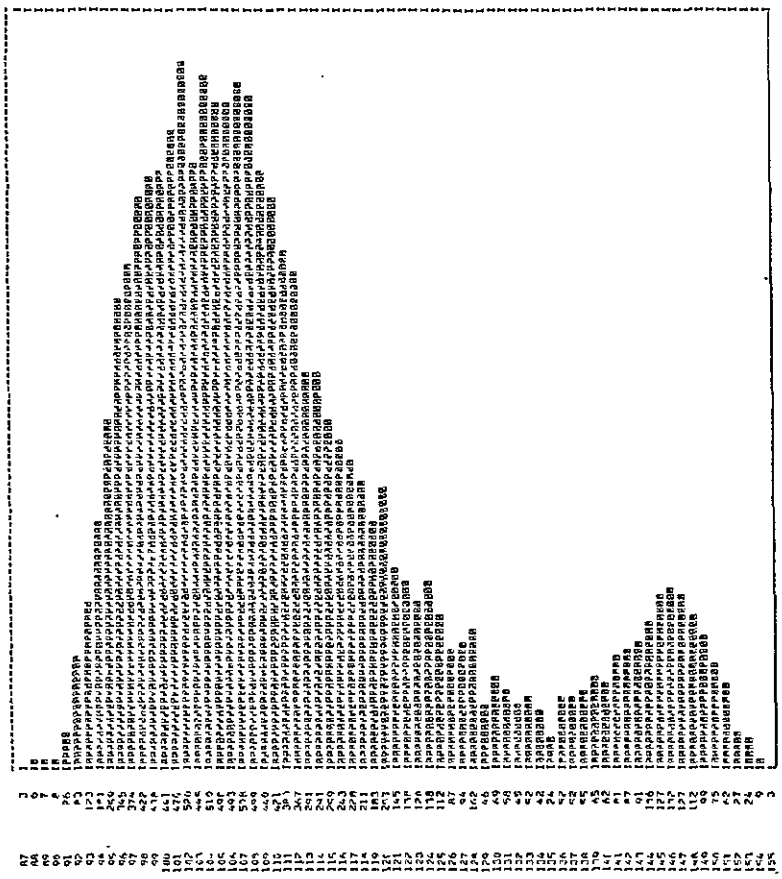

Fig. 102 - Histogram of cover rate of poplar grove no. 4 (of Fig. 101)

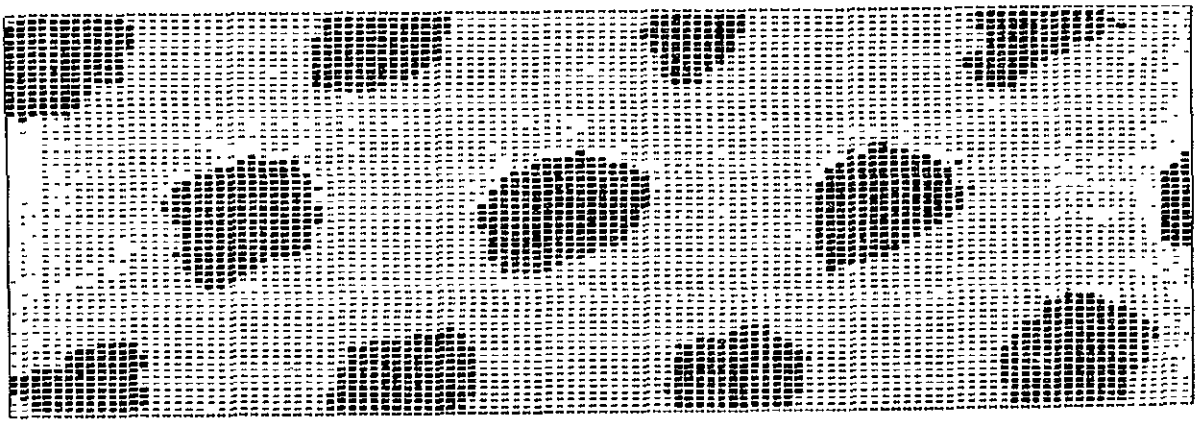

Fig. 103 - Display of some poplar crowns of grove No. 4 (of Fig. 101)

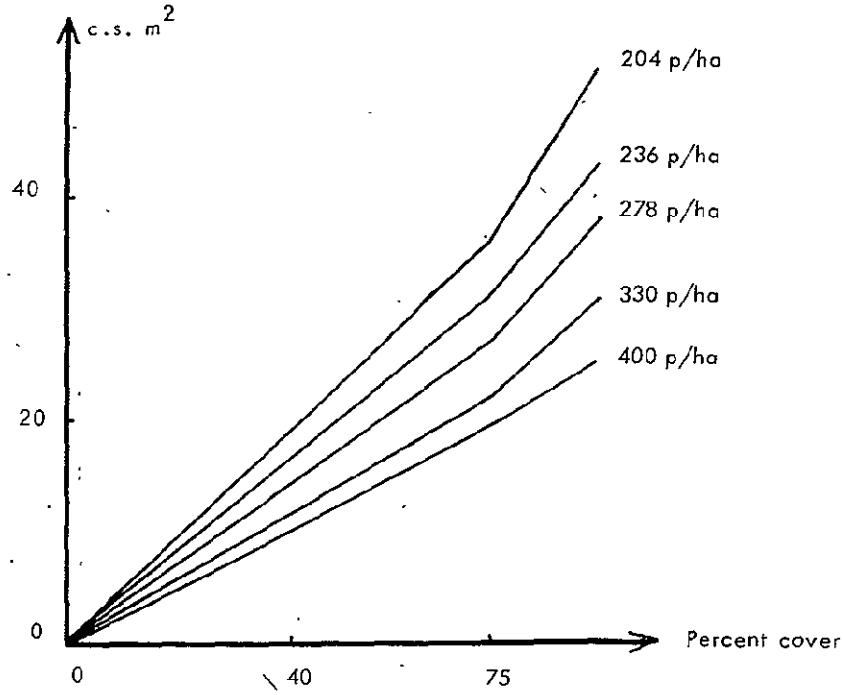

Fig. 104 - Relationship between cover percentage and crown surface (C S) as a function of plantation density

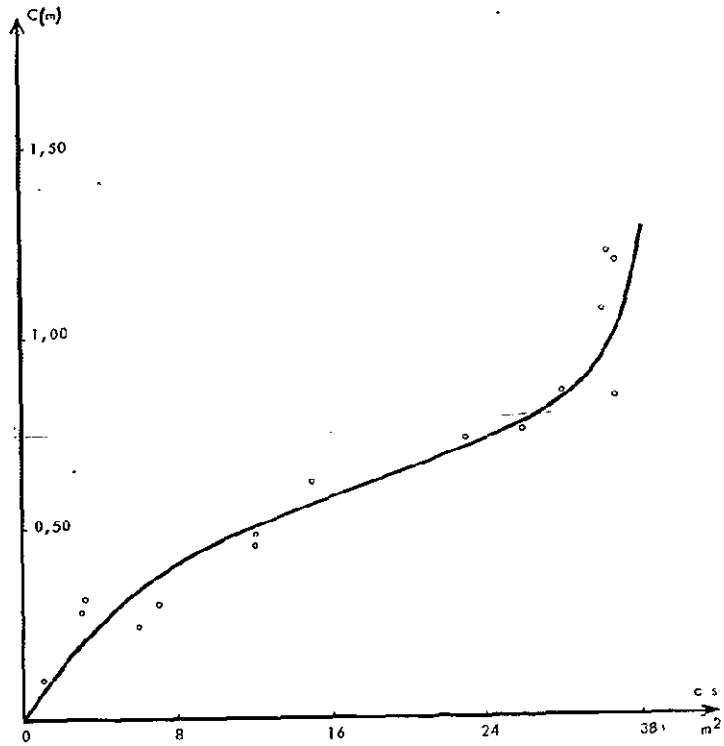

Fig. 105 - Relationship between crown surface (C S) and circumference (C) for 1214 plantations at 204 p/ha density

Table 45 - Example of standing timber evaluation on I 214 fields (density 204 plants/ha)

Ref. field	Microdensitometric cover percentage (%)	Computed Crown Surf. (m^2)	Computed Stem Circ. (m)	Ground measured Circ. (m)	Difference (m)
3	44	23	0.73	0.88	- 0.15
4	21	10.5	0.44	0.37	+ 0.07
41	6	8	0.15	0.10	+ 0.05
5	27	13	0.53	0.48	+ 0.05
52	11	5.5	0.32	0.24	+ 0.08
6	33	16	0.60	0.73	- 0.13
9	84	34	1.24	1.10	+ 0.14
92	34	17	0.62	0.75	- 0.13
94	36	22.5	0.72	0.82	- 0.10
95	33	16	0.60	0.75	- 0.15

4. CONCLUSIONS

'Global' prediction of poplar production is theoretically possible in various environments, without distinction between different varieties, on the basis of the four coverage classes which might be recognized on aerial photographs and of the relationship between coverage and corresponding age classes.

The estimation of standing timber volume is possible on the basis of the biometric relationships (to be established on representative samples) between a remotely measurable parameter and dendrometric characteristics of poplars. As in the forestry tables, this methodology integrates the influence of environmental conditions.

BIBLIOGRAPHY

Internal:

- FLOUZAT, G., "A Preliminary Theoretical Study in Order to Estimate by Remote Sensing the Biomass in a Poplar Site", National Technical Information Service. Weekly Abstracts - NASA Earth Resources Survey Program. NASA CR-146822, July 5, 1976
- "Principe d'étude et mesure globale de la production de bois de peuplier", cours de Technologie Spatiale - Session I: Observation de la Terre. C.N.E.S., Toulouse, March, 1976
- "Inventory and Available Timber Forecast in a Poplar Area (AGRESTE Test Site No. 5)", National Technical Information Service. Weekly Abstracts. NASA Earth Resources Survey Program. NASA-CR
- "Estimation of Timber Volume in a Poplar Plantation by Remote Sensing", National Technical Information Service. Weekly Abstracts. NASA Earth Resources Survey Program. NASA-CR.

CHAPTER 6 - IDENTIFICATION OF BEECH FORESTS

Contributor to the text:

DEJACE, J. (JRC-Ispra Establishment)

Scientific Collaborators:

DORPEMA, B. (JRC-Ispra Establishment)
FASSI, B. (INPL, Turin)
GULINCK, H. (JRC-Ispra Establishment; post-graduate student)
MEGIER, J. (JRC-Ispra Establishment)
MEHL, W. (JRC-Ispra Establishment)
MONDINO, G-P. (INPL, Turin)
SALANDIN, R. (INPL, Turin)
STEIN, A. (JRC-Ispra Establishment)

The inventory of beech forests in northern Italy is considered as an essential part of a broader inventory of natural renewable resources. Actually, beech wood originating from coppice forests could partially substitute poplars for the production of wood pulp. These coppice forests constitute in northern Italy an important unutilized resource, especially in Piemont where they represent a significant fraction of the total forested areas. The identification of these beech forests by remote sensing techniques has to take into account various objective difficulties arising mainly from the mountainous relief of the investigated areas and from the typical mixed composition of the natural deciduous forests.

1. GROUND TRUTH DATA

The area under investigation is situated in the Italian part of the Maritime Alps, south-west of Cuneo (test site no. 3). It covers part of the valley of Stura di Demonte and an affluent called Vallone dell'Arma.

The ground truth, prepared by INPL from infrared aerial photographs (scale 1:17,000), considered the following types of vegetation:

- Chestnut forests on north-oriented slopes at medium altitudes,
- beech forests at higher altitudes and on the edge between the two valleys,
- deciduous forests with closely mixed species,
- crops and meadows at the bottom of the valleys.

A significant portion of the area (rocks, bare soils, villages, etc.) is

not fully characterized.

The ground truth has been reported manually on the 1:25, 000 map and then digitalized following the method described in Chapter IV, sect. 2.2.3.1. Fig. 106 gives the display of digitalized ground truth.

2. MSS DATA AND ITEMS OF CLASSIFICATION

Two LANDSAT scenes, free of clouds over the studied area, were available for this investigation, namely those of July 3rd, 1975 (2162 - 09333) and of September 13th, 1975 (2234 - 09332).

The two scenes were used first separately and later merged into a unique 8-channel scene.

Because of the mountainous relief of the area under investigation, the angle of incident sunlight to the ground varies from 10 to 65°, thus leading to extreme variations in direct irradiance. A complete digitalization of the relief which would have taken account of this relief effect was beyond the scope of this study. A simple solution was therefore adopted by defining two beech classes, one in sunlight (beech 1) and the other in shadow (beech 2).

Spectral signatures, i.e. mean and variance-covariance matrix were obtained for each class on homogeneous training samples covering 40 to 200 pixels.

3. RESULTS

3.1 The best results were obtained, on the July data, with the maximum likelihood method (ML), using probability thresholds for each class (see Appendix, section 4.2.2).
From the performance matrix given in Table 46, one notes the following features:

a) The percentage of correct beech classification (i.e. the ratio of the number of pixels of real beech recognized as beech to the total number of beech pixels on the ground truth) amounts to 63%.

b) If beech, chestnut and mixed deciduous forests were considered as a unique class, the percentage of correct classification would be 76%.

c) Discrimination between beech and chestnut is illustrated by the following figures:

74% (11 + 63) of beech area are classified as deciduous forest (either beech or chestnut),

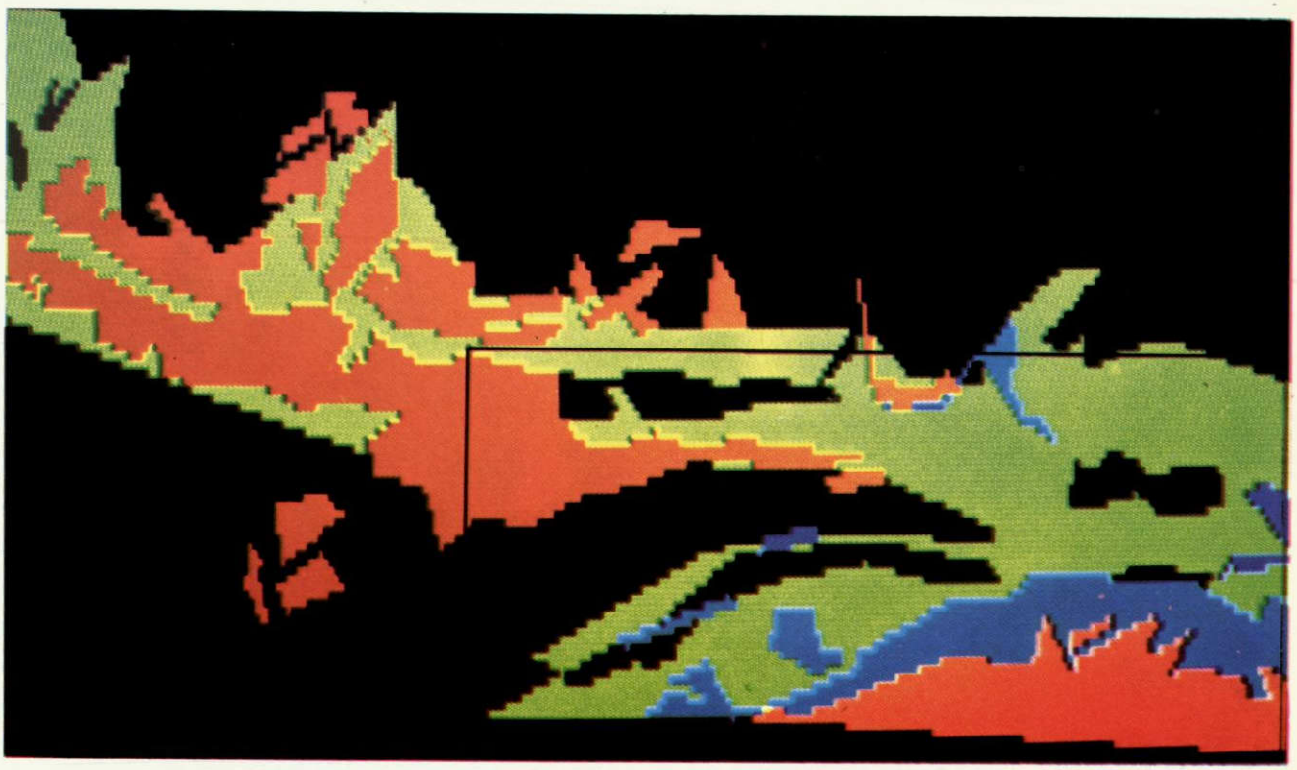

Fig. 106 - Digitalized ground truth, displayed on colour screen. Yellow/green: meadows and crops; blue: chestnut; orange/red: beech

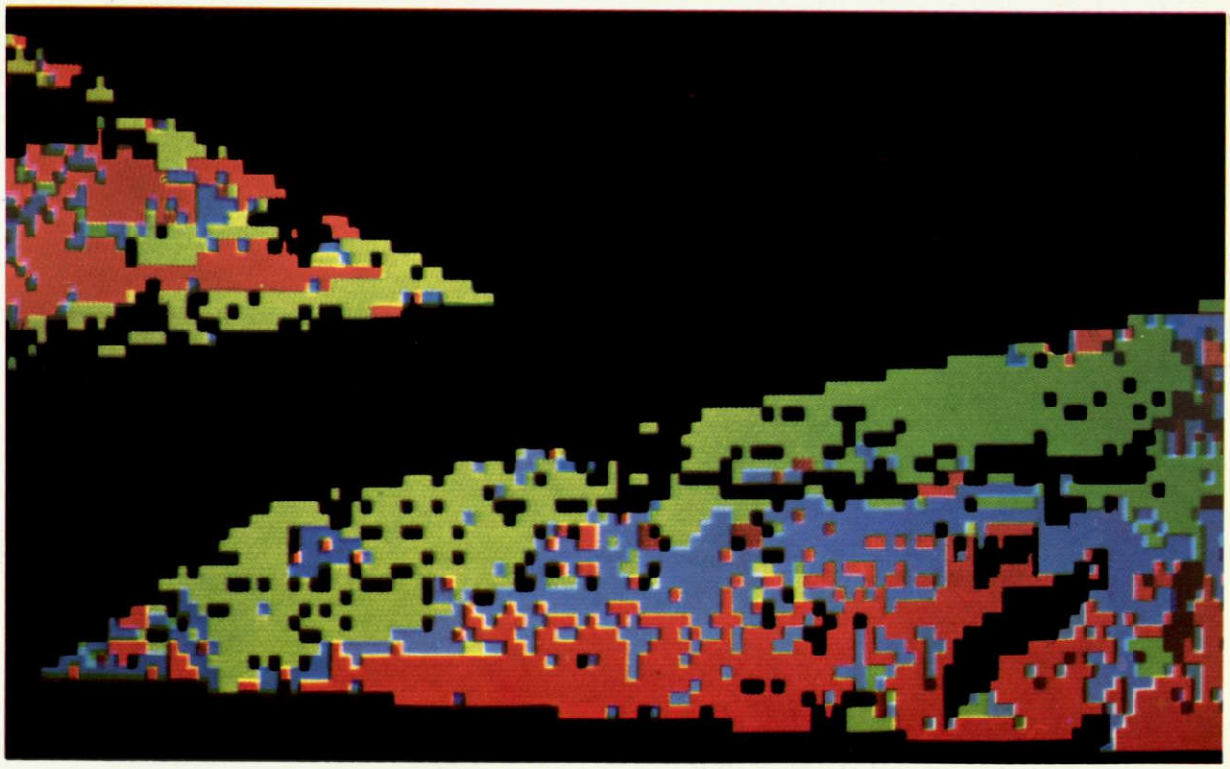

Fig. 107 - Results of classification (ML) of the 7/3/75 scene on the righthand (eastern) part of Fig. 106. Same colour code as in Fig. 106

- among these pixels, 85% (63/74) are correctly classified as beech and thus discriminated from chestnut,
- 67% (50 + 17) of chestnut are classified as deciduous forest,
- among these pixels, 75% (50/67) are correctly classified as chestnut.

d) Finally, the precision on surface estimation (ratio of total number of pixels classified to the number of pixels in the ground truth for a single class) ranges from 81 to 118%.

Because of the limited precision of discrete ground truth, it has seemed unreasonable to still refine the parameters of classification. Figs. 107 and 108 show the results of classification and the display of performance matrix.

3.2 The scene of September 13th (Table 47) gives satisfactory results as far as surface estimation (precision between 82% and 135%) and overall classification of deciduous forests (75% of correct classification) are concerned. But discrimination between beech and chestnut is poorer. This is probably to be related to the plant phenology, the spectral signature of chestnut in early July being influenced by flowering.

3.3 The use of a background class should, in principle, appear more satisfactory since it does not need any arbitrary fixation of threshold. Actually, in this case, this method does not give as good results as the threshold method, even if the number of pixels classified in this background class is artificially reduced by the introduction of a low "a priori" probability.

3.4 Multitemporal analysis starting from an 8-channel scene gives poorer results than the analysis of each single scene, in spite of an increase in computing time (by a factor of 2.8 in this case).

3.5 Modified Euclidean Distance (MED) method brings a relevant reduction in computing time (a factor 4 in this case). This method was applied to the July scene in the three following ways; first on the original data without limiting distance for classes, then on the same data after a principal component transformation and finally on these transformed data by using a limiting distance for each class. Numerical results are given in Table 48. Geographical display of the performance matrix is illustrated in Fig. 109.

One notes that the principal component transformation improves the results of the classification. This can be explained theoretically by the following remarks. In the channel space, reported to principal

Table 46 - Results of classification (ML method with thresholds) on a 7/3/75 scene. (a) in number of pixels, (b) in percentages of ground truth.
Legend: M. C. : meadows and crops; chest. : chestnut; n. cl. : not classified; m. d. f. : mixed deciduous forest; n. ch. : zone not characterized on ground truth; ratio: ratio of classified area to effective area

	Classification					Classification				
Ground - truth		M. C.	chest.	beech	n. cl.		M. C.	chest.	beech	n. cl.
	M. C.	917	116	220	639	M. C.	48	6	12	34
	chest.	144	407	140	127	chest.	17	50	17	16
	beech	299	354	1924	489	beech	10	11	63	16
	m. d. f.	15	32	96	23	m. d. f.	9	19	58	14
	n. ch.	463	56	103	292	n. ch.	51	6	11	32
						ratio	.97	1.18	0.81	
	(a)					(b)				

Table 47 - Results of classification (ML method with thresholds) on a 9/13/75 scene (for legend, see Table 46)

	Classification					Classification				
Ground - truth		M. C.	chest.	beech	n. cl.		M. C.	chest.	beech	n. cl.
	M. C.	1076	118	284	414	M. C.	57	6	15	22
	chest.	112	354	267	85	chest.	14	43	33	10
	beech	448	552	1748	318	beech	15	18	57	10
	m. d. f.	40	50	73	3	m. d. f.	24	30	44	2
	n. ch.	238	33	127	516	n. ch.	26	4	14	57
						ratio	1.01	1.35	.82	
	(a)					(b)				

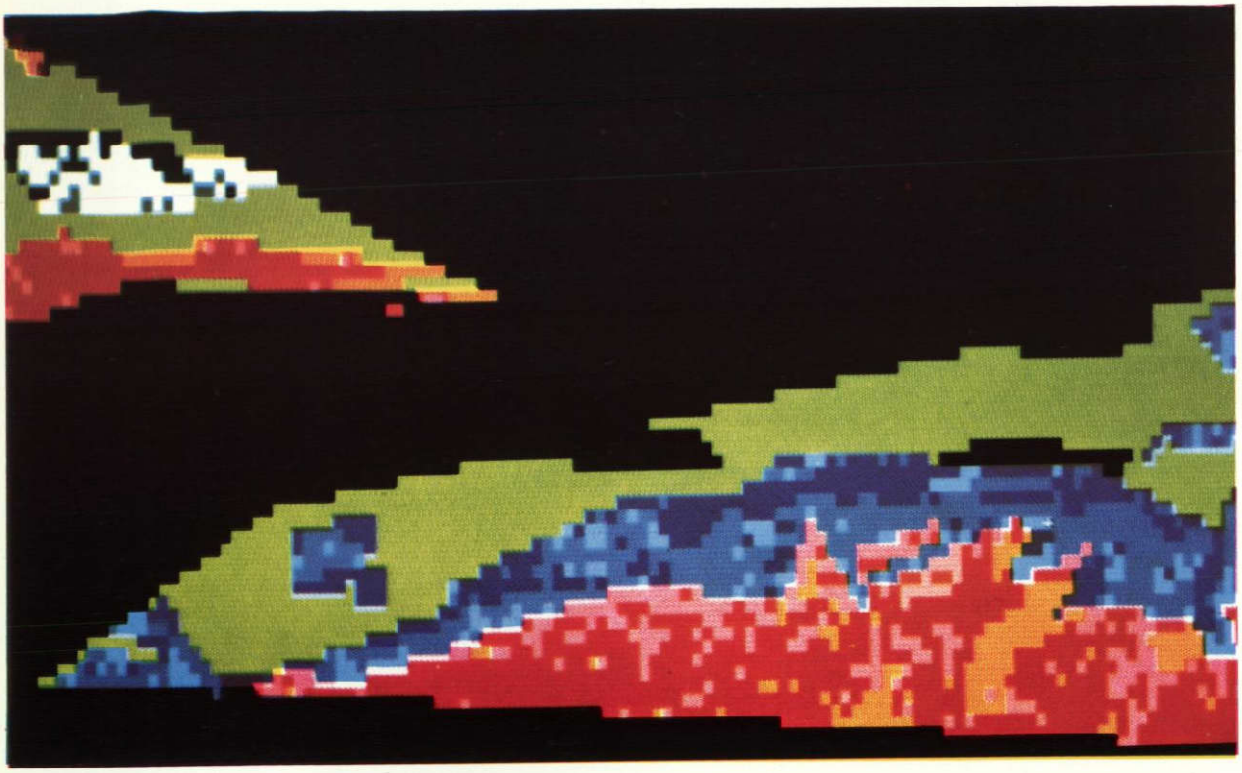

Fig. 108 - Display of performance matrix between ground truth and classification of Fig. 107 (ML method, 7/3/75 scene). Blue: chestnut recogn. as chestnut; light blue: chestnut classif. as beech; dark blue: other chestnut; red: beech recogn. as beech; purple: beech classif. as chestnut; orange/red: other beech; white: mixed deciduous forest classif. as beech; dark green: mixed deciduous forest classif. as chestnut; yellow/light green: crops and meadows (in any classification)

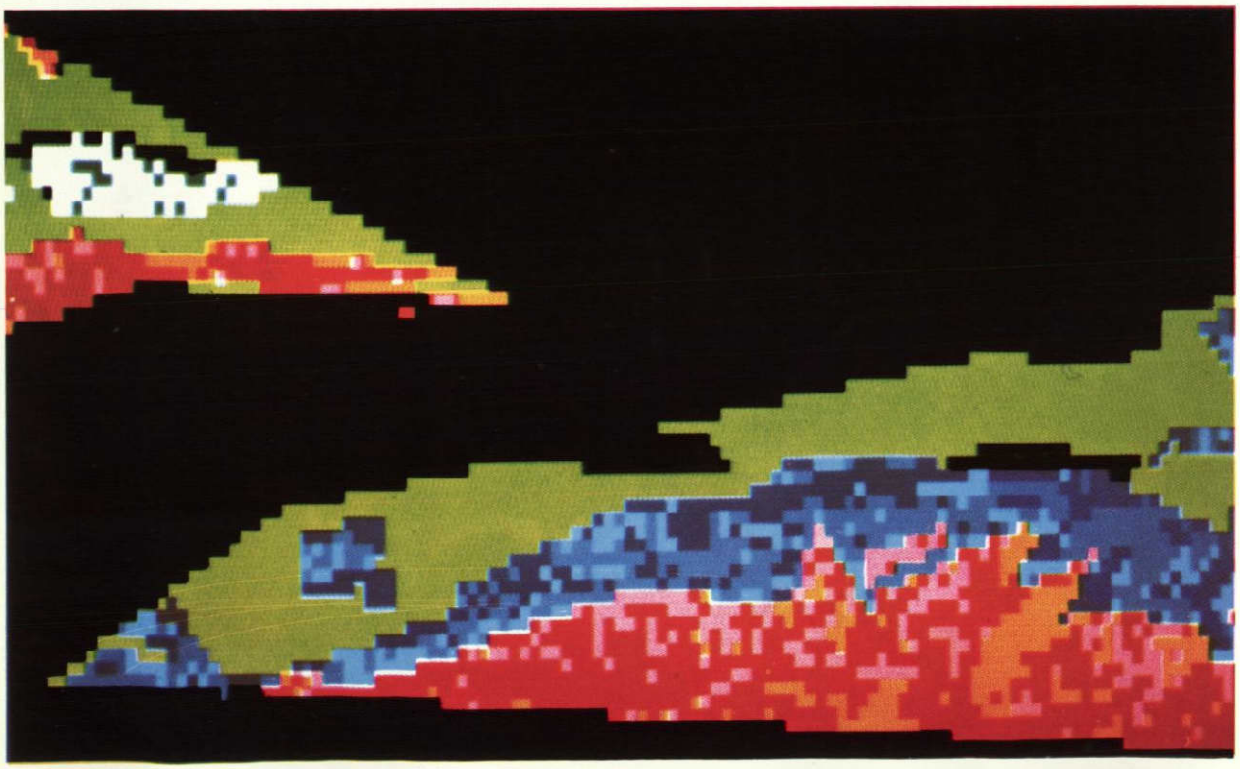

Fig. 109 - Display of performance matrix between ground truth and classification (MED method, 7/3/75 scene). Same colour code as in Fig. 108

Table 48 - Results of classification (MED method) on the 7/3/75 scene. (a) on original data without limiting distance, (b) on data after principal component transformation, without limiting distance, (c) on transformed data with limiting distance. All results are in percentages of ground truth. (For legend see Table 46)

Class / Ground truth	M.C.	chest.	beech	n. cl.	M.C.	chest.	beech	n. cl.	M.C.	chest.	beech	n. cl.
M.C.	46	13	6	35	58	13	7	21	59	6	12	23
chest.	16	63	9	12	15	67	9	9	20	42	23	15
beech	7	24	46	23	12	26	47	16	13	11	62	14
m.d.f.	2	39	39	21	8	38	39	14	10	14	63	13
n.ch.	55	12	6	27	63	11	8	18	62	5	13	20
ratio	1.15	2.12	0.58		0.91	2.06	0.56		1.19	1.04	0.83	
	(a)				(b)				(c)			

Table 49 - Performance matrix, scene of July 5th, extended ratio method with path radiance corrections, results in percentages on ground truth

		Classification	
		Beech	Non-Beech
Ground truth	Beech	83.6	16.4
	Non-Beech	16.2	83.8
Ratio		104.6	96.4

4. CONCLUSIONS

Particular difficulties arise in the application to mountainous regions of remote sensing techniques from satellite with the aim of vegetation classification. Nevertheless, this classification remains possible by such techniques if the algorithms are adapted in such a way to create a class of rejects, which gathers all objects which are not sufficiently characterized on the ground truth. The test used for checking the goodness of classification, the so-called performance matrix, is much more severe than the simple comparison of surfaces where the two types of classification errors, omissions and comissions, always partly compensate each other. It should be emphasized that the confusion matrix takes into account also possible errors in superposition of LANDSAT scanning grid and ground truth document (map or aerial photograph). Under European conditions, where fields or forests are often a few pixels in area, this superposition problem acquires a crucial importance.

The classification methods used so far allow a satisfactory recognition of beech and even its discrimination from other deciduous species (such as chestnut). The better discrimination achieved in July shows the importance of the observation date, which should be carefully studied a priori in collaboration with specialists (in this case foresters).

BIBLIOGRAPHY

Internal:

- DEJACE, J., "Inventaire des hêtraies dans une région des Alpes Maritimes italiennes à partir des données du satellite LANDSAT", Coll. sur l'Utilisation des Satellites en Télédétection, Paris, Sept., 1977
- DEJACE, J., MEGIER, J., MEHL, W., "Computer-aided Classification for Remote Sensing in Agriculture and Forestry in Northern Italy", 11th Int. Symp. on Remote Sensing of Environment, Ann Arbor, Mich., April 1977.

CHAPTER 7 - IDENTIFICATION AND INVENTORY OF FIR FORESTS WITH LANDSAT DATA

Contributor to the text

FLOUZAT, G. (CESR, Toulouse)

Scientific Collaborator on the French test site

Mr. MONCHANT (Centre d'Etude Spatiale des Rayonnements, Toulouse)

Conifer forests constitute in European countries an important timber stock of the mountainous regions. Their economic importance justifies the development of a specific methodology for performing adequate inventories of these resources for land-use purposes.

Objective of this experiment was to establish what level of performances could be achieved in the identification of these woodlands in mountainous conditions. Supervised data processing, on the basis of the ecological knowledge of the forests, allowed an evaluation of the precision obtained in the area measurements. As for the beech investigation, the mountainous relief of the studied area induces great variations in the radiance of the object. The identification of woodlands of a given species requires therefore a representative sampling to be performed under the various standing conditions of a very diversified landscape.

Object of this study was the fir (Abies alba) which is the only coniferous species present in a significant manner in the Pyrenean zone investigated. Therefore the problem of identification is that of a coniferous forest rather than that of fir itself. The test area is rectangular in size (12 x 16 km) and is situated in the central part of the Pyrenees (region of Luchon, south of the AGRESTE test site no. 5).

For a rapid execution of this experiment, LANDSAT transparencies, available from the beginning of the AGRESTE investigation, were used on a single scene (July 27, 1975). Data processing was made on magnetic tapes obtained by digitalization in a microdensitometer.

1. GROUND DATA COLLECTION

1.1 Collection and cartography

The performance definition of such a remote sensing experiment requires that ground reference be collected simultaneously with the imagery.

Therefore, the mapping of fir forests (scale 1 : 50,000) which was drawn up by photo-interpretation of a 1973 aerophotographic survey (performed with two different emulsions, panchromatic and infrared black and white at a scale close to 1 : 25,000) was systematically supervised for every forest site by ground observations made in July 1975. The results obtained after adequate reduction are shown in Fig. 110.

1.2 Analysis of the vegetation map

As for any supervised data processing of LANDSAT imagery, a prerequisite was that sampling should be representative of all the conditions where fir forests are standing. Therefore, a quantification of the standing conditions of these forests in the investigated area was performed on the basis of the vegetation map (scale 1 : 50,000) extracted from the "Foix" sheet of the general vegetation map of France (scale 1 : 200,000). This quantification concerned the parameters altitude, exposition, slope, physionomy and series (see Table 50). The corresponding data were transferred with a kilometric grid on three mapped sheets at scale 1 : 50,000. They included 1658 single points for which information was automatically processed. The stations occupied by fir (167 stands) were then computed. The distribution of these stands in relation to altitude, exposition and slope is roughly illustrated in Fig. 112.

2. SAMPLING METHODOLOGY

2.1 Principle

The samples necessary for supervised data processing are chosen under standing conditions representative of all the fir situations. The geographic localization of such samples is made by taking into account the principal characteristics of the fir stations, obtained by processing of cartographic survey data (see section 2.2). The samples retained are distributed over the whole investigated area, at various altitudes, expositions and slopes in relation to the corresponding frequencies of occurrence. These samples are characterized by their radiance in the 4 LANDSAT channels. On the basis of these results, a final decision is taken of retaining or discarding the various samples:

- those samples are retained which are sufficiently homogeneous and monospecific;
- those samples are discarded which show accidental characteristics in relation to the properties of the investigated object.

The retained samples are used as initiation stage for clustering data processing.

Table 50 - Quantification of the parameters of vegetation distribution

Altitude 20-21-22-23

Exposition 24

0 = flat terrain without definite exposition
1 = north
2 = north-east
3 = east
4 = south-east
5 = south
6 = south-west
7 = west
8 = north-west

Slope 25

0 = 0%
1 = 0-5
2 = 5-10
3 = 10-20
5 = 20-40
7 = 40-80
9 = 80-100

Physionomy 53

0 = cultures
1 = meadows
2 = "landes" (bushlands)
3 = woodlands

Series 54-55

01 = littoral horizons
02 = water edges
22 = poplar grove
03 = quercus suberosa
04 = quercus ilex
05 = quercus pubescens
06 = quercus pedunculata
07 = quercus sessiliflora
08 = pinus marittima
09 = pinus sylvestris
10 = pinus uncinata
11 = fagus sylvatica
12 = abies alba
13 = alpine meadow
14 = good drainage
15 = bad drainage

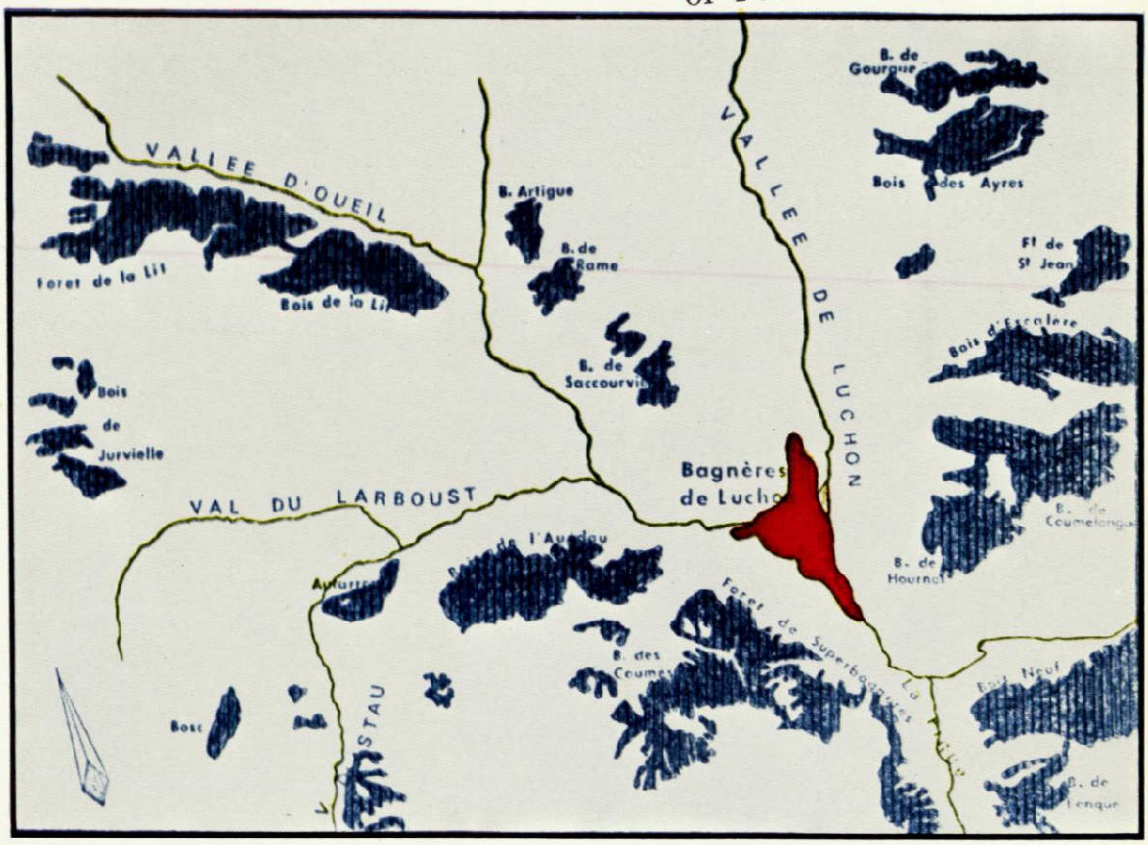

Fig. 110 - Reference map of fir forests from photointerpretation and ground data

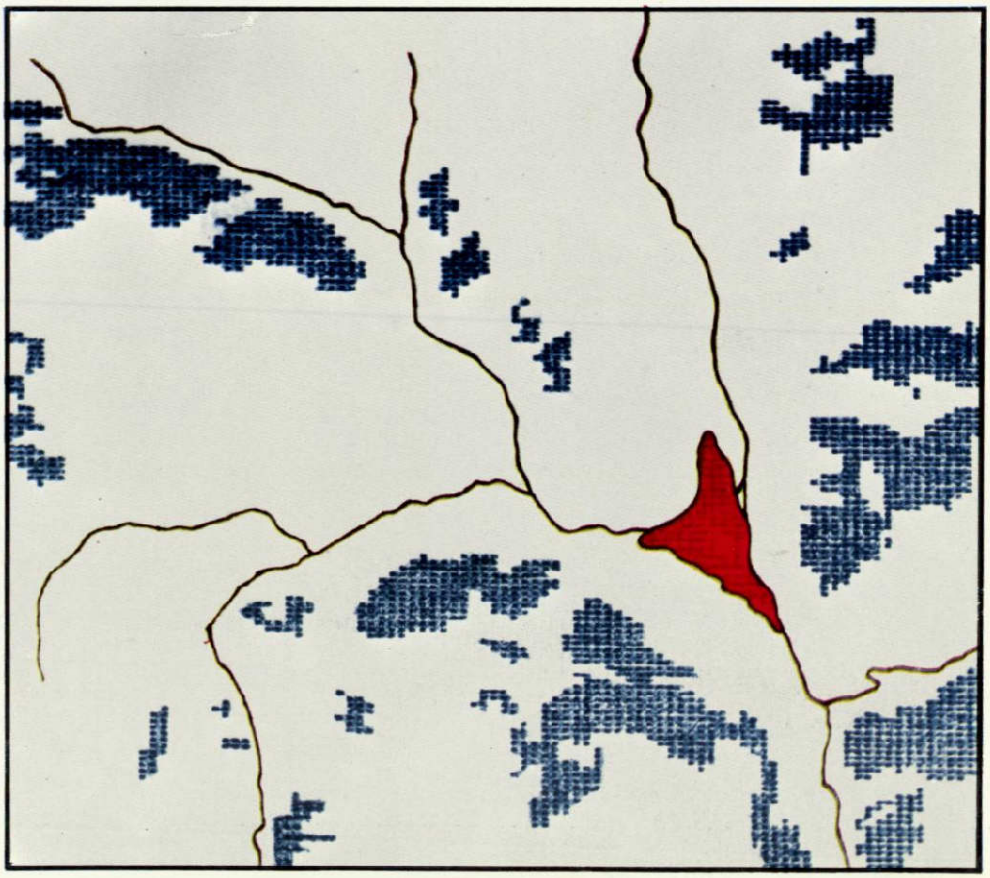

Fig. 111 - Digitized map of fir forests

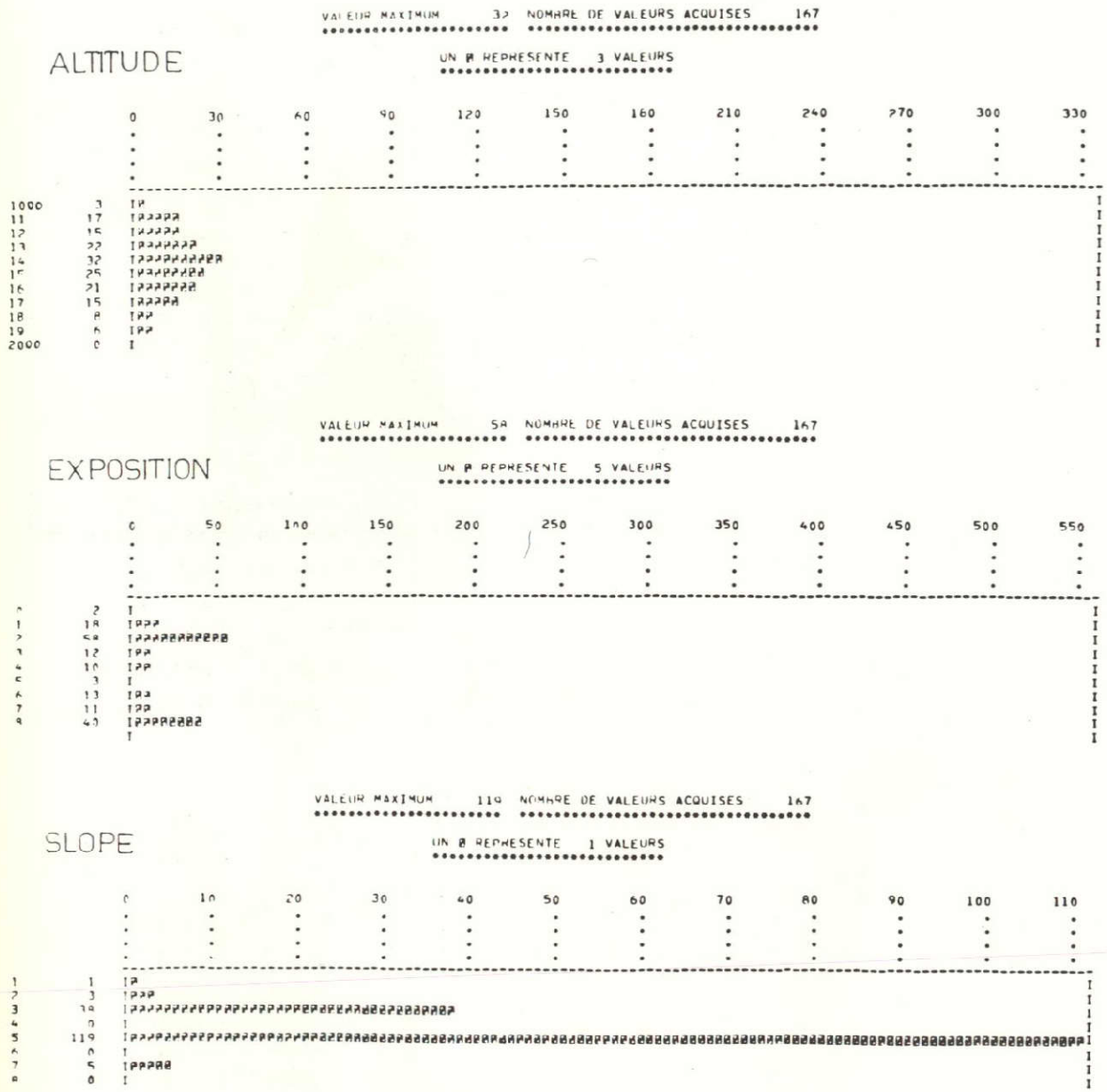

Fig. 112 - Ecological data of vegetation map analysis

2.2 Standing conditions of fir woodlands

Data processing of the results gained from the analysis of the vegetation map allows to define the standing conditions of fir woodlands in relation to various parameters (Fig. 112):

- altitude: in the studied area, fir is present between 1000 and 1900 m. Distribution of the 167 sounding points corresponds to a mean altitude of 1436 m and a 219 m standard deviation, with 88% of total points lying between 1100 and 1700 m;
- exposition: the distribution indicates that the most frequent expositions (69% of total points) are north-east, north-west and north (see also Fig. 113);
- slope: Fig. 114 gives a coherent presentation in relation with slope. It is seen that a great number of points (94% of the total) lies between 10 and 40% in slope.

2.3 Sampling process

Beside the criterion concerning standing characteristics used for the choice of samples, an area criterion had to be adopted. It consisted in retaining samples with an area around 20 grouped pixels in size, a number which allows a better initiation of LANDSAT data processing.

Table 51 indicates the standing characteristics of the 9 retained samples in this first stage. This limited number allows the use of a not-excessively heavy methodology.

Table 51 - Standing characteristics of samples

condition / sample	max. altitude (m)	min. altitude (m)	exposition	slope (%)	number of points
1	1700	1500	north	30	28
2	1600	1340	"	33	30
3	1680	1360	north-east	34	36
4	1400	1140	" "	66	24
5	1600	1380	north-west	35	30
6	1640	1400	" "	50	25
7	1560	1240	" "	71	20
8	1720	1420	" "	64	20
9	1660	1400	north	42	18

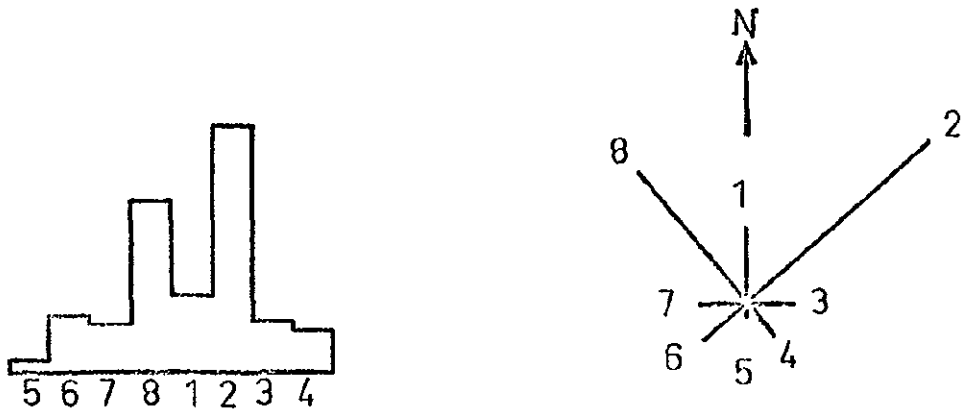

Fig. 113 - Distribution of fir forests in relation to exposition

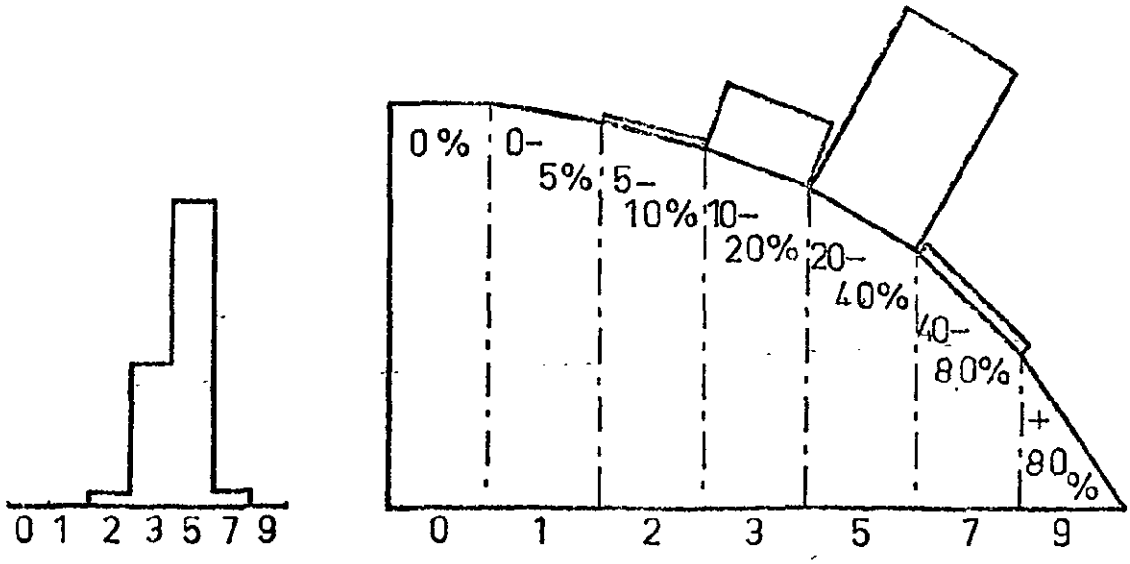

Fig. 114 - Distribution of fir forests in relation to slope

It must be noted that the stations are correctly represented as far as altitude and exposition are concerned, while the slope values appear to be somewhat excessive. This is a consequence of the area criterion since the number of pixels is minimum in samples of less representative slope.

The optical characteristics of the single pixels of the localized samples (see section 3) are now extracted from the 4 channels and the corresponding mean and standard deviation are computed (Table 52).

Table 52 - Optical characteristics of the samples (M = mean; s = standard deviation)

Channel / Sample	MSS 4		MSS 5		MSS 6		MSS 7	
	M	s	M	s	M	s	M	s
1	173.9	3.2	185.8	2.7	149.9	4.6	191.2	3.8
2	172.6	3.0	184.0	2.6	148.0	4.4	189.0	3.4
3	173.6	3.2	181.4	3.5	142.6	4.6	185.9	3.7
4	172.0	3.0	185.7	3.2	150.4	5.1	193.3	7.2
5	172.3	2.6	183.0	4.0	147.5	3.3	186.8	4.2
6	174.5	2.5	180.6	2.7	147.3	3.5	184.9	5.0
7	175.5	2.4	182.4	2.7	150.7	3.9	186.5	3.1
8	173.8	3.2	182.3	5.9	150.7	4.7	184.7	3.9
9			181.4	2.7	148.8	3.5	186.4	3.0

The means appear coherent for all samples in the 4 channels, except for sample no. 4 in channel 7 (higher mean and higher standard deviation). The study of aerial photographs indicates that the corresponding zone does not include a monospecific woodland. In addition, topography of the site lies on the limits of probability conditions of fir presence. This sample is therefore discarded. Another remark might be made on sample no. 8 in channel 5 which exhibits a correct mean but a high standard deviation. Control of this sample does not indicate, however, any abnormal condition and the sample is therefore retained.

3. DATA PROCESSING

3.1

In order to quantify the ground data in view of a performance evaluation, the reference map (Fig. 110) was first digitized with a step equal to the resolution in LANDSAT data processing (1 pixel = 2.5 ha). Results are presented in Fig. 111. The 20 fir forests of the studied area will thus provide 20 single estimations of the inventory efficiency by comparison with results obtained by satellite data processing (see section 4).

3.2

On the other hand, the LANDSAT data available from the four transparencies were digitized with the same step. The optical data obtained were processed as multispectral records. In the present case, a barycentric method (see Appendix, section 4.1.2) was used as classification method supervised with sampling. Fig. 115 shows the results obtained with the 8 retained samples.

3.3

This point-per-point analysis does not take any account of the environment of a given ground station. Furthermore, it results in a spreading of isolated points which are not likely to correspond to any botanical reality but must be put in relation with a shadow effect on leafy vegetal communities. Observations performed during ground control of photo-interpretation did actually establish that pure and homogeneous fir forests are not existing in areas of a few pixels in size. Therefore, a thematic criterion of smoothing the classification results was adopted. Such smoothing applied to LANDSAT data of Fig. 115 eliminates classified detached points and smoothes the contours of forests (Fig. 116).
By this second processing, an automatic inventory of fir forests in the investigated area was achieved.

4. COMPARISON BETWEEN GROUND DATA AND AUTOMATIC INVENTORY RESULTS

The performance definition of the automatic inventory of fir forests is realized by comparing the surfaces of woodlands obtained by map digitalization (Fig. 111) with the surfaces obtained by the LANDSAT data processing described above (Fig. 116).

Values of surfaces are given in the two first columns of Table 53. An evaluation of inventory performances is supplied by the differences between computed and actual surfaces (absolute and relative differen-

ces, third and fourth columns of Table 53).

For all the 20 forests, the global surface difference amounts to 125 ha which corresponds to an overall error of 4.0%. A more accurate evaluation of performances is provided by the characteristics of distribution of the absolute and algebric values of the relative difference (D%) and of the surface difference (D ha). These results are presented in Table 54 for the 20 investigated forests.

Table 53 - Comparison between ground data and automatic inventory results

No.	Name	Reference surface (ha)	Computed surface (ha)	Difference (ha)	Difference (%)
1	Lit (F)	398	396	- 2	- 0.5
2	Lit (B)	176	164	- 12	- 6.8
3	Jurvielle	106	86	- 20	- 18.9
4	Bosc	32	34	+ 2	+ 6.7
5	Astau	62	117	+ 55	+ 88.7
6	Autarrouy	58	81	+ 23	+ 39.7
7	Anedou	256	338	+ 82	+ 32.0
8	Coumes	255	232	- 23	- 9.0
9	Superbagnères	365	318	- 47	- 12.9
10	Artigue	38	34	- 4	- 10.5
11	Rame	48	38	- 10	- 20.8
12	Saccourvielle	54	78	+ 24	+ 44.4
13	Gourgue	68	66	- 2	- 2.9
14	Ayres	152	140	- 12	- 7.9
15	St. Jean	80	75	- 5	- 6.2
16	Escalère	192	210	+ 18	+ 9.4
17	Coumelongue	244	274	+ 30	+ 12.3
18	Hournet	161	157	- 4	- 2.5
19	Bois Neuf	272	330	+ 58	+ 21.3
20	Benque	94	68	- 26	- 27.7
Total		3111	3236		

The differences on the algebric values are evidently smaller because of a compensation effect between over- and underestimated values. However, a general shift leading to globally overestimated results is noted, mostly due to a strong overestimation obtained for a few forests (no. 5, 6, 7 and 12). These forests are localized on steep slopes where physionomy and topography induce a decrease of radiance of leafy trees and their consequent confusion with conifers. Discarding these 4 forests

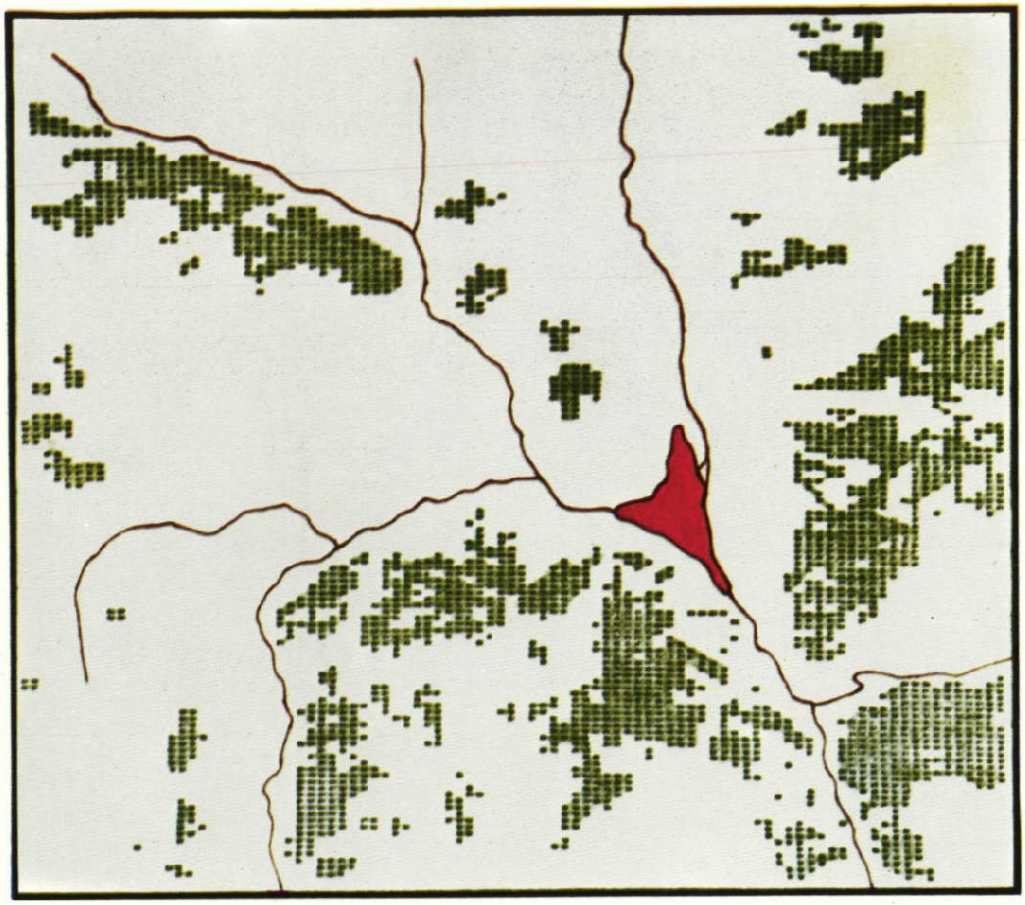

Fig. 115 - Classification results of fir forests from LANDSAT data processing

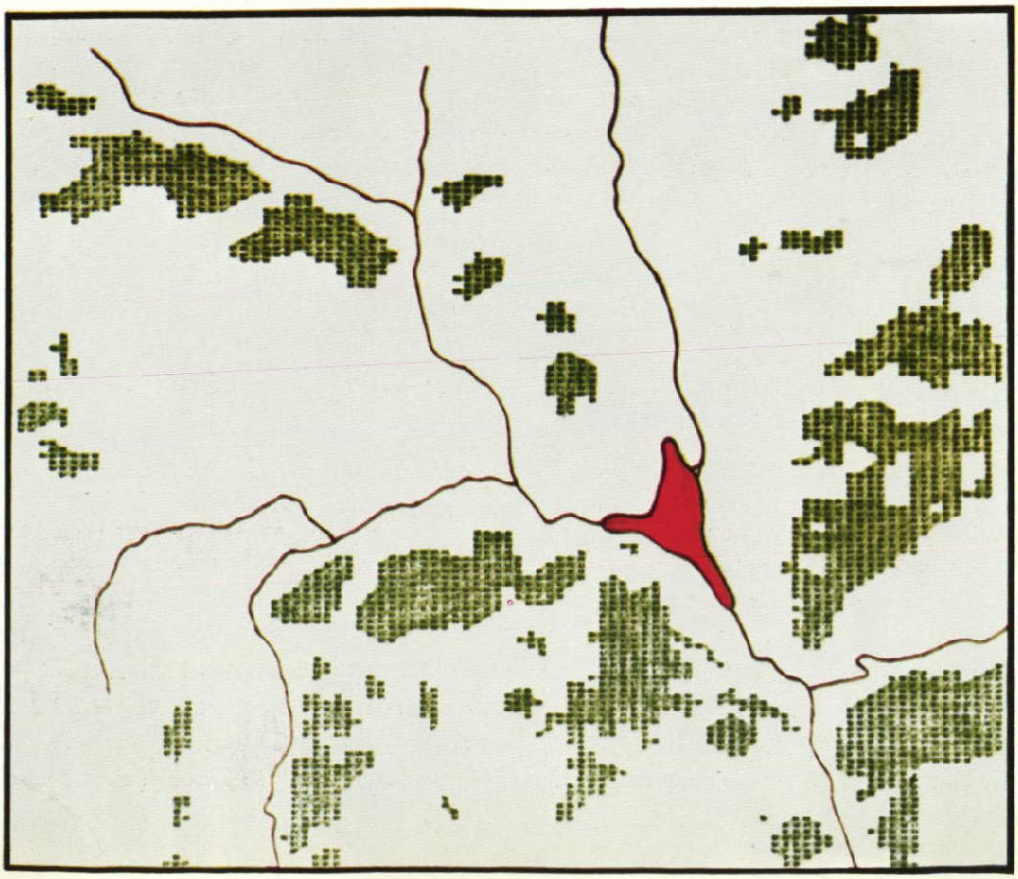

Fig. 116 - Results of the preceding fig. after smoothing

strict necessity of homogeneity tests.

Two types of improvement should be adopted for a more efficient application of the inventory methodology described here. They consist, on the one hand, in the use of LANDSAT CCT magnetic tapes, on the other hand, in a multitemporal analysis of the data. A quick regional surface estimation of coniferous forests in mountains is then likely to be achieved, after reduction of the influence of specific environmental factors on the spectral response of vegetation.

Table 54 - Mean and standard deviation of the absolute (abs.) and algebric (alg.) values of relative difference (D%) and surface difference (D ha), for the 20 investigated forests

	D% (abs.)	D% (alg.)	D ha (abs.)	D ha (alg.)
Mean	19.1	6.4	22.9	6.2
Standard Deviation	20.5	27.6	22.0	31.6

from the computations, results of Table 55 are obtained, which indicate a noticeable overall improvement.

Table 55 - Mean and standard deviation of the absolute (abs.) and algebric (alg.) values of relative difference (D%) and surface difference (D ha) for the 16 retained forests

	D% (abs.)	D% (alg.)	D ha (abs.)	D ha (alg.)
Mean	11.0	- 4.8	17.2	- 3.7
Standard Deviation	7.6	12.8	16.6	24.0

Such improvement might be easily achieved by a multitemporal analysis (for the elimination of the deciduous stations). On the other hand, the surface estimation of single forests would require a higher density of sampling.

5. CONCLUSIONS

Two kinds of factors significantly affect the quality of the surface measurements on fir forests:

- the experimental conditions do not allow a satisfactory identification of fir only on the basis of its spectral signature,
- the spatial resolution of the whole processing procedure is responsible for certain errors in surface measurements.

Nevertheless, it appears that the use of ecological data constitutes an indispensable thematic argument in sampling. The present experiment emphasized the difficulties encountered in the location of stations representative of standing conditions of fir forests and confirmed the

APPENDIX

1. MEASUREMENTS OF ATMOSPHERIC PARAMETERS

(by Maracci, G-C., JRC-Ispra)

A technique based on ground measurements of solar irradiance (H_{sun}) and sky irradiance (H_{sky}), by means of a LANDSAT-compatible radiometer, was developed at the JRC for determining the transmittance (τ) and path radiance (L_p) of the atmosphere [1, 2] The sketch of Fig. 117 where subscripts i correspond to LANDSAT bands i = 4, ... 7, illustrates the transfer of solar energy (H_o) from the sun to the MSS through the diffuse reflection on the ground surface, as well as the atmospheric parameters which affect the satellite data (L).

The figure provides also the most important formulae which may be used in preprocessing transformation in order to express the recorded satellite data in terms of the reflectance ρ which physically characterizes the target.

A systematic program for measurements of atmospheric parameters was carried out on cloud-free days on the test site no. 1 (Po Valley), in 1975, in correspondence to LANDSAT-2 passages. Results from these measurements are shown in Table 56. The values indicate that the masking effect of the atmosphere varies considerably from one day to the other.

The measured atmospheric parameters have been applied, up to now, only to computer classification methods on natural forest with a satisfying improvement of the classification results. Further systematic investigations should be performed in order to evaluate the performances which can be achieved by applying atmospheric corrections to automatic classification techniques.

BIBLIOGRAPHY

Internal:

(1) MARACCI, G-C., STURM, B., "Measurements of Beam Transmittance and Path Radiance for Correcting LANDSAT-data for Solar and Atmospheric Effects", Fifth Conference on Space Optics, October 14-17, 1975, Marseille (France) (1976)

(2) STURM, B., "Determination of Beam Transmittance and Path Radiance in the Four Bands of the ERTS-Satellite", Proc. of DFVLR-Seminar on Remote Sensing, Porz-Wahn (Germany), April 1975.

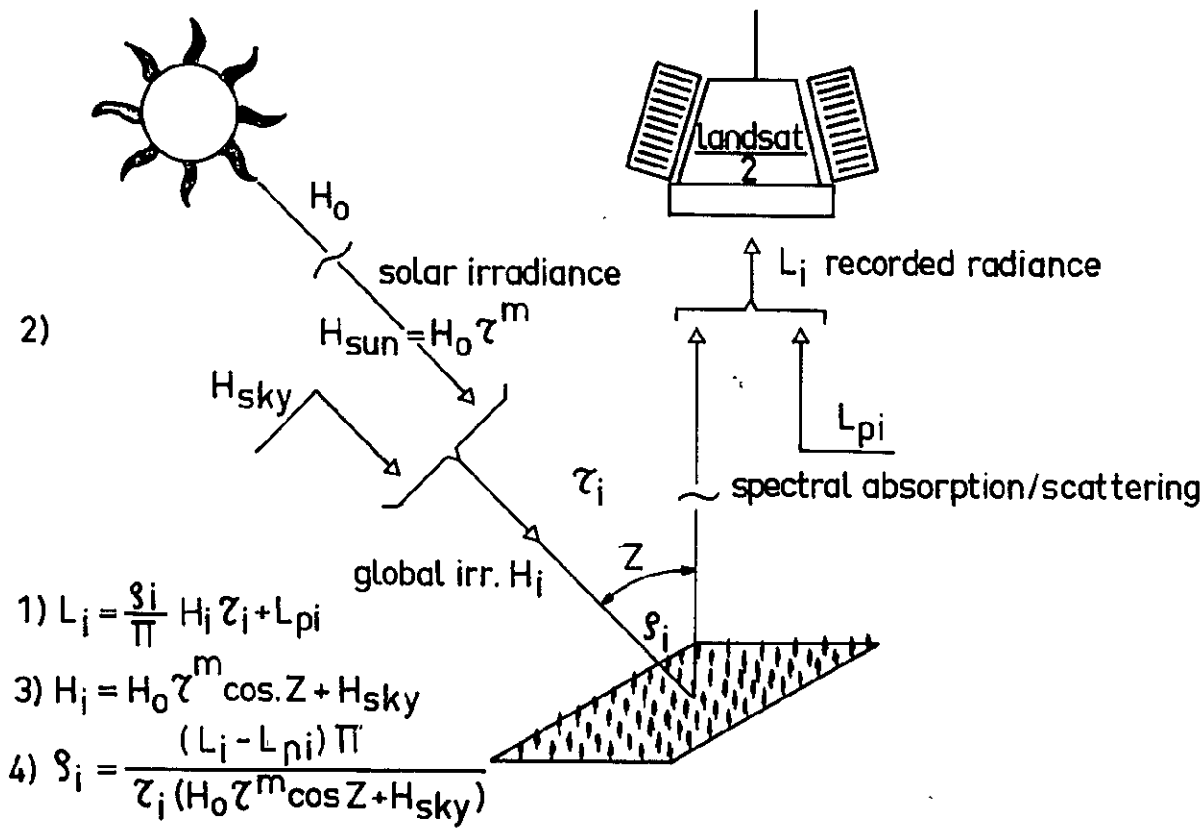

Fig. 117 - Schematic transfer of solar energy from the sun to the LANDSAT-MSS

Table 56 - Measured values of atmospheric parameters, on test site no. 1, in correspondence to LANDSAT-2 passages

Date	Band No	Global Irradiance $H(mW/cm^2)$	Transmittance	Path radiance L_p (mW/cm^2sr)	Equivalent reflectance $(L_p \pi / H \tau)$
22-4-75	4	6 19	0 35	0 32	0 46
	5	9 18	0.44	0 31	0 25
	6	7.72	0 55	0.20	0.15
	7	10.50	0 62	0 19	0 09
28-5-75	4	9.12	0.56	0 28	0 18
	5	12 13	0 63	0 24	0 10
	6	9 67	0.71	0 15	0 07
	7	12.59	0 74	0 13	0 04
3-7-75	4	9 65	0 63	0 27	0 14
	5	12 96	0.70	0 22	0 08
	6	10 67	0 77	0 12	0 05
	7	12 68	0 79	0 11	0 03
21-7-75	4	9 22	0 75	0.21	0.10
	5	13 07	0 79	0 16	0 05
	6	1071	0.85	0 08	0 03
	7	12 96	0 85	0 07	0 02
6-8-75	4	7.44	0.37	0.32	0.37
	5	10.16	0 45	0 30	0 21
	6	8 44	0.55	0 19	0 13
	7	10.34	0 59	0 17	0 09
13-9-75	4	7 85	0 83	0 17	0 08
	5	10.69	0 87	0 12	0 04
	6	8 75	0 91	0 06	0 02
	7	10 41	0 90	0 05	0 02

2. USE OF CAPTIVE BALLOONS FOR SPECTRAL SIGNATURE MEASUREMENTS

(by Maracci, G-C., JRC-Ispra)

The necessity of having a low altitude platform for performing radiometric measurements on trees, and more specifically on poplar afforestations, suggested the use of the captive balloon, which is inexpensive and can be easily controlled from the ground.
A technique was set up to define the signature of poplars by taking profit of the joint experience of CATA, ISP and JRC-Ispra.

2.1 Method

A DELACOSTE captive balloon type V.D. 4 equipped by CATA with an EXOTECH 100 A and a remotely controlled motor OLYMPUS camera, for ground truth documentation, was placed at about 80 m above poplars in order to detect the reflected radiance (R_n) from the tree foliage. At the same time a second EXOTECH, installed on top of the mobile unit and directed toward the zenith, measured the incoming irradiance (I_n). The set up is shown in Figs. 118 and 119.

Sets of data from the two EXOTECHs flowed to the mobile unit where they were recorded every two seconds with a Schumberger data logger. Spectral signatures ρ_n in the four LANDSAT bands were derived from recorded data by means of the simple ratio

$$\rho_n = \frac{R_n}{I_n} \quad (n = 4, \ldots 7) .$$

2.2 Examples of the results

Measurements have been performed on poplar groves at Casale Monferrato on June 3, 1977, from 1.30 p.m. to 3.20 p.m. (sun elevation from 63° 20′ to 48° 48′). They concerned two poplar clones extensively cultivated in the Po Valley (Populus deltoides and Populus americana I 214) and the two concurrent species Salix alba and Robinia pseudo-acacia.

Figs. 120, 121 and 122 illustrate for Salix alba the variations in time (during 1′) which occurred for incoming irradiance (I_n), reflected radiance (R_n) and reflectance (ρ_n), respectively. In spite of strong variations of the incoming irradiance (due to the presence of thin clouds), the reflectance in the 4 bands is relatively constant, the sharp deviations being caused probably by movements of the suspended EXOTECH with wind, as well as to the inhomogeneous foliage coverage. The mean values of 30 measurements (during 1′) are reported in Table 57. The standard error is estimated to be around 5%. One notes from these values that Populus deltoides has the most distinct spectral signature, whereas Salix alba and the poplar clone I 214 are the most likely to be confused.

Fig. 118 - Captive balloon for spectral signature measurements above poplar groves

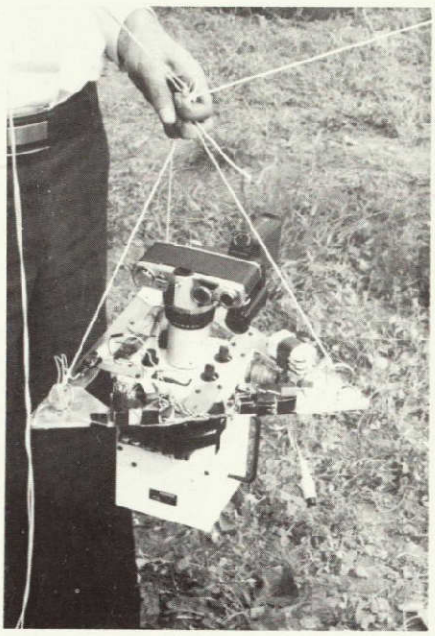

Fig. 119 - Sensors mounted on captive balloon for spectral signature measurements

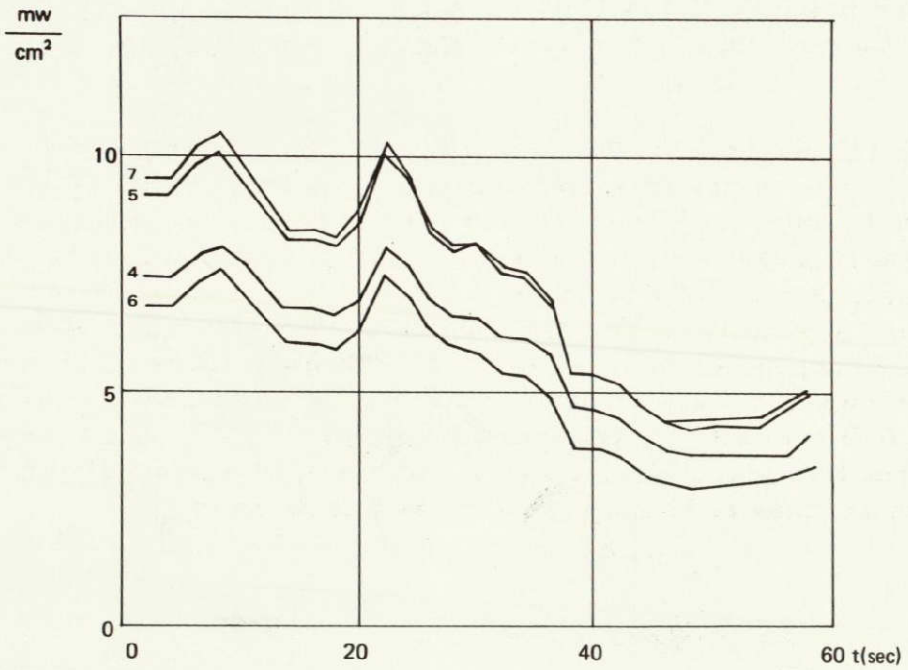

Fig. 120 - Incoming irradiance

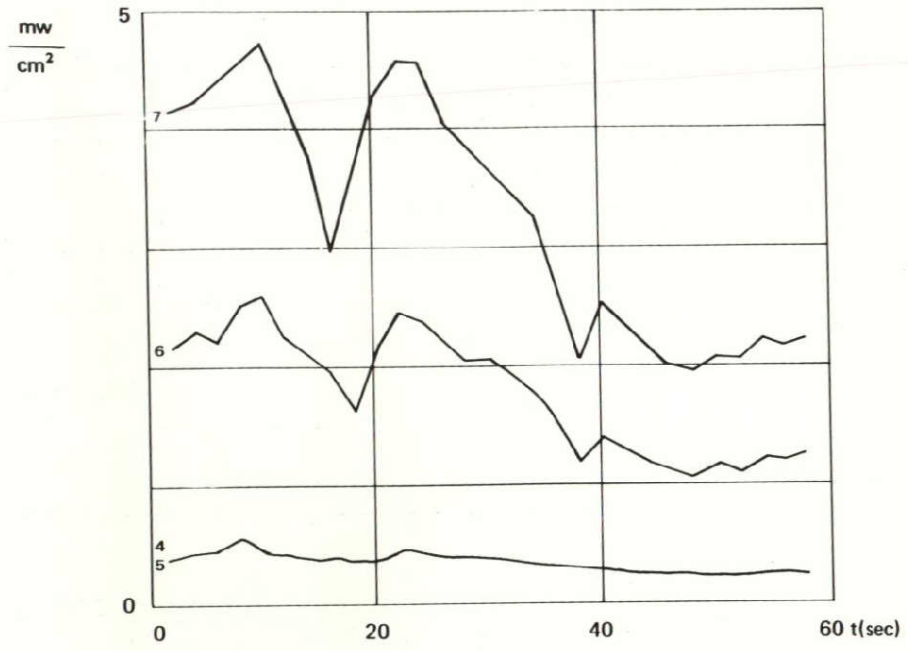

Fig. 121 - Reflected irradiance (Salix alba)

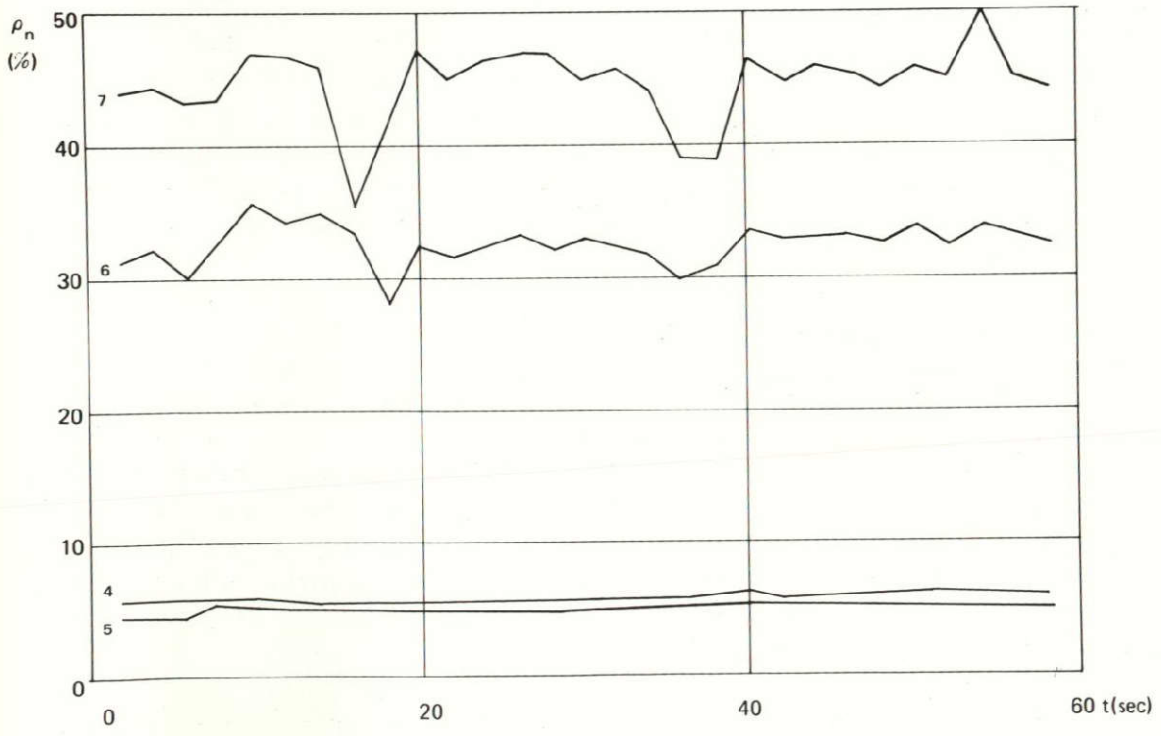

Fig. 122 - Reflectance (Salix alba)

Table 57 - Reflectance measurements on different tree species

Tree Species	Reflectance ρ (%)				
	band 4	band 5	band 6	band 7	time
Populus deltoides	3.18	2.62	26.20	37.33	13h 38m
Salix alba	5.82	4.66	34.12	43.38	14h 15m
Robinia pseudo-acacia	4.10	2.92	33.02	44.20	14h 50m
Populus americana (I 214)	4.92	3.54	36.24	45.51	15h 22m

3. REALIZATION OF A LANDSAT 4-CHANNEL FIELD RADIOMETER

(by Gatelli, E., JRC-Ispra)

The technique of radiometric measurement of landscape features over the agricultural and forest areas of the Italian test sites, either from fixed points or seen as strips of ground from low-altitude aircraft, initially involved a single type of radiometer, the EXOTECH mod. 100.
This radiometer consists essentially of a 4-independent filter optics, aligned with a common centering viewfinder. Due to misalignment of the 4 channels and the necessity of monitoring incoming sun radiation during field operation, a radiometer was developed at the JRC-Ispra obviating the difficulties emerged during the pre-launch phase (Fig. 123).

3.1 Technical description

The 4-way optical waveguide is the basic component which characterizes the performance of this radiometer. The optical layout is shown in Fig. 124. The main body of the guide subdivides into 4 secondary branches, each of which carries a quarter of the incident radiation to the sensors. The entrance section of the guide is accurately positioned with respect to the focal plane of the objective passing through a hole made in the mirror of the viewfinder. Thus, the incident radiation goes directly from the target to the entrance of the optical guide which transmits it to the sensors.

To allow the operator a view of the scene being examined, the radiometer is equipped with a reflex viewfinder with shutter. The operator sees, in the field of the viewfinder, a dark circular area in the centre of the scene, corresponding to the part analyzed by the sensors. In this way it is possible to point exactly the radiometer over the investigated area.

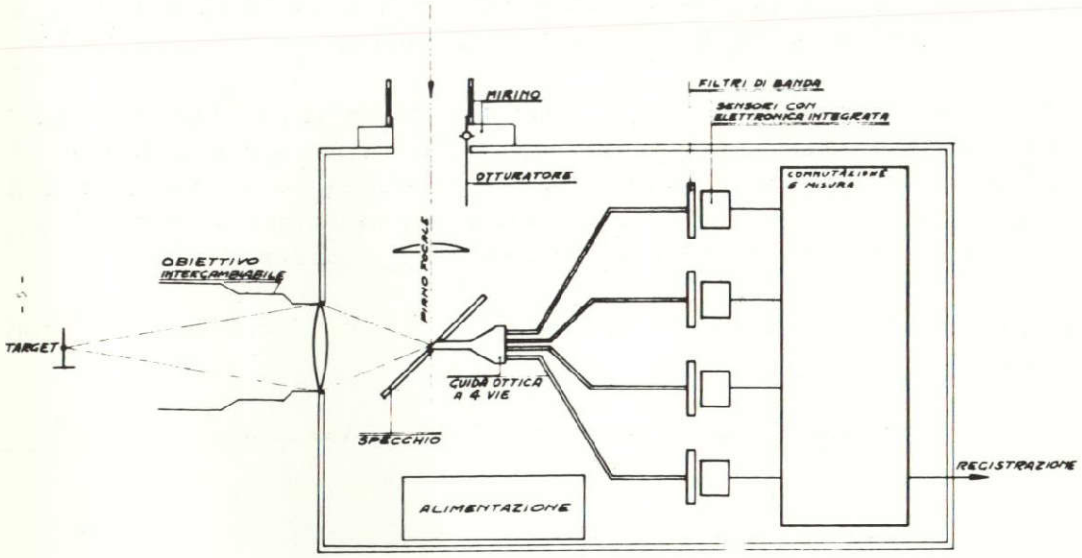

Fig. 123 - Radiometer scheme

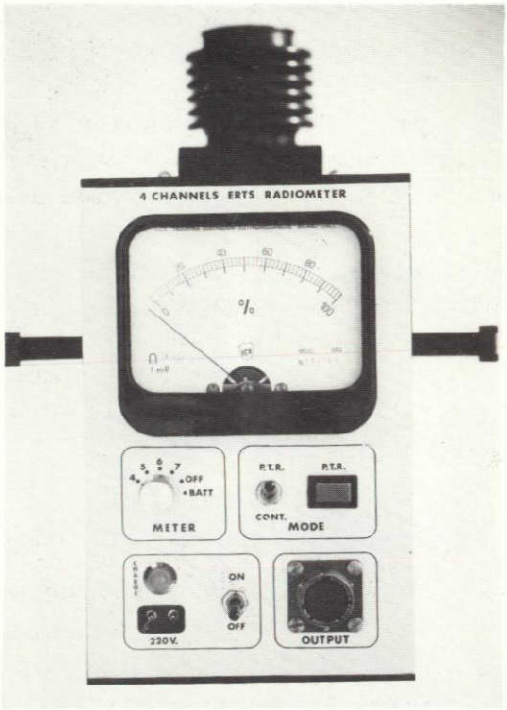

Fig. 124 - Radiometer

The viewfinder is also equipped with a manually controlled shutter with the function to eliminate as much as possible the light entering through the area of the viewfinder during the measurement, under conditions of highly illuminated surroundings.

The radiometer has been mainly used for obtaining radiometric signal profiles in the four LANDSAT channels; the instrument was demonstrated to be particularly suitable also for surveys of targets of small size. In this case pointing is made easier by the design of a viewfinder which allows the display of the area being measured.

In Table 58 the values of the nominal F. O. V. as a function of the used lens, are reported.

Table 58 - Values of nominal F. O. V. for various lenses

Lens	Nom. F. O. V.
50 mm F. 1.8	1^{o}
300 mm F. 4	0.2^{o}
plane	about 50^{o}

Use was made of an opal glass instead of a lens for measurements of the 2π-steradian radiation. The objective is also equipped with a diaphragm allowing a continuous attenuation of the incident radiation.

When the instrument is operated in conjunction with a second radiometer to provide continuous monitoring of a reference panel, the use of the optical attenuator facilitates standardization between the outputs of the 2 radiometers.

The outputs available for signals recording have a level of 0.1 V equivalent to the full scale of the instrument range. In the case of measurements at levels exceeding the normal instrument range the recording outputs keep linear with the incident radiation up to a maximum value of 10 V.

4. DATA PROCESSING METHODS

(by Le Toan, T., CESR, Toulouse and Mégier, J., JRC-Ispra)

4.1 French test sites

4.1.1 Unsupervised classification method

The method developed is a mobile center clustering technique called

"Nuées Dynamiques"[1] . The principle of the method consists of settling clusters around centers G_c^1 chosen randomly on the image. In the next step the process is iterated, i.e. new centers G_c^2, G_c^3, ... G_c^n must be built, and stopped when the centers remain fixed, i.e. when $G_c^n = G_c^{n+1}$ vc.

The method is justified by the fact that the passage from G_c to G_c^1, G_c^2 ... reduces the intra-class variance (of E_c).

To reduce the number of iterations, the area under study is divided into subareas, each of which is a square of 60 x 60 pixels.

Z_{11}	Z_{12}	Z_{13}
Z_{21}	Z_{22}	Z_{23}
Z_{31}	Z_{32}	Z_{33}

The process is applied first to Z_{11}. The iteration number is limited to 5. If after 5 iterations the convergence of the process is not reached, an other random choice is made. When the convergence on Z_{11} is obtained, zone Z_{12} is computed with the last set of centers of Z_{11}.

In the case of LANDSAT imagery, every sub-area corresponds to a zone of about 4.8 km x 3.6 km. Geographically, in such an agricultural zone, 2 contiguous subareas are in most cases included in the same ecological region. This means that the same types of vegetation or land use will very probably be found in 2 contiguous sub-areas. So, in practice, one iteration is necessary for computing Z_{12} with the last centers of Z_{11}. If, however, the "landscape" changes suddenly, then other iterations are needed, or a choice of random initial center must be made. The contiguity concept can be applied in both directions, i.e. lines and columns. Thus, for Z_{21} the initial centers came from Z_{11}.

4.1.2 Supervised classification methods

Several methods were applied, but parametric methods, such as the maximum likelihood ratio, was not utilized since the normal hypothesis for rice field responses is not proved and the a priori occurrence probability of classes is unknown.

- Barycentric method (BM), using weighted euclidean distance between points x_1 and x_2:

$$d^2(x_1, x_2) = \sum_{i=1}^{n} K_i (x_{1i} - x_{2i})^2$$

where K_i = weighting factor for channel i.

The principle consists in choosing K_i to get a maximum of well-classed samples. The process starts with:

$$K_i = \frac{1}{\sigma_i^2},$$

where σ_i^2 is the total variance of samples in channel i.

- Quadratic methods using the following distances:

a) Mahalanobis distance:

$$d^2(x, y_K) = [(x - E(y_K)]^T \sum_K^{-1} [x - E(y_K)]$$

with y_K = set of K^{th} sample (K = 1, 2, 3)

$\sum_K$ = covariance matrix of y_K

E = expectation function.

An alternative method (Fix-Hodges Method) consists in using the Mahalanobis distance and generalizing the K-nearest neighbour rule(2).

b) Sebestyen distance:(3)

$$d^2(x, y_K) = \left|\sum_K\right|^{\frac{1}{n}} \left\{[x - E(y_K)]^T \sum_K^{-1} [x - E(y_K)] + n\right\}$$

with n = number of channels.

This distance minimizes the mean square of the distances from points of every cluster (class) to its barycentre.

c) Chi-square distance:

$$d^2(x_1, x_2) = \sum_{i=1}^{n} K \left[\frac{x_{1i}}{\sum_{i=1}^{n} x_{1i}} - \frac{x_{2i}}{\sum_{i=1}^{n} x_{2i}}\right]^2$$

4.2 Italian test sites

4.2.1 Unsupervised classification methods

Two clustering methods have been used, both utilizing the euclidean distance as similarity measure between data points, and membership

threshold to define the clusters.

The first method[4] constructs the clusters from a random subset of points and attempts to grow the cluster (class) to which a point is attributed by examining also the neighbouring points on the same line. All the points (pixels) of the studied zone are then classified into the various classes defined before, by using euclidean distance between point and mean of the classes. There is no iteration process in this method.

The second method uses all the points of the studied zone in the clustering process. A rejection criterion is also introduced within the points already clustered in order to take into account the evolution of the classes. Several iterations are generally performed in order to ensure a reasonable stability of the results.

4.2.2 Supervised classification methods

- The maximum likelihood method (ML), with normal parameters to describe the training classes, has been used[5]. The following decision law is implemented for vector (point) x:

$$h_k(x) \geq h_\ell(x), \ \forall \ell \neq k \longrightarrow x \in \text{class } k$$

$$\text{where } h_k(x) = \ln P(C_k) - 1/2 \ln\left|\sum_k\right| - 1/2 \left[(x-M_k)^T \sum_k^{-1} (x-M_k)\right]$$

M_k mean vector of class k,

$\sum_k$ covariance matrix of class k.

In the present context, $\ln P(C_k)$ is cancelled from the expression of $h_k(x)$ (see Chapter I, section 3.2.2).

- The modified euclidean distance method (MED)

This method can be considered as formally identical to the ML scheme, but with the assumption that all the covariance matrices describing the class distributions are diagonal. From another point of view it can be seen that the method calculates the euclidean distances between any vector to be classified and the mean vectors of the classes of interest; it then weighs the distances by the variance of the classes; lastly it constructs the following distance between the vector and class C:

$$\sum_{i=1}^{n} \frac{di^2}{v_i} + \ln \prod_{i=1}^{n} v_i \ ,$$

where d_i is the euclidean distance for channel i, v_i is the variance for

channel i, n is the number of channels (dimensions) and the first term is the weighted euclidean distance. The unknown vector is consequently assigned to the class for which the distance just described is minimum. This second method is simpler and much less time-consuming than the ML method.

- Uniformity mapping procedure

This procedure [5] computes the average euclidean distance between a given point and its immediate neighbours. This distance is a measure of the uniformity of the data around the point. A uniformity map is then set up by starting from the uniformity value attributed to each point.

- Determination of performance matrices (PMAT)

This program simply performs a pixel-by-pixel comparison between the discrete version of the ground truth document and the classification results.

If m ground truth categories have been classified into n different classes, then m x n cases are considered in the comparison process and a m x n performance matrix is built.

It is organized in m rows and n columns. Each row contains the number of pixels belonging to the ground truth category - specified as entry of the row - attributed to the various classes by the classification algorithm. Symmetrically, each column contains the number of pixels attributed to the class specified as entry and actually belonging to the various ground truth categories. Each matrix element can be expressed as absolute number of pixels, as percentage of ground truth category pixels (the sum of percentages along each row is 100) or as percentage of total number of pixels attributed to a given class (the sum of percentages along each column is 100).

N.B. In order to avoid confusions, it is spoken of "categories" for ground truth pixels and of "classes" for classified pixels. Each single category does not necessarily correspond to one single class. Depending on the problem, some categories may correspond to one single class and conversely.

- Contour follower routine (DMAP)

This routine is able to take into account, in a pixel-by-pixel comparison performed by PMAT, the pixels situated within a polygon specified by the coordinates of its vertices. The polygon needs not to be convex and may be rather complicated in shape. For instance, a scan line of pixels may be crossed over up to twenty times by the polygon sides.

4.2.3 Interactive System

The classification methods described under 4.2.2 have been, for the greater part, implemented in an interactive mode with a mapped display of the classified results in alphanumeric characters (one character per class). The interactive display terminal used was first a Tectronix 4002 A limited to 80 x 60 characters and at the present stage a Tectronix 4015.1 with a capability of 125 x 80 characters.

BIBLIOGRAPHY

Internal:

- HERZOG, J.H., STURM, B., "Preprocessing Algorithms for Radiometric Corrections and Texture Spatial Features in Automatic Land-Use Classification", 10th Int. Symp. on Remote Sensing of Environment, Ann Arbor, Mich., Oct. 1975.

External:

(1) DIDAY, E., "La méthode des nuées dynamiques et la reconnaissance des formes", Cahiers de l'IRIA, Rocquencourt (France) (1970)

(2) FIX, E., HODGES, J.R., "Discriminatory Analysis", USAF School of Aviation Medicine, Rep. 4 and 11 (1951)

(3) SEBESTYEN, G.S., "Decision-Making Process in Pattern Recognition", The Mac Millan Company (1962)

(4) TURNER, B.J., "Cluster Analysis of Multispectral Scanner Remote Sensor Data", Remote Sensing of Earth Resources, vol. 1 (Shahrokki, Ed.), the University of Tennessee, Tullahoma, Tenn. (1972)

(5) BORDEN, F.Y., APPLEGATE, D.N., TURNER, B.J., LACHOWSKI, H.M., MEREMBECK, B.F., HOOSTY, J.R., "Satellite and Aircraft Multispectral Scanner Digital Data Users Manual", ORSER-SSEC Technical Report 1.75 (1975), Office for Remote Sensing of Earth Resources. The Pennsylvania State University.